Molecular epitope and affinity determination of protein-protein interactions by a combination of biosensor and mass spectrometric methods

“ Molekulare Epitop- und Affinitätsbestimmung von Protein-Protein-Wechselwirkungen durch eine Kombination von biosensorischen und massenspektrometrischen Methoden“

TECHNISCHE UNIVERSITÄT DARMSTADT

at the Department of Chemistry
of the Technische Universität Darmstadt

submitted in fulfillment of the requirements for the
degree of Doctor rerum naturalium
(Dr. rer. nat.)

Doctoral thesis
by Pascal Wiegand

First assessor:	Prof. Dr. Katja Schmitz
Second assessor:	Prof. Dr. Frederik Lermyte

Darmstadt 2024

Date of submission: 18th December 2023

Day of the oral examination: 5th February 2024

Wiegand, Pascal: Molecular epitope and affinity determination of protein-protein interactions by a combination of biosensor and mass spectrometric methods
Darmstadt, Technische Universität Darmstadt,
Year of publication of the dissertation on TUPrints: 2024
URN: urn:nbn:de:tuda-tuprints-267798
Day of the oral examination: 5th February 2024

The present work was carried out from January 2018 to December 2022 under the supervision of Prof. Dr. Dr. h.c. Michael Przybylski at the "Steinbeis Center for Biopolymer Analysis and Biomedical Mass Spectrometry" in Rüsselsheim am Main in collaboration with the working group of Prof. Dr. Katja Schmitz at the Technische Universität Darmstadt. The dissertation was submitted to the Department of Chemistry at the Technische Universität Darmstadt in december 2023.

Die vorliegende Arbeit wurde im Zeitraum von Januar 2018 bis Dezember 2022 unter der Betreuung von Herrn Prof. Dr. Dr. h.c. Michael Przybylski im „Steinbeis Center for Biopolymer Analysis and Biomedical Mass Spectrometry“ in Rüsselsheim am Main in Zusammenarbeit mit dem Arbeitskreis von Frau Prof. Dr. Katja Schmitz an der Technischen Universität Darmstadt durchgeführt. Am Fachbereich Chemie der Technischen Universität Darmstadt wurde die Arbeit als Dissertation, um Dezember 2023, eingereicht.

Table of Contents

Acknowledgment /Danksagung

Eine Dissertation ist mit viel Arbeit verbunden und ohne die Unterstützung anderer kaum zu meistern. Deswegen möchte ich mich an dieser Stelle bei allen bedanken, die mir während der Anfertigung meiner Dissertation zur Seite gestanden haben.

Als erstes Danke ich meiner Frau, ohne ihre Unterstützung wäre es mir nicht möglich gewesen diese Arbeit zu einem Ende zu bringen.

Mein besonderer Dank gilt Frau Prof. Dr. Katja Schmitz, die mir zur Promotionsstelle im Steinbeis Center verholfen hat. Bereits während meiner Zeit als Masterstudent konnte ich, in ihrem Arbeitskreis an der TU Darmstadt, fachlich und persönlich viel von ihr lernen. Die konstruktiven und motivierenden Gespräche waren immer wieder hilfreich und haben zu neuen Ideen für die einzelnen Projekte geführt. Herzlichen Dank auch für die Korrektur dieser Arbeit und die Übernahme als Erstgutachterin.

Im Weiteren bedanke ich mich bei Herrn Prof. Dr. Dr. hc. Michael Przybylski, der mir die Möglichkeit zur Promotion im Steinbeis Center gab und mich stets fachlich unterstützte. Besonders die Möglichkeit zu den verschiedensten Konferenzen zu fahren und dort den Austausch mit anderen Promotionsstudenten zu haben, war ein große Bereicherung für mich. Leider ist er Anfang dieses Jahres verstorben und konnte nicht an der Fertigstellung meiner Arbeit mitwirken. Ich werde seinen Elan und seine Motivation nie vergessen, die ihn bis zum Ende begleitet haben.

Mein besonderer Dank gilt Herrn Dipl.-Phys. Prof. Dr. Wolfgang Kleinekofort, der mich ebenfalls im Steinbeis Center bei meiner Arbeit unterstütze und als Fachprüfer an meiner Disputation teilnimmt. Die Zusammenarbeit mit der Hochschule RheinMain und dem Steinbeis Center wurde durch ihn ermöglicht und die Bachelor- und Masterstudenten, die er zu uns ins Labor führte, waren mir eine große Hilfe.

Außerdem Danke ich Herrn Prof. Dr. Frederik Lermyte für die Übernahme des Zweitgutachters meiner Arbeit und Herrn Prof. Dr. Stefan Zielonka für Teilnahme an meiner Disputation als Fachprüfer.

Speziell bedanke ich mich bei allen meinen ehemaligen Kolleginnen und Kollegen im Steinbeis Center, die mit mir im Labor zusammengearbeitet haben. Da ist Dr. Loredana Lupu, die mich stets bei der Reparatur der MS Geräte unterstütz hat, sowie unsere zahlreichen Konfernzbesuch werden mir stets in Erinnung bleiben. Delia Mihoc und Biljana Brdar, die für gute Laune im Labor gesorgt haben. Dr. Yannick Baschung, der mit mir in meinem ersten Doktorandenjahr, in die USA auf eine Tagung ins schöne San Diego geflogen ist. Stephan Rawer, der als erfahrender Peptidchemiker stets einen Rat bei Problemen hatte und der allein mit seiner Anwesenheit für eine gute Stimmung im Labor gesogt hat.

Für die großartige Unterstützung im Labor bedanke ich mich bei Tamsila Khan (B.Sc.), Daria Holdschick (M.Sc.) und Till Schneider (M.Sc.), die mir mit ihren wissenschaftlichen Arbeiten geholfen haben, diese Arbeit anzufertigen.

Ich danke meiner gesamten Familie und meinen Freunden für die mentale Unterstützung in der letzten Zeit.

Data dissemination

Publications

Parts of the presented Ph.D. project have been submitted for publication or are in preparation for submission.

Loredana-Mirela Lupu, **Pascal Wiegand**, Daria Holdschick, Delia Mihoc, Stefan Maeser, Stephan Rawer, Friedemann Völklein, Ebrahim Malek, Frederik Barka, Sascha Knauer, Christina Uth, Julia Hennermann, Wolfgang Kleinekofort, Andreas Hahn, Günes Barka and Michael Przybylski. Identification and Affinity Determination of Protein-Antibody and Protein-Aptamer Epitopes by Biosensor-Mass Spectrometry Combination. Int. J. Mol. Sci. 2021, 22, 12832.

Delia Mihoc, Loredana-Mirela Lupu, **Pascal Wiegand**, Wolfgang Kleinekofort, Oliver Müller, Friedemann Völklein, Michael O. Glocker, Frederik Barka, Günes Barka, Michael Przybylski. Antibody Epitope and Affinity Determination of the Myocardial Infarction Marker Myoglobin by SPR-Biosensor Mass Spectrometry. J. Am. Soc. Mass Spectrom. 2021, 32(1), 106-113.

Anna Tramarin, Marina Naldi, Genny Degani, Loredana Lupu, **Pascal Wiegand**, Angelica Mazzolari, Alessandra Altomare, Giancarlo Aldini, Laura Popolo, Giulio Vistoli, Michael Przybylski, Manuela Bartolini. Unveiling the molecular mechanisms underpinning biorecognition of early-glycated human serum albumin and receptor for advanced glycation end products. Anal. Bioanal. Chem. 2020, 412, 4245–4259.

Loredana Lupu, **Pascal Wiegand**, Nico Hüttmann, Stephan Rawer, Wolfgang Kleinekofort, Irina Shugureva, Anna S. Kichkailo, Felix N. Tomilin, Alexander Lazarev, Maxim V. Berezovski and Michael Przybylski. Molecular Epitope Determination of Aptamer Complexes of the Multidomain Protein C-Met by Proteolytic Affinity-Mass Spectrometry. ChemMedChem. 2020, 15(4), 363-369.

Pascal Wiegand, Loredana Lupu, Nico Hüttmann, Julia Wack, Stephan Rawer, Michael Przybylski and Katja Schmitz. Epitope Identification and Affinity Determination of an Inhibiting Human Antibody to Interleukin IL8 (CXCL8) by SPR- Biosensor–Mass Spectrometry Combination. J. Am. Soc. Mass Spectrom. 2020, 31(1), 109–116.

International and national presentations

Pascal Wiegand, Loredana Lupu, Nico Hüttmann, Julia Wack, Stephan Rawer, Michael Przybylski, Katja Schmitz. Epitope Identification and Affinity Determination of an Inhibiting Human Antibody to Interleukin IL8 by SPR-Biosensor-Mass Spectrometry Combination. 53rd DGMS Annual Meeting, Münster, Germany. March 1-4, 2020. **Oral presentation**.

Pascal Wiegand, LoredanaLupu, Nico Hüttmann, Julia Wack, Stephan Rawer, Michael Przybylski, KatjaSchmitz. Epitope Identification and Affinity Determination of an Inhibiting Human Antibody to Interleukin IL8 by SPR-Biosensor-Mass Spectrometry Combination. "TUD Doktorandentag", Darmstadt, Germany. January 29, 2020. **Poster presentation**.

Pascal Wiegand, Loredana Lupu, Maxim V. Berezovski, Nico Hüttmann, Alexander Lazarev, Andrés R. A. Marques, Paul Saftig, Michael Przybylski. Epitope Identification of an aptamer complex of Cathepsin D in comparison to an antibody-Cathepsin D complex. 52nd DGMS Annual Meeting, Rostock, Germany. March 10-13, 2019. **Oral presentation.**

Pascal Wiegand, Loredana Lupu, Maxim V. Berezovski, Andrés R. A. Marques, Paul Saftig, Michael Przybylski. Epitope Identification of an aptamer complex of Cathepsin D in comparison to an antibody-cathepsin D complex. 30th MassSpec-Forum, Vienna, Austria. February 19-20, 2019. **Poster presentation.**

Pascal Wiegand, Nico Hüttmann, Julia Wack, Loredana Lupu, Alexander Lazarev, Michael Przybylski, KatjaSchmitz. Identification and Affinity Determination of Antibody Epitopes against the Chemokine CXCL8 by High-Pressure Proteolytic Extraction Mass Spectrometry and Biosensor Analysis. 66TH ASMS Conference on Mass Spectrometry and Allied Topics, San Diego, California, USA. June 3-7, 2018. **Poster presentation.**

Pascal Wiegand, Nico Hüttmann, Julia Wack, Loredana Lupu, Michael Przybylski, Katja Schmitz. Identification and Affinity Determination of Antibody Epitopes against the Chemokine CXCL8/Interleukin-8 by Affinity Mass Spectrometry and Biosensor Analysis. Joint meeting of DGMS and SFSM, Saarbrücken, Germany. March 11-15, 2018. **Poster presentation**.

Declaration / Erklärungen

§8 Abs. 1 lit. c der Promotionsordnung der TU Darmstadt
Ich versichere hiermit, dass die elektronische Version meiner Dissertation mit der schriftlichen Version übereinstimmt und für die Durchführung des Promotionsverfahrens vorliegt.

§8 Abs. 1 lit. d der Promotionsordnung der TU Darmstadt
Ich versichere hiermit, dass zu einem vorherigen Zeitpunkt noch keine Promotion versucht wurde und zu keinem früheren Zeitpunkt an einer in- oder ausländischen Hochschule eingereicht wurde. In diesem Fall sind nähere Angaben über Zeitpunkt, Hochschule, Dissertationsthema und Ergebnis dieses Versuchs mitzuteilen.

§9 Abs. 1 der Promotionsordnung der TU Darmstadt
Ich versichere hiermit, dass die vorliegende Dissertation selbstständig und nur unter Verwendung der angegebenen Quellen verfasst wurde.

§9 Abs. 2 der Promotionsordnung der TU Darmstadt
Die Arbeit hat bisher noch nicht zu Prüfungszwecken gedient.

Darmstadt, den 18.12.2023

(Pascal Wiegand)

1 Abstract

1.1 Zusammenfassung

Den Schwerpunkt der vorliegenden Arbeit bildet die Charakterisierung der Bindestellen (Epitope) von Antikörpern bzw. Aptameren der vier Modellproteine Interleukin-8 (IL8, CXCL8), Cathepsin D (CTSD), α-Glucosidase A (GAA) und Survival Motor Neuron Protein (SMN). Allen Teilprojekte gemeinsam war die Isolierung von potenziellen Epitoppeptiden aus einem enzymatischen Verdau des jeweiligen Proteins durch die Affinitätschromatographie an immobilisiertem Antikörper bzw. Aptamer. Dieser Versuchsaufbau wird Epitopextraktion genannt.[1] Die einzelnen Fraktionen von der Affinitätssäule wurden mittels Matrix-unterstützter Laser-Desorptions-Ionisierungs-Flugzeit Massenspektrometrie (MALDI-tof MS)[2] untersucht, um anhand der Peptidmassen die Epitoppeptide und deren Sequenz zu bestimmen. Zur weiteren Validierung der identifizierten Peptide wurde deren Affinität zu den Antikörpern mittels Oberflächenplasmonenresonanz (SPR)-Biosensoranalyse untersucht.[3] Dabei sollte auch die Epitopextraktion mit Sepharose gebundenem Antikörper mit einer Variante verglichen werden, bei der der Antikörper direkt auf einem SPR-Chip immobilisiert war.[4] Die Epitopcharakteriserung ist beim Verständnis der Funktion von Antikörpern und bei der Entwicklung verschiedenster Bioassays von Bedeutung.

Die Modellproteine stehen alle in Verbindung mit verschiedenen Krankheiten, sei es als Zielproteine bei der Behandlung von Krankheiten oder als potenzielle Biomarker. Dabei wird IL8[5] mit chronisch entzündlichen Krankheiten, wie rheumatoider Arthritis (RA), SMN[6] mit der Muskelatrophie (SMA), und CTSD[7] und GAA[8] mit verschiedenen lysosomalen Speicherkrankheiten in Verbindung gebracht. Die Aufklärung Epitope von Antikörpern an diese Proteine können dabei helfen, deren biologische Funktionen besser zu verstehen. Zum Beispiel inhibiert der Antikörper gegen IL8 dessen Rezeptorbindung und entsprechende Funktionen, kann aber auch zu dessen Nachweis eingesetzt werden. Epitoppeptide können aber auch zur Quantifizierung eines Proteins verwendet werde, das als Biomarker für eine bestimmte Krankheit dient, wie beim SMN-Protein, das ein Biomarker für die spinale Muskelatrophie ist. Bei CTSD wiederum sollten die Bindungsstellen eines Antikörpers mit denen eines Aptamers verglichen werden und die Epitoppeptide von GAA sollten bei der Enzymersatztherapie (ERT) mittels Apherese dabei helfen, Antikörper gegen das Medikament aus dem Blut zu entfernen.

Bei den Epitopextraktionsexperimenten für den Komplex von IL8 mit dem monokonalen Antikörper mAB-I2519 konnten Epitoppeptide besonders gut identifiziert werden, wenn die entsprechenden Antikörper über Protein G an Goldchips gebunden waren. Die Untersuchung von IL8 und seinen Peptiden wurde durch deren relativ starke Bindung an die verschiedensten Oberflächen, wie an die Sepharose 4B, erschwert. Beim Einsatz von Peptiden aus einem tryptischen Verdau ergab sich ein diskontinuierliches Epitop für mAB-I2519, das aus IL8[12-20] und IL8[55-60] besteht. Die Affinitäten der Antikörper-Antigen Komplexe wurden mit dem SPR-basierten Biosensor bestimmt. Die Immobilisierung wurde ebenfalls über Protein G erreicht und ergab stabile und hochaktive Antikörperoberflächen. Für die Wechselwirkung von IL8 mit mAB-I2519 wurde eine K_D von 7,4 nM ermittelt, für das Peptid IL8[12-20] eine K_D von 75,1 µM und für IL8[55-60] von 0,98 mM. Beide Peptide binden den Antikörper im Paratop mit geringer Affinität, weswegen beide in einer bestimmten Konformation präsentiert werden müssen, um den Antikörper mit einer entsprechend hohen Affinität zu binden. IL8[12-20] ist Teil der Rezeptorbindungsstelle und IL8[55-60] ist für die Bindung an Glykane auf Zelloberflächen verantwortlich, was wichtig für die IL8-Gradientenbildung zur Rekrutierung von Leukozyten ist. Daher hemmt mAB-I2519 gleichzeitig die Bindung von IL8 an seinen Rezeptor und an Zelloberflächen und verhindert auf diese Weise dessen biologische Wirkung.

Mit den gleichen Methoden, wie zur Analyse der Interaktion von IL8 mit mAB-I2519, wurden das SMN-Protein und sein monoklonaler Antikörper mAB-7B10 untersucht. Für den Komplex von SMN und mAB-7B10 wurde ein bekanntes Epitop auf den SMN-Protein in Form des tryptischen Peptids rSMN[37-57] extrahiert. Die Epitopextraktion konnte in diesem Zusammenhang auch erfolgreich von einem SPR-Biosensorchip durchgeführt

werden. Die Affinität von mAB-7B10 zu rSMN beträgt 0,25 - 0,69 nM; für das synthetische Epitoppeptid rSMN[37-57] liegt sie bei 3,2 nM. Aufgrund der gut erhaltenen Affinität des Epitoppeptids wurde es erfolgreich in einem Konzeptbeweis für einen diagnostischen Assay eingesetzt, mit dem das SMN-Protein aus biologischen Proben durch Epitopextraktion und MALDI-tof MS quantifiziert werden kann. Geeignete Kalibrierungskurven in Verbindung mit einer ersten erfolgreichen Extraktion des Epitoppeptids aus einer Vollblut-Lysatprobe wurden erhalten. Zusätzlich wurden polyklonale Antikörper mit einem Epitop im C-terminalen Bereich von SMN zusammen mit mAB-7B10 in einen Sandwich-SPR-Assay getestet, der als alternative Strategie zur Quantifizierung des SMN-Proteins eingesetzt werden könnte. Die Signalverstärkung durch den zweiten Antikörper soll dabei zu einem noch sensitiveren Assay führen.

Die Untersuchung der CTSD-Antikörper bzw. -Aptamer-Komplexe und des GAA-Antikörper-Komplexes führten zu keiner eindeutigen Identifizierung von Epitoppeptiden und Bindungsstellen. Dies war vor allem auf die große Menge an unspezifischen Sepharose-bindenden Peptiden, die aus dem jeweiligen Proteinverdau mit Trypsin und Chymotrypsin stammten, zurückzuführen. Zur erfolgreichen Epitopidentifizierung müssten daher alternative Methoden verwendet werden. Um in Zukunft Proteinepitope, die über die Epitopextraktion schwerzugänglich sind, frühzeitig zu erkennen, müssen spezifische Scouting-Experimente für unspezifische säulenbindende Peptide aus Proteinverdauen mit unterschiedlichen Proteasen durchgeführt werden. Dadruch könnte der Schwierigkeitsgrad eines zu bestimmenden Epitopes mit der Epitopextraktionsmethode eingeschätzt werden. Für den GAA-Antikörper war bekannt, dass das Epitope im 70 kDa Fragement des Proteinkomplexes liegen soll, weswegen hier das Epitop zumindest auf eine Region um GAA[317-324], GAA[304-349], und GAA[411-458] eingegrenzt werden konnte.

Zusätzlich zu den experimentellen Laborarbeiten wurden *in-silico* Prädiktoren für die B-Zell-Epitop Vorhersage eingesetzt, um die identifizierten Peptide als Teil eines potenziellen Epitops zu bewerten. Die verwendeten Softwaretools, DiscoTope 2.0,[9] Seppa 3.0,[10] BepiPred 2.0[11] und BCEPS[12] und deren Vorhersagen über die Epitope, beinhalteten die identifizierten Epitope aus den Analysen mit SMN und IL8. Für CTSD und GAA wurden viele der identifizierten Peptide ebenfalls als potenzielle Epitope vorhergesagt, aber wegen des großen Anteils von unspezifischen Bindern konnten keine eindeutigen Epitoppeptide ausgemacht werden. Für die untersuchten Proteine zeigten die Epitopvorhersagen jedoch, dass andere Proteasen, wie Glu-C, Lys-C oder Arg-C, für die Bildung von epitopabbildenden Peptiden von Vorteil gewesen wären, die die potenziellen Epitope nicht an potenziell kritischen Positionen für die Antikörperbindung gespalten hätten. Daher kann die *in silico* Analyse zur Planung und Verbesserung des Versuchsaufbaus für eine bestimmte Epitopidentifizierung beitragen.

Schließlich wurde der enzymatische Verdau von Proteinen unter hohem Druck mit den vier Modellproteinen getestet, da dieser Schritt essenziell für die Epitopextrkation ist. Der Hochdruckverdau wurde unter wiederholten Zyklen von hohem und niedrigem Druck durchgeführt und wird als „*pressure cycling technology*“ bezeichnet.[13] Die Tests wurden mit Trypsin durchgeführt und die erhaltenen Peptide wurden mittels MS charakterisiert. Unter anderem wurden Parameter für die Sequenzabdeckung, Verdauungsgeschwindigkeit, Enzymspezifität und erhaltene Peptidpeakmuster mit einem Standardverfahren unter Atmosphärendruck verglichen. Die Parameter zeigten ähnliche Werte für den Verdau unter atmosphärischem und hohem Druck. Es gibt Anzeichen dafür, dass für den Hochdruckaufschluss wesentlich geringere Mengen des Enzyms verwendet werden könnten, wobei einige Stunden oder weniger für den vollständigen Verdau ausreichen. Dies muss weiter untersucht werden. Außerdem bestätigen diese Experimente, dass Trypsin seine Spezifität und Aktivität unter hohem Druck nicht verändert.

1.2 Abstract

The focus of the present work is the characterization of binding sites (epitopes) of antibodies and aptamers against the four model proteins interleukin-8 (IL8, CXCL8), cathepsin D (CTSD), α-glucosidase A (GAA) and survival motor neuron protein (SMN). Common to all subprojects was the isolation of potential epitope peptides from enzymatic digestion of the respective protein using affinity chromatography with immobilized antibody or

aptamer. This experimental setup is called epitope extraction,[1] and eluated fractions were analyzed by matrix-assisted laser desorption ionization time-of-flight mass spectrometry (MALDI-tof MS)[2] to identify the epitope peptide sequence based on the peptide masses. For further validation of the identified peptides, their affinity to the antibodies was determined by surface plasmon resonance (SPR) biosensor analysis.[3] Epitope extraction with Sepharose-bound antibody was also compared with a variant in which the antibody was immobilized directly on an SPR chip.[4] Epitope characterization is essential for the understanding of antibody function and for the development of various bioassays.

The model proteins are all associated with different diseases, either as target proteins in the treatment of diseases or as potential biomarkers. IL8[5] is associated with chronic inflammatory diseases such as rheumatoid arthritis (RA), SMN[6] with muscular atrophy (SMA), and CTSD[7] and GAA[8] with various lysosomal storage diseases (LSD). The elucidation of the epitopes of antibodies relevant to these proteins can help us understand their biological functions. For example, the antibody against IL8 inhibits its receptor binding and corresponding functions but can also be used for its detection. Epitope peptides can also be used to quantify a protein that serves as a biomarker for a specific disease, such as the SMN protein, a biomarker for spinal muscular atrophy. In CTSD, the binding sites of an antibody should be compared with those of an aptamer, and the epitope peptides of GAA should help to remove antibodies, which are formed against the drug in enzyme replacement therapy (ERT) from blood of patients using apheresis.

In the epitope extraction experiments for the complex of IL8 with the monoclonal antibody mAB-I2519, epitope peptides could be identified particularly well when the corresponding antibodies were bound to gold chips via protein G (PG). The investigation of IL8 and its peptides was complicated by their relatively strong binding to various surfaces, such as sepharose 4B. When peptides from a tryptic digest were used, a discontinuous epitope for mAB-I2519 consisting of IL8[12-20] and IL8[55-60] was obtained. The affinities of the antibody-antigen complex were determined by using the SPR-based biosensor. The immobilization of the antibody via protein G yielded stable and highly active surfaces. For the interaction of IL8 with mAB-I2519, a K_D of 7.4 nM was determined; for the peptide IL8[12-20], a K_D of 75.1 µM and for IL8[55-60] of 0.98 mM. Both peptides bind the antibody paratope with low affinity, which is why both must be presented in a specific conformation in order to bind the antibody with a correspondingly high affinity. IL8[12-20] is part of the receptor binding site, and IL8[55-60] is responsible for binding to glycans on cell surfaces, which is important for IL8 gradient formation required for leukocyte recruitment. Therefore, mAB-I2519 simultaneously inhibits the binding of IL8 to its receptor and cell surfaces, thus preventing its biological effect.

The SMN protein and its monoclonal antibody mAB-7B10 were analyzed similarly to IL8 and its antibody mAB-I2519. For the complex of SMN and mAB-7B10, a known epitope on the recombinant SMN (rSMN) protein was extracted in the form of the tryptic peptide rSMN[37-57]. In this context, epitope extraction was also successfully performed using an SPR-based biosensor. The affinity of mAB-7B10 to rSMN is 0.25 - 0.69 nM; for the synthetic epitope peptide rSMN[37-57], it is 3.2 nM. Due to the well-preserved affinity of the epitope peptide, it was successfully used in a proof-of-concept for a diagnostic assay to quantify the SMN protein from biological samples by epitope extraction and MALDI-tof MS. Appropriate calibration curves in conjunction with a first successful extraction of the epitope peptide from whole blood lysate were obtained. In addition, polyclonal antibodies with an epitope in the C-terminal region of SMN were tested with mAB-7B10 in a sandwich SPR assay, which could be used as an alternative strategy to quantify the SMN protein. The signal amplification by the second antibody could increase the assay's sensitivity.

The examination of the CTSD-antibody and -aptamer complexes, respectively, and the GAA antibody complex did not lead to unambiguous identification of epitopes or binding sites. This was mainly due to the large amount of unspecific sepharose-binding peptides originating from the respective protein digestion with trypsin and chymotrypsin. Therefore, alternative methods would have to be used for epitope identification of these proteins. In order to recognize protein epitopes that are difficult to access via epitope extraction, at an early stage, specific scouting experiments for unspecific column-binding peptides from digestions with different proteases must be carried out in the future. This would allow the determination of the difficulty level of an

epitope to be determined using the epitope extraction method. For the GAA antibody, it was known that the epitope should be located in the 70 kDa fragment of the protein complex, which is why at least the epitope could be narrowed down to a region around GAA[317-324], GAA[304-349], and GAA[411-458].

In addition to the experimental lab work, in-silico predictors for B-cell epitope prediction were used to evaluate the identified peptides a part of a potential epitope. The predictions of the software tools DiscoTope 2.0,[9] Seppa 3.0,[10] BepiPred 2.0,[11] and BCEPS[12] included the epitopes for SMN and IL8. For CTSD and GAA, many of the identified peptides were identified by the epitope predictors, but due to the large proportion of non-specific binders, no unique epitope peptide could be assigned. However, for the investigated proteins, the epitope predictions showed that other proteases, such as Glu-C, Lys-C, or Arg-C, would have been advantageous for the formation of epitope-forming peptides, as they do not cleave at potentially critical positions for antibody binding. Therefore, in-silico analysis can help to design and improve the experimental setup of a particular epitope identification.

Finally, the enzymatic digestion of proteins under high-pressure was tested with the four model proteins, as the digestion is essential for epitope extraction. High-pressure digestion was carried out under repeated cycles of high and low pressure and is referred to as "pressure cycling technology" (PCT).[13] The tests were performed with trypsin, and the peptides were analyzed by MS. Performance parameters such as sequence coverage, digestion speed, enzyme specificity, and peptide peak patterns were compared with a standard procedure under atmospheric pressure. The parameters showed similar values for digestion under atmospheric and high pressure. There is evidence that much lower amounts of the enzyme could be used for high-pressure digestion, with a few hours or less sufficient for complete specific digestion, but this will need further investigation. At last, these experiments confirmed that trypsin does not change its specificity and activity under high pressure.

2 Introduction

The focus of the following work is the analysis of protein-protein interactions (PPI) or protein-antibody interactions by chromatography, mass spectrometry, and a biosensor. Combining these methods yields information about the binding sites and the strength of the interactions. Both are essential characteristics of protein-protein interactions, and they help in the task of finding ways to influence specific proteins. One possible field of application is medicine. For example, many diseases are related to dysfunctional proteins or PPIs for which specific inhibitors can be used as therapeutics. The knowledge about the precise interaction site and its characteristics helps develop such inhibitors. The binding characteristics also lead to insights into biological processes and can be applied to potential diagnostic assays. This chapter will introduce and compare different methods for determining binding sites and affinities compared to the affinity chromatography-mass spectrometry and SPR-based biosensor analysis employed in the presented work. Afterwards, the model proteins used in this work and their relevance to the corresponding diseases will be presented, followed by general experimental procedures and strategies for data evaluation.

2.1 Elucidation of interaction sites

Protein interactions are essential for all living creatures, from bacteria to large animals. The sum of all proteins in a specific organism or compartment is called the proteome, and its composition can change depending on environmental stimuli.[14] In the related field of proteomics, researchers try to measure and identify all proteins of a given proteome and their changes upon specific environmental changes. Researchers have found correlations between all kinds of diseases and changes in the proteome. Similar correlations were found in other "-omics" fields, like glycomics[15], metabolomics[16], and transcriptomics[17]. Each of these fields emphasizes the analysis of a specific substance class, like sugars, metabolites, or RNA transcripts. Combining information from all omics fields will ultimately result in the most detailed description of a specific singular cell and multicellular organisms like animals and humans.[18] The interactome[19], which comprises all interactions of proteins, sugars, DNA, or RNA molecules within an organism or compartment, can be analyzed and understood by combining all omics fields. Detailed knowledge of the interactome could help to predict, prevent, identify, and treat various diseases. Since the human interactome is slightly different for everyone, characterizing a personal interactome could lead to even more precise, personalized treatment strategies for all kinds of diseases.

The most investigated class of biomolecules are proteins. The interactions of proteins and their high abundance in living creatures make them a perfect target for treating diseases, which is why highly advanced analysis methods have been developed.[20] Due to its significance for drug discovery, researchers sometimes refer to the interactome as the characterization of protein-protein interactions, even though the interactome should involve all biomolecular interactions. The characterization of PPIs usually includes the identification of binding sites, kinetics, affinities, and specific mechanisms. Information about residues involved in binding sites helps to understand the underlying binding mechanisms, their impact on protein function, and their response to external forces. The binding affinity and, more importantly, the binding kinetics are directly linked to the underlying binding mechanism and the biomolecule's activity. The combination of all information will characterize the analyzed protein complex formation, dissociation, persistence, and mechanism of function.[21]

2.1.1 Antibody binding structures and affinity

The interaction of proteins with other proteins, carbohydrates, lipids, or small molecules is based on non-covalent interactions: hydrogen bonding, van-der-Waals, hydrophobic, and electrostatic forces.[21] Those interactions occur at the surface amino acid residues of proteins that come into contact. Transition and stable complexes are formed if the binding free energy passes a specific threshold, which can vary greatly. The

formation of protein complexes is critical to all biological functions and effects. Therefore, the identification of binding sites is a crucial part of understanding and influencing biochemical processes. [21]

Antibodies form a particular group of proteins with high specificities and affinities for their target antigen. That is why antibodies are widely investigated as therapeutics and diagnostic agents. Antibodies are part of the innate and adaptive immune systems of vertebrates. Immune cells like leukocytes and B-cells, which produce antibodies, protect vertebrates against chemical pathogens.[22] Different antibodies or immunoglobulin (Ig) subclasses like IgG, IgE, IgM, IgA, and IgD can be distinguished.[23] They differentiate in structure and domain assembly, with each singular antibody having an individual amino acid sequence. They are expressed at different stages during an immune response to pathogens. Nevertheless, they share similar structures and construction features, described in more detail for the IgG antibody class. IgG antibodies consist of two heavy and two light chains (Figure 2.1.1), with Greek β-barrels forming the characteristic structure of globulins.[23] The different chains are connected via disulfide bonds, and each heavy (H) and light chain (L) consists of a constant (C) domain (CH1, CH2, CH3, CL) and a variable (V) domain (VH, VL).[24] The crystallizable fragments (F_C), which results from papain cleavage at the hinge region, consists of the domains CH2 and CH3 and is necessary for immune cell recognition. The variable domains, which are essential for antigen binding, are called antigen-binding fragments (F_{ab}) and consisit of VH-CH1 and VL-CL, which are also created by papain cleavage. The variable regions from heavy and light chains form the 'complementarity determining regions' (CDRs), composed of three hypervariable loops. Those antigen binding loops on the antibody are called paratopes, and the binding site of the antibody paratope on the antigen is called epitope.[24]

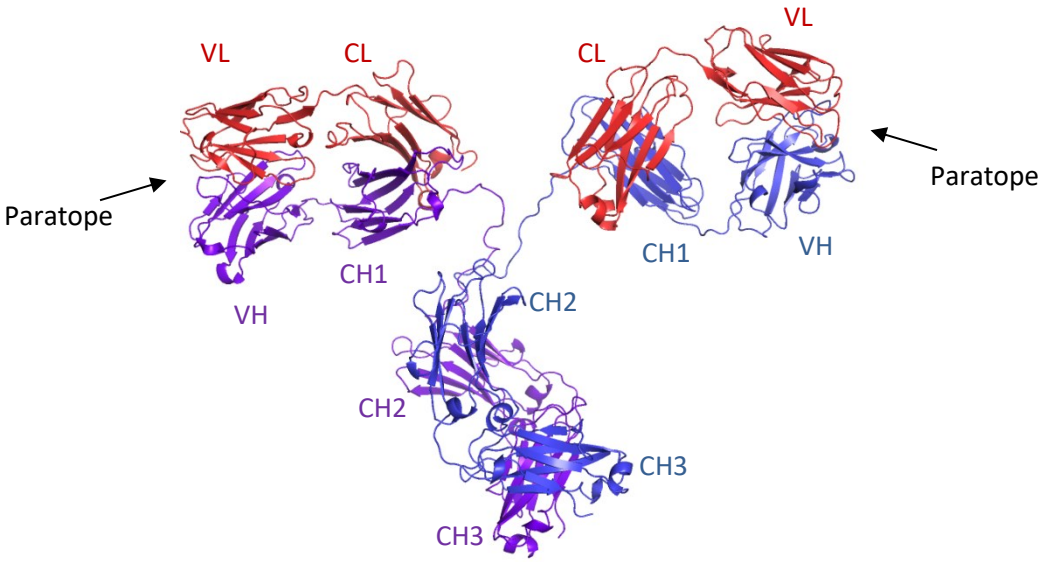

Figure 2.1.1: Example of an antibody crystal structure (PDB: 1IGT) with annotations for key structural characteristics. The two light chains are highlighted in red, and the two heavy chains are shown in shades of blue. (The antibody image was created with PyMOL.[25])

The CDRs from heavy (CDR-H1, CDR-H2, CDR-H3) and light chains (CDR-L1, CDR-L2, CDR-L3) are extensively investigated for common structural and sequence motifs. Different results point to more rigid structural motifs in CDR-H1, CDR-H3, CDR-L1, CDR-L2, and CDR-L3, whereas CDR-H3 shows conformational flexibility and rearrangement upon antigen binding. Several studies have shown the enrichment of aromatic and polar amino acid residues in the CDRs.[26] Despite extensive knowledge about the paratope composition and conformation, predicting corresponding epitopes from a given paratope composition is still challenging. *Vice versa,* it is impossible to predict the paratope only from an epitope sequence or structure. However, prediction attempts of epitope regions on protein antigens have been made based on common motifs, structural similarities, and surface accessibility of amino acid residues. To a certain extent, the prediction of binding to B-cell receptors, T-cell receptors, and the major histocompatibility complexes I and II (MHC-I and MHC-II) seems possible.[27,28] Those predictions should be considered cautiously and must be validated by experimental data. However, the more data is collected, the better the correlating algorithms can be tuned and trained to yield more accurate

predictions, as further discussed in chapter 2.1.3. The location of an epitope on a protein indicates which biomolecular processes a corresponding antibody might interfere with, and which known protein interactions might be inhibited or otherwise modified. Antibody-induced functional inhibition is one approach to treating certain diseases caused by malfunctioning proteins or pathways. One crucial property of antibodies binding to an antigen is described as affinity. The stability of a formed antibody-antigen complex is chracterized by its affinity, where the kinetic parameters for the complex association, dissociation, and free binding enthalpy play a critical role.[29] Therefore, the affinity indicates potential dose-response curves, which show essential parameters for medical applications. The binding of an antibody to an antigen is often described by the lock-and-key model[23], where two complementary shapes bind to each other. However, the "induced fit" model[26] represents the reality more often, and structural changes during the binding event from an antibody to its antigen lead to an even tighter fit. In some cases, conformational changes occur before the actual binding event due to structural flexibility. The corresponding model is called "conformational fit". [24] Those three binding models apply to all protein-protein interactions and not exclusively to antibody-ligand binding. The simplest protein-protein interactions are described as a 1:1-binding event, where one protein molecule binds to one ligand molecule (Figure 2.1.2-A). For the calculation of kinetic and equilibrium constants, the concentration of (c_{AB}) is dependent on the association rate (k_a), dissociation rate (k_d), and concentrations of the interacting proteins (c_A, c_B). At the equilibrium state, the complex formation and complex dissociation occur at equal rates, leading to the equation (2). This binding model is not entirely accurate for antibodies, especially for binding an antigen on a surface (Figure 2.1.2-B). Moreover, the avidity leads to a homo-bivalent binding mode, in which the interplay of multiple binding sites for one target on one ligand facilitates re-binding after dissociation or binding a second target molecule linked to a first one.

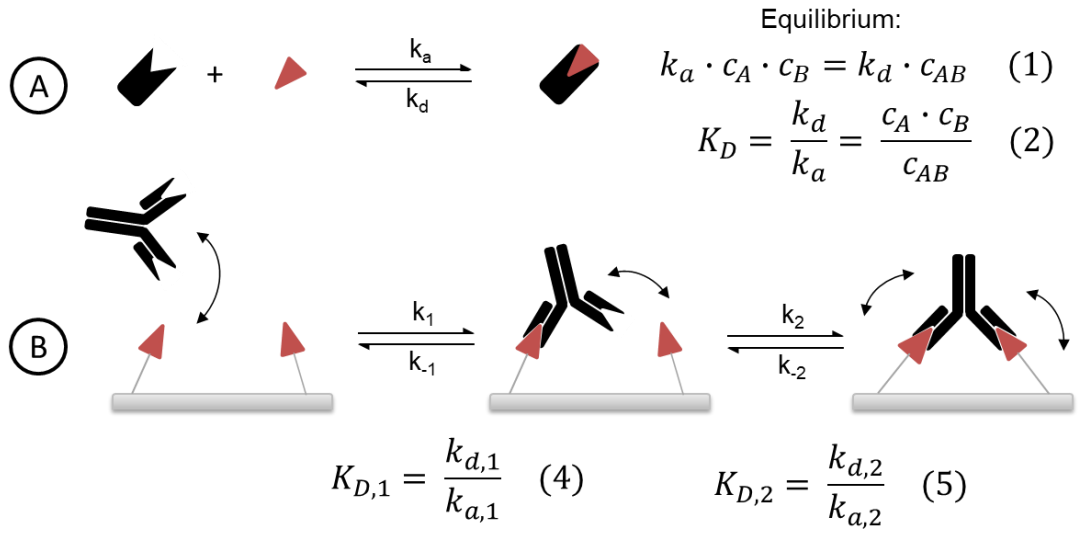

Equilibrium:

$$k_a \cdot c_A \cdot c_B = k_d \cdot c_{AB} \quad (1)$$

$$K_D = \frac{k_d}{k_a} = \frac{c_A \cdot c_B}{c_{AB}} \quad (2)$$

$$K_{D,1} = \frac{k_{d,1}}{k_{a,1}} \quad (4) \qquad K_{D,2} = \frac{k_{d,2}}{k_{a,2}} \quad (5)$$

Figure 2.1.2: Kinetic and affinity binding models. (A) 1:1 binding model with one analyte molecule binding to one ligand molecule. (B) Bivalent binding model for antibodies binding an antigen on a surface. Two binding sites in close proximity allow a much faster second binding event before and after the complex dissociated, creating a seemingly non-dissociating complex. In the case of binding multiple antigens simultaneously on a surface, the dissociation is significantly slower.

In the context of antibody-antigen binding, one antibody molecule has two binding sites for two identical antigen molecules. Therefore, antibodies bind with an avidity of two, leading to nearly irreversible antigen binding, mainly if several antigens are located on the surface of a pathogen or in a protein oligomer. Different kinetic parameters and equilibrium constants arise from this model for a more complex mechanism of association and dissociation. This multiple-parameter system makes comparisons demanding. Therefore, the so-called "functional affinity," according to the 1:1-binding model, is used to determine kinetic parameters and affinity for antibodies to compare more easily to other complex formation and dissociation constants.[30,31] The binding mechanism also correlates with the epitope structure, typically described as continuous, discontinuous, or structural epitope (Figure 2.1.3). A continuous, non-structural epitope binds its target entirely based on its primary structure without requiring a predefined conformational state. Therefore, the consecutive order of

amino acids defines its binding capabilities and mechanism. It could also be possible to have a continuous epitope with a necessary conformation for target binding. It is more likely to be found because, upon a binding event, structural changes are more often necessary to form a stable protein complex. Not all amino acids in a continuous epitope are often necessary for target binding and only provide a specific structure or arrangement of the amino acids participating in the binding event. These epitopes are categorized as discontinuous epitopes, which are partly dependent on their structure. Lastly, the amino acids of an epitope can be spread over the entire length of the primary sequence but are structurally close together on the protein surface to form a complex, discontinuous epitope. [32]

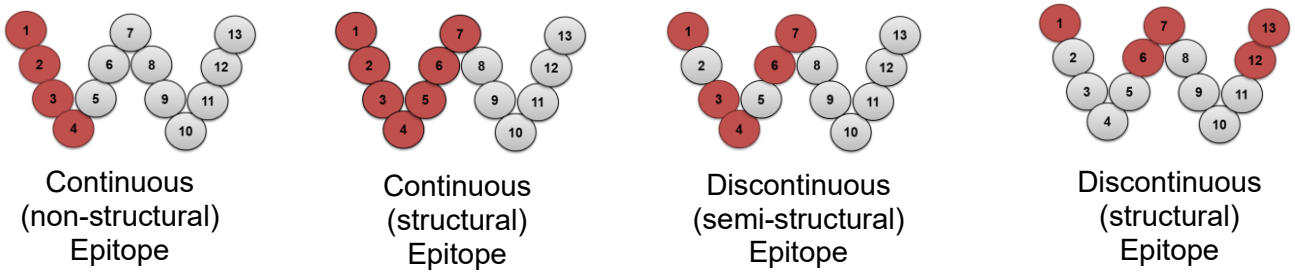

Figure 2.1.3: Antibody, B-cell, and T-cell epitope classification into continuous (linear) and discontinuous epitopes with subgroups for their structural dependency for forming a stable protein complex.

The knowledge of an epitope from an antibody can give insights into specific binding properties and its applicability in certain biochemical assays. For example, a continuous epitope might retain its whole affinity in a small peptide from the protein, which could be used as a biomarker. A discontinuous epitope might be more challenging to use as a peptide biomarker because extracting it from a biological sample is more challenging. If the structure of the related protein is essential for its biological activity, its structural integrity could be tested with an antibody with a discontinuous epitope on the target. Therefore, the epitope type can be exploited in certain biochemical assays to address specific biochemical questions. The epitope and its type must be identified before applying an antibody to those assays. Besides in-silico predictions of epitopes, many experimental methods have been developed for antibody epitope analysis, which will be introduced in the following chapters, as well as an alternative biomolecular class for antibodies in biochemical assays.

2.1.2 Aptamers as alternatives to antibodies

Aptamers are proposed as alternatives to antibodies and are often described as ‘chemical antibodies’.[33–37] Single-stranded oligonucleotide aptamers, either DNA or RNA, are reported to have similar binding capabilities to proteins compared to antibodies.[38] Because of their similar biochemical properties, it should be possible to substitute antibodies with aptamers in biochemical assays, diagnostics, and therapeutics. A general drawback of antibodies is reproducibility issues arising from batch-to-batch variabilities in cell-based production, which are observed for all antibodies and variants.[39] The possibility of producing synthetic aptamers makes them an attractive alternative to antibodies.[36] However, identifying new aptamer ligands is still the biggest challenge. In an in-vitro approach called ‘systematic evolution of ligands by exponential enrichment’ (SELEX), libraries of oligonucleotides are screened against a target protein or other molecules, and potential aptamers are enriched due to their high target affinity.[40] This approach is often complex, yielding numerous potential ligands, which need further characterization regarding their affinity and specificity.[41]

Many assays and potential clinical diagnostics could be performed with aptamers instead of antibodies. For example, in some enzyme-linked immunosorbent assays (ELISA), aptamers have successfully replaced antibodies, called enzyme-linked apta-sorbent assays (ELASA).[36] Because of their high stability and easy

synthesis, aptamers have also attracted considerable interest in nanomaterials.[42] In this context, nanomaterials for diagnostics are functionalized with aptamers to provide biorecognition abilities. Many aptamer-antibody (-hybrid) based assays have been successfully demonstrated for biosensors.[43] Nevertheless, there is no accurate diagnostic tool based on aptamers yet besides many research applications. Despite their potential in research applications, aptamers face challenges in replacing the well-established antibody-based assays. The detailed analysis of aptamer-protein complexes lags behind compared to the extensive characterization of antibody-based complexes.[43] Bridging the expertise and knowledge gap between these two fields is crucial for expanding the application of aptamers in diagnostics.

In the field of therapeutics, only one aptamer drug was approved in 2004.[44] The drug Pegaptanib sodium from Eyetech Pharmaceuticals/Pfizer, which is an RNA aptamer binder for the vascular endothelial growth factor (VEGF), which is applied for the treatment of age-related macular degeneration (AMD) and diabetic macular oedema.[44] It belongs to a class of VEGF inhibitors and initially showed great success. However, antibody-based inhibitors that got an FDA-approval soon afterwards showed superior performance.[45] For both aptamer and antibody-based drugs, VEGF inhibitors showed weak long-term stabilization of the eyesight in patients with ocular vascular disease. Therefore, in long-term treatment, none of the therapies seems optimal. These examples of antibodies that outperform corresponding aptamers reduce the interest in aptamer research as therapeutics. It remains uncertain if aptamers are less efficient as therapeutics than antibodies, and the investigation of aptamer epitopes could help by the identification of effective aptamers. Moreover, it is interesting to investigate whether different epitopes are accessible with aptamers than with antibodies.

2.1.3 In-silico analysis of antibody epitopes

Nowadays, in-silico prediction tools are widespread in biochemistry. In epitope analysis, the prediction of B-cell or antibody epitopes was extensively studied. Especially in epitope-peptide-based vaccine development, B-cell (or T-cell) epitope prediction tools are intensively investigated.[46–48] The B-cell epitope (BCE) prediction tools are generally divided into linear/continuous and conformational/discontinuous BCE prediction tools. The main difference between those tools is the information needed for BCE prediction. Linear BCE predictors, like BepiPred-2.0[11], BCEPS[12], ABCpred[49], LBtope[50], SVMTrip[51], and iBCEL-EL[52] utilize the protein sequence, whereas conformational BCE predictors, like DiscoTope-2.0[9], Epitopia[53], CBtope[54], EPVSR[55], ELLIPRO[56] and SEPPA 3.0[10] utilize additional available information from protein 3D-structures for BCE predictions. In general, the BCE predictors are composed of three components.

The first component sets specific physicochemical parameters for the characterization of amino acid sequences, like hydrophobicity, surface accessibility, and flexibility. The second component includes datasets of identified epitope and non-epitope sequences, which are analyzed regarding their characteristic physicochemical parameters and amino acid composition. The third component is a specific machine learning (ML) algorithm, often described by the term “classifier” because it classifies an amino acid as part of an epitope or not. All kinds of ML algorithms, like support vector machines (SVM), artificial neural networks (ANN), and random forest regressions (RFR), are used for epitope predictions.[46] Those classifiers are usually trained and tested on known datasets of epitopes for their performance and accuracy. A known set of epitope data is used for training the classifier, and another set of epitope data is used to test the correctness of the predictions. The identification of ratios between true positive/negative and false positive/negative hits with a known set of epitope data usually describes the correctness of the prediction or prediction performance. Widely adopted performance metrics are the area under a receiver operator characteristics curve (ROC AUC), accuracy (ACC), F1-score, and the Matthews correlation coefficient (MCC).[57,58] There is no consistent usage of one parameter, and it is rare in the literature that all mentioned parameters are used. This makes it challenging to compare the performance of the different prediction tools. Additionally, the epitope data used for classifier training and cross-validation vary significantly, and databases could be incomplete, making the performance comparison even more complicated. [46–48] Therefore, the performance of the respective method is often reported for each analyzed protein or protein

class in a corresponding publication. For example, the improved DiscoTope 2.0 prediction tool showed a set of different protein AUC values between 0.75 and 0.95, with even one outlier of 0.2.[9] The reported AUCs for different prediction tools are between 0.55 - 0.9 (0.5 corresponds to a coin flip). High AUC values are often only reached in the initial publication for specific proteins. Subsequent research, which uses established prediction tools as a standard for comparison of a new prediction tool, fails to accomplish the initially reported performance.[9–12,49–56,59] Therefore, the methodological approach for epitope predictions and the kind of analyzed protein influence the prediction outcome. The different prediction performances were already discussed in the improved DsicoTope 2.0[9] publication, where proper benchmarking of conformational epitope prediction from 3D structures was suggested. Considering biologically active protein complexes as a prediction basis for better access to "real" surface-accessible protein sites could also reduce false positive results.

Taken together, it seems necessary to use several prediction tools and find a consensus sequence as a potential BCE that would subsequently be validated experimentally.[60,61] In this work, four BCE prediction tools were tested for BCE validation of the identified epitopes on the model proteins used in this work, namely DiscoTope-2.0[9], SEPPA-3.0[10], BepiPred-2.0[11], and BCEPS[12]. The four selected prediction tools are accessible as web applications, providing easy access and usability. DiscoTope-2.0 and SEPPA-3.0 use crystal structures of the analyte proteins as a basis for the predictions, enabling the prediction of discontinuous/conformational epitopes. BepiPred-2.0 and BCEPS only employ the primary protein sequence to predict an epitope, which makes them better suited to predict continuous epitopes. The methodologies applied in DiscoTope-2.0 and SEPPA-3.0 are similar but use different definitions of solvent accessible surface areas (SASA), residue neighboring, clustering, and propensity scores for the amino acids being part of a BCE. BepiPred-2.0 and BCEPS consist of machine learning algorithms, which use physicochemical properties of amino acid residues like hydrophobicity, surface accessibility, and structural flexibility of primary sequences from epitope and non-epitope data to differentiate between them. Various ML algorithms are employed; BepiPred-2.0 utilizes a random forest regression algorithm, while for BCEPS, multiple approaches were tested, with a support vector machine algorithm demonstrating the best performance.

Nevertheless, the prediction accuracy for linear epitopes remains low because roughly 90 % of all epitopes are conformational epitopes.[32] The prediction of conformational epitopes is more accurate, but more information is needed for the analysis. In particular, information about the 3D structure is required but often unavailable.[47] This challenge might be overcome by combining new and continuously advancing protein structure prediction tools based on state-of-the-art deep learning algorithms, like AlphaFold,[62,63] with the BCE prediction tools. Producing a linear epitope-peptide-based vaccine is significantly simpler than developing a conformational epitope-based vaccine. Consequently, a linear epitope proves more appealing than a conformational epitope for the development of epitope-based vaccines.[48] Therefore, a higher interest in optimizing and developing linear epitope prediction tools seems to exist. The same seems true for epitope peptide-based biomarkers because linear epitopes are experimentally easier to identify, characterize, and apply in specific bioanalytical assays.[64–66]

2.1.4 Methods for determination of protein and peptide binding affinities

A ligand pair's binding strength or affinity determines if a complex will form and its stability after formation.[29] These parameters guide the development of drugs and diagnostic tools. Several methods have been established to determine affinity. Methods like enzyme-linked immunosorbent assays (ELISA)[67], fluorescence-based methods (e.g. fluorescence polarization (FP)[68]), ultracentrifugation (UC)[69], isothermal titration calorimetry (ITC)[70,71], biolayer-interferometry (BLI)[72], surface plasmon resonance spectroscopy (SPR)[73], and quartz crystal microbalance (QCM)[74] are commonly used to characterize biomolecular interactions.[29,75]

These methods rely on different physical principles for measuring heat changes, optical changes, or mass changes of biomolecules when interacting (Table 2.1.1). Direct measurement of a ligand binding event is often preferred because these methods can be highly specific for the investigated interaction and provide real-time kinetic data. Moreover, the ITC is an example of a homogeneous assay. It does not need any molecular

separation of the investigated molecules and can be measured from a simple, mixed solution. No chemical modification of the analyzed biomolecules is necessary for signal generation because the released heat upon protein binding is measured in a closed compartment and monitored over time. Therefore, the ITC can determine thermodynamic parameters (ΔH, ΔS, ΔG), binding affinities (K_D, K_A), and stoichiometry.[76,77] Another direct and homogeneous assay is the FP, but one of the investigated biomolecules needs a fluorescent label to record any binding signal. The labeling itself can influence the binding properties of a biomolecule and needs careful monitoring.[78,79] SPR-, QCM-, and BLI-based biosensors are also direct measurements of biomolecular interactions, but one ligand must be immobilized on a surface, and the analyte binds from a solution to the immobilized ligand. Therefore, they are considered heterogeneous assays. The advantages are the high specificity and accuracy that can be acquired with these setups. Challenges for these assays are the ligand immobilization step and unspecific interactions of proteins with the biosensor surfaces, which can strongly influence the experimental outcome.

Table 2.1.1: Commonly used methods for analyzing protein interactions and general method traits.

Method	Description	Direct/Indirect Measurement	Homogen./Heterogen. Assay	Label Required
ITC	Measurement of heat changes.	Direct	Homogeneous	No
FP	Measurement of changes in fluorescence polarization.	Direct	Homogeneous	Yes
SPR	Monitoring of refractive index changes on a sensor.	Direct	Heterogeneous	No
QCM	Measurements of mass changes on a quartz crystal.	Direct	Heterogeneous	No
BLI	Monitoring of interference-pattern changes on a biosensor.	Direct	Heterogeneous	Yes
UC	Separation of molecules based on sedimentation.	Indirect	Heterogeneous	No
ELISA	Detection of molecules using enzymatic reactions.	Indirect	Heterogeneous	Yes

Indirect measurement methods are another assay group, including UC and ELISA. For these assays, the binding event is indirectly measured by the concentration determination of an unbound ligand (e.g., UC) or an enzymatic reaction enabled by the binding event, releasing a photosensitive product, which is measured with optical detectors (ELISA). UC and ELISA are considered heterogeneous assays because a molecular separation step is involved during the experimental procedure. The UC does not need a label, but an ELISA depends on a labeled biomolecule. Indirect assays are often more versatile in their application and enable high-throughput screening, making them very attractive to pharmaceutical companies. However, they are more prone to false positive or negative results without carefully selecting control samples. The different methods for the analysis of protein interactions follow different physical principles, but the calculation of affinities and kinetic constants are similar for each. The equilibrium equation (Figure 2.1.2) and resulting constants are calculated to the Langmuir (1:1) binding model (Figure 2.1.4), which was developed for the adsorption of gas molecules on a surface.[74,80] According to the 1:1 single binding model, a monolayer of ligand (A) molecules adsorbs to the surface of a receptor (B) and forms a monolayer on it.

1:1 Molecular Binding **According to Langmuir**

$$A + B \rightleftharpoons AB \quad \Longrightarrow \quad \theta = \frac{K \cdot c_A}{1 + K \cdot c_A} \qquad (6)$$

Θ = fractional surface saturation
K = Langmuir adsorption or equilibrium constant
C_A = Free ligand concentration

Figure 2.1.4: Molecular binding of a ligand to its receptor on a surface according to 1:1 stoichiometric reaction,[74,80] corresponding to the surface absorption of a molecular monolayer from Langmuir.

Therefore, the fractional surface saturation depends on the ligand-receptor complex (AB) concentration and the free ligand concentration (A). Both can be determined with the presented biochemical methods, and together with the Langmuir binding model, the equilibrium and kinetic constants are calculated. For the example of SPR-based biosensors, the calculation will be discussed in more detail because it is the method used in the presented work for measuring binding affinity and kinetics. SPR biosensors have become a comprehensive tool for biomolecular interaction studies. They find their use in clinical research laboratories as diagnostic tools for the investigation of cancer, infectious diseases, and food allergens.[81,82] The principle of any SPR measurement is the interaction of light with a thin metal film when light hits a metal film at a certain angle. The Kretschmann arrangement is commonly used to accomplish a suitable experimental setup for biochemical analysis (Figure 2.1.5-A). A gold-coated glass slide is mounted on top of a prism through which incident light passes, and the gold surface reflects the light. If p-polarized light enters at a specific angle (resonance angle), it creates an evanescent field that penetrates the gold film and several 100 nm into the adjacent medium, decreasing exponentially with the distance to the gold surface. At the surface of the gold layer, the evanescent field excites the electrons, now called plasmons. SPR is sensitive to refractive index changes of the medium adjacent to the metal-dielectric interface, so anything entering the evanescent field's region changes the resonance angle. Therefore, if an antigen flows over a gold chip and binds to an immobilized antibody, the resonance angle shifts accordingly. As light is shone onto the surface at different angles, the resonance angle can be detected as a distinct dark spot because, in the case of resonance, the surface plasmons absorb nearly all the energy of the light so that the reflected light is attenuated. The shift in resonance angle or change in position of the dark spot on the detector is then recorded over time for monitoring antigen-antibody complex formations (Figure 2.1.5-B).[73,83]

As mentioned, any change in refractive index will influence the resonance angle. Therefore, an antigen entering the evanescent field without an immobilized antibody will also change the resonance angle, but the shift is much smaller without a specific binding event, as the antigen is not enriched on the surface. Likewise, a change in solvent composition can lead to significant changes in resonance angle. Therefore, a reference measurement is always necessary to compensate for the general resonance shift due to changes in the medium. A response curve (sensorgram) is recorded over time by following the resonance angle shift, which is translated into resonance units by the detector. To record the association between an immobilized antibody, or any other ligand, and its antigen, an antigen solution flows over the chip until saturation of the surface at the equilibrium is observed. Afterwards, only the buffer without antigen flushes the antigen out to record the dissociation (Figure 2.1.5-C). In the last step, any remaining antigen on the surface is flushed out with a regeneration solution to prepare the chip for the next injection with the antigen solution at varying concentrations. Different response curves at varying concentrations are necessary for the calculation of reliable kinetic and equilibrium constants.[3,73,84]

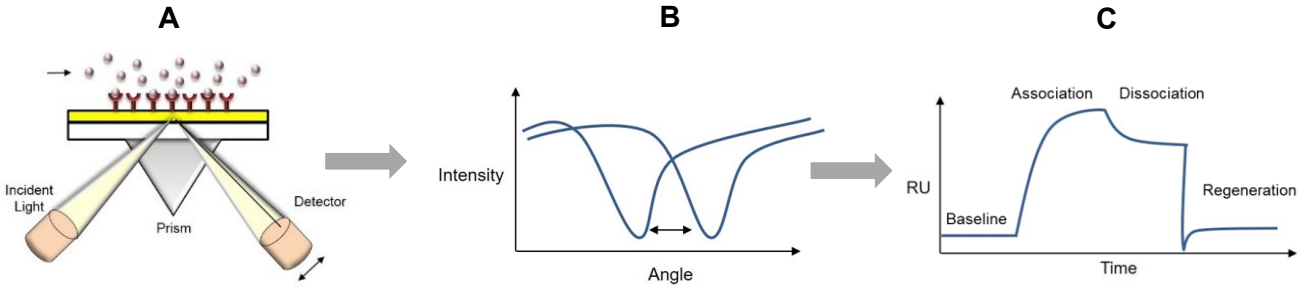

Figure 2.1.5: Scheme of the SPR-based biosensor in (A) Kretschmann configuration with an immobilized antibody and injected antigen in the flow chamber. Binding events lead to (B) a resonance angle shift that is translated into (C) resonance units (RU) and monitored over time for kinetic and affinity evaluations.

The previously mentioned complex-concentration time-dependent reaction equation (7) can be used to describe the association phase of the complex.[84] The concentration of the immobilized ligand (c_B) corresponds to the difference between the complex concentration at equilibrium state ($c_{AB,\ max}$) and the actual complex concentration (c_B). Furthermore, the injected analyte concentration (c_0), together with the linear relation of the response (R) and concentration changes, leads to the transformation of equation (7) to equation (8) for the

complex formation, which depends on the maximum response reachable in a specific experimental setup (R_{max}). Similarly, the dissociation curve can be described from the reaction equation (9), which originates from equation (8) and the absence of any injected analyte ($c_0 = 0$). The corresponding integrated reaction equations for the association and dissociation can be calculated, and with non-linear fitting of corresponding SPR data sets, the k_a and k_d can be determined. .[84]

$$\frac{d_{c_{AB}}}{dt} = k_a \cdot c_A \cdot c_B - k_d \cdot c_{AB} \quad (7)$$

$$\frac{dR}{dt} = k_a \cdot c_0 \cdot (R_{max} - R) - k_d \cdot R \quad (8)$$

$$\frac{dR}{dt} = - k_d \cdot R \quad (9)$$

The final equation for calculating equilibrium constants (11; here K_D) corresponds to the Langmuir 1:1 binding isotherm and can be derived from the reaction equation (10) at the dynamic equilibrium state with the response measured at the equilibrium (R_{eq}). The application of suitable fitting algorithms for corresponding data sets allows the calculation of the dissociation constant K_D.

$$\frac{dR}{dt} = k_a \cdot c_0 \cdot \left(R_{max} - R_{eq}\right) - k_d \cdot R_{eq} = 0 \quad (10)$$

$$R_{eq} = \frac{c_0 \cdot R_{max}}{c_0 + K_D} \quad (11)$$

Commercially available biosensors commonly employ a Kretschmann configuration as their experimental setup. However, different experimental setups like grating coupled, or fiberoptic SPR-based biosensors are also used.[83] The techniques are very similar in exploiting the SPR phenomenon, and each offers certain advantages for the analysis of specific analytes. Of all setups, the Kretschmann configuration offers the most versatile application range among commercially available instruments. Regarding the sensitivity of the SPR-based biosensors, specific enhancements can be accomplished without changing the metal surface, laser, detector, or metal surface functionality. The sensitivity of a Kretschmann-SPR depends strongly on the size of the analyte (molar mass), with larger analytes causing larger shifts of the resonance angle upon specific binding events. Therefore, the smaller analyte should be immobilized for corresponding SPR measurements, or the analysis becomes significantly more challenging. For very weak interactions, only a very low amount of analyte is bound; therefore, only a minimal resonance angle shift is obtained. The most straightforward improvement strategy for increased sensitivity is the modification of the metal surface and its functionalization without exchanging any instrumental component.[3] Examples of those modifications are graphene-based surfaces with varying metal layers.[85,86]

Various methods have been developed to immobilize biomolecules on metal surfaces. Commonly used gold chips can be functionalized by organic compounds with at least one thiol group. The sulfur-containing thiol forms a strong but non-covalent bond with the gold atoms on the chip surface. Therefore, any thiol-group-containing molecule can act as a spacer or linker group on the gold surface to immobilize biomolecules.[87] The most stable surfaces are obtained with long alkyl chains, which stabilize themselves upon binding on top of a sensor chip. A cysteine-rich protein can be directly immobilized on the gold surface. However, it may lose its folding upon binding on the surface because, more often, the cysteine residues are essential for the structure in the form of disulfide bonds. Small chemical compounds like bifunctional alkanes or short polyethylene glycols (PEG) with one thiol group and a carboxyl or amine group are used more often. The hydrophobic alkyl chains or hydrophilic oligoethylene chains self-assemble to form a monolayer on the gold surface anchored by the thiol headgroups, while the tail functionality can be used for covalent binding of biomolecules. Those kinds of surfaces are called self-assembled monolayers (SAM).[88] Additionally, a dextran functionalized SAM-gold surface is the most used chip because the oligosaccharide suppresses non-specific surface interactions and helps to maintain ligand activity by providing a hydrophilic surface and blocking contact with the otherwise hydrophobic surface. Specific surface modifications are preferable for certain applications. For example, a plain bifunctional alkane layer is often well-suited for analyzing single monomeric proteins. However, polyethylene glycol surfaces are more

advantageous for analyzing a specific protein in a more complex sample mixture (e.g., serum) because they show less fowling and less non-specific interaction with a wide range of serum proteins.[88–90]

For the immobilization of antibodies, several strategies are applicable. In this work, the bifunctional SAM-layer consisted of 16-mercaptohexadecanoic acid (16-MHDA; MHDA) and was further modified by a carboxy-dextran layer or by functionalization with protein G for directed antibody immobilization.[91,92] In any case, carboxyl groups on the chip surface were initially activated with EDC/NHS for covalent protein or antibody immobilization.[93] The biggest difference for the used surfaces is the antibody immobilization modes. In the case of the dextran (a) or plain MHDA-chip (b), the antibody is randomly oriented on the gold surface, and in the case of protein G (PG; C) as linker-layer, the antibody is so oriented on the chip surface that all F_{ab} sites are pointed away from the chip surface and are accessible for protein binding (Figure 2.1.6).[94–97]

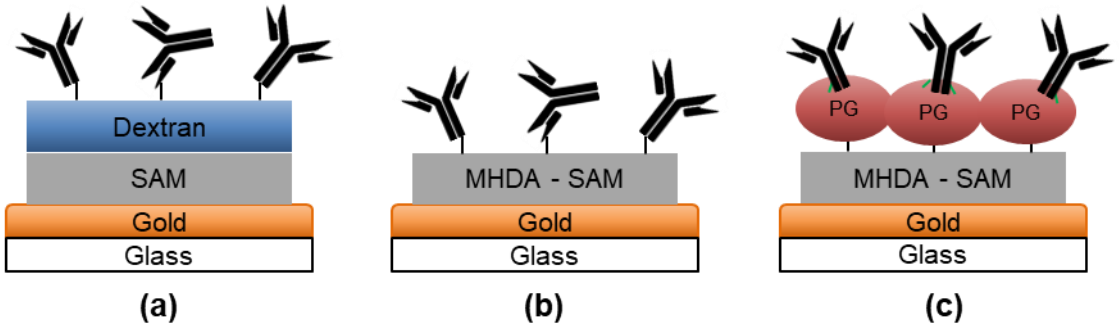

Figure 2.1.6: Immobilization strategies used in this work. (a) Randomly oriented immobilized antibody on a gold chip functionalized with (a) carboxy-dextran, or (b) MHDA. In the case of (c) PG as a linker between the MHDA and antibody, the antibody F_{ab} site is oriented away from the gold surface, and for covalent immobilization, the antibody F_c part is crosslinked via dimethyl pimelidate (DMP) to the PG.

In covalent-oriented antibody immobilization, PG is first covalently immobilized, to which the antibody of interest binds non-covalently via its F_c-domain. Both are covalently connected with the crosslinker dimethyl pimelimidate (DMP) via closely located primary amines (e.g., from lysine residues).[94] The immobilization by protein G should lead to highly active antibody surfaces as the variable domains face away from the surface towards the analyte solution. Challenges to the creation of a highly active antibody surface can arise from the crosslinker that might inactivate the antibody by modifying the paratope so that it cannot bind its antigen. Therefore, crosslinker concentrations must be thoroughly assessed for optimal antibody activity. The randomly oriented antibody immobilization bears the risk of partially inactivating the antibody by being immobilized via amines close or directly inside the paratope region, and unspecific F_c interactions might occur, too. Generally, an antibody surface via PG is more active but needs more sophisticated experimental procedures.[91,94] The combination of affinity/kinetic data with information about the position of the molecular interaction sites will result in more precise protein complex characterizations, which the biosensor can enable. In the subsequent chapter, the epitope extraction method via affinity chromatography will be introduced as to how it could be combined with the SPR-based biosensor for simultaneously obtaining epitope sequences and affinity data.

2.1.5 Methods for epitope identification

Multiple methods have been applied for binding site analysis, including X-ray crystallography[98–100], nuclear magnetic resonance spectroscopy (NMR)[101,102], cryo-electron microscopy (cryo-EM)[103–105], alanine scan[106,107]/peptide mapping[108], proton-deuterium exchange mass spectrometry (HDX-MS)[109,110], chemical crosslinking mass spectrometry (CC-MS)[111,112], and many others. These methods can be divided into two categories.

The first category can be defined as "structure-based methods"[1,113], including NMR, and cryo-EM. Those methods utilize different physicochemical phenomena to provide the positions of the individual atoms of a protein-ligand-complex with resolutions of a few angstroms. In the analysis of structural data from a protein-protein complex, the binding site is defined as the region(s) with the closest distance between protein and ligand atoms. Typical distances for the non-covalent interactions are 0.2 - 0.5 nm.[114] For all those methods, expensive equipment, very pure samples, high protein amounts, and long experimental times are needed. The results are precise, have a high resolution, and show an accurate image of a protein-ligand complex. The second category of methods can be defined as "function-based methods".[1,113] The function-based methods either rely on the test of protein fragments or mutants for their target binding capability. In footprinting methods, a ligand causes or prevents a specific protein complex modification, which can be detected afterwards. The alanine scan and peptide mapping methods are in the category of protein fragment or mutant binding assays. The oldest and best-known method is the "pep-scan" or "alanine-scan".[106,107] The pep-scan method focuses on analyzing the binding of synthetic peptide fragments that cover the sequence of a protein. The goal is to identify the binding peptides from the binding site. The alanine scan has a slightly different approach. Here, a single amino acid exchange is utilized either in the complete protein or in previously identified binding peptides to identify the most crucial amino acid residues for binding by detecting reduced binding. The binding detection can be done with any suitable binding assay discussed in the previous chapter.

HDX- and CC-MS belong to the footprinting assays. Binding sites are discriminated from non-binding sites by (1) labeling the protein-ligand complex with ligand-bound regions protected from labeling, (2) fragmentation of the protein-ligand complex with ligand-bound regions protected from fragmentation, and (3) mass spectrometric analysis of the fragments that bind to the protein or that are not retained by the protein.[109–112] In HDX-MS, the protein-ligand complex is labeled with deuterium by exchanging hydrogens from the backbone of the primary protein structure. Surface-accessible sites are more susceptible to the exchange of hydrogen for deuterium. Therefore, hydrogens within the protein and hydrogens covered in the protein-ligand complex are less accessible for deuterium exchange. HDX locations are identified by "freezing" the HD exchanged state by lowering the pH, which leads to the protonation of all unprotonated peptide bonds, and further exchange is stopped. Subsequently, the protein is fragmented by enzymatic digestion (e.g., pepsin). Afterwards, MS-based methods, like LC-MS, can be used for peptide fragment analysis and identification. Several control experiments are necessary to verify the identified binding sites. Most important is the HDX with the protein alone for reference on the digestion itself and to assign peptides from inaccessible sites that are not deuterated. Deuterium abundance heat maps indicate the potential binding sites as regions with low deuterium abundance.[109,110]

In CC-MS, a chemical crosslinker connects protein and ligand near the binding site in the protein-ligand complex. After enzymatic digestion (e.g., with trypsin or chymotrypsin), the peptide fragments are analyzed by MS, too. The binding site peptide conjugates are often demanding to identify because subsequent MS/MS fragmentations might result in inconclusive spectra. Therefore, the chemical crosslinkers often carry a cleavable site, such as a photosensitive site, which is cleaved by irradiation. Crosslinker concentration and incubation time are crucial for a successful CC-MS experiment because too high concentrations and long incubation times may lead to random cross-linking events. Different crosslinkers must be tested to find a suitable crosslinker to account for binding site shape and amino acid composition.[111,112]

Another MS-based method for binding site identification is based on affinity chromatography, which is primarily used for protein purification. It is often referred to as the "epitope fishing", "peptide mapping", or "epitope extraction" method.[1,4,115] Affinity chromatography uses specific protein-protein interactions to separate a specific protein from a mixture. The respective ligand is immobilized on a solid column media, holding back the protein of interest while other proteins are washed out. This type of chromatography is often applied to antibody/antigen purifications.[116] Therefore, it was first applied to the identification of antibody epitopes and named "epitope extraction".[117] As in other MS-based methods, an enzyme is used for protein digestion, and the resulting digestion mixture is incubated with an affinity column to separate binding peptides from non-binding peptides (Figure 2.1.7). This method's crucial part is distinguishing peptides that bind non-specifically to the

column from peptides that bind specifically to the antibody. Otherwise, they might be wrongly annotated as specific ligand-binding peptides. Depending on the extent of column-binding peptides, the subsequent data analysis can be challenging and may lead to an unsuccessful epitope identification.

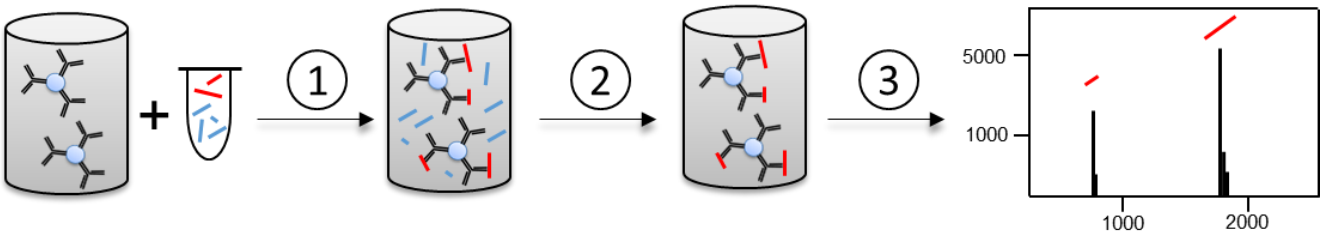

Figure 2.1.7: Principle of the epitope extraction method. An antibody is immobilized as a specific "ligand" and incubated (1) with a digested protein for peptide isolation. All non-binders are washed out (2), and the specific binding peptides are eluted (3) from the column. Subsequent MS analysis of the eluted fractions is executed for the identification of peptides from the binding site.

Moreover, not all proteases are equally suited for digestion. If the enzyme cleaves the binding site at an essential position for ligand binding, the affinity might be lost entirely, and no peptide fragments will be identified as specific ligand binders. The affinity needs to be conserved in the resulting peptide fragments to identify a binding site reliably, and different enzymes may need to be tested for successful binding site identification. The previously discussed MS-based methods, HDX and CC-MS, do not have these limitations. However, labeling with deuterium or crosslinking also needs extensive optimization. The resulting MS spectra are more complex and need more extensive analysis than the relatively simple results from an epitope extraction experiment. The simplicity of the experimental setup makes it possible to apply epitope extraction to a large range of protein-ligand complexes, where one ligand (antibodies, proteins, carbohydrates, DNA) is immobilized, and a digested target protein is used for binding site identification.

2.1.6 Mass spectrometry

Mass spectrometry (MS) is an extensively employed technique for determining molecular masses, structures, and concentrations, which finds application in nearly all pharmaceutical and medical fields. From the identification and quantification of synthetic molecules to biomarkers in the field of omics, MS is one of the most versatile techniques. Moreover, MS instruments can measure small and large molecules at very low concentrations, making them perfect for the research and development of new ways to treat diseases. [118] The working principle for all MS instruments is very similar: MS techniques measure the masses of molecules that must be transferred into the gas phase with simultaneous ionization.[119] The ionized molecules travel through an electric field, where they are accelerated to different velocities according to their mass. They can be distinguished based on the time they require to hit a detector, the angle by which they are deflected in a magnetic field, or the specific frequency at which they pass an oscillating quadrupole to reach the detector. Therefore, the mass-to-charge ratio decides how molecules travel through the analyzer before hitting the detector. Three key components form the basis of each mass spectrometer: ionizer, mass analyzer, and detector. Soft ionization methods are best suited for the analysis of biomolecules because they leave the target molecule intact during the evaporation and ionization process.[120] Examples of those soft ionizing methods are the "matrix-assisted laser desorption ionization" (MALDI)[2] and the "electrospray ionization" (ESI)[121]. In the mass analyzer, molecules are separated by their mass-to-charge ratio in various ways. The basis for molecule separation is an electric field, which influences either the velocity or the traveling path of ions before they hit the detector. Examples of those are the "time-of-flight" (tof) and quadrupole (Q) mass analyzers. The combinations used in this work are a MALDI-tof MS and an ESI-Q-MS.

In MALDI-tof MS measurements, the sample solution is combined with the dissolved matrix substance, and both are spotted on a metal target plate. The sample and matrix are usually dried under room temperature until they

crystalized, and no solvent is left. In the instrument, a pulsed laser is directed at the crystallized sample matrix mixture, which leads to the vaporization of the mixture, and the matrix molecules get charged. Afterwards, the matrix molecules transfer their charge to the sample molecules, and the ionized sample molecules enter the tof-mass analyzer. In MALDI, the matrix molecules protect the sample molecules against the laser energy and help to prevent an excess of transferred energy to the biomolecules, which otherwise would lead to their fragmentation. In the tof-analyzer, the time after which the molecules hit the detector correlates to their charge and mass. At the same charge, heavier molecules need more time to travel through the tof-analyzer and hit the detector later than lighter molecules. Matrix substances are usually aromatic compounds with carboxyl functionality to provide an acidic milieu for more efficient positive charge transfer to the analyte molecules.[122,123]

The ESI-Q-MS ionizes the sample solution by spraying it through a charged needle, creating charged droplets. Charge transfer is usually enhanced by acidic solutions, which provide excess protons to charge the analyte molecules positively. Due to reduced pressure in the instrument, the liquid from the analyte droplets evaporates, leaving a charge on the sample molecules. The charged molecules are accelerated towards an oppositely charged metal plate and enter the quadrupole mass analyzer. Before hitting the detector, the differently sized (mass) and charged molecules travel in a specific trajectory between the metal rods in the alternating quadrupole field. The alternating quadrupole field functions as a mass filter and only allows molecules in a specific mass range to pass the field in a specific trajectory, allowing them to hit the detector.[124] One key difference between MALDI-tof MS and ESI-Q-MS is the resulting mass spectra. MALDI typically leads to low-charged biomolecules, whereas ESI leads to different multiply-charged ions. Therefore, the ESI mass spectra need more complex and more extensive analysis.

2.1.7 Epitope identification by affinity-SPR-MS

The affinity isolation of epitopes or other binding site-forming peptides (BP) has been applied in many protein-protein, -sugar, -antibody, and -aptamer studies.[1,125] An overview article on epitope extraction/excision describes the application and development of mass spectrometry-based epitope mapping methods over the last ~ 30 years.[1] Early attempts to automate and streamline epitope extraction were made in the group of Michael Przybylski[126,127] by utilizing a surface acoustic wave (SAW) biosensor as an affinity separation tool combined with ESI-MS fraction analysis. A similar workflow was later chosen for the SPR measurements with combined MALDI-tof MS fraction analysis as employed in this work. The epitope extraction from an SPR biosensor chip is similar to that from an affinity column. An initial incubation of the immobilized antibody with the digested analyte protein is followed by several washing steps with final acidic elution of specifically bound peptides and subsequent MALDI-tof MS fraction analysis (Figure 2.1.8). The combination of affinity and epitope analysis provides several advantages. Comparison of the affinity of an intact protein-ligand to its digestion could indicate the nature of the epitope because a linear epitope is expected to retain a similar affinity to the intact protein. A discontinuous or complex epitope of many protein sites would be expected to show manifold reduced affinities. However, a manifold decreased affinity could indicate a suboptimal enzyme choice because the epitope sequence could be cleaved in an affinity-reducing or losing position. Therefore, a first affinity estimate of the related epitope peptides could show the difficulty level of the epitope extraction experiment and guide the whole experimental setup for subsequent analysis. Moreover, the experimental setup could be expanded for biomarker development and research of specific protein interactions. Its practicality will be evaluated in the presented work.

Exemplary publications from the working group Przybylski and collaborations are summarized to present the scope for the analyzed proteins and their antibodies with the epitope extraction and excision method. The most intensively researched biomolecular interaction seems to be antibody-antigen interactions.[4,125,126,128–133] In the case of a linear epitope, like for the α-galactosidase A and its antibody, the results show a high affinity for the protein antibody complex (K_D = 16 nM), which was well conserved in the identified and synthesized epitope peptide (K_D = 39 nM).[4] For the analysis of an HLA-B27-homodimer and its antibody, a disulfide bond linked epitope peptide-conjugate sequence was detected with a K_D of 40 nM.[131] A more complex antibody epitope was

seen for the recombinant *mycobacterium tuberculosis* Ag85B antigen and anti-Ag85 antibodies with medium affinities (K_D = 0.6 - 9.2 µM) of several antigen variants to the antibodies.[129]

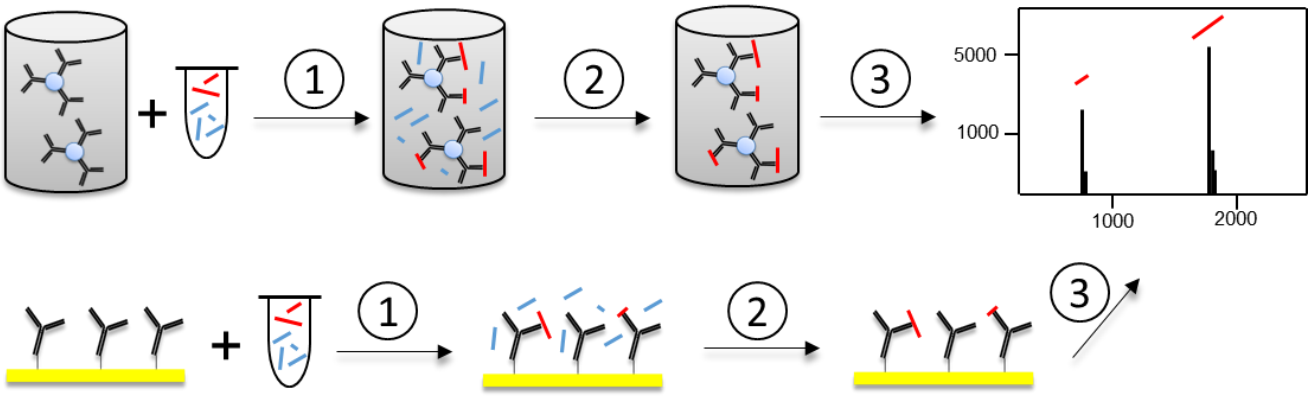

Figure 2.1.8: Scheme of the epitope extraction via affinity column and SPR biosensor chip. The first step is incubating the digested analyte protein with the immobilized ligand (1), then washing out all non-binding peptide fragments (2) until no more peptides elute. Then, an acidic buffer solution is applied to elute specifically bound peptide fragments (3). The eluates from washing steps and final acidic elution are collected and analyzed by MALDI-tof MS (3).

The mentioned SAW-based biosensor and ESI-MS combination was tested on several proteins with linear epitopes and high affinities for the antibody-antigen interactions (K_D = 10 - 50 nM).[126] These examples suggest a suitable affinity range for the successful epitope identification of antibody-antigen interactions via epitope extraction and excision in the µM to nM range and potentially even lower affinities, considering the following examples of non-antibody analysis. The analysis of the protein-protein interaction of VC1-HSAgly led to a K_D of 0.6 µM with a complex interaction suggested by determined SPR interaction curves and multiple protein sites being in contact for the interaction.[134] In comparison, DNA-Aptamer protein interactions of the protein C-Met and two aptamers showed K_D values between 0.2 - 0.5 µM, with one aptamer having a linear and the other a discontinuous binding site and for the C-Met aptamers, the combination of SPR and MS was also successfully tested.[135] The weakest analyzed interaction was a protein-carbohydrate ligand pair, galectin-3 and lactose.[136] The K_D value for the interaction of the intact protein with the sugar was 4.8 µM, and for the identified epitope peptides, between 2 - 12 mM, which was determined on a SAW biosensor. These results show that even very weak interactions can be analyzed by the epitope extraction, and in the case of an antibody-antigen interaction, the affinity of corresponding epitope peptides can be very low and still get identified if the specificity of the peptides is high enough. However, the potential experimental effort to search for an optimal enzyme or suitable support material for the column was also recognized, and in specific cases, much optimization is necessary.[132,133] Therefore, epitope identification is not always straightforward, and challenging epitope identifications seem highly dependent on the investigated protein and antibody.

2.1.8 Methods of proteolytic digestion

One essential step in the presented epitope extraction method, and also in many other techniques employed in proteomics,[137] is the efficient digestion of the target protein. Much effort has been made to develop fast and reproducible procedures for enzymatic digestion. Attempts to improve the digestion speed are ongoing. Many methods are used today to accelerate enzymatic digestions, like high-temperature, microwave, solvent, or high-pressure assisted digestions.[137] Moreover, various enzymes are available for protein digestion, with trypsin being the most commonly used.[138] Trypsin is available in different variations regarding purity, specificity, and activity towards its cleavage sites, located on the C-terminal side of lysine and arginine residues in a protein sequence.[139] Still, even optimized enzymes are imperfect and can lead to semi-specific and unspecific cleavage events due to unfavorable amino acid compositions at the cleavage sites.[140] Those unspecific cleavage events arise partly from

the enzyme itself, buffers, and non-MS grade enzyme preparations can contain different enzyme isoforms, exhibiting slightly broader specificities. For specific applications, switching to other enzymes like chymotrypsin, Lys-C, Lys-N, Arg-C, or Glu-C is possible and might be necessary for specific applications.[141]

For evaluation of digestion performance in terms of acceleration and cleavage products, methods are compared to a "standard procedure". Since trypsin is the most extensively used enzyme in proteomics research, it is considered the "standard enzyme". Therefore, digestions with trypsin under its "standard conditions" are compared to a new method or procedure. Trypsin's optimal activity is reached at pH 7 - 9, 37 °C, in a wide range of salt buffers, with typical enzyme-to-protein ratios of 1:200 to 1:20 and incubation times between 3 - 20 h.[142] The incubation time highly depends on the target protein stability and how easily trypsin can reach its cleavage sites. A general approach involves protein denaturation before digestion. Disulfide bonds significantly contribute to protein stability. Because of that, the disulfide bonds are reduced, and the back reaction is permanently blocked by cysteine alkylation. Trypsin is partly resistant to organic and chaotropic solvents, which can be used to enhance protein denaturation. Alternatively, heat denaturation is used along with disulfide bond reduction and alkylation to enhance protein unfolding for subsequent digestions.[143] Since the digestion time is highly dependent on the target protein itself, a balance between protein denaturation and optimal conditions for trypsin activity must be found. Therefore, different approaches with microwave heating, high-pressure, and ultra-sonication try to accomplish high enzyme activity and protein denaturation. Another approach utilizes immobilized trypsin for fast and reusable enzyme applications.[144]

In this work, the influence of high-pressure cycling is evaluated on different proteins and trypsin for accelerated and reproducible digestion. Pressure Biosciences Inc. made the pressure cycling technology (PCT) commercially available for research with an instrument called Barocycler 2320 EXT.[145] Pressure cycling is accomplished in a PCT tube that holds the digestion mix in the pressure chamber of the Barocylcer. Water influx into the pressure chamber leads to high pressures of up to 45 kpsi (3102 bar). For pressure cycling, high pressure is maintained for a certain amount of time, followed by pressure release before pressure increases again. This way, the hydrophobic protein core is expected to be flushed with water, accelerating denaturation and structural destabilization.[146] Even in high-pressure cycling, reduction, and alkylation are often necessary for good digestion results. This technology was applied to several proteins to test the acceleration rate of the digestion compared to standard atmospheric digestion, which can be accessed on the PBI website.[147–149]

2.2 Protein targets and ligands for interaction studies

The following chapters introduce the studied proteins and associated diseases. Moreover, the amino acid sequences, known crystal structures (hypothetical, simulated structures, if no crystal structure was available), investigated ligands, and related diseases are summarized.

2.2.1 Interleukin-8 / CXCL8

Interleukin-8 (IL8; CXCL8) is an essential chemokine, and as a chemotactic cytokine, it coordinates the migration of immune cells during inflammatory processes.[150,151] IL8 is released to activate leukocytes upon injuries or after pathogen or bacterial invasion.[152] The IL8 secretion creates a decreasing gradient away from the site of inflammation and reaches into neighboring blood vessels. There, IL8 binds to glycosaminoglycans (GAG) on epithelial cells to form a stable gradient. Leukocytes follow the IL8 gradient and secrete more IL8 and other inflammatory cytokines like IL1 and TNF-α at the site of inflammation. The secretion of IL1 and TNF-α leads to more IL8 expression and functions as a self-enhancing process for a stable gradient formation. Finally, the leukocytes fight invading pathogens or bacteria through phagocytosis.[152,153] In some cases, the overproduction of IL8 is correlated with autoimmune diseases like rheumatoid arthritis and psoriasis.[154,155] Moreover, IL8 acts as an angiogenesis factor. As one example, endothelial cells secrete IL8 to stimulate the growth of new blood

vessels. Some tumor cells secrete IL8, too. In this case, blood vessels grow toward the tumor cells and supply them with nutrients for continuous growth.[156,157] These facts make IL8 an interesting target for the treatment of diseases and as a biomarker. [5,158–160] Several IL8-inhibiting anti-IL8 antibodies are developed as a potential therapeutic for IL8-related diseases. The antibody HUmAX-IL8 entered clinical phase I trials as an IL8 inhibitor to support established cancer treatments.[159] High serum IL8 concentrations seem to correlate with a poor outcome of established cancer therapies, and reduction of high elevated IL8 concentrations could increase the chances of successful treatment.[160] However, the disease-related mechanism does not seem fully understood, making developing and testing such a hypothesis very challenging. Therefore, no FDA or EMA-approved antibody-based IL8 inhibitors are currently on the market. Due to the limited success of antibody-based therapeutics for targeting IL8, the focus lies on the development of receptor antagonists in the form of small molecules.[5] The sequence and structure of IL8 are highly investigated and characterized, making subsequent analysis much more accessible. The unprocessed IL8 protein is expressed as a 99 amino acid-long precursor. After cleaving off the N-terminal signal peptide of 20 amino acids, additional processing leads to different IL8 isoforms with varying lengths.[161] The most abundant and biologically active isoform in humans is IL8[6-77], a 72 amino acid-long protein, which is utilized in this work (Figure 2.2.1).[162–164] The structure features a C-terminal α-helix, three antiparallel β-sheet, an extensive loop structure, an unstructured N-terminus, and two disulfide bonds.[164,165]

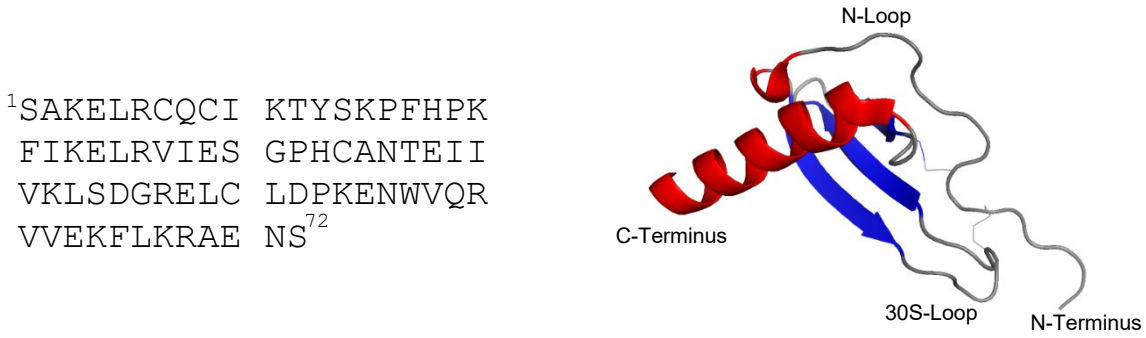

Figure 2.2.1: Amino acid sequence of the utilized recombinant expressed IL8 in E.coli and crystal structure (PDB-ID: 1IL8)[166] with α-helical sequence parts in red, β-sheets in blue, and loop/unstructured sequence regions in grey. (The protein image was created with PyMOL.[25])

The disulfide connection gives it the systemic name CXCL8. It indicates that IL8 belongs to a chemokine class with two N-terminal cysteine residues separated by one amino acid (= ”CXC”) that form intramolecular disulfide bonds with the remaining two cysteine residues.[164,166] The α-helix and the close surface β-sheet enable dimerization at higher concentrations ($K_{D,Dimer}$ ~ 10 µM)[167], which reduces receptor binding capacity.[168] The G-protein coupled receptors (GPCR), CXCR1, and CXCR2, on leukocytes, interact with IL8 with an affinity of 1 - 2 nM (K_D).[157,164] Receptor binding is mediated by the N-terminal ELR-motif, the N-loop, and 30S-loop structures, which bind to the receptors in a two-step mechanism.[169–172] Briefly, the ELR-site captures the corresponding binding region on the CXCR1/2 together with the 30S-loop. After structural rearrangement, the N-loop binds to its corresponding binding domain. Another essential chemotaxis function arises from the α-helix, which binds to GAGs on endothelial cells and forms a stable gradient for leukocyte recruitment in blood vessels. [169–172] The structural features and known interaction sites of IL8 help the investigation of molecular inhibitory mechanisms. The binding sites of inhibitors, like anti-IL8 antibodies, need to be identified for such explanations. The monoclonal anti-human IL8 antibody, mAB-I2519, produced in mice, was used in ELISA and western blot assays to detect and quantify IL8.[156,173–176] It strongly inhibits granulocyte movement towards an IL8 gradient.[171,172] However, the epitope and affinity of mAB-I2519 on IL8 are unknown. Hence, understanding the corresponding epitope could provide insights into the inhibition mechanism. It could clarify whether the antibody directly blocks a receptor binding site or interferes by sterically preventing the interaction of the chemokine’s binding sites with the receptor.

2.2.2 Cathepsin D

Cathepsin D (CTSD) is an aspartic protease with pepsin-like cleavage behavior that processes, degrades, and activates proteins and peptide hormones.[177] Those enzymes are to a great extent housekeeping proteins. They are active in lysosomes, which are acidic cell compartments for the metabolic degradation of various substances. As one of many lysosomal hydrolytic enzymes[178], CTSD has endopeptidase activity and degrades denatured and misfolded proteins.[177] It influences the activity of other proteins and enzymes by cleavage at specific sites.[7] CTSD has many substrates, but its well-studied role in the homeostasis of neuronal proteins seems to dominate.[179,180] Down-regulation of CTSD is connected to many neurodegenerative diseases, like Parkinson's, Alzheimer's, and Huntington's disease, as well as several neuronal ceroid lipofuscinoses (NCL) forms.[177] Different NCL subtypes are linked to specific gene mutations, which lead to reduced or non-detectable CTSD activity. NCL belongs to the lysosomal storage disorders (LSD).[181,182] Here, the inability of CTSD to degrade its substrates leads to protein accumulation and aggregation in neurons, which results in neuronal dysfunctions. LSDs can be diagnosed by gene analysis but are challenging to treat. Besides chaperone therapies that aim to stabilize defective proteins to restore their function, enzyme replacement therapy (ERT) is one of the few FDA-approved treatment strategies.[183] In ERT, a recombinant variant of the missing or dysfunctional enzyme is administered to compensate for the missing enzyme. The big challenge for this kind of treatment is successfully transporting the recombinant enzyme to its destination. For the treatment of NCL-10, a recombinant CTSD was developed, but the challenge for the recombinant enzyme is to get through the blood-brain barrier.[183] Besides its involvement in neuronal diseases, CTSD is also correlated with breast cancer and might serve as a biomarker and therapeutic target for tumor growth inhibition.[184]

The biomolecular processing of CTSD is very complex. The 52 kDa precursor enzyme is enzymatically cleaved and finalized by cathepsin B and L, which results in a heavy chain of 34 kDa and a light chain of 14 kDa, which forms together the final CTSD enzyme (Figure 2.2.2).[7,177] The pro-CTSD (pCTSD) is enzymatically inactive but is suggested to serve as a messenger protein. The single-chain CTSD shows already low enzymatic activity, which is fully obtained after final maturation. Moreover, CTSD is a glycoprotein with reported O-glycosylation[185] at T52 and N-glycosylations[186] at N123 and N252 (aa numbering according to Figure 2.2.3).

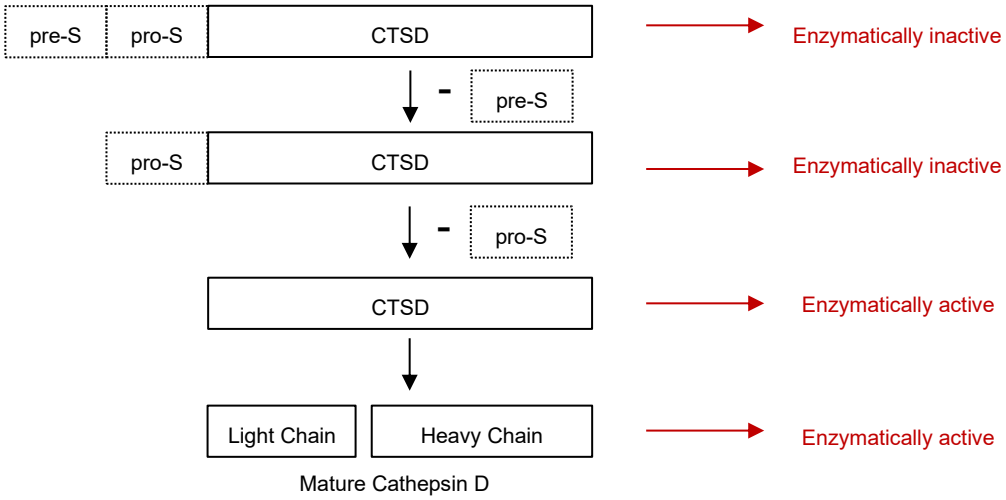

Figure 2.2.2: Processing of the precursor CTSD biomolecule in the ER. After the expression of the Pre-pro-CTSD, the pre-sequence is cleaved off during the transfer to the extracellular medium. Then, under acidic conditions, in the lysosomes and with the help of other cathepsin enzymes, the mature CTSD molecule is obtained.

The two aspartic acid residues, D33 and D231, which are closely located in the 3D-structure at the interface of the light and heavy chain (Figure 1.2.3-C), are necessary for enzyme activity. The protein is stabilized by extended β-sheets, which are present in the predicted I-Tasser pro-protein structure (Figure 2.2.3-B) and in the experimentally determined protein crystal structure from the PDB data bank (Figure 2.2.3-C). In this study, a pCTSD variant (Figure 2.2.3-A) was used as a model protein, which was obtained from the Saftig group at the University of Kiel, where it was tested as a potential drug in the ERT of NCLs.[183,187] The sequence is similar to the wild-type pro-CTSD sequence with a His-tag at the N-terminal protein site.

A

^{1}HHHHHHALAL VRIPLHKFTS IRRTMSEVGG SVEDLIAKGP VSKYSQAVPA VTEGPIPEVL KNYMDAQYYG
EIGIGTPPQC FTVVFDTGSS NLWVPSIHCK LLDIACWIHH KYNSDKSSTY VKNGTSFDIH YGSGSLSGYL
SQDTVSVPCQ SASSASALGG VKVERQVFGE ATKQPGITFI AAKFDGILGM AYPRISVNNV LPVFDNLMQQ
KLVDQNIFSF YLSRDPDAQP GGELMLGGTD SKYYKGSLSY LNVTRKAYWQ VHLDQVEVAS GLTLCKEGCE
AIVDTGTSLM VGPVDEVREL QKAIGAVPLI QGEYMIPCEK VSTLPAITLK LGGKGYKLSP EDYTLKVSQA
GKTLCLSGFM GMDIPPPSGP LWILGDVFIG RYYTVFDRDN NRVGFAEAAR L^{402}

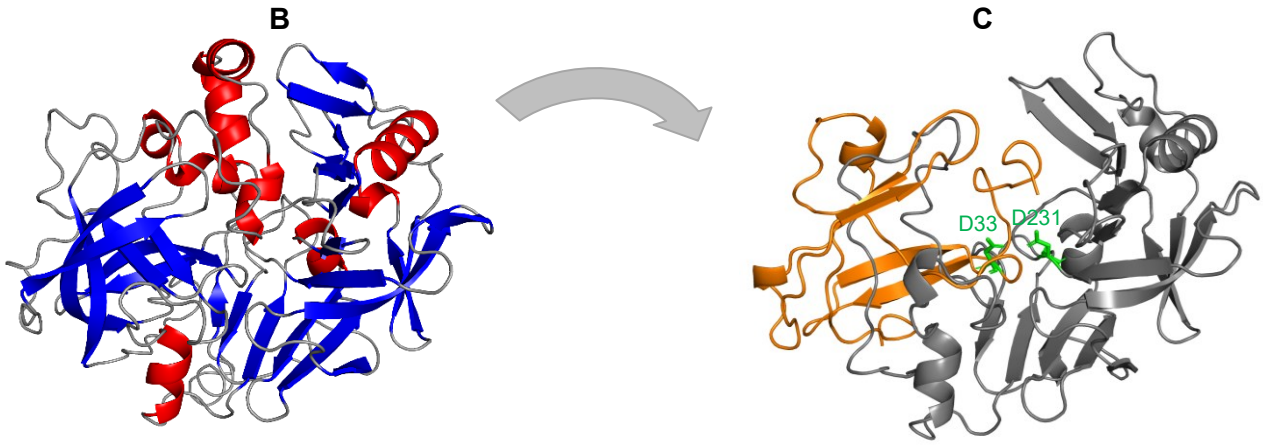

Figure 2.2.3: (A) Sequence of pro-cathepsin D (pCTSD) used as a model protein in this work. (B) I-Tasser model for a predicted structure in comparison to the crystal structure of (C) matured CTSD with highlighted aspartic acid residues (D33, D231) in the actives site and the light chain displayed in orange and the heavy chain in grey (PDB-ID: 1ILYW). (The protein image was created with PyMOL.[25])

Antibodies have been developed by the Saftig group for their potential use as a biomarker in cancer research and diagnostics of NCLs. An aptamer against CTSD was obtained from the Berezovsky group. The binding mode of both was investigated in this work. The CTSD-aptamer is a DNA-aptamer with 80 bases and a 5'-aminohexane linker (Figure 2.2.4).

5'-/5AmMC6/ CTC CTC TGA CTG TAA CCA CGA TTT CGA TCG CTC TGA GAC
TGC CAA CGT CCC ACC ATT CGC GCA TAG GTA GTC CAG AAG CC -3'

Figure 2.2.4: Cathepsin D DNA-aptamer (CTSD-Apt) of 80 bases with the 5'-aminohexane tag for immobilization via EDC/NHS chemistry to carboxyl groups.

2.2.3 Alpha-glucosidase A

One of the first lysosomal enzymes discovered was α-glucosidase A (GAA), which enzymatically breaks down glycogen in the lysosomes.[188] It was identified in the 1960s as a cause of Pompe disease, a hereditary LSD,[188,189] in which a gene defect leads to an inefficient GAA or lack thereof. The absence of GAA leads to the accumulation

of its substrate glycogen in lysosome, leading to cardiac and skeletal muscle cell apoptosis.[190] Mutations at various positions in the GAA sequence can influence GAA processing, activity, and transport. Therefore, many mutations in the GAA gene are associated with a GAA deficiency and Pompe disease.[8] Infantile-onset Pompe disease (IOPD)[190], represents the most severe form, which causes severe symptoms in the first year of life and leads to death in the same period without treatment. A less severe form is the late-onset Pompe disease (LOPD)[190], which can manifest anytime after the first 12 months of life. The progression of this disease is much slower, and cardiac muscle weakness is not severe. However, significant muscle weakness is still observed, leading to immobility and severe muscle damage in the respiratory system. GAA is produced as a 110 kDa precursor molecule with a mannose-6-phosphate (M6P) glycan modification required for efficient transport to the lysosomes.[191] Moreover, as a glycoprotein, GAA carries several N-glycosylation sites at N71, N164, N321, N401, N583, N813, and N856.[191,192] The maturation of GAA includes several processing steps, which lead to a multicomponent enzyme complex with a 70 kDa, 19 kDa, 10 kDa, and 4 kDa fragment (Figure 2.2.5).[193] The enzyme activity is reported for the matured GAA and 76 kDa complex.

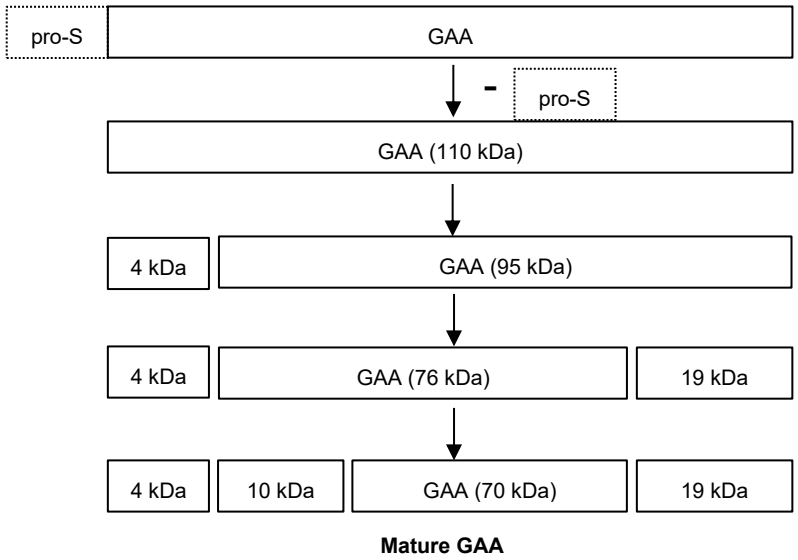

Figure 2.2.5: Processing of the precursor GAA biomolecule. According to the predicted translation product of the GAA gene, a pro-sequence is cleaved off the GAA, and the 110 kDA precursor molecule is obtained. After two additional processing steps, the 76 kDa, 4 kDa, and 19 kDa GAA complex forms, and in the final step, an additional 10 kDa fragment gets cleaved off the 76 KDa fragment to yield the multicomponent GAA enzyme complex.[193]

Efforts to treat Pompe disease led to its first FDA-approved enzyme replacement therapy (ERT) in 2006. It consists of human GAA recombinantly produced in CHO cells (Myozyme, Sanofi Genzyme).[194,195] The drug is a GAA precursor molecule of 883 amino acids, which is matured after lysosomal uptake as previously described. The sequence of myozyme is available from the drugbank[196], and homology modeling with I-Tasser shows a very similar structure to the matured GAA (Figure 2.2.6). The ERT with myozyme led to significant improvement in patients' treatment outcomes. However, it does not cure the disease. For IOPD patients, a shortened life span and significant symptom manifestations are observed.[197] Attempts to improve the drug efficiency for ERT aim at more efficient drug transport to the lysosomes by extending M6P functionalization.[198] Besides the ERT, gene replacement therapies (GRT) are under investigation and show promising results in animal studies but have not yet been tested in clinical studies.[199] One challenge with ERT is the different responses of individual patients.[200] A test for cross-reactive immunological material (CRIM) has been suggested. Patients with residual GAA present (CRIM-positive), react much better to the ERT than patients without any GAA production (CRIM-negative).[201,202] In CRIM-positive patients, the host immune system was exposed to GAA, and no strong immune response to the recombinant enzyme occurred. In CRIM-negative patients, the host immune system recognizes the GAA during the ERT as foreign enzymes and tries to remove it from the body altogether. In the case of a CRIM-negative test, an immune tolerance induction (ITI) by administration of rituximab, methotrexate, and intravenous

immunoglobulins (IVIG) is performed, which significantly improves the ERT outcome.[203–205] Other attempts to deal with immune responses to ERT include the prediction of anti-drug antibody (ADA) formation by combining gene analysis with protein phenotype data.[205] To enhance the effectiveness of the ERT, a viable approach would involve eliminating the autoimmune antibodies formed against a recombinant enzyme. Therefore, it would be necessary to identify epitopes targeted by antibodies in patients post Myozyme administration and remove these antibodies from the bloodstream using epitope peptides through apheresis. To test the epitope extraction on GAA, the epitope from an anti-GAA antibody was attempted to identify. The monoclonal mouse anti-human GAA antibody (IgG2a; Clone: 43G7; NMB-MUB0707P; Biozol) was chosen for the first epitope extraction with GAA. The mAB-43G7 was produced against human GAA and the epitope was not precisely reproted but mAB-43G7 bound to the 76 kDa and 70 kDa GAA-fragment in an western blot experiment.[206] The 70 kDa GAA-fragment covers the GAA[196-706] in the presented sequence (Figure 2.2.6).

A

1 AHPGRPRAVP TQCDVPPNSR FDCAPDKAIT QEQCEARGCC YIPAKQGLQG AQMGQPWCFF PPSYPSYKLE
NLSSSEMGYT ATLTRTTPTF FPKDILTLRL DVMMETENRL HFTIKDPANR RYEVPLETPH VHSRAPSPLY
SVEFSEEPFG VIVRRQLDGR VLLNTTVAPL FFADQFLQLS TSLPSQYITG LAEHLSPLML STSWTRITLW
NRDLAPTPGA NLYGSHPFYL ALEDGGSAHG VFLLNSNAMD VVLQPSPALS WRSTGGILDV YIFLGPEPKS
VVQQYLDVVG YPFMPPYWGL GFHLCRWGYS STAITRQVVE NMTRAHFPLD VQWNDLDYMD SRRDFTFNKD
GFRDFPAMVQ ELHQGGRRYM MIVDPAISSS GPAGSYRPYD EGLRRGVFIT NETGQPLIGK VWPGSTAFPD
FTNPTALAWW EDMVAEFHDQ VPFDGMWIDM NEPSNFIRGS EDGCPNNELE NPPYVPGVVG GTLQAATICA
SSHQFLSTHY NLHNLYGLTE AIASHRALVK ARGTRPFVIS RSTFAGHGRY AGHWTGDVWS SWEQLASSVP
EILQFNLLGV PLVGADVCGF LGNTSEELCV RWTQLGAFYP FMRNHNSLLS LPQEPYSFSE PAQQAMRKAL
TLRYALLPHL YTLFHQAHVA GETVARPLFL EFPKDSSTWT VDHQLLWGEA LLITPVLQAG KAEVTGYFPL
GTWYDLQTVP VEALGSLPPP PAAPREPAIH SEGQWVTLPA PLDTINVHLR AGYIIPLQGP GLTTTESRQQ
PMALAVALTK GGEARGELFW DDGESLEVLE RGAYTQVIFL ARNNTIVNEL VRVTSEGAGL QLQKVTVLGV
ATAPQQVLSN GVPVSNFTYS PDTKVLDICV SLLMGEQFLV SWC 883

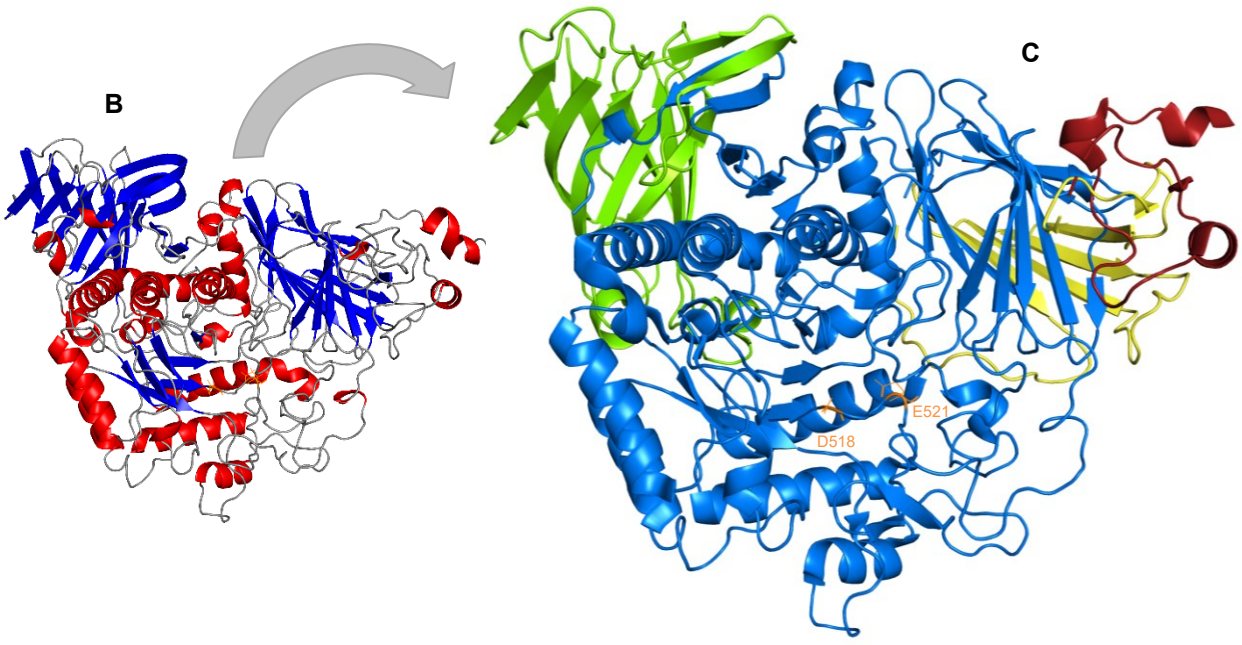

Figure 2.2.6: (A) Sequence of Myozyme, the precursor protein used for studying GAA and its antibodies. (B) An I-Tasser homology model prediction with the myozyme sequence. (C) The crystal structure of matured GAA with active sites D518 and E521 (orange sticks) with the 4 kDa fragment in dark red, 10 kDa fragment in yellow, 19 kDa fragment in green, and the 70 kDa fragment in light blue. (PDB-ID: 5KZW). (The protein image was created with PyMOL.[25])

2.2.4 Survival Motor Neuron Protein

The survival motor neuron protein (SMN protein) is present in the cytoplasm and nucleus of nearly all human cells, with a wide range of functions. It is involved in RNA/DNA processing, cell signaling, endocytosis, autophagy, and neuronal skeleton formation.[207,208] Its involvement in small-nuclear ribonucleotide protein (snRNP) formation, also called spliceosomes, seems most significant.[209] Those complexes are essential for mRNA processing, and subsequent translation processes depend on them. This function explains why the SMN protein is found in almost all body cells and shows how crucial it is for any body compartment to function correctly. Decreased SMN protein concentrations are caused by homozygous deletion of the SMN1 gene, which leads to spinal muscle atrophy (SMA).[210] There is an SMN2 gene from which much less SMN protein is produced and can not compensate for the loss of the SMN1 gene. The motor neuron network is most severely influenced, with pathological conditions involving general muscle fiber loss and especially neuron degeneration in the spinal cord.[208]

SMA is classified into 5 subtypes according to their severity and the onset of disease-related symptoms.[210] The 5 SMA types can be further categorized into prenatal onset (onset: < 1 month; type 0), early onset (onset: 0-6 months; type 1), and late-onset (onset: < 18 months for type 2 and 3; and onset 10-30 years for type 4).[211] Type 0 and 1 SMA patients have drastically reduced life expectations. Type 2 patients can reach adulthood, and type 3 and 4 SMA patients have nearly average life expectancies.[210] Other SMA classifications include mobility milestone accomplishments, like the ability to sit, stand, and walk.[210,211] To understand the different SMA phenotypes, a look at the SMN1 and SMN2 genes is necessary. The SMN1 gene is responsible for producing full-length (fl) SMN protein. Humans have a second gene, known as the SMN2 gene, capable of producing approximately 10 % fl-SMN protein along with truncated SMN variants.[6,209] Therefore, it is not possible for the SMN2 gene to fully compensate for the SMN protein translation. However, the copy number of the SMN2 gene differs in individuals from 1 - 4, and a higher copy number is seen in SMA type 3 and 4 patients, which leads to less severe phenotypes.[211,212] Both genes consist of 3 exons (6,7,8) spliced to the transcript for SMN protein translation. The only difference is a synonym point mutation in exon-7, which causes a C-T change.[211] This creates a so-called exonic splicing silencer (ESS) site, prompting exon-7 to be skipped during mRNA transcription. Consequently, the resulting mRNA encodes mainly a C-terminally truncated SMN protein variant, which is called SMNΔ7. Those variants seem to lack self-oligomerization ability, which significantly decreases their cellular stability and ability to get correctly incorporated into certain snRNP - complexes.[6,207,208] Especially, axon outgrowths and dendrites in the spinal cord need higher concentrations of SMN protein to function correctly. It is still unclear if the SMN-related snRNP complexes splice specific motor neuron-related proteins or if the SMN protein is needed in the axons for motor neuron functions. There are indications for both.[208] Because of its broad presence in the human body, the current hypothesis emphasizes the SMN protein's role in mRNA trafficking to the axons and its translation to locally essential proteins.[209]

Despite the complex interaction scheme of the SMN protein and its incompletely understood function, there are several treatment strategies for SMA and several available FDA-approved drugs.[212] Protein-based therapy approaches seek to correct the expression of the SMN protein by modifying RNA splicing using oligonucleotides, as seen in Nusinersen (Spinraza) and Risdiplam. These treatments enhance the incorporation of exon-7 in the transcript. Another FDA-approved gene therapy option introduced in 2019 is Onasemnogen-Abeparvovec (Zolgensma).[211,212] The diagnostics of SMA include gene analysis after a physician suspects an SMA case. Several countries have now executed SMA newborn screenings to determine the prevalence and frequency of SMA occurrence in the corresponding populations. In 2019, the results from a newborn genetic screening (NBS) in Germany were published, which found an incidence rate of 1:7524.[213,214] Those analyses included the previously reported correlation with SMN2 gene copy number and amount of expressed SMN protein.[215–217] However, the SMN2 copy number and amount of expressed SMN protein can vary significantly, which defines the disease severity. Therefore, determining the SMN protein concentrations in each patient might benefit the appropriate treatment strategy.[215,218] It is essential to know that the mother contributes SMN protein to the unborn in the fetus, which decreases rapidly in the first three months of life if the infant cannot generate its own SMN protein. This biological process must be considered when measuring SMN protein concentrations in infants.[216] Dominant

for the SMN quantification from blood samples are ELISA-based.[217,219] The reported concentrations of SMN protein levels for healthy individuals are in the range of 30 - 70 ng protein / 1 mL of whole blood. The SMN protein level in SMA patients is reported to be 5 - 20 ng protein / 1 mL of whole blood, and correlations for the SMN gene copy number with SMN protein levels are observed.[215,217,219]

The role of SMN protein in snRNP complexes was extensively studied with a monoclonal mouse anti-human SMN protein antibody (mAB-7B10)[220], which was first reported in a publication from 2000.[221] This antibody was also used for specific SMN protein detection from HeLa cell extracts in two different snRNP complexes via immune-affinity chromatography. Immunoprecipitation and pull-down assays were conducted using cell lysates to characterize SMN complexes and interactions.[222–224] Its epitope was localized in the first 30 amino acids in the N-terminal part by SMN fragment analysis.[221,225,226] Further characterization of the mAB-7B10 - SMN protein complex by peptide mapping of overlapping peptide sequences from SMN[1-30] revealed the epitope sequence [12]PEQEDSVLFR[20] (Figure 2.2.7). The epitope peptide is suggested as a potential tag-sequence for recombinant proteins for the isolation and purification of expressed proteins by affinity chromatography with the mAB-7B10.[227] Later, the epitope data was confirmed by a peptide microarray with amino acid substitution to distinguish between well-conserved and exchangeable amino acids in the epitope sequence.[228] While writing the dissertation, no crystal structure for the SMN protein was available. I-Tasser predictions were unattainable due to an inaccurate crystal structure in the database for homology modeling.

Figure 2.2.7: Amino acid sequence of the recombinant SMN protein with N-terminal tag sequence for purification after expression. The tag sequence carries an His6-tag (H4 - H9) and a T7-tag (M21 – G31). The tag-sequence on the N-terminal site covers 35 amino acids (M1 - F36), the native human SMN sequence starts with amino acid A37, the mAB-7B10 epitope is highlighted in blue, and the epitope for the polyclonal antibodies (pAB) in orange.

While the mAB-7B10 epitope sequence is identified, no affinity for the antibody-protein or antibody-peptide complex is reported. The linear epitope may exhibit high affinity, presenting an opportunity for leveraging an SPR/AC-MS-based diagnostic assay for the identification and quantification of SMN protein. Because SMA is connected to a truncation of SMN in the C-terminal end, two antibodies produced against the C-terminus are investigated for their use in a bioassay for identification of its absence. The polyclonal antibodies (pAB) against the synthetic peptide with the sequence [309]GYYMGFRQNQKEGRCSHSLN[329] (rSMN[309-329]) are produced in rabbits by the company immunoGlobe® on the request of the Steinbeis Center. Briefly, the cysteine residues are easily oxidized, which could create antibodies specific only to one isoform of the SMN protein. Therefore, the cysteine residue (C323) is exchanged for α-aminobutyric acid (Abu) to avoid any inconvenience with the specificity of the produced antibodies. The resulting peptide derivative is then coupled to keyhole limpet hemocyanin (KHL)[229,230], which is used to immunize two rabbits. The immunization is repeated three times with three weeks in between before the first large bleeding of both rabbits, resulting in antibody preparations IG1106-1 and IG1107-2. After two more immunizations, another large bleeding lead to IG1106-2 and IG1107-2 fractions. Each antibody preparation is affinity purified with the epitope peptide, which carries no cysteine or Abu. Instead, a serine is at position 323 to avoid the extraction of antibodies specific to the Abu residue. The characterization of the prepared antibodies can be found in chapter 5.4.

3 Aims of the thesis

The identification and characterization of epitopes and, in general, binding sites of any protein-protein complex is essential for the development of new drugs, bioassays, and clinical diagnostics. In this work, epitopes of specific antibodies against four model proteins will be analyzed, and the method for epitope identification should be improved.

The first goal was the identification of epitopes from antibodies and one aptamer against three model proteins, namely IL8 (mAB-I2519), CTSD (AB-1, AB-2, CSTD-aptamer), and GAA (mAB-43G7). The information on the epitope sequence and its location on the proteins can give insights into the mechanisms of inhibitory antibodies, like that against IL8. The SMN protein and its antibody (mAB-7B10) epitope sequence were known, but the affinity was unknown. Therefore, the affinity of the SMN - mAB-7B10 and the IL8 - mAB-I2519 complex and their epitope peptides was also determined. This information can tell how well the affinity is retained in the epitope peptides and what kind of epitope is present. Additionally, the affinity of two antibodies produced against the C-terminal sequence of SMN was compared to the mAB-7B10, which could be used in an SPR-based biosensor assay to determine ratios of truncated and non-truncated SMN protein levels.

Furthermore, this information guides assay development and corresponding improvements. The epitope comparison of antibodies and aptamers was investigated on the model protein CTSD to investigate the differences and similarities of these biomolecule classes. The antibody epitopes on GAA are investigated for their potential use in the apheresis of patients under ERT to remove the autoimmune antibodies formed against the drug after treatment.

The epitope extraction method has the potential to be used as a diagnostic assay, which utilizes epitope peptides as biomarkers. Therefore, an antibody with a linear epitope, which retains a strong affinity to the antibody, would be ideal. The proof-of-concept was done on the model protein SMN, its antibody mAB-7B10, and its synthetic epitope peptides. The results would be applied to other proteins and their ligands, like the CTSD and its DNA-aptamer if possible. The bioassay should consist of three steps: (1) the digestion of a sample, (2) the epitope extraction, and (3) epitope peptide quantification by MALDI-tof MS analysis. Several additions and modifications were tested for the epitope extraction method to evaluate its potential as a diagnostic tool.

The first addition was a chip-based extraction platform that should reduce sample consumption and permit simultaneously recording affinity data from an SPR-based biosensor together with sequence data from MALDI-tof MS measurements. This experimental setup will be tested on the different model proteins, depending on the outcome of the corresponding epitope identification experiments. The enzymatic digestion of proteins is a crucial step for epitope identification by epitope extraction and for the intended use of epitope peptides as biomarkers. Therefore, an alternative to the standard digestion at atmospheric pressure, high-pressure digestion, was tested on enzymatic digestions with trypsin.

With regard to the enzyme used for digestion, the design of an epitope extraction experiment is somewhat limited. The gold standard trypsin is the first choice for any investigation. It leads to well-ionizable peptide fragments but could, incidentally, cleave the epitope, leading to fragments with weak antibody binding. Therefore, four different in-sillico B-cell epitope prediction tools are investigated. These tools could indicate potential epitopes on a tested protein, and comparison to the cleavage sites of proteolytic enzymes might guide to an optimal experimental setup.

4 Material and Methods

4.1 Common Materials and Chemicals

All materials and chemicals used in this work were purchased from the following manufacturers/distributers, if not specified otherwise: Carl Roth (Karlsruhe, GER), Carbolution (Saarbrücken, GER), Iris Biotech (Marktredwitz, GER), Merck (Darmstadt, GER), Merck Novabiochem (Darmstadt, GER), Rapp Polymers (Tuebingen, GER), Sarstedt (Nümbrecht, GER), Sigma Aldrich (Taufkirchen, GER), VWR (Darmstadt, GER), Acros Organics (Fair Lawn, USA), Fluka (München, GER), Thermo Fisher Scientific (Hampton, USA), Riedel-de Haën (Seelze, GER).

4.1.1 Buffers and Solutions

Buffers and aqueous solutions were always prepared with MilliQ filtered water (MQ; Merck Millipore System), and the pH was adjusted with HCl and NaOH. The following table summarizes the buffers and solutions used in this work (Table 4.1.1).

Table 4.1.1: Used buffers and solutions.

Buffer/Solution	**Composition**
General	
Phosphate buffered saline (PBS); pH 7.4	137 mM NaCl; 2.7 mM KCl; 40 mM NaH_2PO_4; 1.8 mM KH_2PO_4
Phosphate buffered saline T (PBST); pH 7.4	PBS; 0.1 % Tween-20
Blocking buffer; pH 8.5	1 M ethanolamine
AmBic buffer; pH 7-9	10 - 100 mM ammonium bicarbonate
Affinity Chromatography	
Coupling buffer; pH 8.5	0.2 M $NaHCO_3$; 0.5 M NaCl
Washing buffer-1	1 mM HCl
Washing buffer-2; pH 4	0.2 M NaAc; 0.5 M NaCl
Washing buffer-3; pH 8	0.1 M Tris-HCl; 0.5 M NaCl
Storage buffer; pH 8	100 mM ammonium bicarbonate
SPR-based Biosensor	
Activation solution (EDC/NHS)	20 mg/mL EDC; 5 mg/mL NHS
Coupling buffer B; pH 5	30 mM NaAc
SDS-PAGE	
Tris buffer-1; pH 6.8	1.5 M TRIS-HCl
Tris buffer-2; pH 8.8	0.5 M TRIS-HCl
Tris buffer-3; pH 8.8	2.5 M TRIS base
SDS solution	10 % SDS
APS solution	10 % APS
Laemmli buffer	20 % glycerol; 2 % SDS; 1 % mercaptoethanol; 0.01 % bromphenol-blue; 100 mM Tris buffer pH 6.8

4 % Tris-stacking gel (2 gels)	30 % acrylamide/bisacrylamide (1.32 mL); 0.5 M Tris buffer pH 6.8 (3.78 mL); 10 % SDS (150 µL); MQ (6 mL); 10 % APS (75 µL); TEMED (15 µL)
12 % Tris-separating gel (2 gels)	30 % acrylamide/bisacrylamide (6 mL); 1.5 M Tris buffer pH 6.8 (3.75 mL); 10 % SDS (150 µL); MQ (5.03 mL); 10 % APS (75 µL); TEMED (7.5 µL)
14 % Tris-separating gel (2 gels)	30 % acrylamide/bisacrylamide (7 mL); 1.5 M Tris buffer pH 6.8 (3.75 mL); 10 % SDS (150 µL); MQ (4.03 mL); 10 % APS (75 µL); TEMED (7.5 µL)
16 % Tris-separating gel (2 gels)	30 % acrylamide/bisacrylamide (8 mL); 1.5 M Tris buffer pH 6.8 (3.75 mL); 10 % SDS (150 µL); MQ (3 mL); 10 % APS (75 µL); TEMED (7.5 µL)
Tris-Running buffer	25 mM TRIS; 193 mM glycine; 3.5 mM SDS
4 % Tricine-collection gel (1 gel)	30 % acrylamide/bisacrylamide (0.66 mL); 2.5 M Tris buffer pH 8.8 (0.76 mL); MQ (3.42 mL); 10 % APS (150 µL); TEMED (5 µL)
12 % Tricine-separation gel (1 gel)	30 % acrylamide/bisacrylamide (3 mL); 2.5 M Tris buffer pH 8.8 (5 mL); MQ (0.89 mL); 10 % APS (100 µL); TEMED (6 µL)
Tricine-Running buffer	0.1 M TRIS; 0.1 M tricine; 3.5 mM SDS
Colloidal Coomassie solution	0.12 % Coomassie brilliant blue; 20 % methanol; 10 % acetic acid
Western blot	
TBS buffer	20 mM TRIS; 0.2 M NaCl
TBST buffer	TBS buffer; 0.1 % tween-20
TBS blocking buffer	TBS buffer; 1 % BSA
Transfer buffer	48 mM TRIS; 39 mM glycine; 20 %methanol; 0.04 % SDS
Ponceau S solution	0.5 % Ponceau S; 5 % acetic acid
Staining solution	0.48 mM 4-chloro-naphthol; 50 mM TRIS-HCl; 0.2 M NaCl; 17 % methanol
MALDI-tof MS	
2,5-dihydroxy benzoic acid (DHB)	20 mg/mL; 50 % ACN; 0,1 % TFA
Super-DHB	50 mg/ml; 50 % ACN; 0,1 % TFA
α-hydroxy cinnamic acid (HCCA) Sinapic acid(SA) solution A	Saturated solution; 50 % ACN; 0,1 % TFA Saturated sinapic acid in ethanol
Sinapic acid (SA) solution B	Saturated sinapic acid solution; 50 % ACN; 0,1 % TFA
3-hydroxypicolinic acid (3-HPA)	Saturated 3-HPA; 50 % ACN; 0,1 % TFA; 10 mg/mL diammonium hydrogen citrate
HPLC	
Eluent A	99.9 % ACN; 0.1 % TFA
Eluent B	99.9 % MQ; 0.1 % TFA
Seal wash solution	10 % MeOH in MQ

4.1.2 Antibodies, proteins, and standards

Antibodies and proteins are listed in the following table (Table 4.1.2).

Table 4.1.2: Antibodies, proteins, and standards used in this work.

Antibodies/Proteins	Manufacturer	Specification
Interleukin 8 (IL8)	WG Schmitz, TU Darmstadt, GER	Human interleukin-8 / CXCL8 (1-72)
Monoclonal anti-human IL8	Sigma Aldrich, Steinheim, GER	Monoclonal anti-human interleukin 8 IgG mouse, i2519
Bovine serum albumin (BSA)	PAA Laboratories, Pasching, AUT	Bovine serum albumin fraction V, K41-001
Trypsin	Promega, Walldorf, GER	Trypsin sequencing grade, V5111
Chymotrypsin	Promega, Walldorf, GER	Trypsin sequencing grade, V1061
Lys-C	Promega, Walldorf, GER	Trypsin mass spectrometry grade, V1671
PNGF	Promega, Walldorf, GER	PNGase F, V483A
Horse myoglobin	Sigma-Aldrich, Missouri, USA	Myoglobin from horse heart, M-1882
Monoclonal anti-myoglobin	Santa Cruz Biotechnology, Oregon, USA	Mouse monoclonal anti-myoglobin IgG, sc-393020
Polyclonal anti-horse myoglobin	Bethyl Laboratories, Montgomery, USA	Goat polyclonal anti-horse myoglobin antibody, A150-103
Recombinant SMN (SMN)	Immunoglobe, Himmelstadt, GER	Recombinant human SMN protein, M180806
Monoclonal anti-human SMN	Immunoglobe, Himmelstadt, GER	Mouse monoclonal anti-human SMN antibody, 7B10, 0176-01
Polyclonal anti-human SMN	Immunoglobe, Himmelstadt, GER	Rabbit polyclonal anti-human SMN antibody
Myozyme (GAA)	Sanofi Genzyme, Cambridge, UK	Recombiant human alpha glucosidase, alfa alglucosidase for pompe treatment
Monoclonal anti-human GAA	Biozol, Eching, GER	Mouse anti-human alpha-glucosidase antibody, 43G7, NMB-MUB0707P
Cathepsin D	WG Saftig, CAU Kiel, GER	Recombinant human cathepsin D
Anti-human cathepsin D (1)	WG Saftig, CAU Kiel, GER	Polyclonal anti-human cathepsin D antibody
Anti-human cathepsin D (2)	WG Saftig, CAU Kiel, GER	Polyclonal anti-human cathepsin D antibody
Cathepsin D Aptamer	Integrated DNA Technologies, USA	Cathepsin D aptamer, ref. no. 187556225
Anti-rabbit HRP	Santa Cruz Biotechnology, Oregon, USA	Mouse anti-rabbit IgG-HRP, sc-2357
Anti-mouse HRP	Sigma-Aldrich, Missouri, USA	Rabbit anti-Mouse IgG (whole molecule) - peroxidase antibody, A9044
Protein G	Sigma-Aldrich, St-Louis, USA	Protein G from *Streptococcus sp.*
mPAGE Color Prestained Ladder	Merck Millipore, Darmstadt, GER	Ladder for SDS-PAGE, 10-203 kDa
Protein Ladder 94964	Sigma-Aldrich (Merck), Darmstadt, GER	Ladder for SDS-PAGE, 8-245 kDa

4.1.3 Affinity column material, resins, and chips

All used affinity media for affinity chromatographic experiments and resins for solid-phase peptide synthesis are listed in the following table (Table 4.1.3).

Table 4.1.3: Used column media, synthetic resins, and biosensor chips.

Name	Manufacturer	Specification
CNBr-activated sepharose 4B	GE Healthcare, Uppsala, SWE	Pre-activated (CNBr) beads for direct immobilization of proteins, 17-0430-01
SelfPack POROS 20 EP	PerSeptive Biosystems, Massasuchetts, USA	Pre-activated (Epoxy) beads for direct immobilization of proteins, 1-6128-10
TentaGel PHB (high swelling)	Rapp Polymer, Tübingen, GER	Polystyrene resin, loading capacity: 0.27 mmol/g, HQ28013
PS-PHB-Arg(Pmc)-Fmoc	Rapp Polymer, Tübingen, GER	Polystyrene resin with preloaded Fmoc-Arg(Pmc)-OH, loading capacity: 0.59 mmol/g, H0370751317
PS-PHB-Lys(Boc)-Fmoc	Rapp Polymer, Tübingen, GER	Polystyrene resin with preloaded Fmoc-Lys(Boc)-OH, loading capacity: 0.74 mmol/g, H0370751317
PS-PHB-Ser(tBu)-Fmoc Wang resin	Rapp Polymer, Tübingen, GER	Polystyrene resin with preloaded Fmoc-Ser(tBu)-OH, loading capacity: 0.66 mmol/g H0751501323
Bare gold SPR chip	Sofchip, Florida, USA	Size 12x12x0.9mm; Catalog No. 1000003-3
Carboxylated dextran SPR chip	Sofchip, Florida, USA	Size 12x12x0.9mm; Catalog No. 1511123-3

4.2 Devices and software

The following tables summarize the devices and software used in this work (Table 4.2.1).

Table 4.2.1: Devices used.

Device	Name	Manufacturer
MALDI-tof mass spectrometer	Autoflex III Smartbeam	Bruker Daltonics, Billerica, USA
HPLC	2795 Alliance HT instrument	Waters, Massachusetts, USA
HPLC	Vanquish HPLC System	ThermoFisher Scientific, Langerwehe, GER
UV-Vis detector	Ultimate3000 Variable Wavelength Detector	ThermoFisher Scientific, GER
SPR-based biosensor	SR7500DC SPR system	Reichert Technologies, Buffalo, USA
Peptide synthesizer	ABI 433 A peptide synthesizer	Applied Biosystems, Darmstadt, GER
High-pressure digestion device	Braocycler 2320 EXT	Pressure Biosciences, Massachusetts, USA
Nitrogen generator	NM32LA	Peak Scientific, Frankfurt, GER
Water purification system	Direct-Q 3UV, ultrapure (Type 1) water	Merck Millipore, Massachusetts, USA
Lyophylisator	Alpha 1-2 LD plus	Christ, Osterode, GER

Centrifuge	Biofuge 13	Heraeus, Hanau, GER
Centrifuge	Biofuge primo	Heraeus, Hanau, GER
Concentrator	Concentrator 5301	Eppendorf, Hamburg, GER
Ultrasonic bath	Transonic 570	Elma, Singen, GER
Horizontal shaker	KS 260 basic	IKA, Staufen, GER
Thermoshaker	Biometra TSC ThermoShaker	Analytik Jena, Jena, GER
Scanner for Gels	Stylus Office BX535WD	Epson, Suwa, JP
Precision Balance	PJ3600 DeltaRange	Mettler Toledo, Columbus, USA
Electronic precision and analytical balance	ALJ 160-4M	KERN, Balingen, GER
SDS-Gel casting and running devices	Mini-PROTEAN® Tetra Vertical Electrophoresis Cell, 4-gel, for 1.0 mm thick hand-cast gels	BioRad Laboratories, Feldkirchen, GER

Table 4.2.2: Software used.

Software	**Instrument/Data**	**Manufacturer**
FlexControl 3.3	MALDI-tof MS control software	Bruker Daltonics, Billerica, USA
FlexAnalysis 3.3	Mass spectra	Bruker Daltonics, Billerica, USA
mMass[231–233]	Mass spectra	Martin Strohalm
Integrated SPR Autolink	SPR-based biosensor, sensorgram	Reichert Technologies, Buffalo, USA
Trace Drawer 1.7.1	Sensorgram	Reichert Technologies, Buffalo, USA
MassLynx 3.3	HPLC; chromatogram	Waters, Massachusetts, USA
Chromeleon 7	HPLC; chromatogram	ThermoFisher Scientific, Langerwehe, GER
PBI Barocycler 2320 EXT control software	Instrument control	Pressure Biosciences, Massachusetts, USA
SynthesisAssist 3.1	Instrument control, peptides synthesizer	Applied Biosystems, Darmstadt, GER
ImageJ[234]	SDS-PAGE and Western blot image processing	Wayne Rasband
Pymol[25]	Crystal structure image preparation with PDB files	Schrödinger
MS Tools[235]	MS Data, Protein Map preparation	MS Tools

4.3 Peptide and protein purification and separation methods

4.3.1 Buffer exchange via spin-filter

Proteins that needed to be dissolved in a specific buffer for biosensor or mass spectrometric analysis were transferred into a suitable one via spin-filter with a molecular-weight-cutoff (MWCO) of 10 kDa (Roti-Spin MINI; Carl Roth; Karlsruhe, GER). Sample volumes up to 500 µL were suitable for the used spin-filters.

Before sample loading, the spin-filter was washed twice with 500 µL of ethanol (70 %) and twice with 500 µL of ultrapure water (MQ) by centrifugation at 10,000 rpm for 2-10 min. After emptying the spin-filter, 50-500 µL of the sample was loaded and washed 5 times by adding 50-500 µL of the desired buffer (PBS or MQ). After

centrifugation at 10,000 rpm for 2-10 min, samples were stored in microcentrifugation tubes (MCT) in the refrigerator at 4 °C or in the freezer at -20 °C for later use.

4.3.2 RP-C18-HPLC

The reversed-phase C-18 high-performance liquid chromatography (RP-C18-HPLC) was used with a binary solvent system consisting of 0.1 % trifluoric acid (TFA) in MQ and 0.1 % TFA in acetonitrile. The silica-based column material is functionalized with alkanes of different lengths (C18 = 18 alkyl groups) to separate peptides and proteins according to their hydrophobicity. In this work, RP-HPLC was used to purify peptides after their synthesis. A C18 column (250 mm × 4.6 mm) from Interchim (Interchrom-KR5C18-25QK) with a 2795 Alliance HT HPLC instrument or a C18 column (150mm x 4.6 mm) from Macherey-Nagel (Nucelosil 100-5 C18 Nautilus; Macherey-Nagel, Düren, GER) with a Vanquish HPLC System were employed. The binary solvent system for gradient formation consisted of solvent A (0.1 % TFA in MQ) and solvent B (0.1 % TFA in ACN). A UV-Vis multiwavelength detector from ThermoFisher (ultimate 3000) was used for retention time monitoring at 220 nm and 280 nm.

Peptide IL8[12-20] (TYSKPFHPK) was purified via RP-HPLC in several semipreparative runs with the Interchrom-KR5C18-25QK column at a flow rate of 1 mL/min and 50 °C. After 5 minutes of column equilibration with 90 % solvent A, the peptide was eluted by a continuous gradient over 20 minutes from 90 % to 70 % solvent A. The column was flushed with 10 % solvent A for 10 minutes and re-equilibrated for 5 minutes at 10 % solvent A. Several aliquots of 5 µL (100 mM) crude peptide IL8[12-20] were injected, and purified fractions were collected and lyophilized.

Peptide IL8[55-60] (ENWVQR) was purified via RP-HPLC in several semipreparative runs with the Interchrom-KR5C18-25QK column at a flow rate of 1 mL/min and 50 °C. After 5 minutes of column equilibration with 90 % solvent A, the peptide was eluted with a continuous gradient over 30 minutes from 90 % to 80 % solvent A. The column was flushed with 10 % solvent A for 10 minutes and re-equilibrated for 5 minutes at 10 % solvent A. Several aliquots of 5 µL (100 mM) crude peptide IL8[55-60] were injected, and purified fractions were collected and lyophilized.

Peptide IL8[55-72] (ENWVQRVVEKFLKRAENS) was purified via RP-HPLC in several semipreparative runs with the Nucelosil 100-5 C18 Nautilus column at a flow rate of 1 mL/min and 45 °C. After 5 minutes of column equilibration with 75 % solvent A, the peptide was eluted by a continuous gradient over 25 minutes from 75 % to 55 % solvent A. The column was flushed with 10 % solvent A for 10 minutes and re-equilibrated for 5 minutes at 75 % solvent A. Several aliquots of 40 µL (10 mM) crude peptide IL8[55-72] were injected, and purified fractions were collected and lyophilized.

Peptide rSMN[38-57] (MSSGGSGGGVPEQEDSVLFR) was purified via RP-HPLC in several semipreparative runs with the Nucelosil 100-5 C18 Nautilus column at a flow rate of 1 mL/min and 30 °C. After 5 minutes of column equilibration with 80 % solvent A, the peptide was eluted by a continuous gradient over 20 minutes from 80 % to 74 % solvent A. The column was flushed with 10 % solvent A for 10 minutes and re-equilibrated for 5 minutes at 80 % solvent A. Several aliquots of 60 µL (5 mM) crude peptide rSMN[38-57] were injected, and purified fractions were collected and lyophilized.

Peptide rSMN[37-57] (AMSSGGSGGGVPEQEDSVLFR) was purified via RP-HPLC in several semipreparative runs with the Nucelosil 100-5 C18 Nautilus column at a flow rate of 1 mL/min and 30 °C. After 5 minutes of column equilibration with 80 % solvent A, the peptide was eluted by a continuous gradient over 20 minutes from 80 % to 70 % solvent A. The column was flushed with 10 % solvent A for 10 minutes and re-equilibrated for 5 minutes at 80 % solvent A. Several aliquots of 60 µL (5 mM) crude peptide rSMN[38-57] were injected, and purified fractions were collected and lyophilized. The combined fractions for each peptide were reinjected to verify the

successful purification with the corresponding gradients, and all results can be found in the corresponding results chapters.

4.3.3 ZipTip for sample desalting

Before mass spectrometric (MS) analysis, samples with too high concentrations of salt or other additives that are not MS-compatible were purified by reversed-phase ZipTips (Merck Millipore, Darmstadt, GER). ZipTips are micro-pipette tips with a C_4- or C_{18}- reversed-phase chromatography medium, which are widely applied for peptide and protein purification. Both ZipTips were used similarly with a 0.5-10 µL pipette.

First, the ZipTip was wetted with 10 µL of 100 % ACN three times by aspirating and discarding the ACN. ZipTips were equilibrated with 10 µL 0.1 % TFA in MQ (three times) by aspiration and dispensation in the same way as before. The sample was acidified by adding TFA to a final concentration of 0.1 %. The sample was loaded by aspirating and dispensing 10 µL of the sample ten times. Afterwards, the sample was washed with 10 µL of 0.1 % TFA in MQ by aspiration and discarding the solution. For elution, 10 µl of 90/10 (v/v) ACN/MQ with 0.1 % TFA was aspired. Eluted samples were stored at -20 °C or lyophilized for later use.

4.3.4 SDS-PAGE

The sodium dodecyl sulfate-polyacrylamide gel electrophoresis (SDS-PAGE) separates proteins by size after being uniformly, negatively charged by SDS and moving in an electric field through a polymeric gel. For gel preparation, 2 glass slides were cleaned and placed in the casting frame from Biorad (Table 4.2.1). At first, the mixture for the separating gel (Table 4.1.1) was activated by adding APS and TEMED to start the polymerization process, and the mixture was filled up to three-quarters between the glass slides. After overlying with ethanol, the gel was left for 15 minutes for polymerization. Afterwards, the ethanol was removed, and the mixture for the stacking gel (Table 4.1.1) was likewise prepared and added with a comb for the sample pocket formation. After 15 minutes, polymerization was completed, and the gel was directly used or covered in wet tissues and stored at 4 °C.

For electrophoresis, gels were mounted into the running chamber from Biorad (Table 4.2.1), the running buffer (Table 4.1.1) was added, the comb was removed, and the sample pockets were filled with 15-20 µL sample in Lämmli-buffer (Table 4.1.1). Lämmli-diluted samples were heated for five minutes to 95 °C before loading the sample onto the gel. 5 µL standard protein ladder (Table 4.1.2) was added for mass comparison, and the gel running chamber was closed. A constant voltage of 100 V was applied for 3-5 hours and stopped when the running front started to move out of the gel. The gels were removed from the chamber and washed three times with MQ. To stain the proteins, the gel was incubated with Coomassie blue solution (Table 4.1.1) overnight at room temperature, followed by destaining with 20 % methanol with 10 % acetic acid in MQ for 2-4 h. The gel was documented with a scanner/printer from Epson.

4.3.5 Western Blot and Dot Blot

After a gel-electrophoresis, a Western blot can be performed to stain the separated proteins specifically with corresponding antibodies. In an electric field, the proteins from a gel are transferred to a PVDF membrane. The membrane is then incubated with a primary and a secondary antibody. The secondary antibody is conjugated with an enzyme, and incubation with a suitable substrate leads to the formation of a dye (e.g., fluorophore) that indicates the presence of the specific protein-antibody complex at the respective position on the membrane. A Western blot with direct spotting of proteins onto a membrane without previous separation by SDS-PAGE but with the same detection and staining procedure is called a dot blot.

For every Western blotting experiment, a semi-dry Western blotting instrument was used (Table 4.2.1). For semi-dry blotting, the PVDF membrane was incubated in methanol. Afterwards, Whatman paper, PVDF membrane, and the prepared gel were incubated in the blotting buffer (Table 4.1.1) before forming the transfer stack. At first, a layer of wetted Whatman paper was placed on the anode of the semi-dry blotter, overlayed with the PVDF membrane, gel, and another layer of Whatman paper in that order. After closing the semi-dry blotter, a constant current of 90 mA was applied for 90 minutes. The protein-loaded PVDF membrane was blocked by incubation in the blocking buffer (Table 4.1.1) for one hour, followed by incubation with 5 mL of 0.1 - 1 µg/mL primary antibody solution (Table 4.1.2) in TBS-T (Table 4.1.1) for two hours. The membrane was washed three times and incubated with 5 mL of 2 µg/mL secondary antibody solution (Table 4.1.2) in TBST buffer for two hours. Finally, the membrane was rewashed three times with TBS-T and then incubated with blot staining solution (Table 4.1.1) for 5 - 10 min. until a suitable band signal intensity was reached. The Western blot was documented with an Epson scanner/printer.

The dot blot procedure started with activation of the PVDF by incubation in methanol followed by washing with blotting buffer (Table 4.1.1) and spotting 5 µL of protein solution onto a stripe of the PVDF membrane at various concentrations. After the spots were allowed to dry at room temperature, the membrane was again socked in methanol, washed with blotting buffer (Table 4.1.1), and the immune-staining procedure was carried out as described for the Western blot.

4.4 MALDI-tof mass spectrometry

If not stated otherwise in the results section, samples were directly analyzed by MALDI-tof MS with the following procedures and chemicals. All MALDI-tof MS analyses were performed with a Bruker autoflex III smartbeam (Table 4.2.1). Peptide mixtures were measured with 2,5-dihydroxybenzoic acid (DHB) or α-cyano-4-hydroxycinnamic acid (HCCA) and proteins with super-DHB (SDHB) as the matrix. All matrix compounds were dissolved in 50 % acetonitrile in water supplemented with 0.1 % TFA. DHB was used at 20 mg/mL solution, HCCA as a saturated solution, and SDHB as a 50 mg/mL solution. The targets for spotted samples were either an “MTP 384 target plate polished steel BC” or “MTP AnchorChip 800/384 T F” from Burker Daltonics Inc.

0.7 µL (20 mg/mL) of matrix solution and 0.7 µL of sample were spotted and mixed on a MALDI target and left to dry at room temperature. After the sample was dry, the plate was put into the MS instrument and measured. Peptide measurements in the mass range of 400 - 4000 Da were primarily carried out in reflector mode (Method: RP; Figure 4.4.1), and large peptides and proteins with a mass above 4000 Da were measured primarily in linear mode (Method: LP; Figure 4.4.1). With the RP method, 75 % laser intensity and 2000 laser shots were usually used to record proper signals, and the LP method was used with 90 % laser intensity and 5000 laser shots.

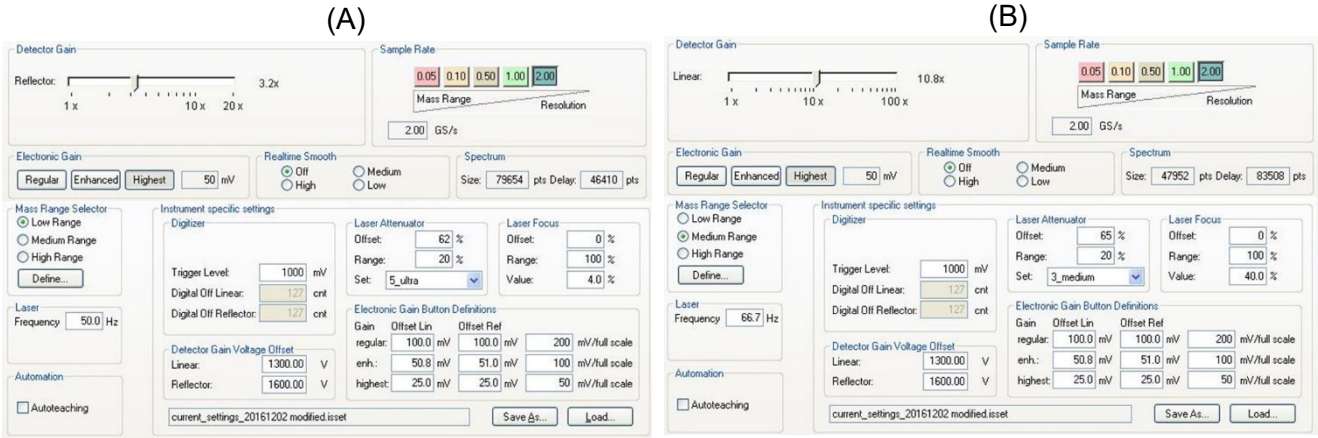

Figure 4.4.1: Autoflex III smartbeam (Bruker Daltonics Inc.) instrument-specific settings for measuring peptides in the reflectron mode (A) and large peptides and proteins in linear mode (B).

Both peptides and proteins were primarily measured in positive mode. Before each series of measurements, external calibration was done with the calibration solutions spotted and dried with the same matrix used for spotting the samples. An Agilent calibration solution (Table 4.1.2) was used for the mass range from 400 - 4000 Da and a mixture of myoglobin and BSA (both with > 90 % purity determined by SDS-PAGE) for the masses higher than 4000 Da. The MALDI-tof MS instrument was controlled with the FlexControl software from Bruker Daltonics, and the first mass spectra analysis was with the flexAnalysis software from Bruker. Usually, the final analysis of the recorded mass spectra was performed with Mmass[233], and the protein maps were created with MS tools[235,236].

4.5 Peptide synthesis

Peptides were synthesized by Fmoc-based solid-phase peptide synthesis (SPPS) with the ABI 433 A peptide synthesizer (Table 4.2.1). The synthetic method is based on the coupling of amino acid derivates to each other in a controlled way so that only the desired peptide chain is formed on a solid support medium (resin). The amino acid derivates usually carry a permanent protection group on the side chain and a temporary Fmoc-protection group on the amino group. This way, only the free carboxyl group is activated with HBTU/DIPEA and bound to a resin with an appropriate linker and functionality (e.g., an amino group). Afterwards, the Fmoc-group is cleaved off under basic conditions (e.g., piperidine or piperazine), and the coupling step is repeated until the desired sequence is obtained. In the last step, the peptide is cleaved off the resin, often along with the side chain protection groups under acidic conditions (if the linker is acid-labile). Precipitation of the peptide in diethyl ether (DE) or methyl-tert-butylether (MTBE) removes many side products from protecting group cleavage. The final purification of the peptides was accomplished by HPLC.

For automated solid-phase peptide synthesis, the ABI 433 A peptide synthesizer was loaded with solvents for washing, coupling, deprotection, and amino acid derivatives (Table 4.5.2). The amino acid derivatives Fmoc-Ala-Oh, Fmoc-Cys(Trt)-OH, Fmoc-Asp(OtBu)-OH, Fmoc-Glu(OtBu)-OH, Fmoc-Phe-OH, Fmoc-Gly-OH, Fmoc-His(Trt)-OH, Fmoc-Ile-OH, Fmoc-Lys(Boc)-OH, Fmoc-Leu-OH, Fmoc-Met-OH, Fmoc-Asn(Trt)-OH, Fmoc-Pro-OH, Fmoc-Gln(Trt)-OH, Fmoc-Arg(Pbf)-OH, Fmoc-Ser(tBu)-OH, Fmoc-Thr(tBu)-OH, Fmoc-Val-OH, Fmoc-Trp(Boc)-OH and Fmoc-Tyr(tBu) from either Novabiochem (Merck Schuchart OHG, Hohenbrunn, GER), GL Biochem Ltd (Shanghai, CH) or Applied Biosystems (Warrington, UK) were used. Usually, 0.1 mmol of resin was used with a reaction vessel volume of 8 mL. 10 eq. Fmoc-amino acid derivative, 9.95 eq. HBTU, and 20 eq. DIPEA was used with 0.1 mmol of resin. Fmoc-amino acid derivatives were preloaded into their cartridges as a dry powder. The ABI 433 A peptide synthesizer was controlled by the ABI 433 A peptide synthesizer control software. All synthesis options have several presets, and modules (Table 4.5.1) used to program a synthesis sequence. The programmed sequence of the FSPPS started with resin swelling, followed by deprotection of the preloaded amino acid and repetitive coupling/deprotection until the amino acid sequence was completed (Table 4.5.3). The synthesis sequence consisted of modules (Table 3.5.1) containing the times/volumes/amounts for each washing, incubation, coupling, and deprotection step. After the synthesis, the resin was dried from residual DCM at room temperature. The peptide was cleaved off the resin, and the side-chain protecting groups were removed by incubation with 5 mL of 95 % TFA, 2.5 % tri-isopropylsilane, and 2.5 % MQ for three hours at room temperature. Peptides were precipitated by pouring the reaction mixture into 20 mL of ice-cold MTBE. The MTBE was removed by centrifugation and decanting. The peptide was resuspended twice in MTBE, followed by centrifugation and decanting. Finally, the precipitated peptide was dried, dissolved in 50:50 ACN/MQ, and lyophilized. The experimental procedure from the ABI 433 A peptide synthesizer included monitoring the N-terminal Fmoc-deprotection after each coupling step. For that purpose, a UV detector measured the dibenzofulvene-piperidine adduct at 301 nm after each coupling step. Additionally, the deprotection step was repeated automatically if necessary. The monitoring data of the synthesized peptides are attached in the appendix and referenced in the corresponding results chapter.

Table 4.5.1: Module descriptions for creating a peptide sequence for FSPPS with the ABI 433 A peptide synthesizer.

Code	Module-Name	Procedure description
A	Activation HBTU	The Fmoc-AA is initially dissolved in 1.8 mL of NMP, and 2.2 mL 0.45 M of HBTU in DMF are added to the cartridge for activation. The dissolution process is accelerated by nitrogen bubbling supply and lasts 6 minutes.
B	Deprotection UV*7%	The reaction vessel is flushed with NMP, and piperidine is added to a final concentration of 21 % piperidine. The reaction vessel is vortexed for 5 minutes. UV detector line is flushed with methanol. 21 %piperidine in NMP is partly supplied to the UV detector and to the waste. UV measurement at 301 nm. If the intensity of the UV signal exceeds 7 % of the previous deprotection, the deprotection is repeated (max 4 times).
C	-	-
D	NMP Washes	The reaction vessel is flushed 4 times with NMP. The last washing fractions are supplied to the activator vessel for a later washing step of the resin (Module d).
E	Transfer	1 mL 2 M DIEA in NMP is supplied to the Fmoc-AA cartridge and mixed with nitrogen supply for 15 seconds. The cartridge content is then supplied to the reaction vessel. Vortex of the reaction vessel is turned on.
F	*Clean Cartridge & Couple	*If the cartridge content is supplied to the reaction vessel, this module starts. The cartridge is flushed and drained 4 times with NMP. 10 times; the reaction vessel is vortexed for 15 secs and an additional 13 seconds vortex off.
I	Vortex (5 min)	Vortex of the reaction vessel is turned on for 5 minutes.
b	*Cond. Deprotection * 750 300s	*If the UV signal of the "deprotection UV*7%" is not under 7 % of the previous deprotection step, this additional deprotection procedure is activated. Modification of Module B contains 10 minutes of vortexing with 21 %piperidine and repetition for max. 5 times.
c	DCM Washes	The reaction vessel is flushed 6 times with DCM.
d	NMP Wash from Activator	NMP from the activator vessel is supplied to the reaction vessel, vortex on for 3 seconds, and drained to the waste. Repetition of 3 times.
e	MeOH, NMP to Aux.	Lines to the detector are flushed with MeOH and NMP.
f	*Cond.Extended Coupling* 15 min	*If module b was needed in a previous Fmoc-AA coupling step, instead of module F, module f is utilized. Instead of repeating "vortex on 15 seconds/vortex off 13 seconds" 10 times, it is repeated 30 times.
g	Reset to Channel 2	Set UV detector on with measurement setup at 301 nm.

Table 4.5.2: Solvent and reagent preparation for the ABI 433 A peptide synthesizer. The respective amino acid derivatives are separately weighted into their cartridges.

No.	Solvent/Reagent
1	Piperidine
2	0.45 M HBTU in DMF
3	2 M DIEA in NMP
4	Dichloromethane (DCM)
5	N-methyl-2-pyrrolidone (NMP)
6	Methanol
7	0.1 mmol resin
8	Fmoc-AA derivative

Table 4.5.3: ABI 433 A peptide synthesizer sequences for the synthesized peptide IL8[12-20], IL8[55-60], IL8[11-23], IL8[55-72], rSMN[37-57], and rSMN[38-57]. Modules are described with a one-letter code and are listed in the following table. Utilized resins were PS-PHB-amino acid derivative Fmoc-protected media with corresponding C-terminal amino acids of the respective sequence.

Cycle	Name	Modul-Series	No. of Repetitions
1	Complete Wash	E, c, D	1
2	Single Couple	B, b, A, D, E, F, f, d, i	8
3	Final Deprotection	B, b, I, D, c, c	1

4.6 Protein Digestion

Trypsin or chymotrypsin were used to digest proteins for sequence analysis via mass spectrometry and epitope extraction. Both enzymes show optimal activity at pH 7 - 9. Trypsin cleaves at the C-terminal side of lysine and arginine, whereas chymotrypsin cleaves mainly at the C-terminal side of phenylalanine, tryptophan, threonine, leucine and at a lower activity after methionine, alanine, glutamic acid, and aspartic acid. Recommended enzyme-to-protein ratios range from 1:200 to 1:20 (w/w) and depend on the protein stability (chapter 2.1.8).

4.6.1 Preparation of cysteine-rich proteins for in-solution digestion

Proteins were dissolved/diluted in 100 mM ammonium bicarbonate (AmBic; pH 8) to a final concentration of 0.1 mg/mL. To reduce the disulfide bonds, 2 µL of 100 mM dithiothreitol (DTT) was added to 100 µL of the 0.1 mg/mL protein solution and incubated at 95 °C for 20 minutes. After cooling to room temperature, 4 µL of a 1 M iodoacetamide (IAA) solution in MQ was added and incubated for one hour in the dark. Finally, 2 µL of a 1 M DTT solution was added and incubated for 30 minutes in the dark for IAA quenching. Afterwards, the alkylated proteins were stored at 4 °C (short term) and -20 °C (long term) or used immediately. Preparations of larger amounts for the digestions were scaled up to 1 mL (0.1 mg/mL) protein solutions.

4.6.2 In-solution digestion of proteins at standard conditions

To 100 µL of a 0.1 mg/mL alkylated protein solution, trypsin or chymotrypsin were added in an enzyme-to-protein ratio of 1:20 (w/w) (1 µL; 0.5 mg/mL), and incubated at 37 °C for 3-20 hours. For quenching the enzyme, 1 µL of concentrated HCl was added. Analysis by MALDI-tof MS was performed immediately, or the samples were stored at -20 °C. Different enzyme-to-protein ratios and variations of the incubation time are indicated in the respective results section.

4.6.3 In-solution digestion of proteins at high pressure

The Braocycler 2320 EXT (Table 4.2.1) was used for high-pressure digestion and utilized pressure cycling technology (PCT). The sample is filled into a “Pressure-Cycle-Technology” (PCT) tube that withstands the high pressure created by pumping water into the pressure chamber of the instrument. High pressure (max. 45 kpsi; 3102 bar) was maintained for an adjustable time, and then the chamber was released to atmospheric pressure. One high and low-pressure phase forms one cycle, and 1 - 300 cycles are used during digestion.

100 µL of a 0.1 mg/mL solution of alkylated protein with trypsin or chymotrypsin (1:20 (w/w) enzyme-to-protein ratio) was filled into a PCT tube and put into the pressure chamber of the Braocycler 2320 EXT. The adjustable parameters like temperature, cycle mode (pressure time on/pressure time off), number of cycles, and pressure were adjusted for each enzyme-protein pair. The limits for all parameters are listed below (Table 4.6.1). Different enzyme-to-protein ratios and variations of the incubation time are indicated in the respective results section.

Table 4.6.1: Barocycler settings for trypsin and chymotrypsin.

Enzyme	Temperature (°C)	Pressure (kpsi)	Pressure time on/pressure time off (s/s)	Number of cycles
Trypsin	37 - 50	20 - 35	50/10	15 - 300
Chymotrypsin	37 - 50	25 - 45	50/10	15 - 300

4.6.4 In-gel digestion of proteins

The protein of interest was separated by SDS-PAGE. The resulting band was cut out from the gel with a scalpel and diced into small pieces, that were transferred into a microcentrifuge tube (MCT). 200 µL of MQ was added, incubated for 5 minutes, and then removed. Subsequently, the gel was incubated with 200 µL AmBic : ACN (1:1 (v/v)) for 10 minutes. After removing the AmBic : ACN solution, 100 µL of ACN was added, and the mixture was incubated for 5 minutes. Again, the ACN was removed, and the gel pieces were dried under reduced pressure in a concentrator at 45 °C for 5 minutes. 30 µL of 10 mM DTT in 50 mM AmBic was added to the gel pieces, followed by 45 minutes of incubation at 56 °C. The MCT was cooled to room temperature. 30 µL of 100 mM IAA in 50 mM AmBic were added and incubated for 45 minutes in the dark. Afterwards, washing with 200 µL of MQ, 200 µL (1:1) AmBic : ACN, 100 µL ACN, and drying in the concentrator was repeated as described above. 30 µL of 0.02 µg/µL trypsin solution in 50 mM AmBic with 10 % ACN was incubated with the gel pieces for 30 minutes at room temperature. After adding 30 µL of 50 mM AmBic, the suspended gel pieces were incubated at 37 °C overnight. The next day, 1 µL of formic acid was added, and the supernatant was collected in another MCT. Twice 50 µL of 50 % ACN with 0.1 %TFA were incubated with the gel pieces for 45 minutes, and the supernatant was added to the previous one. The gel was incubated with 100 µL 90 % ACN with 0.1 % TFA for 10 minutes in the last extraction step. All supernatants were pooled and dried in the concentrator at 60 °C for 10 - 30 minutes under reduced pressure. Finally, the extracted digestion mixture was analyzed by MALDI-tof MS.

4.6.5 Deglycosylation of N-glycosylated proteins

Peptide-N-Glycosidase F (PNGF) digestion of whole proteins was carried out with 1 µL aliquots of (10 u/µL) PNGF solution (Table 4.1.2) added to 100 µg of recombinant GAA (0.5 mg/mL) in 50 mM ammonium hydrogen carbonate (pH 8). The reaction mixture was incubated at 37°C for 18 hours, and the deglycosylation reaction was quenched by freezing at -20°C.

Alternatively, 10 µg of digested protein were deglycosylated directly after proteolysis without any work-up. 1 µL (10 u/µL) PNGF was added to the prepared alkylated peptide mixture, which was then incubated for 4 h at RT and frozen before MS analysis. The deglycosylation efficiency was analyzed by SDS PAGE and mass spectrometry.

4.7 Affinity Chromatography and Mass Spectrometry

Epitope Extraction and Excision are affinity chromatography-based methods combined with mass spectrometry (MS) used for epitope identification, which was extensively discussed in the introduction (chapter 2.1.5).

4.7.1 Affinity column preparation

The used microcolumns had a bed volume of 500 µL and an outlet filter with a 10 µm pore size. Washing steps are described as column volumes (CV), and the washing was done by manual pipetting and gravity or centrifugal flow (Table 4.1.1). Three different column materials were tested and compared: (a) CNBr-activated sepharose, (b) Tentagel M NH_2, and (c) POROS EP. The difference in the experimental procedure was the column media preparation. After the addition of the ligand, all further steps were the same.

Column media preparation

(a) 30 mg of CNBr-activated sepharose was incubated with 0.5 mL of 1 mM HCl for 15 minutes at room temperature and washed with 5 CV of washing buffer and 5 column volumes of coupling buffer (Table 4.1.1).

(b) 90 mg Tentagel M NH_2 was washed with 10 column volumes of washing buffer followed by incubation with 5 % glutaraldehyde in water (v/v) for 2 h. Afterward, it was washed with 3 CV of washing buffer and 3 CV of coupling buffer (Table 4.1.1).

(c) 5 mg POROS EP was washed with 10 CV of coupling buffer (Table 4.1.1).

Ligand immobilization

Each column medium was incubated with ligand (20-50 µg antibody) in 300 µL of coupling buffer (Table 4.1.1) for 3 h on a shaker at RT. Afterwards, the column was washed with 5 CV of washing buffer and 5 CV of blocking buffer and was incubated in blocking buffer (Table 4.1.1) for 2 h at RT. After washing with 5 CV of washing buffer and 10 CV of 50 mM AmBic buffer (Table 4.1.1), the column was stored in AmBic buffer at 4 °C until later use.

Control column preparation

The procedure for column media preparation was carried out with the coupling buffer (Table 4.1.1) containing no antibody in the ligand immobilization step. Afterwards, the column was washed with 5 CV of washing buffer and 5 CV of blocking buffer (Table 4.1.1) and incubated with it for 2 h. Final wash steps with 5 CV of washing buffer and 10 CV of 50 mM AmBic buffer (Table 4.1.1) and columns were stored as described above.

4.7.2 Protein and Epitope Extraction from an Affinity Column

The following protocol was applied to each column material, and changes to either buffer composition, additives, or extent of washing are described in the respective results sections. 10 - 30 µg of protein / digested protein in 50 mM AmBic or PBS buffer were pipetted in the respective micro-column with/without immobilized antibody and incubated for 3-20 h at RT under gentle shaking. The column was washed with 15 - 40 CV of 10 mM AmBic or PBS buffer. The last washing step consisted of 3 CV of 10 mM AmBic followed by elution of specifically bound protein/peptides with 2 CV of 0.1 % TFA in MQ. The supernatant with protein/digested protein, washing fractions (especially the last washing fraction), and the elution fraction were collected in MCTs for MS analysis. Before MS analysis, the fractions were concentrated at 45 °C in a concentrator under reduced pressure until 20 - 40 µL remained. If the supernatant or the last washing step contained high salt concentrations or other additives, the samples were desalted via C_{18}-ZipTips after the concentration step.

4.7.3 Epitope Extraction of biological samples

The experimental setup was similar to the epitope extraction (chapter 4.7.2), but sample preparation before digestion was necessary. Briefly, the whole blood cell lysate samples were received from the University Hospital in Gießen from the group of Prof. Dr. med. A. Hahn. The samples were purified with 10 kDa MWCO spin-filters (chapter 4.3.1), and additional standard digestion was followed according to chapter 4.6.2.

4.7.4 Epitope Excision from an affinity column

The following protocol was applied to each column material, and changes to either buffer composition, additives, or extent of washing are described in the respective results sections. 10 - 30 µg of protein in 50 mM AmBic or PBS buffer were pipetted into the microcolumn with/without immobilized antibody and, under gentle shaking, incubated for 3-20 h at RT. The column was washed with 10 - 20 CV of 10 mM AmBic or PBS buffer. 250 µL (2 µg/mL) trypsin in 50 mM AmBic was added to the column. After incubation at 37 °C for 3-20 h, 15-40 CV

of 10 mM AmBic or PBS were used for washing. The last washing step consisted of 3 CV of 10 mM AmBic followed by elution of specifically bound peptides with 2 CV of 0.1 % TFA in MilliQ water. The supernatant with protein, washing fractions (especially the last washing fraction after trypsin treatment), and the elution fraction were collected in MCTs for MS analysis. Before MS analysis, the fractions were concentrated at 45 °C in a concentrator under reduced pressure until 20 - 40 µL remained. If the supernatant or the last washing step contained high salt concentrations or other additives, the samples were desalted via C_{18}-ZipTips after the concentration step.

4.8 Surface Plasmon Resonance Spectroscopy

The SPR-based biosensor used in this work consisted of a Kretschman configuration with various coatings of the use biosensor chips, described in the following chapters.

4.8.1 Instrument specifications

The SPR instrument used for all experiments was an SR7500DC SPR system from Reichert Technologies (Table 4.2.1) equipped with a syringe pump SR8500 of 250 µL, enabling flow rates between 0.1 - 3000 µL/min. The autosampler SR8100 allows sample injection with 100, 250, and 500 µL loop sizes. Finally, the SR7500DC SPR system utilizes a 2-channel fluidic system in serial connection (Figure 4.8.1). The fluidic system allows the analysis of the same sample injection over the sample and reference channel for optimal data referencing. Furthermore, the instrument manufacturer claims a measurable affinity range between 1 mM - 1 pM, low noise of 0.05 µRIU, and low drift of 0.01 µRIU/min with a high sensitivity that allows the measurement of molecules as small as 100 Da. Biosensor chips used in this work consisted of gold-coated glass slides (Table 4.1.3). The glass slide dimensions are 0.9 x 12 x 12 mm (thickness/length/width) with a 50 nm thick gold layer and a chrome oxide binding layer between the glass and gold. Surface functionality consists of a customized self-assembled monolayer, as described below. The SPRAutolink software was used for data acquisition, and the TraceDrawer software from Reichert Technologies was used for data processing.

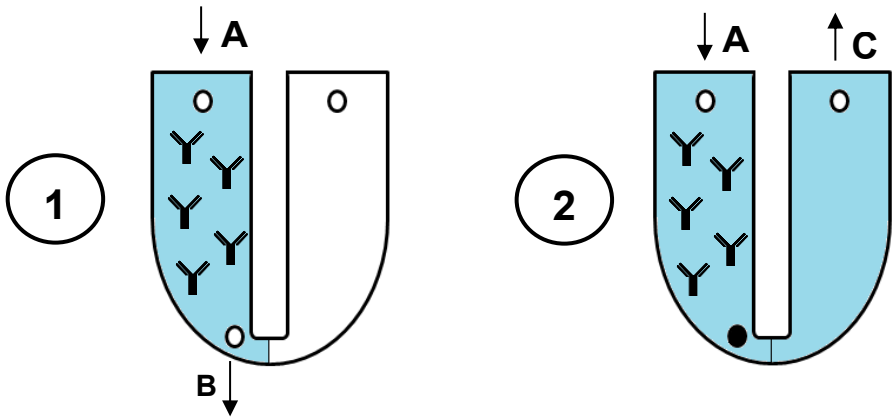

Figure 4.8.1: Scheme of the flow cell utilized by the SR7500DC SPR system from Reichert Technologies in serial mode. Two flow paths can be selected: (1) only through the first channel via inlet A and outlet B when the channel valve B is opened. The first channel is the sample channel because the immobilized ligand sits there. (2) through both channels consecutively with a closed valve B for outlet at point C. Therefore, the second channel is the reference channel without an immobilized ligand.

4.8.2 Ligand Immobilization

In general, the immobilization comprises 3 steps: (1) chip preparation, (2) immobilization of the bivalent monolayer, and (3) immobilization of the ligand on the chip. In a few cases, a pre-functionalized chip (with dextran) was purchased, and steps (1) and (2) were not necessary.

Steps (1) and (2) were performed outside of the instrument (Figure 4.8.2). A new or previously used chip (12 x 12 x 0.9mm; Sofchip, USA; Cat. 1000003-3) was rinsed with 70 % ethanol and M. Afterwards, the chip was incubated 5 times in a 2:1 (v/v) mixture of concentrated sulfuric acid (H_2SO_4) and hydrogen peroxide (H_2O_2) for 5 minutes and rinsed with MQ between incubations. Then, the chip was rinsed with MQ / 70 % ethanol and dried under a nitrogen (N_2) jet. 5 mL (1 mg/mL) of MHDA ($HS(CH_2)COOH$) dissolved in ethanol (EtOH) was added to the dry chip in a glass vessel. The chip was incubated on a shaker for 18 h at room temperature. The next day, the chip was again rinsed with MQ and 70 % ethanol and dried under a nitrogen jet. The functionalized chip was then stored at 4 °C or was immediately used.

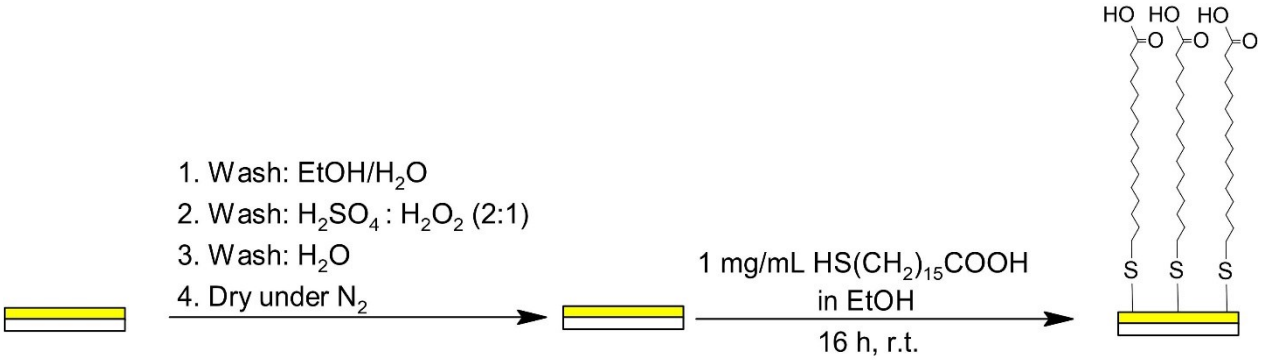

Figure 4.8.2: Scheme of the biosensor chip preparation steps for generating a self-assembled monolayer (SAM) of 16-mercaptohexadecanoic acid on a gold surface.

Step (3) was carried out in the instrument. For this purpose, the chip was placed on top of the prism and underneath the flow cell. For ligand immobilization, a 250 µL-loop was used with a flow rate of 25 µL/min; if not otherwise indicated, the complete loop volume was injected. The immobilization happened while the sample flowed over the chip (association phase). Afterwards, the running buffer flushes out all unbound ligands (dissociation phase). The association and dissociation phases were seen for every injection. After each sample injection, the loop and needle were washed twice with 500 µL flow buffer (PBS; Table 4.1.1). Two different ligand immobilization methods were applied: (a) one leading to a covalent, randomly oriented immobilization of proteins/antibodies/aptamers on an MHDA or dextran chip and (b) another one leading to covalent oriented immobilization of antibodies on an MHDA chip employing protein G (Figure 2.1.6).

For (a) the covalent, randomly oriented immobilization, the sample and reference channel were activated by injection of 20 mg/mL EDC and 5 mg/mL NHS in MQ (association: 7 min.; dissociation: 5 min.; 25 µL/min.; 175 µL), followed by injection of the ligand at a concentration between 4 - 200 µg/mL in 30 mM sodium acetate buffer pH 5 (assssociation: 10 min.; dissociation: 5 min.; 25 µL/min.; 250 µL) only over the sample channel. 1 M ethanolamine (pH 8.5; association: 10 min.; dissociation: 5 min.; 25 µL/min; 250 µL) was injected twice over both channels to block unreacted, activated carboxyl groups.

For (b) the covalent oriented immobilization, 200 µg/mL protein G in 30 mM sodium acetate buffer at pH 5 (association: 10 min.; dissociation: 5 min.; 25 µL/min.; 250 µL) were immobilized in random orientation with surface activation and blockage as described above. After surface blocking, 4 - 100 µg/mL antibody in PBS were injected (associtation: 25 min.; dissociation: 8 min.; 10 µL/min; 250 µL) only into the sample channel. For covalent antibody conjugation to the protein G, 30 mM dimethyl pimelimidate (DMP) in 0.2 M sodium borate was injected (association: 25 min.; dissociation: 8 min.; 10 µL/min; 250 µL) only into the sample channel. For

blocking of partially unreacted DMP molecules, 0.1 M glycine with 10 mM HCl was injected once (association: 2 min., dissociation:5 min.; 25 µL/min; 50 µL) into both channels or 2 injections of 1 M ethanolamine (pH 8.5; association: 10 min.; dissociation: 5 min.; 25 µL/min, 250 µL) were applied.

After both immobilization steps, the immobilized ligand was equilibrated for 3 - 18 h at 5 - 25 µL/min with PBS before any analyte injection.

4.8.3 Affinity measurements with SPR

SPR experiments for affinity determination consist of two phases: the association phase, in which the analyte solution flows through the channels, and the dissociation phase, in which only flow buffer runs into the channels without the analyte, to wash out the bound analyte molecules. Both phases are set for a specific time, specified below, and varied according to the loop size and flow rate. In the case of very slow complex dissociations, the dissociation time can be prolonged to obtain a sufficient signal for affinity and kinetic calculations. Furthermore, only the sample buffer is injected in the same way for compensation of any buffer effects. After each buffer and sample injection, a regeneration of the chip surface is followed by complete removal of the bound analyte molecules under acidic conditions to provide a free antibody for the next analyte injection. Therefore, one sample cycle consisted of one buffer injection, one sample, and one regeneration injection. This cycle was repeated for each analyte concentration. The flow buffer was PBS or PBST, and the samples were diluted in flow buffer prior to injection. Usually, a 1:2 dilution series of the sample with the flow buffer was prepared in a concentration range between 1 nM - 100 µM.

One sample cycle with a 250 µL-loop and a flow rate of 25 µL/min started with a buffer injection with 10 min. association and 5 min. dissociation, followed by sample injection with 10 min. association and 5 min. dissociation. Usually, a regeneration solution was injected for 0.5 - 2 min. association and 10 min. dissociation if the complex was not completely dissociated after the dissociation phase (seen as an upwards baseline drift). The regeneration solution consisted of 10 -100 mM glycine with 10 - 100 mM HCl or 0.1 % TFA in MQ. The measured angle shifts are expressed in response units (µRIU). The response was measured continuously throughout the experiments to detect any baseline drift during the measurements. After the measurements, binding curves were obtained by double referencing, which includes three referencing steps. At first, the sample and reference channel signals were subtracted for each buffer and sample injection. Afterwards, the buffer signal difference was subtracted from the sample signal difference to obtain response curves specific for the ligand analyte interaction. These response curves were fitted according to a 1:1 binding model or others with the Tracedrawer software from Reichert Technologies.

4.8.4 Epitope Extraction from an SPR chip by SPR/MS

For all experiments, a 250 µL-loop was used, flow rates were varied, and the flow buffer was either PBS or 10 mM AmBic buffer. The eluate from the chip was collected for further mass spectrometric measurements. The first experimental step was to dilute the digested protein in running buffer (PBS or AmBic) to a final concentration between 20 - 200 µg/mL of digested protein. The immobilized ligand was incubated with the digestion mixture at a low flow rate between 5 - 10 µL/min for 50 - 100 min. Afterward, the chip was flushed for 2 - 6 h with a flow buffer at 5 - 25 µL/min. For specific epitope peptide elution, 0.1 % TFA in MQ or 10 mM glycine with 100 mM HCl was injected for 2 - 5 min. Afterward, collected fractions were concentrated in a vacuum concentrator at 45 °C, or a C_{18}-ZipTip was used for sample desalting and concentrating. Each fraction was then analyzed by MALDI-tof MS and, prior to those measurements, stored in the freezer at - 20 °C.

4.9 Websites and parameters for in-silico B-cell epitope predictions

The prediction tools are presented in chapter 2.1.3, and used parameters for each are described here (Table 4.9.1). DiscoTope-2.0 and BepiPred-2.0 tools needed no additional parameters or prediction threshold adjustments and were used as accessed on their websites.[237,238] SEPPA-3.0 needed the setting of a prediction threshold, which was set to 0.089 by selecting the antigen type as "secreted" and "Homo".[239] BCEPS was the tool with the most adjustable features. Here, the SVM algorithm was selected with specified epitope size (standard 16 amino acids with a threshold of 0.7), the output was set to "extended B-cell Epitopes", and epitope features like glycosylation, flexibility, accessibility, and hydrophobicity were selected.[240] The same settings were used for all tested proteins.

Table 4.9.1: Summary of used B-cell epitope prediction tools with the corresponding link to their websites, their required input file formats, and category of epitope prediction (L = linear; D = discontinuous) are shown.

Tool	Link	Category	Input
Discotope 2.0	http://tools.iedb.org/discotope/help/	D	PDB
BepiPred 2.0	http://tools.iedb.org/bcell/	L	FASTA
SEPPA 3.0	http://www.badd-cao.net/seppa3/submission.html	D	PDB
BCEPS	http://imbio.med.ucm.es/bceps/	D/L	FASTA

5 Results and Discussion

In this work, interleukin-8 (IL8), cathepsin D (CTSD), alpha-glucosidase A (GAA), survival motor neuron protein (SMN), and their antibody/aptamer ligand interaction were investigated. At first, sample purity and identity were verified by SDS-PAGE and MALDI-tof MS measurements of intact and enzymatically digested protein. Furthermore, the digestion efficiency was tested under standard and high-pressure conditions. Afterwards, the prepared digestions were used for epitope identifications via affinity chromatography (AC) - and surface plasmon resonance biosensor chip (SPR) based epitope extraction or excision experiments. The interactions were further characterized for IL8 and SMN by experimentally determining the binding strength of the intact proteins and synthetic epitope peptides to the corresponding antibodies. The combination of information about epitope position and its binding strength to its target assists in evaluating experimental data on their plausibility and reliability. The combined data finally confirm or dismiss the identified peptides as epitopes and indicate how well they reflect the actual binding site. The found epitope peptides were also compared to the sequences predicted by freely available B-cell epitope prediction tools and have been reviewed on their usefulness for the design of epitope extraction experiments. For optimization of the SPR-based analysis, different surface modifications were tested for horse heart myoglobin (HHM), and the gained knowledge was applied to the analysis of IL8. The last chapter presents the work on an AC-based epitope extraction method for quantifying proteins via MALDI-tof MS with the SMN protein and its antibody.

5.1 Method development on interleukin-8 and mAB-I2519

The IL8/CXCL8 used in this work was produced in *E.coli* in the WG of Katja Schmitz from TU Darmstadt. It was purified via cation exchange chromatography and size exclusion chromatography (SEC), and protein identity was confirmed by Western Blot. The anti-IL8 antibody (mAB-I2519) binds and inhibits IL8, as previously discussed, and the reason for this should be investigated with the epitope characterization. The knowledge obtained by the characterization of IL8 and mAB-I2519 regarding the experimental procedures should be applied to the other investigated proteins in this work.

5.1.1 Protein characterization by enzymatic digestion, MALDI-MS, and SDS-PAGE

As a first model protein for characterization and epitope determination, the small, 72 amino acid-long human IL8 protein with no PTMs seemed ideally suited. The first step for the protein analysis was an SDS-PAGE of the recombinantly expressed IL8. The SDS-PAGE with different IL8 concentrations showed two unexpected bands (Figure 5.1.1). A band around 8.4 kDa was expected for the IL8 protein, but the band was split into two bands. Analysis of the band intensities with ImageJ indicates a sample purity of 75 %. However, only two significant signals are present, and the identity of the higher band might be an impurity, contamination, or a result of insufficient protein denaturation. Insufficient IL8 denaturation seemed possible because it is known to be very stable, and a prolonged time for the denaturation might be necessary. Therefore, contamination or impurity of IL8 in the form of differently present isoforms seemed less likely. Additionally, enzymatically digested IL8 samples were spotted on the gel to confirm complete digestion by the absence of intact IL8 protein. All atmospheric and high-pressure digestions showed no intact IL8 and impurity band, confirming that the impurity is a protein.

In the MALDI-tof MS measurement of the native IL8 (Figure 5.1.2), the expected $[M+H]^+$-peak of 8382.7 m/z was found (measured m/z = 8382.2). The second most abundant signal in the mass spectrum at m/z = 16746.1 correlates with the IL8 dimer-mass ($[2M+H]^+$ = 16746.3 m/z). Therefore, the MALDI-tof MS analysis suggests a highly pure sample. Therefore, the IL8 digestion with trypsin and chymotrypsin should cover the complete sequence.

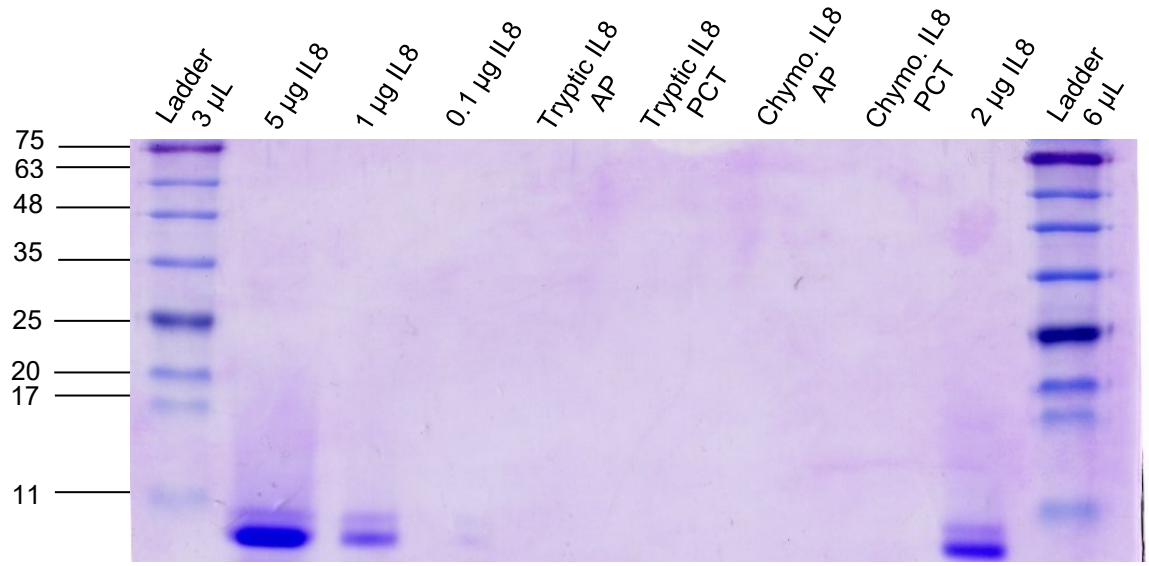

Figure 5.1.1: Tricine-SDS-PAGE of different IL8 samples on a 12 % acrylamide/bisacrylamide gel. 2 µg of tryptic and chymotryptic IL8 treated under atmospheric pressure (AP) and high-pressure cycling technology (PCT) were analyzed. 0.1 - 5 µg of native IL8 were also analyzed as references.

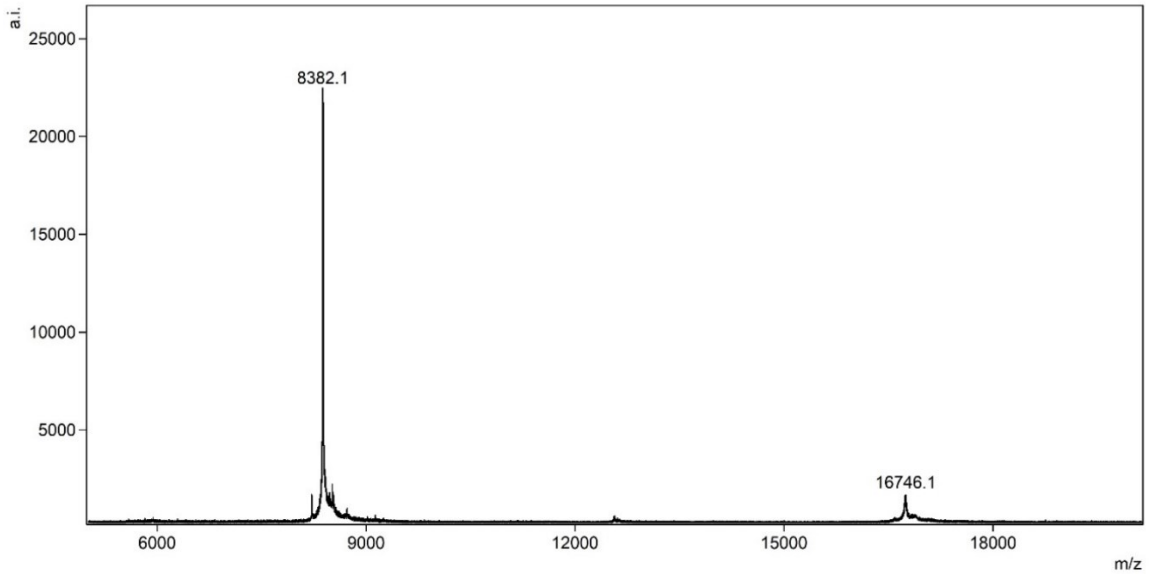

Figure 5.1.2: Native MALDI-tof MS of IL8 for protein identification. IL8 monomer $[M_{theo.} + H]^{1+}$ = 8382.7 m/z and dimer $[2\ M_{theo.} + H]^{1+}$ = 16746.3 m/z. (Method: LP; Matrix: SDHB)

Trypsin digestion of IL8 and subsequent MALDI-tof MS analysis revealed a high sequence coverage with only a few amino acids missing from the N-terminus of the protein (Figure 8.2.1, Figure 5.1.3). The protein map shows the identified tryptic and semi-tryptic peptide fragments as bars under the corresponding amino acid sequence of IL8. 97 % of the IL8 protein sequence was recovered from the digestion mixture. This high sequence coverage (SC) showed IL8 with no significant other signals for impurities or contamination. Moreover, the fully trypsin-specific peptide fragments had the highest intensities in the recorded mass spectra of 89 %, seen in the corresponding mass spectrum, peak table, and table for digestion characteristics (Figure 5.1.6; Table 8.1.1; Table 5.1.1). It demonstrated the high specificity and activity of the used trypsin. Fragments corresponding to semi-specific trypsin cleavage were also identified but with much lower intensities in the mass spectra. The protein map does not represent this information, and the mass spectra must be reviewed. The impact of semi-specific tryptic peptide fragments on the epitope extraction experiments is difficult to estimate. On the one hand, the

semi-tryptic peptide fragments create more overlapping sequences, making it easier to identify epitopes if the enzyme cleaves in the middle of an epitope. On the other hand, the lower signal intensities in the mass spectra may correlate with lower concentrations, which could make it challenging to identify these fragments in an epitope extraction experiment. The lower signal intensities in the mass spectra may also attributed to the amino acid composition. Another important criterion for the characterization of the digestion is the number of skipped cleavage sites, so-called missed cleavage sites (MCS). For the digestion of IL8 with trypsin, 14 peptide fragments without MCS and 12 peptide fragments with equal or more than one MCS were found. Many examples of particular amino acid compositions that drastically lower trypsin activities have been reported in the literature. One example in the tryptic trypsin digest is found at K23 (Figure 5.1.3), where a peptide fragment with and without an MSC was detected, indicating incomplete digestion. Other examples are seen at position K15, followed by a proline on the C-terminal site, which inhibits trypsin very strongly, and where the concatenation of lysine and arginine residues inhibits trypsin activity, as previously reported.[138,241]

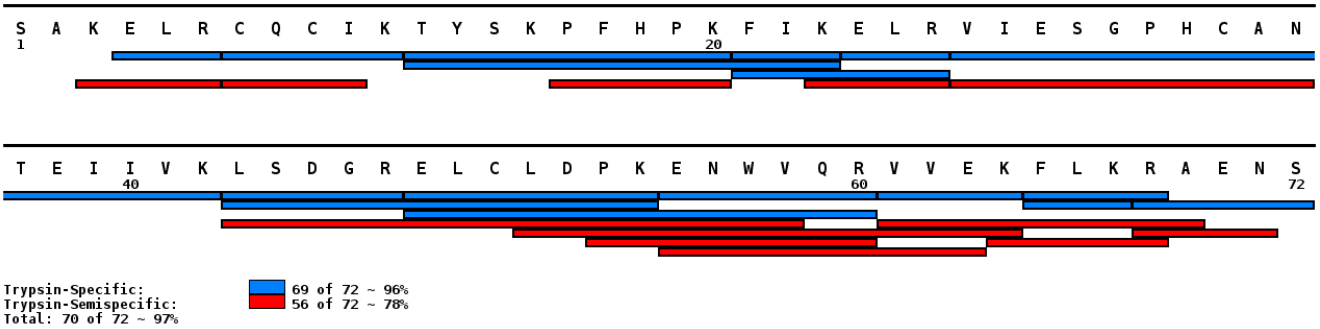

Figure 5.1.3: Protein map of the analyzed tryptic digestion of IL8 following the standard protocol. The trypsin-specific and semi-specific peptide fragments are highlighted in blue and red, respectively, and the overall sequence coverage was 97 %.

The peptide composition starts to stagnate at some point in the digestion. This stagnation can be seen as an endpoint at which a characteristic digestion pattern for a specific protein is obtained (further discussed in chapter 3.1.2). The influence of the MCSs on the epitope extraction experiments is difficult to judge, too, because smaller fragments enable narrower and more precise epitope identification. In case of too small fragments, the affinity might be lost, so that these peptides might not be extracted. Moreover, the affinity should be conserved for larger fragments. However, if they are too large, the actual epitope and essential amino acids for binding are not apparent. Here, the typical length of an antibody or B-cell epitope could be considered a good measure for digestion evaluation. The smallest identified antibody epitopes were not shorter than four amino acids, and most fragment sizes ranged between 8 and 22.[1] All peptides in the digestion with a length between 4 and 22 amino acids could be extracted for a meaningful epitope characterization. For the digestion of IL8 with trypsin under standard conditions, 22 of the 26 identified lie in this range and cover 97 % of all amino acids. Therefore, it could be possible to identify an epitope peptide in the corresponding epitope extraction in chapter 5.1.3.

For comparison, IL8 was also digested with chymotrypsin and analyzed by MALDI-MS as an alternative for the tryptic digest. Due to the much broader enzyme specificity (high-rate cleavage sites: T, F, W, L; lower rate cleavage sites: M, A, D, E)[242], it was expected that only short peptides would be detected and over-digestion could be observed. Those expectations were partly fulfilled, as seen in the protein map (Figure 5.1.4; Figure 8.2.2; Table 8.1.2). The identified peptides were in the same mass range as the tryptic ones (400 - 2000 Da), but the C-terminus of IL8 appeared over-digested. All sequence regions, except for IL8[58-72], were presented by more than one peptide fragment. All 25 peptide fragments had sizes between 4 - 22 amino acids with a sequence coverage of 93 %, making reliable epitope identification challenging. The difficulty might be the C-terminal site, if part of an epitope, because the corresponding peptides had a low intensity in the mass spectra, indicating low concentrations.

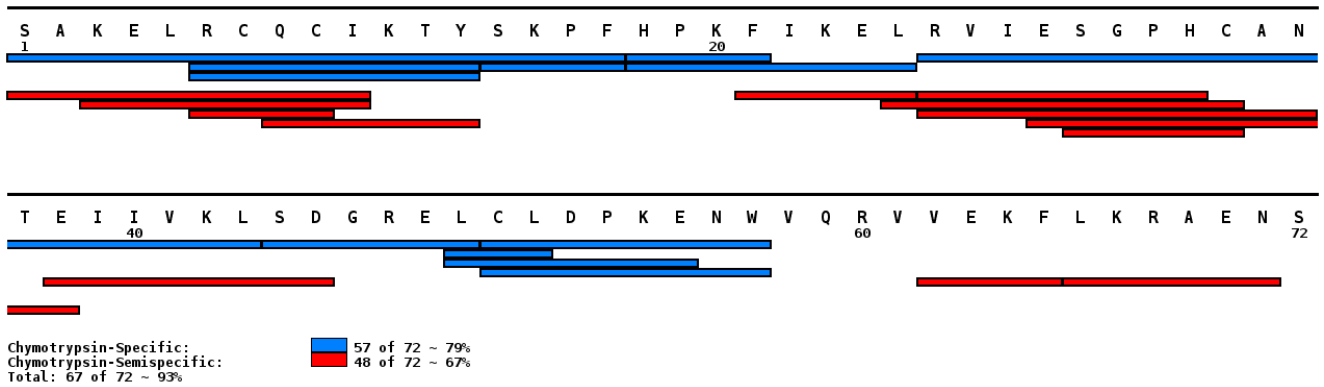

Figure 5.1.4: IL8 protein of the digestion with chymotrypsin highlighting the identified chymotryptic specific and semi-specific peptide fragments.

5.1.2 Tryptic digestion of IL8 under atmospheric and high pressure

In the present study, the standard digestion at atmospheric pressure (AP) at 37 °C was compared to the high-pressure cycling technology (PCT) digestion using standard procedures at the same temperature with the "standard enzyme" trypsin. Chemicals or solvents for protein denaturation were excluded, as they are often incompatible with MALDI-tof MS measurements (e.g., urea) or following epitope extraction experiments (e.g., ACN). For the digestion comparison regarding digestion speed and peptide digestion pattern, purification steps before the epitope extraction were avoided, and no additional chaotropic substances were added. IL8, as a small model protein, should enable easy comparison of the different digestion procedures. With respect to the identified peptides (Figure 5.1.5), both AP and PCT digestion procedures led to very similar digestion patterns.

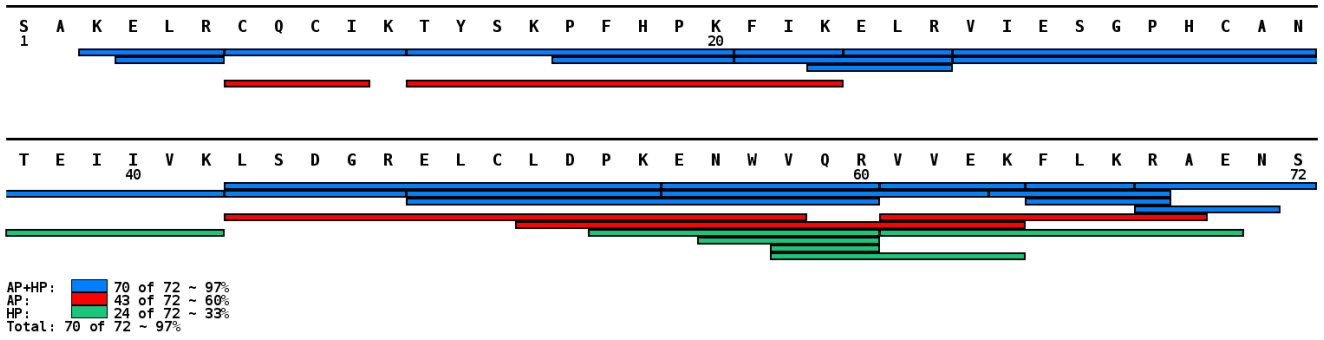

Figure 5.1.5: Protein map of the tryptic digestion of IL8 under AP and PCT conditions. Identical peptide fragments in AP and PCT digestion are shown in blue bars, red bars are peptide fragments only identified in the AP digestion, and green bars are peptide fragments only identified in the HP digestion.

Both digestions looked very similar when comparing the amount of identified peaks, specific tryptic peptide fragments, missed cleavage sites, and sequence coverage (Table 5.1.1). MALDI-tof mass spectra revealed no peaks above 2 kDa; like the protein maps, they were overall very similar (Figure 5.1.6).

Table 5.1.1: Comparison of digestion characteristics obtained under AP and PCT conditions for IL8. Incubation time was 18 h for AP-digestion and 2 h for PCT-digestion. Other parameters were identical for both digestions. MSC = missed cleavage site; SQ = sequence coverage; TS = trypsin-specific peptides.

Digestion	Peaks (No.)	Amount TS (%)	Relative Intensity TS (%)	MSC = 0	MSC ≥ 1	SQ (%)
AP	26	58	89	12	14	97
PCT	26	62	89	12	14	97

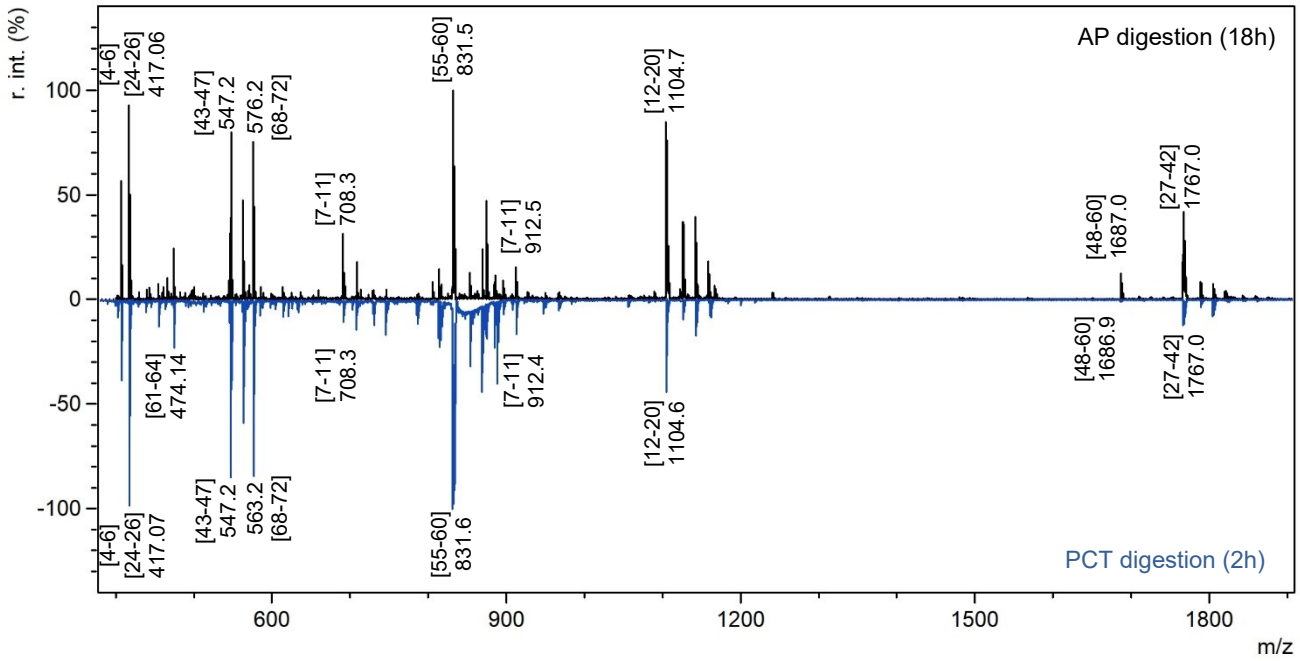

Figure 5.1.6: Mass spectra for comparing the tryptic digestion of IL8 digestion under AP- and PCT conditions via MALDI-tof MS analysis. Mass spectrum of the tryptic IL8 digestion under AP conditions for 18 h (black trace) and under PCT treatment for 120 cycles (blue trace). (Method: RP; Matrix: DHB)

The differences regarding the tryptic peptide composition were minor, especially considering the relative intensity of the differing peptides for each digestion (Table 8.1.1; Table 8.1.22). The same was observed for the trypsin-specific peptides, making 89 % of the total peak intensities in the mass spectra for both digestions. To further investigate if the PCT procedure improves the digestion rate (enzyme activity), the enzyme-to-protein ratio was reduced to 1:100, and the digestion under AP and PCT conditions was stopped after different incubation times by adding 0.1 % HCl. After 30, 90, and 180 minutes or cycles (1 cycle = 1 min.), the digestion was analyzed by MALDI-tof MS. No intact IL8 was detected for either method at any incubation time. The digestions looked very similar, with only minor differences in the MALDI-tof mass spectra (Figure 5.1.7). The more intense peaks showed a similar pattern for all incubation times. Differences were only seen in the higher mass range and for low-intensity peaks. Over time, the peaks at higher masses disappear, but no additional smaller peaks appear because corresponding smaller fragments were seen from the beginning. The progress of digestion was evaluated by the number of identified peaks and missed cleavage sites (Table 5.1.2). Over time, the number of missed cleavage sites reduced substantially, and the final digestion pattern seemed to be reached after 90 minutes for the PCT digestion as opposed to 180 minutes for AP digestion. The comparison indicates a faster digestion progression with the PCT method.

Table 5.1.2: Comparison of atmospheric and high-pressure digestion after different times (AP: 30, 90, 180, and 1080 minutes; PCT: 30, 90, 180 cycles). The number of identified peaks, the percentage of semi-/tryptic peptide fragments, and peptides with 0, 1, and more missed cleavage sites (MSCs) are shown.

Characteristics	AP-30	AP-90	AP-180	AP-1080	PCT-30	PCT-90	PCT-180
Identified Peaks	**57**	**42**	**32**	**31**	**46**	**32**	**28**
Amount TS (%)	51	50	62	52	57	47	54
Relative Intensity TS (%)	73	75	90	80	82	78	75
MSC 0	13	12	11	12	12	14	12
MSC 1	10	11	7	10	13	10	11
MSC >1	**28**	**19**	**14**	**9**	**21**	**8**	**5**
SQ (%)	100	100	100	100	100	100	100

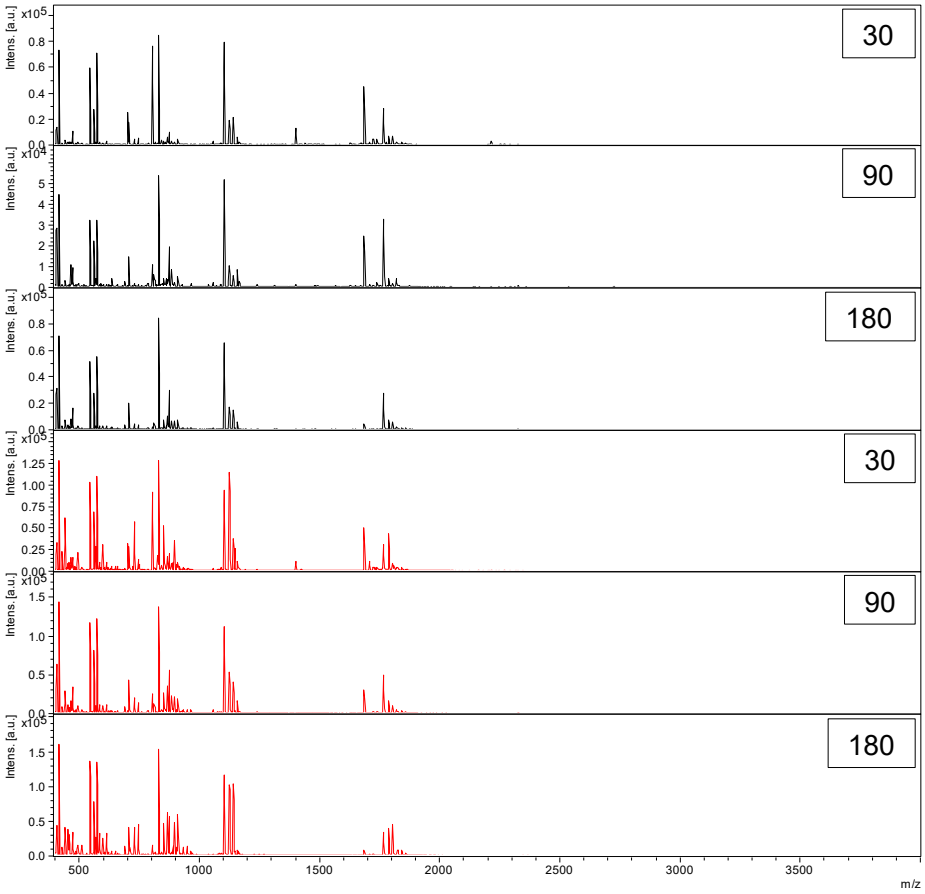

Figure 5.1.7: Modified tryptic digestion of IL8 to monitor AP- and PCT-digestion advancement over time. MALDI-tof MS spectra are shown until the mass range of 4 kDa. Complete images are shown in the appendix. (Method: RP; Matrix: DHB)

In conclusion, the PCT protocol cuts the reaction time nearly in half if the previously determined digestion pattern is used as an endpoint for digestion. The rate of digestion depends on the protein stability in the solution and the protein-to-enzyme ratio. Therefore, already reduced and alkylated IL8, with reduced stability, seems to get digested very fast under either condition, and an incubation time of 18 h under 37 °C is unnecessary.

5.1.3 Epitope identification of IL8 and mAB-I2519 by AC- and SPR-MS

The prepared mAB-I2519 antibody column based on CNBr-activated Sepharose 4B was initially tested for the protein extraction of intact IL8 to confirm its integrity. A control column with ethanolamine-blocked active sites was used, and the standard protein extraction protocol (see chapter 3.8.2) was applied to the antibody and control column. The acidic elution from both columns contained IL8, indicating a strong non-specific binding of IL8 to the sepharose 4B (see Figure 5.1.8; Figure 5.1.9; Table 5.1.3). Therefore, it was expected to identify both column binding peptides and specific mAB-I2519 binding peptides in the following epitope extractions, which could make epitope identification challenging.

Table 5.1.3: Peak table for control and mAB-I2519 affinity column fraction analysis by MALDI-tof MS. Injections of native IL8.

Experiment	Theo. Mass	Exp. Mass	Error	Peak-Identity
Control-Injection	8382.7	8382.0	-0.7	IL8
Control-Elution	8382.7	8382.5	-0.2	IL8
mAB-I2519-Injection	8382.7	8382.6	-0.1	IL8
mAB-I2519-Elution	8382.7	8381.9	-0.8	IL8

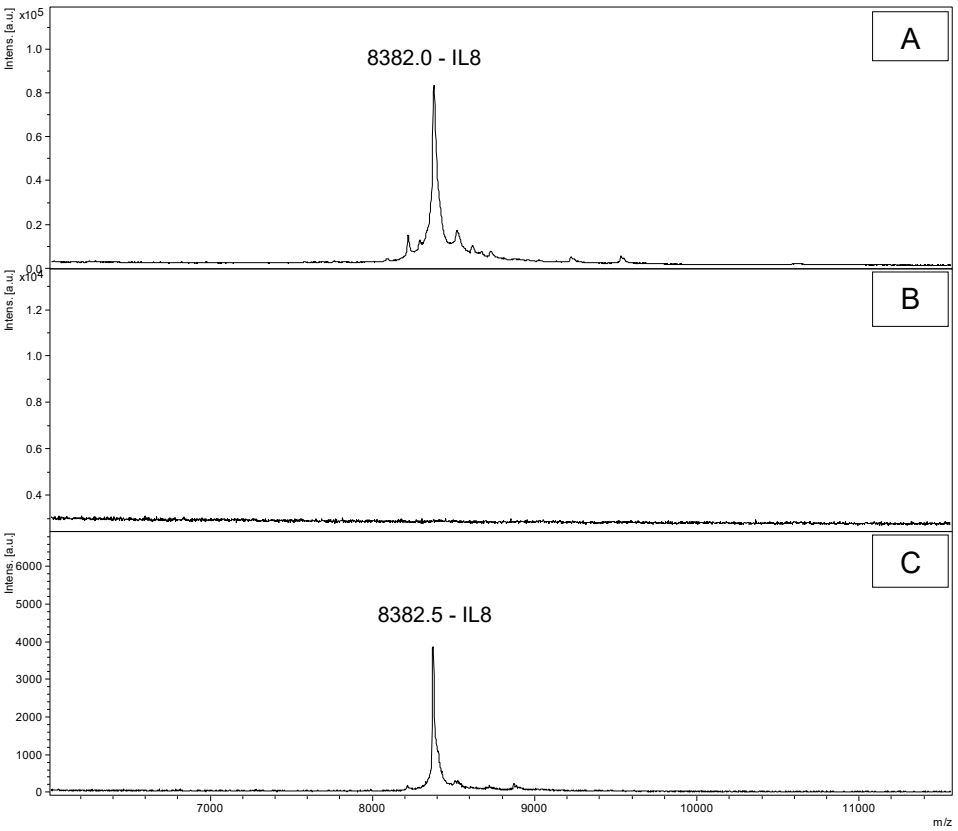

Figure 5.1.8: MALDI-tof MS spectra of the protein extraction control with ethanolamine-blocked CNBR-activated sepharose 4B and recombinant IL8. The binding buffer and washing buffer were 10 mM AmBic, and for elution of bound peptides, 0.1 % TFA was used. Spectra: (A) Intact IL8 before incubation; (B) last washing step; (C) acidified elution. (Method: LP; Matrix: SDHB)

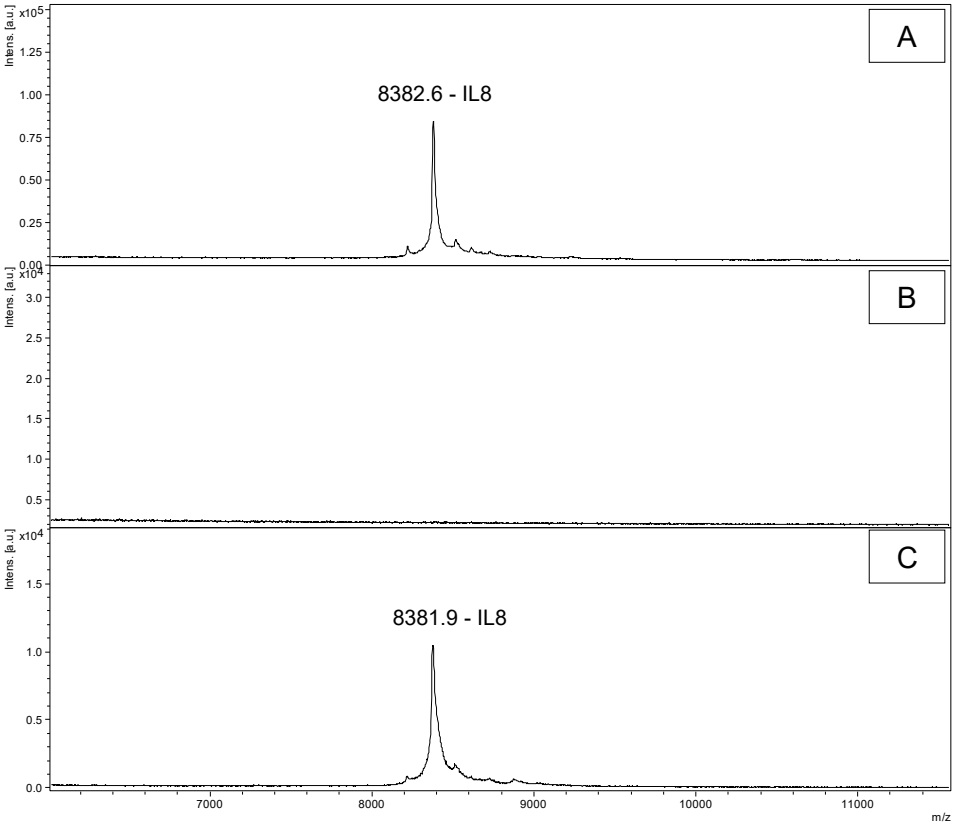

Figure 5.1.9: MALDI-tof MS spectra of the protein extraction with immobilized mAB-I2519 on Sepharose 4B and recombinant IL8. The binding buffer and washing buffer were 10 mM AmBic, and for elution of bound peptides, 0.1 % TFA was used. (A) Intact IL8 before incubation; (B) last washing step; (C) acidified elution. (Method: LP; Matrix: SDHB)

To avoid the extraction of column-specific peptides, different column materials were compared. In addition to sepharose 4B, Tentagel M NH_2 and POROS were tested for epitope extraction with IL8 digested by trypsin. Starting with the Sepharose 4B, 50 mg of column material was incubated with 10 µg tryptic IL8 for 3 hours. Washing and elution fractions were then analyzed by MALDI-tof MS (Figure 5.1.10, Table 5.1.4). The eluted fraction revealed two distinct peaks at m/z 831 (IL8[55-60]) and m/z 1104 (IL8[12-20]). Both correspond to tryptic peptides from the IL8 digestion that bind to the sepharose 4B without any immobilized antibody. A repetition of the experiment gave the same result. When using 50 mg Tentagel M NH_2 and POROS as affinity column media, both peptides (m/z 831 (IL8[55-60]) and m/z 1104 (IL8[12-20]) were also obtained after acidic elution. So, the tryptic IL8 peptides (IL8[55-60]; IL8[12-20]) bind to all tested column media. Different washing buffers were tested to prevent or reduce non-specific binding. Besides the low salt buffer, AmBic (10 mM), PBS, PBS with 0.1 % BSA, and PBS with an additional 0.5 M NaCl were tested but led to the same result (data not shown). Since no differences in the performance of the different column media and buffers were found in the control experiments, Sepharose 4B was chosen for the further epitope extraction experiments, as it was the most commonly used column media in the lab, the immobilization procedure for antibodies was well-established, and the eluted peptides had comparably low intensities indicating low number of bound peptides. 10 mM AmBic was kept as a washing buffer due to its compatibility with MALDI-tof MS.

The antibody column was incubated with 10 µg of tryptic IL8 for 3 hours, and the collected washing and elution fractions were analyzed by MALDI-tof MS (Figure 5.1.11). The last washing fraction was free of any peptide fragments, and the acidified elution showed two distinct peaks at m/Z 831 and 1104 (IL8[55-60]; IL8[12-20]; Table 5.1.4). Other peaks in the spectra represented sodium or potassium adducts of the identified peptides, and no other peaks corresponded to tryptic IL8 peptides. Repetition of the epitope extraction with immobilized antibody and tryptic IL8 yielded the same two distinct peptides. The presented results for control and antibody experiments leave an unclear picture of the epitope on IL8. However, there are indications that the two peptides still represent epitope peptides.

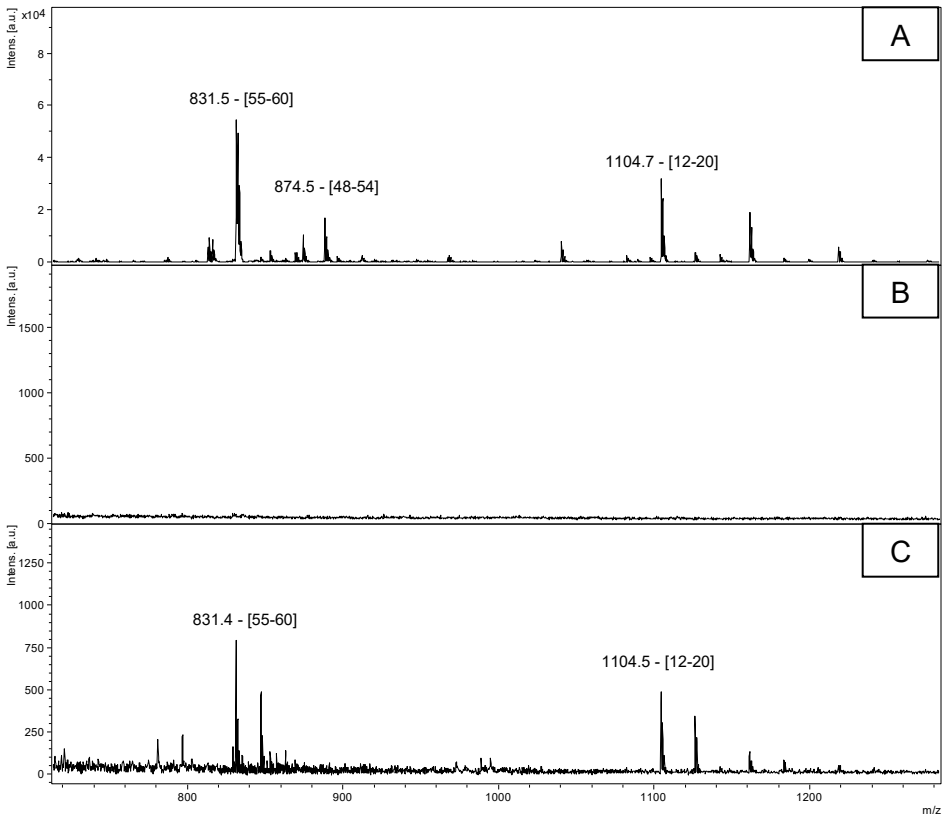

Figure 5.1.10: MALDI-tof MS spectra of the epitope extraction with ethanolamine-blocked Sepharose 4B and tryptic IL8 as a control experiment. The binding buffer and washing buffer were 10 mM AmBic, and for elution of bound peptides, 0.1 % TFA was used. (A) Tryptic digestion of IL8; (B) last washing step; (C) acidified elution. (Method: RP; Matrix: DHB)

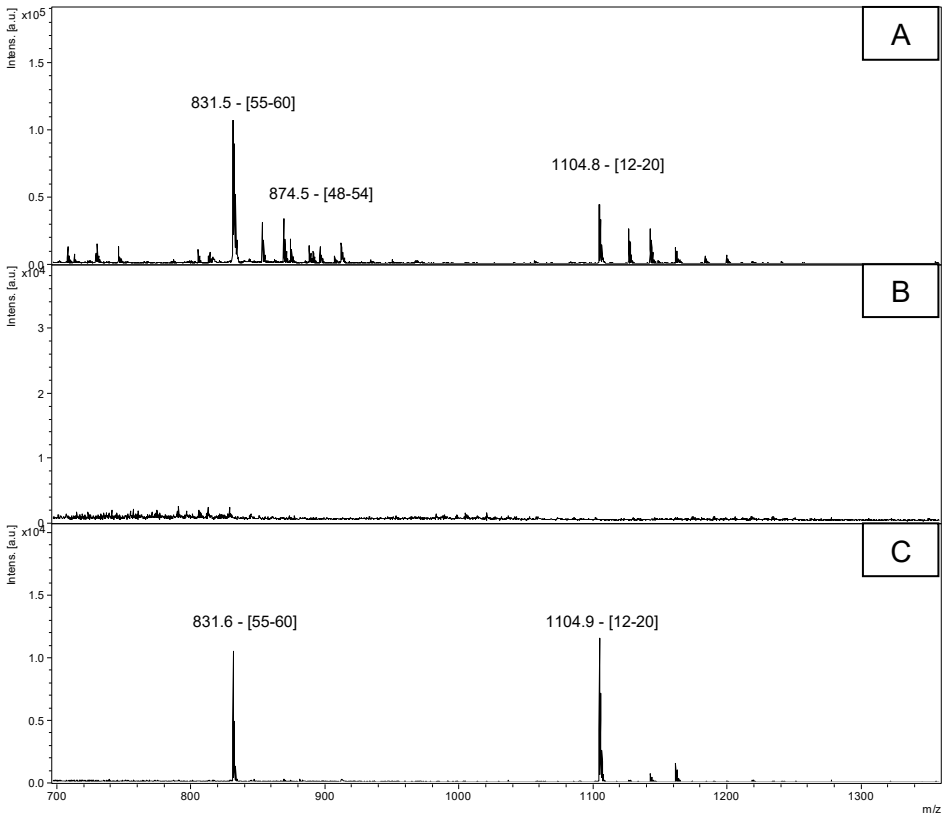

Figure 5.1.11: MALDI-tof MS spectra of the epitope extraction with mAB-I2519 immobilized on Sepharose 4B and tryptic IL8. The binding buffer and washing buffer were 10 mM AmBic, and for elution of bound peptides, 0.1 % TFA was used. (A) Tryptic digestion of IL8; (B) last washing step; (C) acidified elution. (Method: RP; Matrix: DHB)

Table 5.1.4: Peak table for control and mAB-I2519 affinity column fraction analysis by MALDI-tof MS. Injections of tryptically digested IL8.

Experiment	Theo. Mass	Exp. Mass	Error	Peak-Identity
Control-Elution	831.4	831.4	0	IL8[55-60]
Control-Elution	1104.6	1104.5	-0.1	IL8[12-20]
mAB-I2519-Elution	831.4	831.6	0.2	IL8[55-60]
mAB-I2519-Elution	1104.6	1104.9	0.3	IL8[12-20]

The comparison of signal intensities for the different elutions (see Figure 5.1.10-C and Figure 5.1.11-C) indicates much higher concentrations for the peptides from the mAB-I2519 column. However, absolute intensities for different MS experiments can vary significantly. Therefore, relative peak intensities are more reliable for comparisons. Here, the intensity of IL8[55-60] was always lower than the one for IL8[12-20], except for the elution from the mAB-I2519 column. Showing a relative increase in IL8[12-20] compared to IL8[55-60] in the elution, pointing to a specific binding of IL8[12-20] to mAB-I2519. However, no absolute statements about the epitope composition can be made at this point. Important epitope criteria are their surface accessibility to bind the antibody paratope region. The surface accessibility is demonstrated by highlighting the identified epitope peptide candidates in an available IL8 crystal structure from the PDB database with PDB-ID 3IL8 (Figure 5.1.12). It becomes evident that both sequences are located spatially close together and on the protein's surface. Therefore, both peptides potentially form a discontinuous epitope but, unfortunately, bind non-specifical to other surfaces, too.

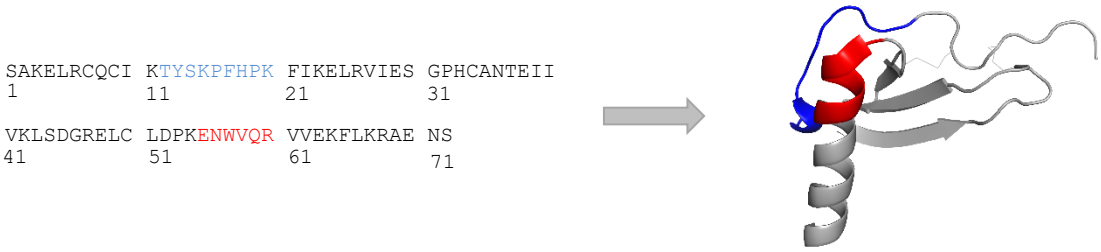

Figure 5.1.12: Amino acid sequence of IL8 with highlighted potential epitope sequences (left). Identical epitope sequences are highlighted in the crystal structure of IL8 (PDB-ID: 3IL8) in the corresponding colors. (The protein image was created with PyMOL.[25])

Another look into the list of identified peaks/peptides from the tryptic digestion of IL8 with a focus on the sequence regions IL8[12-20] and IL8[55-60] (Table 5.1.5) shows that other peptides within those regions were present, too. However, none of the other peptides were seen in any eluate. Mainly, prolonged peptide fragments were detected, which seem to show no improved affinity to mAB-I2519, and it might even be reduced because they were not detected in the acidic elutions. The prolonged peptides generally have very low intensities in the mass spectra, which indicate a low concentration, limiting their detectability in the corresponding extraction experiments. Further verification of peptides IL8[55-60] and IL8[12-20] as specific binders for mAB-I2519 was necessary. For this purpose, IL8 digestion with chymotrypsin was evaluated for an epitope extraction experiment.

Table 5.1.5: Part of the peak table from tryptic digested IL8 (Table 8.1.1) showing the identified peptides from the sequence regions IL8[12-20] and IL8[55-60] and related peptides.

S/N Ratio	Exp. Mass	Fragment	Misc.	Theo. Mass	Sequence	Error
337.0	1104.9	[12-20]	0	1104.6	TYSKPFHPK	0.3
4.8	1493.0	[12-23]	1	1492.8	TYSKPFHPKFIK	0.2
10.8	625.6	[16-20]	0	625.3	PFHPK	0.3
325.2	831.7	[55-60]	0	831.4	ENWVQR	0.3
93.7	1687.0	[48-60]	1	1686.8	ELCLDPKENWVQR*	0.2
6.0	1740.9	[51-64]	2	1739.9	LDPKENWVQRVVEK	-1
6.8	1056.8	[53-60]	1	1056.6	PKENWVQR	0.2
77.0	1158.8	[55-63]	1	1158.6	ENWVQRVVE	0.2

* cysteine residues carry carbamidomethylations.

The chymotrypsin cleavage sites in the IL8 sequence and the potential epitope sites show different possibilities for the experimental outcome. Suppose the identified tryptic peptides belong to the epitope region; in that case, peptides obtained by chymotryptic cleavage would contain only parts of these tryptic peptides and thus may not bind strongly enough to be extracted, or the smaller peptides still bind the antibody, confirming the potential epitope regions as a real epitope. The extraction of other parts of IL8 would suggest the opposite and lead to a rejection of the tryptic peptides as epitopes. Of all chymotryptic IL8 peptide fragments from the sequence regions IL8[12-20] and IL8[55-60] that were found in the digestion, no peptide fragment contained the entire length of either of the potential epitope peptides (Table 5.1.6). The epitope extraction would show if the affinity to the antibody is retained. Washing and acidic elution fractions from the epitope extraction with the chymotryptic digestion of IL8 under standard conditions (AP) were analyzed by MALDI-tof MS (Figure 5.1.13). No peptides could be detected in either eluate fraction from the control and mAB-I2519 column experiments. The repetition of both experiments led to the same result. Therefore, the expectation of chymotrypsin cleaving in a crucial sequence position for the antibody and Sepharose 4B binding seemed to be fullfilled. These results support the hypothesis that the tryptic peptides identified bind to the antibody and Sepharose 4B.

Table 5.1.6: Peak table of selected identified peptide fragments from the chymotryptic IL8 digestion (Table 8.1.2), which correspond to the potential epitope sites IL8[55-60] and IL8[12-20].

Exp. Mass	Slice	Misc.	Theo. Mass	Sequence	Error
-	[12-20]	-	-	TYSKPFHPK	-
2058.6	[1-17]	4	2059	SAKELRCQCIKTYSKPF*	-0.5
1128.9	[6-13]	0	1128.5	RCQCIKTY*	0.3
812.1	[8-13]	1	812.4	QCIKTY*	0.3
478.2	[14-17]	0	478.3	SKPF	0
528.3	[18-21]	0	528.3	HPKF	0
1011.9	[18-25]	2	1011.6	HPKFIKEL	0.3
-	[55-60]	-	-	ENWVQR	-
874.7	[49-55]	2	874.4	LCLDPKE*	0.3
1004.9	[50-57]	2	1004.5	CLDPKENW*	0.4
1061.9	[50-57]	2	1061.5	CLDPKENW*	0.4

* cysteine residues carry carbamidomethylations.

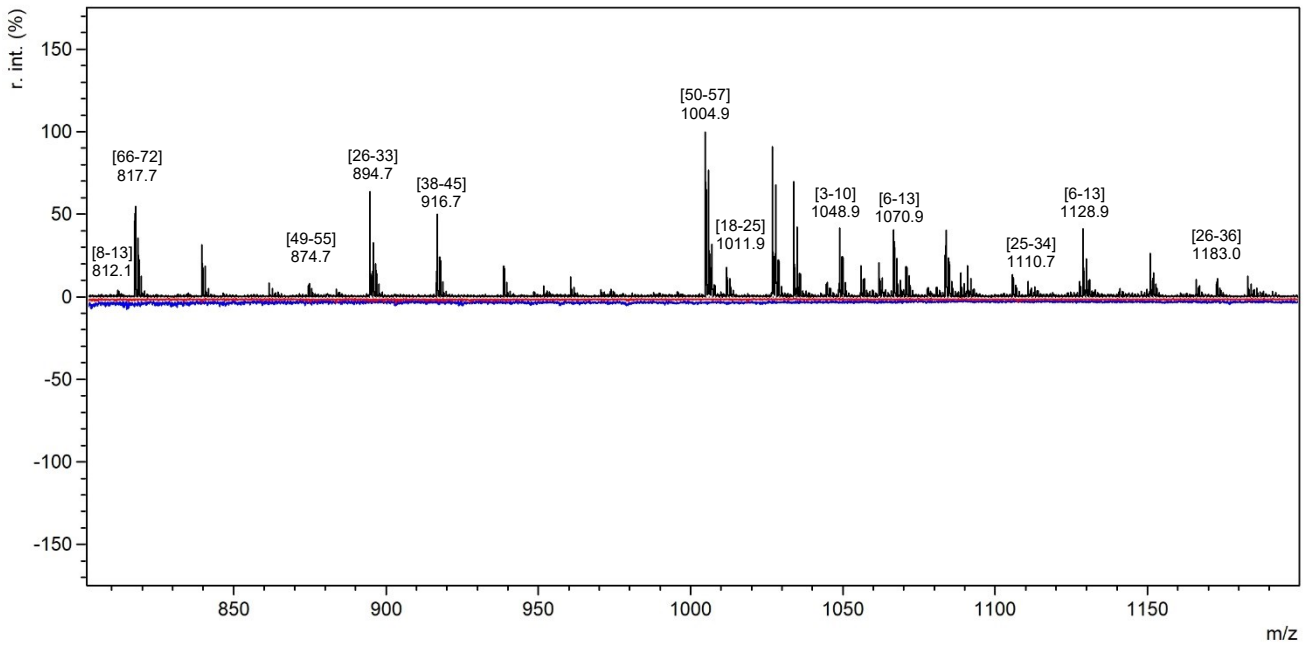

Figure 5.1.13: Overlay of the MALDI-tof MS spectra from the chymotryptic IL8 digestion (black), acidic elution from the control column (red), and acidic elution from the mAB-I2519 column (blue). The appendix lists the complete chymotryptic digestion (Table 7.1.2). (Method: RP; Matrix: DHB)

As a complementary experimental setup for epitope identification, epitope excision was attempted. For those experiments, aliquots of alkylated IL8 were incubated with the antibody-functionalized sepharose and unfunctionalized sepharose as control. Trypsin and chymotrypsin were added in separate experiments to digest those parts of the protein not protected during antibody binding. The control experiments showed no signals from the IL8 digestions with trypsin and chymotrypsin. The experiments with IL8 bound to the antibody yielded no conclusive results in that detected peaks could not be matched to a specific tryptic or chymotryptic peptide fragment from the digestion (data not shown). It is possible that the antibody was partially digested, too, and the observed peaks correlate to antibody fragments. This hypothesis could not be verified because the manufacturer did not publish the antibody sequence, which is, therefore, unknown. Because of those results, epitope excision was not further investigated for the IL8-mAB-I2519 complex.

Epitope extraction on an SPR biosensor system was tested as an alternative experimental setup. For this purpose, the SPR gold chip was functionalized with a 16-MHDA-SAM layer and decorated with mAB-I2519. Here, two antibody immobilization methods were used without and with protein G (PG) for specific antibody orientation. In a control experiment, the tryptic IL8 digestion was injected over the SPR chip without immobilized mAB-I2519. For immobilization with PG, PG was immobilized without antibodies as a control. 10 mM ammonium bicarbonate was used as a running buffer, and fractions were collected after injection (fraction F1), washing (fractions F2-F7), and acidic elution (fraction F8). Each fraction was analyzed by MALDI-tof MS. First, the results for the antibody immobilization without PG are discussed. The control experiment (see Figure 5.1.14; Table 5.1.7; Figure 8.2.35) led to two distinct peaks for IL8[12-20] and IL8[12-23], which had not been detected before. However, no peak for the IL8[55-60] was detected. The acidic eluate from the chip with immobilized antibody contained peaks for IL8[12-20], IL8[14-20], and a small peak for IL8[12-23] (see Figure 5.3.2; Table 5.1.7; Figure 8.2.36). The very low intensity for the IL8[55-60]-peak and IL8[12-20] identification in the corresponding control experiment resemble the results from the sepharose 4B experiments. One difference is seen in the elution of IL8[55-60]. For the mAB-I2519 chip, IL8[55-60] was detected until washing fraction F4 and only until F2 from the control chip. The longer retention time of IL8[55-60] on the mAB-I2519 chip suggests a stronger binding to the antibody. IL8[12-20] shows the same elution profile from the control and mAB-I2519 chip.

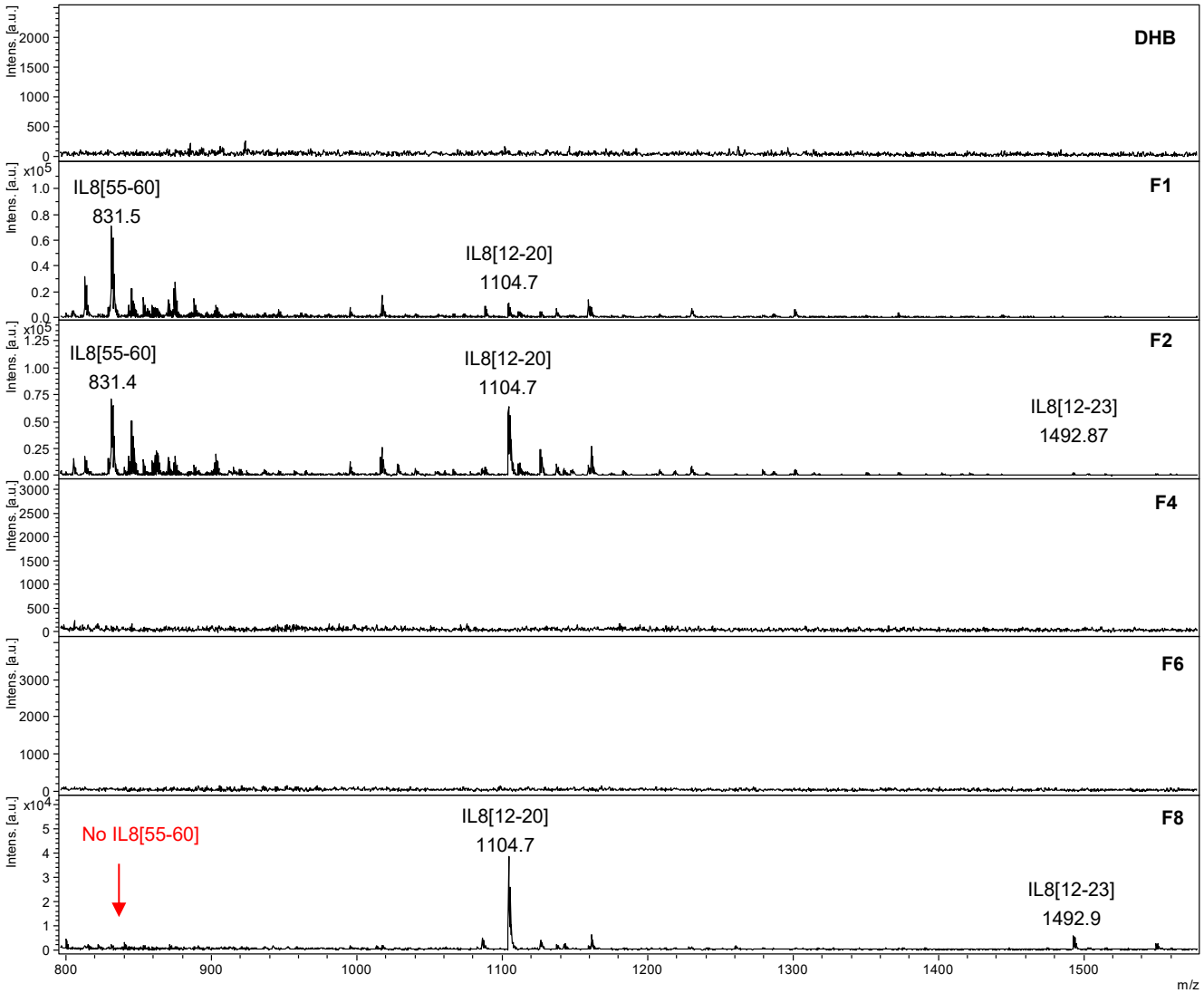

Figure 5.1.14: MALDI-tof MS analysis of collected fractions from the control experiment for the epitope extraction on the 16-MHDA chip. F1 (Injection; 60 minutes; 5 µL/min), F2-F7 (Washing; every 20 minutes; 5 µL/min), and F8 (Acidic elution; 3 minutes; 50 µL/min). All fractions were concentrated to 20 µL and for a better overview not all fractions are shown. (Method: RP; Matrix: DHB)

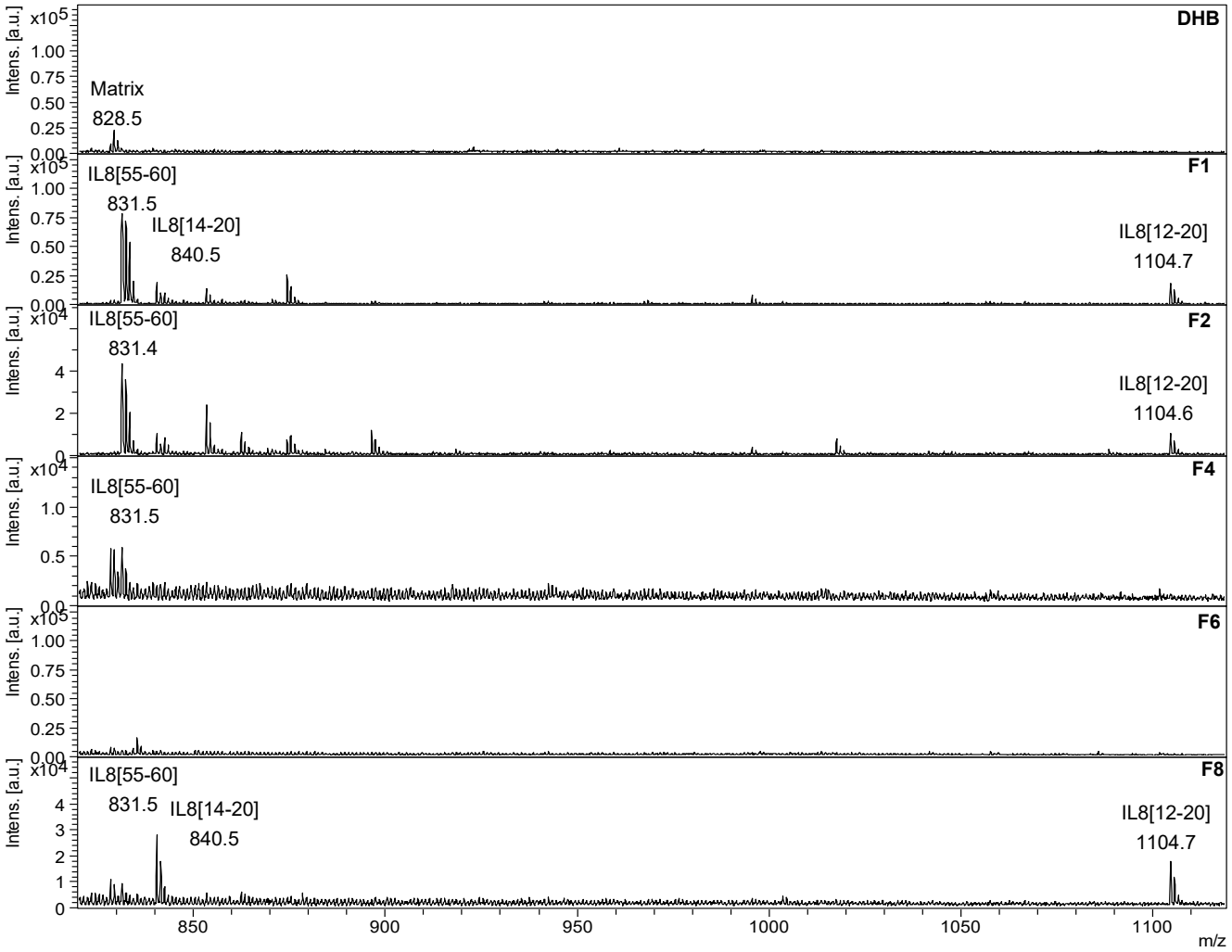

Figure 5.1.15: MALDI-tof MS analysis of collected fractions from the mAB-I2519 experiment for the epitope extraction on the 16-MHDA chip. F1 (Injection; 60 minutes; 5 µL/min), F2-F7 (Washing; every 20 minutes; 5 µL/min), and F8 (Acidic elution; 3 minutes; 50 µL/min). All fractions were concentrated to 20 µL. (Method: RP; Matrix: DHB)

Table 5.1.7: Peak table for acidic elution from control and mAB-I2519extracion on the 16-MHDA SPR chip (Figure 5.1.14; Figure 5.1.15)

Experiment	Theo. Mass	Exp. Mass	Error	Peak-Identity
Chip-Control-Elution	1104.6	1104.7	0.1	IL8[12-20]
Chip-Control-Elution	1492.9	1492.8	0.1	IL8[12-23]
Chip-mAB-I2519-Elution	831.5	831.6	0.1	IL8[55-60]
Chip-mAB-I2519-Elution	840.5	840.5	0.0	IL8[14-20]
Chip-mAB-I2519-Elution	1104.6	1104.9	0.3	IL8[12-20]

The sensorgrams from both experiments (control: Figure 8.2.35; mAB-I2519 chip: Figure 8.2.36) showed no differences between sample and reference channel in both cases. The injection was visible in the sensorgram with a corresponding increase in the baseline, but no specific difference was seen for the digestion mixture injection. The concentration of 4 µM digested IL8 protein paired with a potentially low affinity of both potential epitope-forming peptides yielded to no detectable binding event, whereas control injections with intact IL8 showed explicit antibody binding. Before testing chip surface modifications, the epitope extraction experiment was repeated with PBS as a running buffer. Control and antibody experiments showed no peptides in the acidified elutions. Again, the low affinity might explain why the antibody retained no peptides for longer, and the much higher salt concentration led to a quick washout of the related peptides. IL8, inparticular, showed high

non-specific surface binding in all experimental setups. Therefore, different chip surfaces and antibody immobilization strategies were tested for epitope determination and affinity determinations (more in chapters 5.1.6 and 5.1.7). The antibody immobilized via PG seemed a promising alternative because it should provide a much better accessibility of the immobilized antibody's paratope. The control experiment with immobilized PG (Figure 8.2.37) was carried out with 10 µg of tryptic IL8 for injection. Fractions of injection, wash, and elution were collected and analyzed by MALDI-tof MS (Figure 5.1.16 ; Table 5.1.8Table 5.1.8). A clear difference was seen between the injection (F1) and elution fraction (F6). In the injection-F1 and all other collected fractions, no IL8[12-20] was found. This was surprising because the IL8 digestion had always contained that peptide. IL8[55-60] was last seen in fraction-F3, and from elution-F6 on, no more peptides were eluted off PG. To see no retained peptides was unexpected but indicated that the PG covered the 16-MHDA-coated surface, and that the IL8 peptide fragments did not bind to the PG. Another observation was a polymeric contamination in the collected fractions, which could have arisen from tween-20 (T20). However, it was primarily seen from the PG chip preparations despite extensive washing and preparation of the instrument. The related sensorgrams (Figure 8.2.37) showed no significant binding events but indicated harsh regeneration/acidic elution conditions for injecting 0.1 % TFA in MQ by subsequent baseline drift. Finally, the control experiment revealed no binding peptides to the PG-16-MHDA chip surface, but it was unexpected that IL8[12-20] was not detectable.

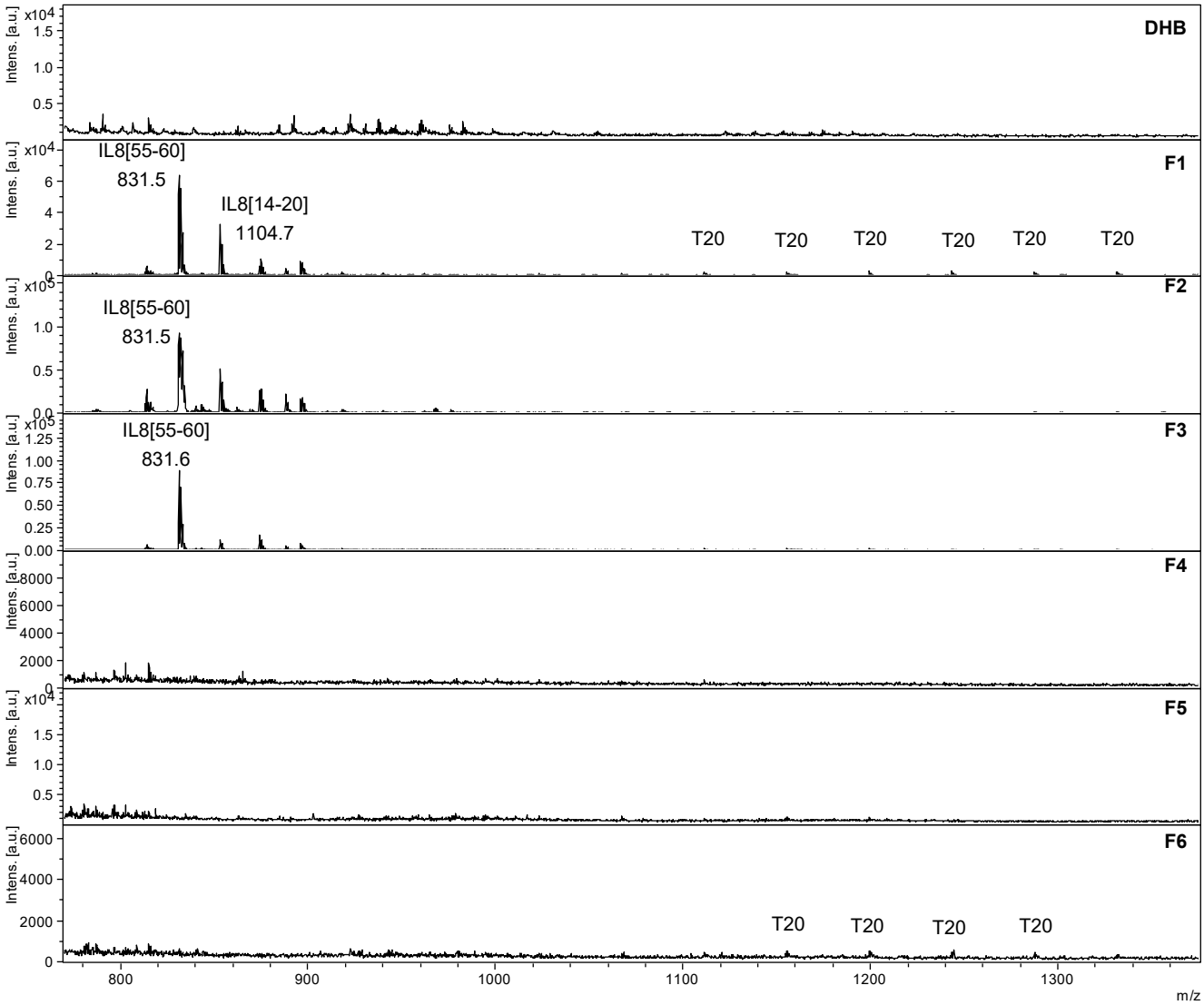

Figure 5.1.16: MALDI-tof MS analysis of collected fractions from the control experiment for the chip-epitope extraction with immobilized protein G on a 16-MHDA chip. Shown fractions F1 (Injection; 60 minutes; 5 µL/min), F2-F5 (Washing; every 20 minutes; 5 µL/min), and F6 (Acidic elution; 3 minutes; 50 µL/min) were concentrated to 20 µL. Tween-20 (T20) from a previous experiment was identified in fraction-F1 and partly in elution-F6. (Method: RP; Matrix: DHB)

Epitope extraction with mAB-I2519 non-covalently immobilized on the SPR-chip via protein G was performed likewise. Similarly, collected fractions were analyzed (Figure 5.1.17, Table 5.1.8, and Figure 8.2.37). The injection fraction-F1 and subsequent washing step fractions F2-F3 contained the same peptides as the control experiment. In the eluate, peptide IL8[12-20] is seen, and IL8[55-60] is also present with very low intensity. IL8[12-20] was not found in the injection, and the polymeric contamination was again observed. Later, the contamination source was identified as Tween-20 (TW20) from reused injection vials, which were not adequately cleaned. TW20 is frequently used to suppress unspecific surface interactions of proteins and surfaces. Therefore, it might reduce the surface binding capability of IL8[12-20], which was why it was not seen in the control experiment. TW20 might not have influenced the specific binding of IL8[12-20] to mAB-I2519 and therefore was seen in the corresponding epitope extraction experiment. Interestingly the addition of TW20 was always avoided for epitope extraction experiments because peptide signals are entirely suppressed in MALDI-tof MS measurements above a particular concentration of TW20. Besides the differences in eluted peptides during epitope extraction, the TW20 did not appear to have influenced the antibody immobilization, and the sensorgram (Figure 8.2.37) shows a reasonable immobilization rate of the antibody.

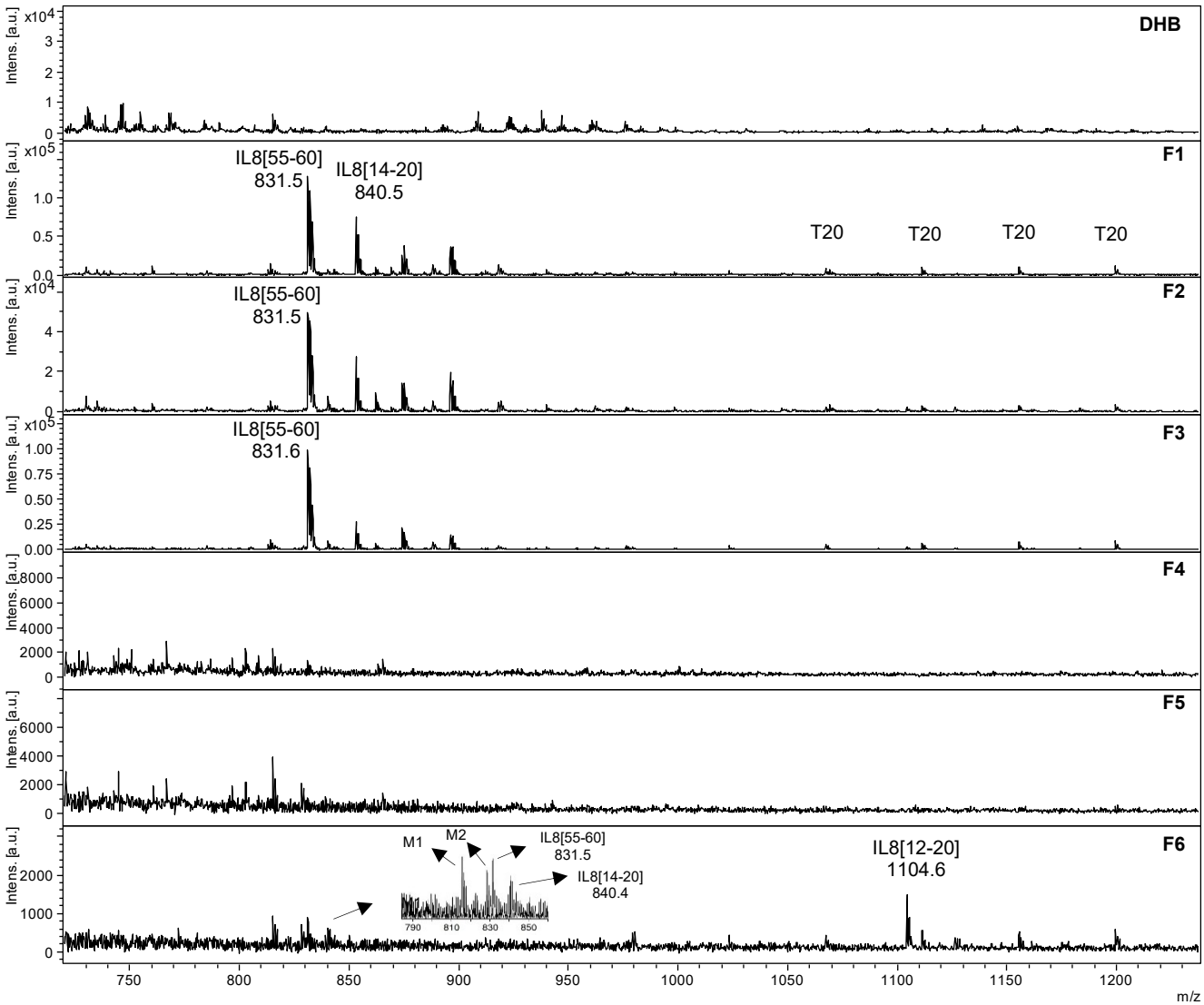

Figure 5.1.17: MALDI-tof MS analysis of collected fractions from mAB-I2519-chip epitope extraction with antibody immobilized via protein G on a 16-MHDA chip. Shown fractions F1 (Injection; 60 minutes; 5 µL/min), F2-F5 (Washing; every 20 minutes; 5 µL/min), and F6 (Acidic elution; 3 minutes; 50 µL/min) were concentrated to 20 µL. Tween-20 (T20) from a previous experiment was identified in fraction-F1, -F2, -F3, and partly in elution-F6. M1 and M2 in elution-F6 denote matrix signals. (Method: RP; Matrix: DHB)

The injection of tryptic IL8 causes a slight increase of the difference between the sample and reference channel, which indicates a binding event. This was the first time that a difference between the control and antibody chip (or column) was seen in the presented experimental setup. Still, the low intensity of IL8[55-60] might indicate that it is a fragment of a larger sequence region forming a discontinuous epitope. Indeed, it seems very likely that both protein regions (IL8[12-20] and IL8[55-60]) form a discontinuous epitope together.

Table 5.1.8: Peak table for acidic elution from control and mAB-I2519 experiment on the 16-MHDA SPR chip with immobilized protein G.

Experiment	Theo. Mass	Exp. Mass	Error	Peak-Identity
Chip-mAB-I2519-Elution	831.5	831.5	0.0	IL8[55-60]
Chip-mAB-I2519-Elution	840.5	840.4	-0.1	IL8[14-20]
Chip-mAB-I2519-Elution	1104.6	1104.6	0.0	IL8[12-20]

5.1.4 In-silico analysis of IL8 antibody epitopes

The identified IL8 epitope peptides were evaluated with the four B-cell epitope prediction tools, DiscoTope 2.0, Seppa 3.0, BepiPred 2.0, and BCEPS. The IL8 protein map (Figure 5.1.18) shows the experimentally identified epitopes and the predictions' results. At first sight, the discontinuous B-cell epitope prediction tools, DiscoTope 2.0 and Seppa 3.0, cover a much smaller sequence on IL8 as an epitope than the continuous prediction tools, BepiPred 2.0 and BCEPS. Different parameter settings for the epitope probability threshold could narrow the immunogenic regions but with the potential risk of missing some immunogenic sites. Therefore, the standard settings for the prediction tools were kept for comparison. The predictions contain parts of the experimentally identified epitope, indicating high immunogenicity in regions [12-20] and [55-60] on IL8. Assuming that the consensus of all prediction tools indicate the sequence regions with the highest immunogenicity, the amino acids H18, K20, N56, K67, and R68 of IL8 are left as best candidates for being part of an epitope. Except for K67 and R68, consensus amino acids are present in the identified epitope. Considering the overlap of at least three out of the four predictions, the protein sites [14-24], [44-46], [55-57], [60-60], [63-64], and [67-68] should also exhibit high immunogenicity.

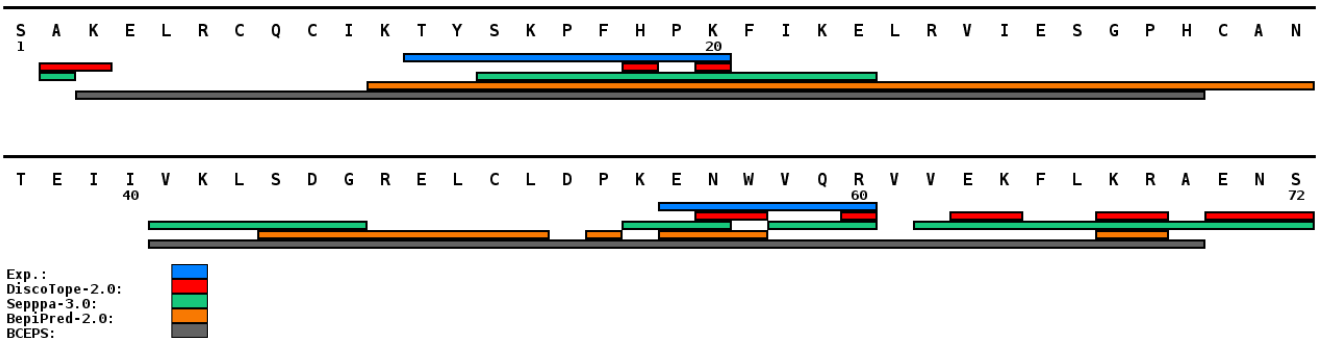

Figure 5.1.18: Protein map of IL8 with experimentally determined epitope and results from the four prediction tools DiscoTope-2.0, Seppa-3.0, Bepipred-2.0, and BCEPS.

The long overlapping regions between the consensus of the prediction and the experimentally identified epitope candidates point to a correct identification of the epitope for the IL8-mAB-I2519 complex. However, according to the prediction, region [14-24] could already be long enough to form a linear epitope. Alternatively, both peptides could form a discontinuous epitope. Comparing the potential epitope regions in the crystal structure of IL8 (Figure 5.1.19), both cases seem possible. Moreover, the identified epitope candidate [55-60] might be shortened, and the epitope is located at the N-terminus of the α-helix.

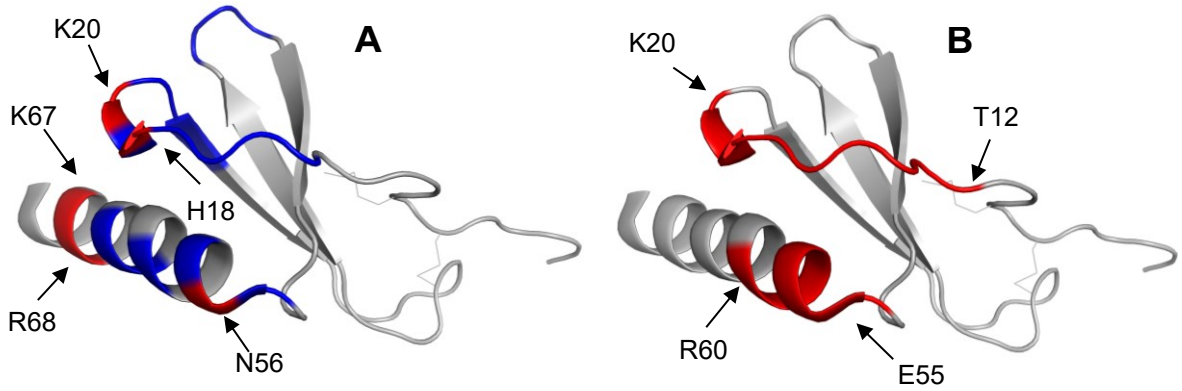

Figure 5.1.19: Identified epitopes highlighted in the crystal structure of IL8 (PDB: 1IL8). (A) shows the experimentally identified epitope in blue (B) consensus sequence of the predictions shown in red, highlighting the potentially most immunogenic amino acids. (The protein images were created with PyMOL.[25])

In principle, the epitope predictions could indicate suitable enzymes for specific protein digestions and corresponding epitope extraction experiments. Here, trypsin and chymotrypsin were used, and according to the predictions, both yield peptides that are short, leading to potentially reduced affinities that make detection in an epitope extraction experiment less likely. Therefore, digestions with Arg-C or Lys-C could have led to prolonged peptides around the potential epitopes. Therefore, the predictions could have helped in the enzyme choice and guidance of the experimental setup.

5.1.5 Epitope peptide synthesis by SPPS

As described before, the potential epitope peptides were synthesized via FSPPS with standard fmoc-chemistry, monitoring the coupling efficiency after each coupling step by measuring the absorption of the Fmoc-deprotection solution at 301 nm on an automated peptide synthesizer. The peptides IL8[12-20] and IL8[55-60] showed a constant signal for the deprotection of the fmoc-group after each step, representing good synthesis profiles (Figure 8.2.3). Resins preloaded with fmoc-protected amino acid derivatives were used; therefore, the first step of the synthesis started with deprotection. Each deprotection was repeated at least once to confirm that the deprotection was successful. A derivative of the epitope peptide IL8[55-60], IL8[55-72], was synthesized with a C-terminally extended sequence for additional affinity tests. Deprotection monitoring showed a slight drop in the absorption maxima after coupling amino acids R60 and V61 (Figure 8.2.4). However, the drop was not substantial, and a sufficient amount of the peptide should be synthesized for HPLC purification. However, in the case of a second synthesis, double coupling steps could be implemented for R60 and V61 to maximize the coupling efficiency. A common reason for reduced coupling efficiencies is the formation of secondary structures or aggregations of the growing peptide on the resin, which impairs subsequent amino acid binding. Overall, the three synthesized peptides showed reasonable synthesis profiles for further purification and characterization by HPLC and MALDI-tof MS. For IL8[12-20], the resin was preloaded with a fmoc-protected lysine derivative; for IL8[55-60], a preloaded resin with fmoc-protected arginine was used. The three peptides IL8[12-20], IL8[55-60], and IL8[55-72] were successfully purified by HPLC (Figure 8.2.5; Figure 8.2.6; Figure 8.2.7; Figure 8.2.8; Figure 8.2.9; Figure 8.2.10). The characterization by MALDI-tof MS (Figure 8.2.11) showed the expected masses for the peptides, measured from the collected and combined fractions after the purification (Table 5.1.9).

Table 5.1.9: Summary of the IL8 peptide synthesis. Chromatograms and mass spectra are in the appendix. . GT = gradient time frame; RT = retention time.

Name	Sequence	Gradient (% Solvent A)	GT (min.)	RT (min.)	Purity (%)	Calc. Mass ($[M+H]^+$)	Exp. Mass ($[M+H]^+$)
IL8[12-20]	TYSKPFHPK	90 to 70	20	12.9	97.2	1104.6	1104.7
IL8[55-60]	ENWVQR	90 to 80	25	17.8	94.1	831.4	831.3
IL8[55-72]	ENWVQRVVEKFLKRAENS	75 to 55	25	20.0	99.6	2231.2	2231.1

5.1.6 Test of antibody SPR-chip immobilization strategies with myoglobin as a model protein

The MHDA and dextran gold chips seemed to fail to analyze the mAB-I2519-IL8 interaction in all detail. The recorded sensorgrams carried artifacts from the non-specific interaction of IL8 with the chip surface, which made affinity and kinetic calculations very challenging. The analysis of the synthetic epitope peptides showed the same difficulty. Furthermore, the mAB-I2519 seemed to lose its activity comparably fast after the injection of 1 - 2 protein dilution series, and it was not easy to find a suitable regeneration solution. The antibody seemed more stable on the dextran chip than on the MHDA chip, but the non-specific surface interactions were present in both cases. The corresponding results are shown in chapter 5.1.7. The previous success with a PG-modified biosensor chip led to a more precise investigation of its performance in SPR-related affinity and kinetic analysis of IL8 and its antibody mAB-I2519. Covalent antibody immobilization was accomplished by chemical crosslinking of the antibody and PG by dimethyl pimelimidate (DMP). The test system for the immobilization optimization was a set of myoglobin–antibody pairs, commonly used as model systems in the research laboratories at the Steinbeis Center. After the initial tests of the immobilization strategy, Daria Holdschick executed the optimization experiments on the SPR-based biosensor with horse heart myoglobin (HHM) and monoclonal/polyclonal anti-myoglobin antibodies as part of her master thesis[243], and some parts of the results were used for a review article on the combination of SPR and MS.[244]

First, the HHM and a polyclonal anti-horse heart myoglobin antibody produced in goats (pAB-A150) were tested on MHDA and MHDA-PG. The cross-linking of PG and antibody with DMP was done according to Makaraviciute et al.[94], and the execution of the presented results was done by Daria Holdschick, as indicated in the corresponding figure legends. The antibody immobilization efficiency, activity, and stability were compared for both immobilization strategies. For this purpose, the crosslinking of antibody and PG via DMP had to be optimized. Therefore, a solution of 4 µg/mL pAB-A150 in PBS (250 µL) was injected with different DMP concentrations (0.4 - 30 mM) in sodium borate buffer (0.1 - 0.2 M).[243] The stability of the immobilized protein was tested by injections of regeneration solution (0.1 M glycine in 20 mM HCl). At a DMP concentration of 30 mM in 0.2 M sodium borate buffer (10 µL/min flow rate and 250 µL injection volume), nearly no baseline decrease was detected after the injection of the regeneration solution, indicating that the antibody was stably immobilized.[243] Higher concentrations of DMP could also produce a stable antibody surface but were avoided because too high concentrations could decrease antibody activity. The random antibody immobilization on MHDA via EDC/NHS at 80 and 160 µg/mL pAB-A150 was compared to 4, 80, and 160 µg/mL pAB-A150 immobilization on PG-prepared MHDA chips (Figure 5.1.20), which stayed stable after the injection of the regeneration solution.

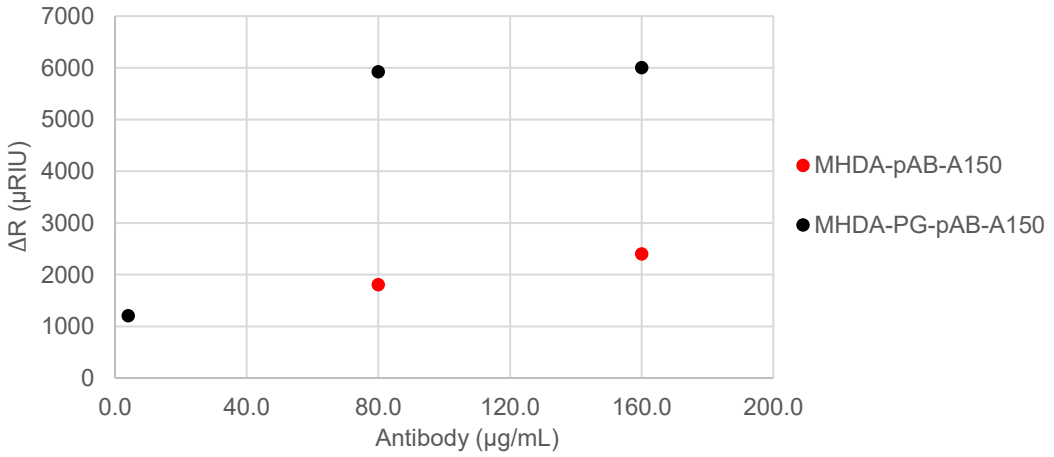

Figure 5.1.20: pAB-A150 concentrations for chip immobilization via EDC/NHS and PG/DMP represented by the shift difference of resonance units before and after antibody injection (ΔR, µRIU). The data are from experiments done by Daria Holdschick and by myself.

The response of the SPR signal was proportional to the amount of immobilized antibody, which enabled a comparison of the different immobilization levels on the differently modified chips. Both 80 and 160 µg/mL antibody concentrations seemed to saturate the chip surface. However, the PG enabled much higher antibody loadings on the chip surface, and even the low concentration of 4 µg/mL led to a detectable antibody immobilization. The immobilization via PG-DMP led to 2.5 to 3.3 times higher levels of antibody immobilization, and 4 µg/mL antibody on MHDA-PG resulted in nearly 70 % of the immobilization level obtained with 80 µg/mL on MHDA. The higher antibody densities on the surface will result in more flexibility and space for experimental adjustments. While the amount of immobilized antibody was important, the activity of the antibody after immobilization was decisive. Therefore, injections of HHM should show how much of its antigen the immobilized antibody could bind. As the immobilization level of 80 µg/mL pAB-A150 on an MHDA-chip was comparable to that of 4 µg/mL pAB-A150 on MHDA-PG, chips prepared with these concentrations were used for comparison. HHM was injected in concentrations between 0.16 - 10 µM on both chips, and the resulting sensorgrams were analyzed by fitting the data to a 1:1 binding model with the software Tracedrawer (Table 4.2.2) to obtain the kinetic constants k_{on} and k_{off} from which the K_D was calculated. The MHDA chip showed an R_{max} of 40 µRIU for a 2.5 µM HHM injection and no further increase with 5 and 10 µM HHM. The MHDA-PG chip showed an R_{max} of 48 µRIU for 2.5 µM and an R_{max} of 66 µRIU for 10 µM HHM. Despite the somewhat lower antibody amount on the MHDA-PG chip, the antibody surface could bind considerably more HHM. This confirms the expectation that an antibody immobilized in an oriented fashion should exhibit higher activity than a randomly oriented one. The quality of the produced data was better for the MHDA-PG chip, especially for the complex dissociation. For the MHDA chip, no significant dissociation was observed, which led to the seemingly low K_D of 23 nM, which seemed falsified by the nearly absent dissociation of the formed antibody-HHM complex. On the MHDA-PG chip, a proper complex dissociation was observed, and a K_D of 146 nM was calculated, which seemed to represent the actual binding strength. Moreover, the results produced with the MHDA-PG chip showed better reproducibility and quality of the corresponding fits. However, the data fittings suggested a non-1:1 binding event for the interaction of pAB-A150 with HHM, which is most likely explained by the polyclonality of the antibody.[243]

This first set of results should be confirmed by analyzing a monoclonal anti-myoglobin antibody. For this purpose, the monoclonal anti-myoglobin antibody, mAB-A6, was tested. 12, 20, and 40 µg/mL (V = 250 µL) of mAB-A6 antibody was immobilized via PG and DMP crosslinking for immobilization efficiency evaluation with the previously determined experimental conditions (Figure 5.1.21). The immobilization efficiency seemed reasonable, but for mAB-A6, a saturation of the PG seemed to occur already at 40 µg/mL. To avoid high antibody concentrations on the surface, which could have been disadvantageous for recording proper dissociation curves, 20 µg/mL mAB-A6 was chosen for the kinetic analysis, which indicated a K_D between 1 - 2 µM.[243]

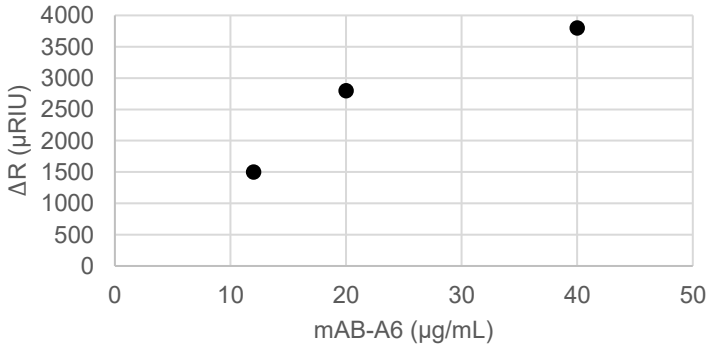

Figure 5.1.21: Immobilization efficiency of mAB-A6 via PG and DMP on MHDA at 12, 20, and 40 µg/mL in PBS buffer in relation to the shifted SPR signal R (µRIU). The experiments were carried out by Daria Holdschick, and the data was used to create the figure shown.

For both antibodies, pAB-A150 and mAB-A6, the epitope extraction with MHDA-PG chips was done, too.[243] The epitope extraction for mAB-A6 was done before[245] and was reproduced partly by Daria Holdschick[243] because of inconsistencies in the prepared HHM digestions, and the epitope for the pAB-A150 was successfully determined.[243,244] Therefore, the successful use of an MHDA-PG chip for epitope extraction was confirmed.

5.1.7 SPR measurements of protein- and peptide-mAB-I2519 complexes

The IL8-mAB-I2519 complex was characterized on an SPR biosensor with different gold chip modifications. Dextran, MHDA, and modified MHDA chip surfaces were tested for optimal kinetic and affinity data recording. The epitope extraction method was also tested and optimized for the application to MHDA and MHDA-modified surfaces.

5.1.7.1 Method development for characterization of the IL8-mAB-I2519 complex by SPR

For the first analysis of the IL8-mAB-I2519 interaction, the antibody was immobilized on a pre-functionalized dextran-gold chip (Sensorgram for immobilization: Figure 8.2.44). IL8 injections over the immobilized mAB-I2519 showed high surface binding, seen in the high signal on the reference channel, and difficulties with the regeneration conditions, indicated by the baseline drift after regeneration, in the raw sensorgram (Figure 5.1.22). The IL8 concentrations of 1.5 and 3 µM showed the expected curve shapes for single-site binding and normal response ranges. However, higher IL8 concentrations of 6 and 12 µM led to an unexpected and unproportional increase in the measured responses. The unproportional signal intensity increase might be linked to IL8 dimer formation at higher concentrations ($K_{Dimerization}$ ~ 10 µM)[167]. Therefore, IL8 concentrations above 1.5 µM were avoided. A proper regeneration solution could not be identified with high salt concentrations or acidified glycine solutions, and the 0.1 % FA in MQ was used for the following experiments. The baseline drift was not observed in other experiments with FA as part of the regeneration solution. Therefore, it seemed more likely to be a specific problem with IL8 and dextran. Interestingly, the signal drift of the reference channel after regeneration rises proportionally to the increasing IL8 concentration, also indicating a strong binding of IL8 to the dextran on both surfaces.

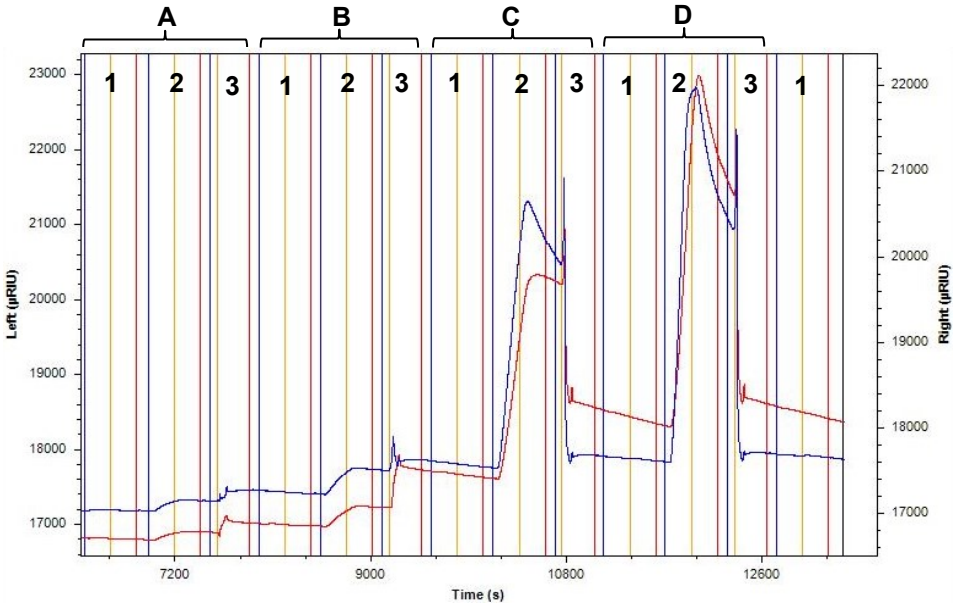

Figure 5.1.22: Raw sensorgram for buffer (PBST; **1**), sample (**2**), and regeneration solution (**3**) injections. The sample channel (left; blue) and reference channel (right; red) are shown with vertical lines indicating the start of injection (blue), the start of dissociation (yellow), and the end of dissociation (red). 1.5, 3, 6, and 12 µM IL8 (A, B, C, D) were injected in PBST, starting with the lowest concentration. The regeneration solution consisted of 0.1 % formic acid in MQ.

However, an IL8 concentration-dependent response increase was detected. Therefore, an IL8 dilution series with more samples in the concentration range was set up (1:2 dilution of 1.5 µM) to evaluate complex formation and dissociation. The subsequent IL8 injections between 47 and 1500 nM showed reasonable association and dissociation patterns for the double-referenced sensorgrams, yielding a K_D of 82.2 nM (Figure 5.1.23; Table 5.1.10). The highest concentration of 1.5 µM IL8 showed an unexpected association curve shape, and the

1:1 binding model was even less suitable to fit the dissociation curve. No plateau was seen for the association phase, indicating a continuous binding of the IL8 to the antibody and dextran on the chip surface. Therefore, the dissociation phase starts before reaching a plateau, and the dissociation of IL8 from the antibody might be overlapped by the dissociation of IL8 from the dextran. Subtracting the reference channel/buffer injection from the sample channel (= double referencing) should compensate for the IL8-dextran interaction, but it did seem to be enough for compensation, and the immobilized antibody might have reduced the non-specific interaction of IL8 with dextran. The results with dextran-modified gold chips seem biased and can not provide a definitive affinity for the interaction but a range for the affinity and kinetic parameters. Therefore, other chip surfaces were tested.

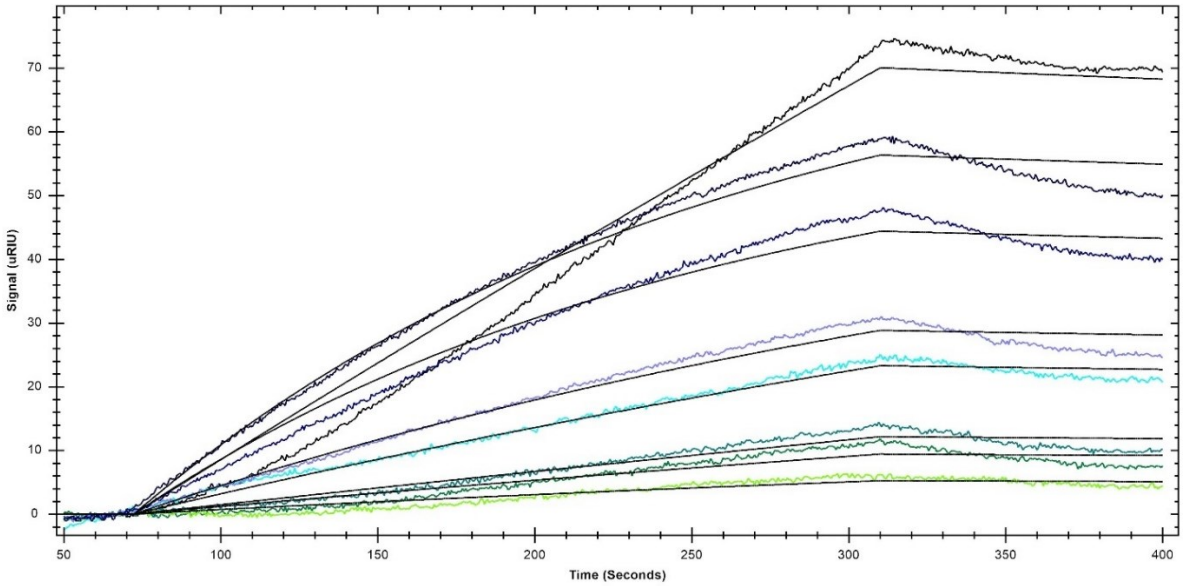

Figure 5.1.23: Sensorgram of a native IL8 dilution (47-1500 nM (light green to black); PBST) over the mAB-I2519 immobilized on a dextran functionalized gold chip. Colored lines represent the measured and processed signals, and black straight lines represent the 1:1 binding fit. The calculated K_D value for the interaction was about 82.2 nM.

Table 5.1.10: Determined kinetics, affinities, and errors for the IL8 - mAB-I2519 interaction on a dextran functionalized gold chip with a global 1:1 binding fit.

Sample	ka (1/(M*s))	Error	kd (1/s)	Error	K_D (nM)	Error (nM)	Chi^2 (µRIU^2)
Native IL8 dilution	3.48×10^3	$\pm 0.05 \times 10^3$	2.86×10^{-4}	$\pm 0.22 \times 10^{-4}$	82.2	±7.5	3.3

For comparison with the dextran-modified surface, an MHDA-functionalized gold chip was used without a spacer between the immobilized antibody and the MHDA-SAM (Sensorgram for immobilization: Figure 8.2.45). For the injections of the sample and regeneration solutions, a strong baseline drift combined with a strong binding of the IL8 to the surface was observed in the raw sensorgram (Figure 8.2.46). Regeneration with 0.1 % FA in MQ and 0.1 M NaCl pH 2 was tested, which showed similar results. Therefore, the MHDA chip was unsuitable for analyzing the IL8-mAB-I2519 complex. The epitope peptides should also be analyzed, and fewer non-specific interactions of those with the chip surfaces were expected. However, the injection of those over the immobilized mAB-I2519 on an MHDA chip showed similar surface binding and regeneration difficulties (data not shown).

The inconsistent results with MHDA-coated gold chips did not reveal reliable affinity and kinetic constants for the interactions of IL8 protein-, IL8[55-60]-, or IL8[12-20]- antibody interactions. Therefore, the previously introduced antibody immobilization via protein G (chapters 4.8.2 and 5.1.6) was used to analyze the IL8-mAB-I2519 interaction. An MHDA-PG chip was prepared with 250 µL of mAB-I2519 (20 µg/mL) for the interaction analysis (Figure 8.2.47). The sensorgram for the injections of IL8 dilutions showed much better quality and

consistency, and the corresponding kinetic and affinity calculations yielded a K_D of 7.4 nM with a fast association and slow dissociation of the protein antibody complex. Moreover, the injection of 800 nM IL8 yielded a R_{max} of 152 µRIU, doubling the intensity reached on the dextran or MHDA chip. The complex dissociation was still challenging to detect because the mAB-I2519-IL8 complex seemed very stable. Apparently, the oriented antibody immobilization with higher antibody activity positively affected the experimental outcome. The experiments with IL8 confirmed that, after immobilization via protein G, the mAB-I2519 is much more stable on the surface, with less degradation after regeneration and proportional response increase for increasing concentrations of IL8.

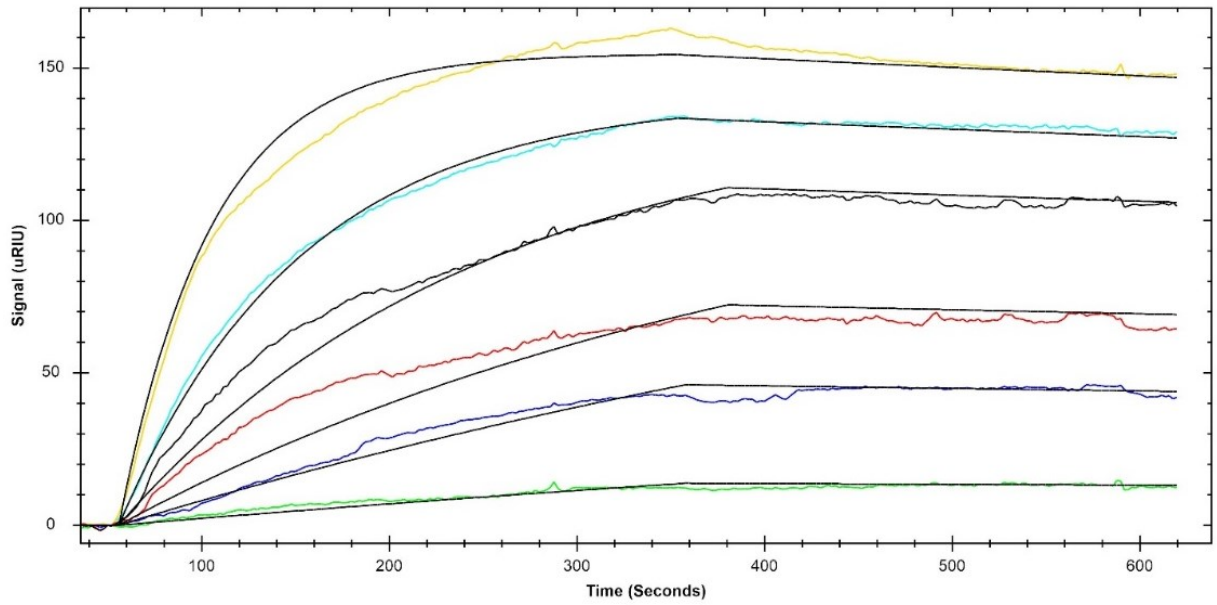

Figure 5.1.24: Double referenced response curves for 25 (green), 50 (blue), 100 (red), 200 (black), 400 (cyan), and 800 (yellow) nM IL8 injections (colored curves) over an mAB-I2519 functionalized PG-MHDA-gold chip. Curve fitting with a 1:1 binding fit (black curves) estimated a K_D of 7.4 nM.

The peptides IL8[12-20] and IL8[55-60] were tested similarly with the oriented immobilized mAB-I2519 (Figure 5.1.25). Epitope peptide IL8[12-20] showed a regular concentration-dependent signal, and a K_D in the micromolar range (K_D = 76.1 µM) was calculated. Compared to experiments without protein G immobilization, the 1:1 binding model led to a reasonable fit, with a fast association and dissociation. For IL8[55-60], a much lower affinity (K_D = 0.98 mM) was observed, and much higher concentrations were needed for actual binding detection. Both peptides showed low maximum response values, which resulted partly from their small molecular size (MW(IL8[12-20] = 1102 Da and MW(IL8[55-60] = 832 Da). Compared to the high affinity of full-length IL8 to mAB-I2519, those low affinities are consistent with the notion that both peptides are part of a discontinuous epitope. This hypothesis of both peptides forming a discontinuous epitope was further tested by simultaneous injection of both peptides at an equimolar concentration of 300 µM ((Figure 5.1.25-C). Indeed, both peptides can bind to the mAB-I2519 simultaneously, as seen in the increased response at 25 µRIU for the injection of both peptides together compared to 7 µRIU for IL8[55-60] and 16 µRIU for IL8[12-20] alone. Therefore, the hypothesis of a discontinuous epitope is further supported. However, it is still possible that the discontinuous epitope is comprised of additional sites of the IL8 protein, which were not detected in the epitope extraction experiments. The in-silico analysis suggested a longer sequence at the C-terminal helix as an epitope-forming sequence region at IL8[55-72], which was not present as a peptide in the tested digestions. Therefore, peptide IL8[55-72] was also synthesized and tested on a similarly prepared mAB-I2519 MHDA-PG chip. Another mAB-I2519-PG-MHDA-chip was prepared for the test of IL8[55-72] (Figure 8.2.39). The proper antibody immobilization was confirmed with a 100 nM IL8 injection, which showed a highly active and immobilized antibody (Figure 8.2.48).

Table 5.1.11: Determined kinetics, and affinity constants, and errors for native IL8, IL8[55-60], IL8[12-20] - mAB-I2519 interaction on a PG-MHDA functionalized gold chip. The curve fitting used a 1:1 binding model with global parameter settings.

Sample	ka (1/(M*s))	Error	kd (1/s)	Error	K_D (M)	Error (M)	Chi^2 (µRIU^2)
Native IL8	2.52×10^4	$\pm 0.01 \times 10^4$	1.87×10^{-4}	$\pm 0.08 \times 10^{-4}$	7.41×10^{-9}	$\pm 0.36 \times 10^{-9}$	16.72
IL8[55-60]	2.83×10^1	$\pm 2.19 \times 10^1$	2.80×10^{-2}	$\pm 0.07 \times 10^{-2}$	9.87×10^{-4}	$\pm 0.20 \times 10^{-4}$	1.42
IL8[12-20]	2.60×10^2	$\pm 1.16 \times 10^2$	1.95×10^{-2}	$\pm 0.75 \times 10^{-2}$	7.51×10^{-5}	$\pm 0.78 \times 10^{-5}$	1.98

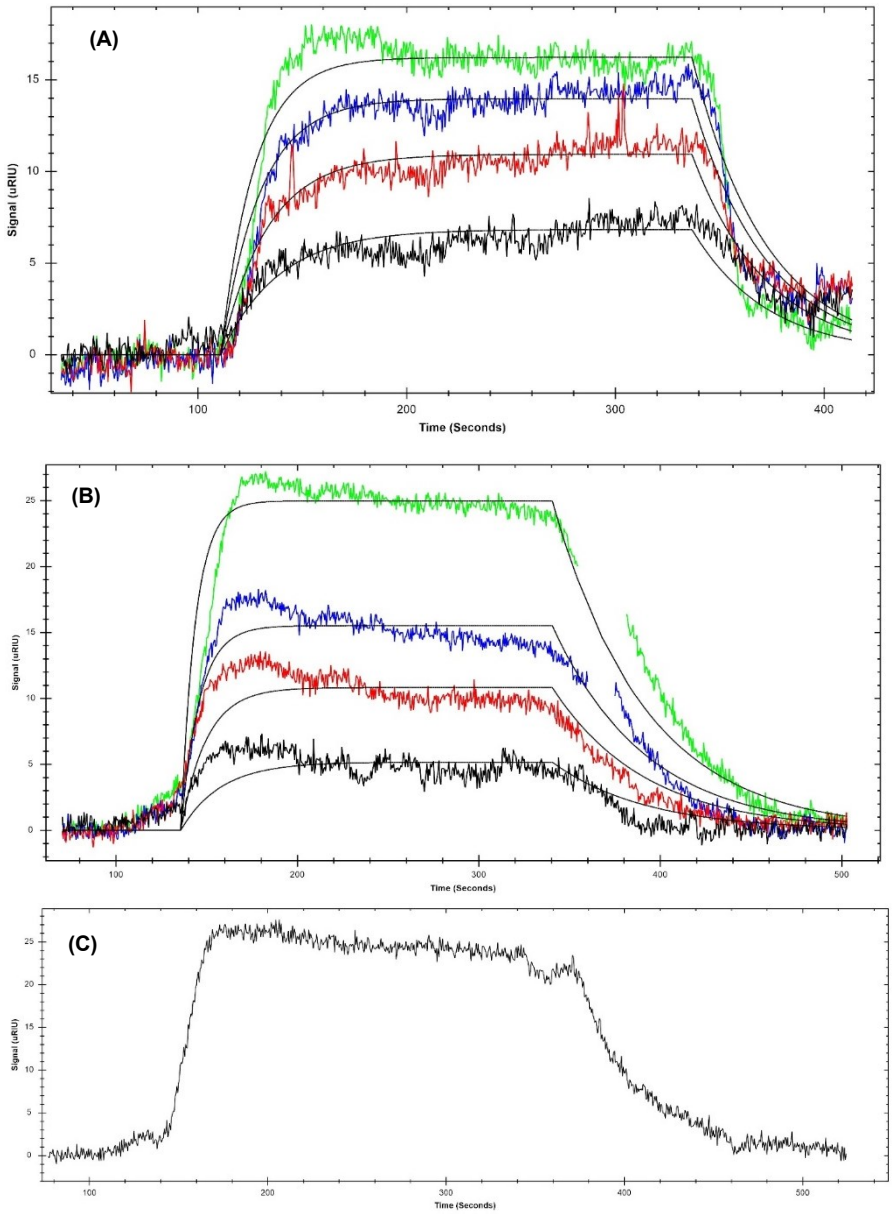

Figure 5.1.25: Double-referenced response curves for epitope peptide injections over an mAB-I2519 functionalized PG-MHDA-gold chip (colored lines). (A) 300 - 1200 µM IL8[55-60] and (B) 100 - 400 µM IL8[12-20] were injected and fitted to a 1:1 binding model (black lines). Estimated K_D value for IL8[55-60] of 0.98 mM and IL8[12-20] of 75.1 µM. (C) A mixture of 300 µM IL8[12-20] and IL8[55-60].

The injection of IL8[55-72] over the mAB-I2519 led to a negative response for the double-referenced response curve, and subsequent experiments also showed negative values, which made determining an affinity for IL8[55-72] impossible and, at the same time, indicate a stronger binding to the reference channel. Due to this non-specific interaction, it was impossible to say whether the epitope region on the C-terminal helix on IL8 is

extended. The reference channel was coated with protein G, meaning the C-terminal peptide seemed to bind to protein G. A potential explanation might be that the many positively charged amino acids in the C-terminal peptide, Il8[55-72], could bind to the negatively charged protein G. Assuming a similar pI of the used protein G (Table 4.1.2) to its native pI, which was calculated from the sequence available on UniPort (protein G UniProt-Code: Q54181), it has a pI of 4.34. Therefore, it would be negatively charged at a pH of 7.4 (pH of PBS), and it would be possible that IL8[55-72] binds to it.

Finally, the previously mentioned average epitope length of 8 - 22 amino acids[1] should be considered for evaluating IL8[55-72] as an epitope peptide. The peptide IL8[12-20] contributes potentially 9 amino acids to the antibody binding, which would be already enough to form an epitope according to the literature. However, the results presented point to a discontinuous epitope, considering the low affinity of IL8[12-20] to mAB-I2519. Therefore, IL8[55-60] could contribute another 6 amino acids and IL8[55-72] another 22 amino acids to the epitope. IL8[12-20] and IL8[55-60] come to an epitope of 15 amino acids, which could be enough to bind mAB-I2519 with a high affinity. The IL8[12-20] and IL8[55-72] would yield an epitope of 31 amino acids, probably containing many non-epitopic amino acids. Therefore, IL8[12-20] and IL8[55-60] seem more likely to form the actual epitope core. Moreover, the C-terminal IL8 sequence forms an α-helix, and some of the amino acids from the C-terminal site, IL8[55-72], would not contribute to antibody binding because the amino acid residues on one side of the α-helix usually contribute to protein binding. This would be entropically disadvantageous for the unstructured IL8[55-72] peptide, reducing the antibody binding even if a few more amino acids on the C-terminal part of IL8 would belong to the epitope region.

5.1.7.2 SPR-based epitope extraction

The first epitope extraction experiments were done on an MHDA chip (Figure 5.1.14; Figure 5.1.15), which showed non-specific binding of the peptides to the chip surface, and no clear response was recorded for a binding event. The affinity and kinetic constants were yielding low affinities for the epitope peptides, meaning that much higher digestion concentrations would be necessary for producing a detectable specific response increase for the binding event to the mAB-I2519. However, higher digestion concentrations would not solve the difficulties with the non-specific interactions. Therefore, higher antibody loadings on the chip surface seemed more desirable, which could not be accomplished with the MHDA chips, and the MHDA-PG chips were instead tested for epitope extraction.

To omit the non-specific interaction of the positively charged peptides with protein G, PG was only immobilized on the sample channel to non-covalently immobilized mAB-I2519 (Figure 8.2.37 - A+B), and this experimental setup was tested for potential application in the epitope extraction experiments. Comparison of a native IL8, alkylated IL8, tryptic IL8, and buffer injection showed a well-working experimental setup (Figure 5.1.26). The native IL8 showed the highest response maximum, while the alkylated IL8 yielded a slightly lower response along with a strong upwards drift, which is typical for unspecific surface binding. The IL8 denaturation led to an affinity loss and stronger non-specific interaction with the chip surface. For the native IL8, a slight upwards drift was also detected and compared to the alkylated IL8, leading to the hypothesis of denatured IL8 binding strongly to any surface. Indeed, unstructured peptides and proteins can bind metal surfaces.[246,247] There are attempts to characterize the proteins and their degree of binding surfaces in a non-specific manner, and the MHDA surface was reported to show reduced non-specific interactions which a variety of serum proteins.[247,248] Therefore, the challenges of non-specific surface binding were known but needed to be characterized for an individual protein in the specific experimental context. Compared to the native and alkylated IL8, the affinity for the tryptic IL8 was substantially reduced but not completely lost, in line with the hypothesis of the discontinuous epitope. Overall, the oriented antibody immobilization on MHDA-PG chips yielded much higher surface loadings, which made it much easier to detect the binding of the tryptic digestion of IL8 to the antibody. Because of these successful experiments, the MHDA-PG chips were used for the previously shown epitope extractions (Figure 5.1.16, Figure 5.1.17), which indicated the extracted tryptic IL8 peptides, IL8[12-20] and IL8[55-60], also as an epitope.

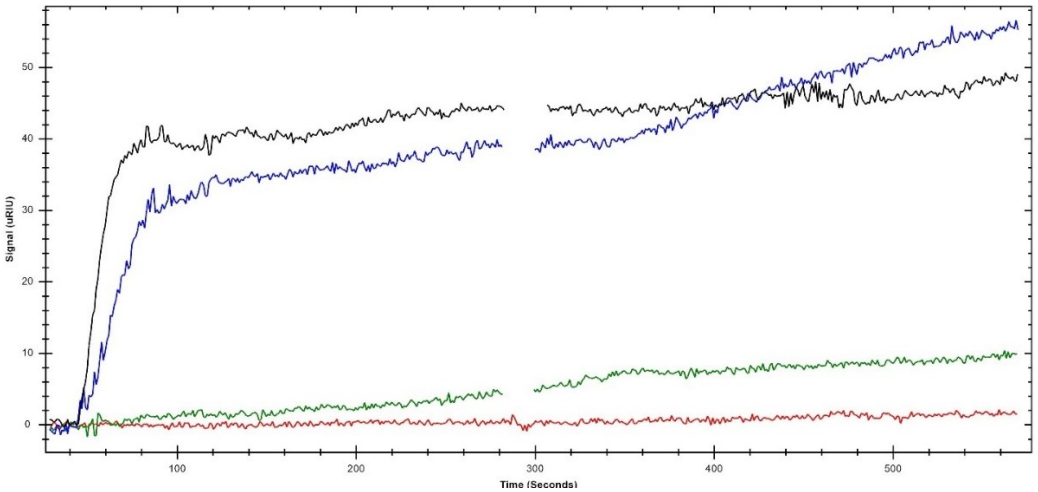

Figure 5.1.26: Sensorgram of 480 nM native IL8 (black), 480 nM alkylated IL8 (blue), 480 nM tryptic IL8 (green), and PBS (red) injections. All injections were done at 50 µL/min.

One downside of the non-covalent antibody immobilization is that each experiment needs a new antibody coating, but the antibody should be independent of any regeneration conditions, ensuring optimal antibody activity for each experiment. Additionally, the experimental setup with non-covalently immobilized antibodies would make control tests more flexible and investigations of crossreactivities to other biomolecules more accessible. The presented IL8-mAB-I2519 complex characterization supports the advantages of the MHDA-PG chips, which can be a superior alternative for proteins with challenging analysis of their binding capabilities.

5.2 Analysis of cathepsin D - aptamer and - antibody complexes

The pro-cathepsin D (pCTSD) variant from WG Saftig from the University of Kiel was first analyzed by SDS-PAGE and MALDI-tof MS. After protein identification and sequence confirmation of enzymatically digested pCTSD; epitope extraction was performed with anti-pCTSD antibody, anti-CTSD antibody, and a CTSD-aptamer. Briefly, the aptamer and one of the antibodies were produced against the native cathepsin D (CTSD-aptamer; anti-CTSD antibody), and the other antibody was produced against the pro-peptide of CTSD, which is part of the pCTSD (anti-pCTSD[7-21] antibody). A detailed introduction of the antibodies and aptamer is presented in chapter 1.2.2. The anti-CTSD antibody is a polyclonal antibody, which is important to remember because it will most likely have several epitopes on CTSD. The antibody and aptamer epitopes should be compared to show differences and similarities for the different ligand classes.

5.2.1 Protein characterization by enzymatic digestion, MALDI-MS, and SDS-PAGE

The analysis of pCTSD via SDS-PAGE (Figure 5.2.1) revealed several distinct bands for the intact pCTSD. At higher concentrations, two bands were detected around 48 kDa, one below the 63 kDa marker band and another around 180 kDa. The bands at 48 kDa seem slightly higher than the theoretical mass of pCTSD of 43,7 kDa, showing the presence of PTMs, which were expected due to the expression in HEK-cells.[187] The double band has been reported by the Saftig group at the University of Kiel, too, and corresponds to different isoforms with differing PTMs of pCTSD. The higher bands disappear at lower concentrations and could originate from pCTSD aggregation products at higher concentrations. Different amounts of pCTSD were loaded onto the gel to compare the digestion efficiencies. 1 µg aliquots of the tryptic and chymotryptic digestions showed no intact protein in the gel, neither for the digestion at AP- nor under PCT- conditions. Separate fractions from the samples

loaded onto the gel were also analyzed by MALDI-tof MS. The MALDI-tof MS measurement of intact pCTSD (Figure 5.2.1) showed two double peaks at 21.4/23.8 and 43.7/47.5 kDa. The peak at 43742.1 m/z corresponds to the singly charged pCTSD mass ($[M_{theo.} + H]^{1+}$ = 43681.6 m/z), and the higher peak with a maximum at 47561.5 m/z belongs to modified pCTSD (PTMs). The 21.4/23.8 m/z peaks belong to the modified and unmodified doubly charged pCTSD, and around 15 kDa, a small peak for the triply charged pCTSD was seen. No signals were detected at higher masses, and the detected signals' intensity was comparable low. The laser intensity was adjusted to 95 % to record the mass spectra, and 10000 laser shots were needed to record the signal intensities shown.

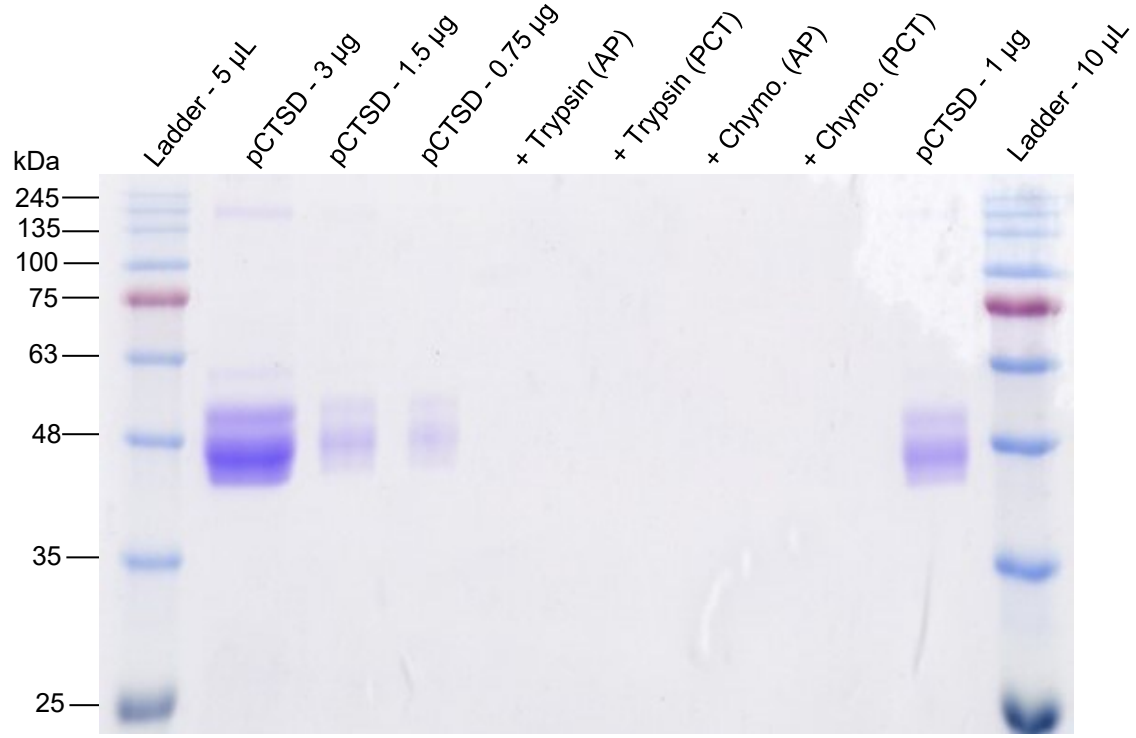

Figure 5.2.1: Tris-SDS-PAGE of pCTSD at different amounts (0.75 - 3 µg) applied to a 14 % acrylamide/bisacrylamide gel. 1 µg of tryptic and chymotryptic pCTSD were used. Both enzymes were digested under atmospheric (AP) and high-pressure cycling (PCT) conditions. 5 and 10 µL ladder were loaded in the first and last column.

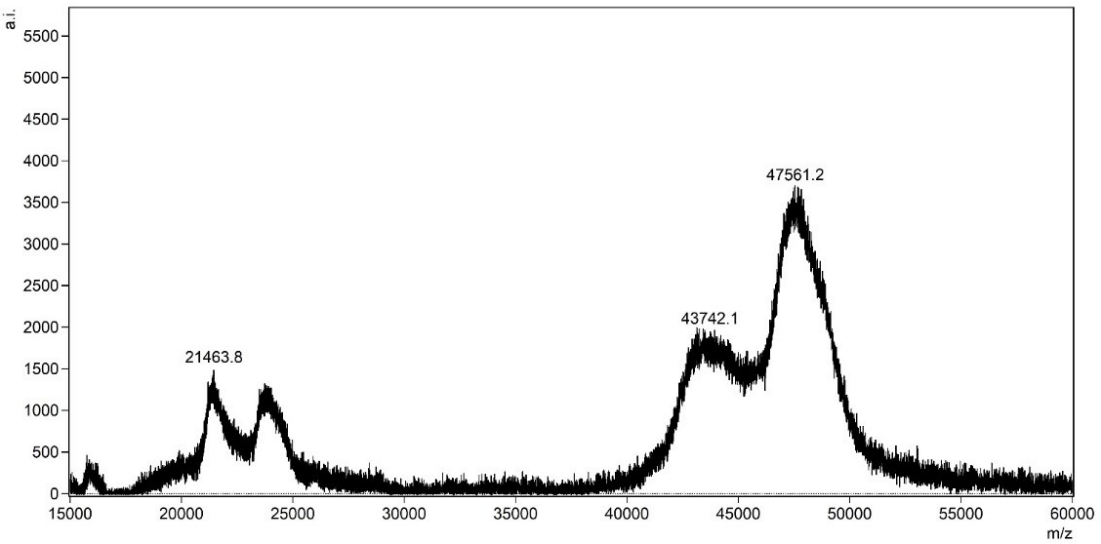

Figure 5.2.2: Native MALDI-tof MS of pCTSD for protein identification. Expected peak for $[M_{theo.} + H]^{1+}$ = 43681.6 m/z. (Method: LP; Matrix: SDHB)

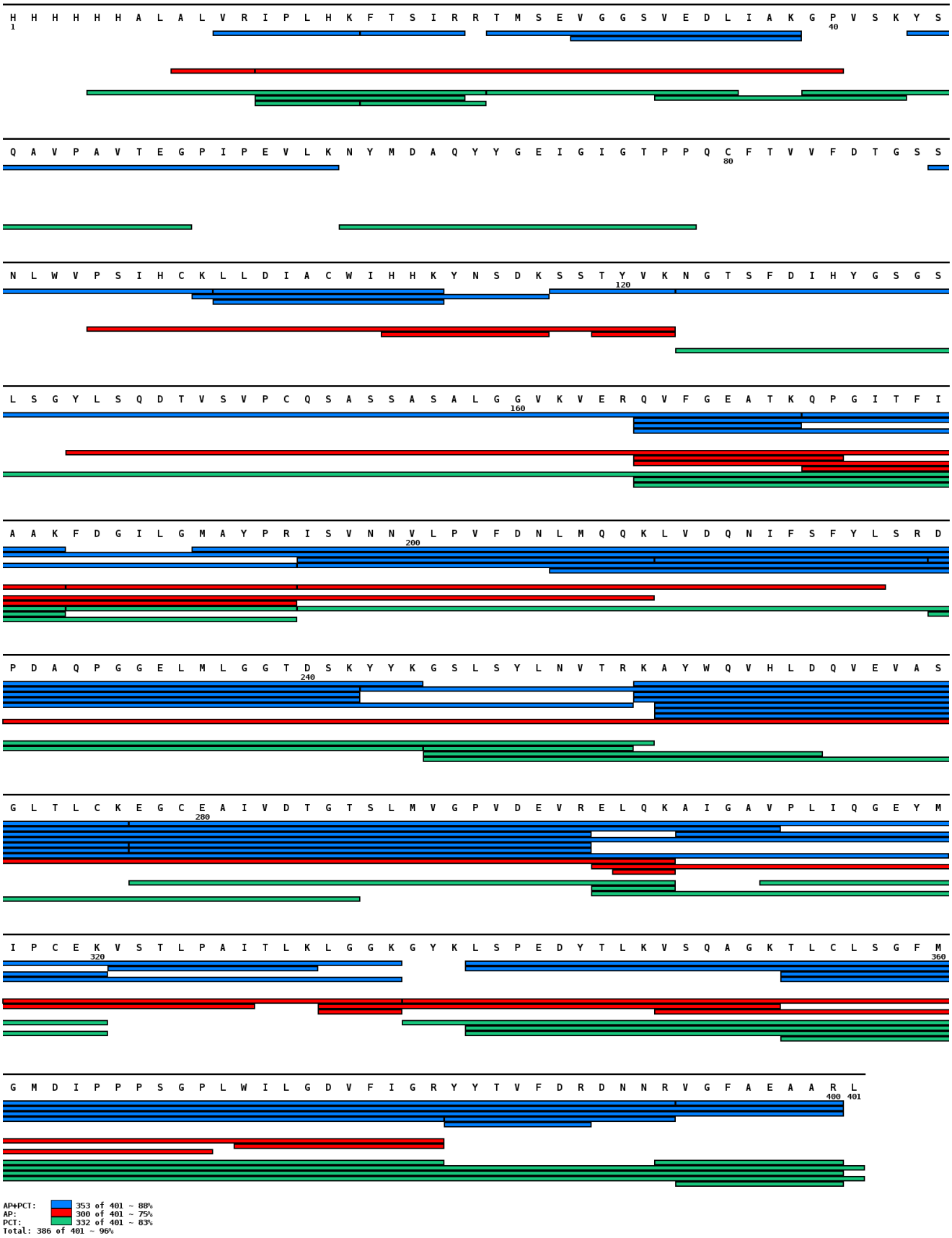

Figure 5.2.3: Protein map of the tryptic digestion of pCTSD under AP and PCT conditions for 120 minutes and 120 cycles, respectively. Identical peptide fragments in AP and PCT digestion are shown in blue bars, red bars are peptide fragments only identified in the AP digestion, and green bars are peptide fragments only identified in the HP digestion.

PCTSD was subjected to tryptic and chymotryptic digestion under AP and PCT conditions. The analysis of the tryptic digestion by MALDI-tof MS (Figure 8.2.14; Figure 8.2.12; Table 8.1.3; Table 8.1.4) and the corresponding protein map showed a high sequence coverage of 90 %. The N-terminal sequence part was underrepresented in the protein map, and despite PTMs, like glycosylations at T52, N123, and N252, the corresponding peptides were identified in the digestion. The tryptic digestion of pCTSD confirms that the prepared glycoprotein was a mixture of low and high-abundant PTMs. The pCTSD, expressed in HEK-cells, was not glycosylated to an extent where it would not be possible to use in an epitope extraction experiment. The pCTSD was treated with PNGF to remove the N-glycosylations but did not significantly increase the sequence coverage (data not shown). Therefore, no further treatment of the pCTSD with PNGF was done to remove any N-glycans. The digestion of pCTSD with chymotrypsin (Figure 8.2.15; Figure 8.2.13; Table 8.1.5; Table 8.1.6) showed a similar pattern. The N-terminal sequence part was also underrepresented. However, peptides complementary to the tryptic digestion were identified, resulting in a total sequence coverage for both digestions of 99 %. Therefore, both digestions could be used in separate experiments for epitope identification, making it very likely to identify epitopes. For the digestion with trypsin, the trypsin-specific peptide fragments formed over 80 % of the peptides, regarding the relative intensity of the trypsin-specific peptides to the semi-specifically produced peptides (Table 5.2.1).

The high-pressure digestion was also tested for the trypsin digestion of pCTSD, and the critical parameters, i.e., peak number, missed cleavage sites, and sequence coverage, obtained after 120 minutes to 120 cycles of PCT digestion were compared to normal digestion under atmospheric pressure for 1080 minutes (Table 5.2.1). The digestion peak pattern was very similar for all conditions, with a slightly reduced sequence coverage and trypsin-specific peptides for the AP digestion at 1080 minutes, indicating a slight over-digestion. Comparing the mass spectra and especially the protein map (Figure 5.2.3), the similar digestion pattern was reflected by the large overlapping amount of peptides in both digestions, which form the majority of the highest intense peaks for all digestions (83 - 87 %). Therefore, the similarity of the digestions indicates well-working trypsin under both conditions with minor differences, and the digestions under PCT conditions were used for the epitope extraction conditions.

Table 5.2.1: Comparison of tryptic digestion characteristics obtained under AP and PCT conditions for pCTSD. Incubation time was 18 h for AP-digestion and 2 h for PCT-digestion. Other parameters were identical for the digestions. MSC = missed cleavage site; SQ = sequence coverage; TS = trypsin-specific peptides.

Digestion	Peaks (No.)	Amount TS (%)	Relative Intensity TS (%)	MSC = 0	MSC ≥ 1	SQ (%)
AP-1080	62	63	83	29	33	90
AP-120	54	76	88	23	31	96
PCT-120	65	72	87	25	40	96

5.2.2 Binding site identification of an antibody and aptamer to pCTSD

The tryptic and chymotryptic digestions of pCTSD were used for the epitope extraction experiments with the CTSD-aptamer and two antibodies. The control experiments for the pCTSD digestions with trypsin and chymotrypsin were carried out with pre-activated sepharose 4B according to the previously described protocols (chapter 4.7). A slightly higher amount of 15 µg digested pCTSD was diluted in PBS for column incubation. The column was washed with 35 CV of 5 mM AmBic buffer, followed by acidic elution with 0.1 %TFA in MQ. MS-analysis of selected fractions of the control experiment with Sepharose 4B beads showed a lot of column-material-binding peptides in the elution and no peptides in the last washing step (Figure 8.2.16). Repeating the control experiments with the same column and another digestion batch led to slightly different results, as summarized in the corresponding table (Table 5.2.2). The identified sequence parts for the control experiment with the tryptic pCTSD digestion were [13-31], [39-54], [101-111], [184-196], [225-255] and [307-329]. Those pCTSD regions share no common motif, charge, or biochemical properties from which a common sepharose-binding ability could be derived (analysis not shown). The eluting peptides were not identical in the repeated control experiments, which most likely originated from the different digestion batches used in the experiments.

The differences in the used digestion batches were illustrated in the peptide [101-111], which was alkylated to different extents in the digestions and the corresponding extracted peptides, too.

Table 5.2.2: Peak table of identified trypsin-digested pCTSD peptides in the acidic elution from control experiments. If a peptide was identified in both experiments, the S/N, meas. mass and error are reported for experiment E1.

S/N	Meas. mass	Fragment	Theo. mass	Error	Exp. No.
12.8	1211.8	[13-22]	1211.7	0	E1
17.7	923.1	[23-31]	923.4	0.3	E1
26.4	1589.8	[39-54]	1589.8	0	E1
11.3	1348.7	[101-111]	1348.7	0	E1
75.2	1405.7	[101-111]*	1405.7	0	E2
15.6	1239.6	[184-194]	1239.6	0	E1/E2
11.6	1439.8	[184-196]*	1439.7	-0.1	E2
.6	2386.0	[225-247]	2386.1	0.1	E1
11.2	1563.8	[243-255]	1563.8	0	E1
51.2	1676.9	[307-320]	1676.8	-0.1	E1
5.6	815.5	[322-329]	815.5	0	E2

* cysteine residues carry carbamidomethylations.

A similar control experiment was done with the chymotryptic pCTSD digestion, which showed similar ([9-18], [94-110], [245-252]) and new ([64-85], [113-141], [149-158], [275-289], [344-357], [384-396]) sequence regions as column binders (Table 8.1.7; Figure 8.2.17), which are summarized in a protein map (Figure 5.2.4). Again, the data from the repeated experiments differ. Moreover, the identified sepharose-binding peptides differ for the experiments with trypsin and chymotrypsin. The overlapping regions [13-18], [101-110], and [245-252] identified in both control experiments seem to exhibit comparable high affinities to the sepharose. However, it was an open question of how to exclude or include the unspecifically binding peptides in the discussion about epitope and non-epitope regions. It seemed plausible to consider only the control data of the tryptic digestion for epitope extraction with trypsin and the same comparison for chymotrypsin. The peptides from both control experiments cover a large part of the pCTSD sequence, and it seemed very likely that overlapping peptides would be found in the epitope extraction experiments. Comparing the initial digestions of pCTSD with trypsin (Figure 8.2.14) and chymotrypsin (Figure 8.2.15), the digestion with trypsin seemed to represent the protein better when it comes to the number of peptides from each sequence region. However, both digestions showed similar values for the digestion performance criteria, like sequence coverage (Table 5.2.1). Those findings illustrate the challenges with “unspecific” column binding peptides, namely their lack of predictability.

In the epitope extraction experiments for antibodies and the tryptic digestion of pCTSD, the anti-pCTSD[7-21] antibody epitope extraction was intended as an additional control because of its known epitope sequence [7-21]. The control experiment had already identified one epitope-derived peptide [13-22] as a non-specific column binder, so the epitope overlaps with the sepharose binding site. Furthermore, the epitope extraction for the anti-pCTSD antibody and the anti-CTSD antibody with the tryptic digestion of pCTSD did not reveal any new peptides from the digestion in the acidic elution (data not shown). Therefore, the epitopes might overlap with the peptides from the control experiment (Figure 5.2.4), or trypsin cleaved the epitope sequence, which made antibody binding impossible. Therefore, the epitope extraction was repeated for both antibodies with the chymotryptic digestion of pCTSD.

The repeated epitope extraction with anti-pCTSD[7-21] and chymotryptic digestions of pCTSD yielded the peptide pCTSD[1-20] and several additional peaks/peptides compared to the control experiment (Figure 5.2.5;

Figure 8.2.18; Table 8.1.8). Newly identified peptides without any overlapping sequence from the control experiments with chymotrypsin were [34-46], [55-60], [266-272], [322-329], [333-338], and [367-372]. The peptides [34-36] and [322-329] overlap with peptides found in the control experiment with trypsin but not in the control experiments with chymotrypsin, leaving it open if they bind the sepharose and the antibody. Moreover, several extracted peptides overlap partially with peptides from the control experiments, namely [86-112], [137-155], [235-263], and [339-354]. It was also impossible to tell if these peptides bound the antibody and sepharose or only one of them. The peptides [55-60], [266-272], [333-338], and [367-372] seemed to bind with higher certainty to the antibody, even though the antibody was produced against the N-terminal sequence [7-21]. It can happen that for digestions with a high extent of unspecific peptide binders, antibodies are also bound unspecifically or specifically. Anti-pCTSD and anti-CTSD antibodies were produced in rabbits. Therefore, a similar peptide binding pattern was expected because of the results from the control experiments. However, the polyclonal anti-CTSD antibody will likely have several epitopes on the CTSD, which should be kept in mind.

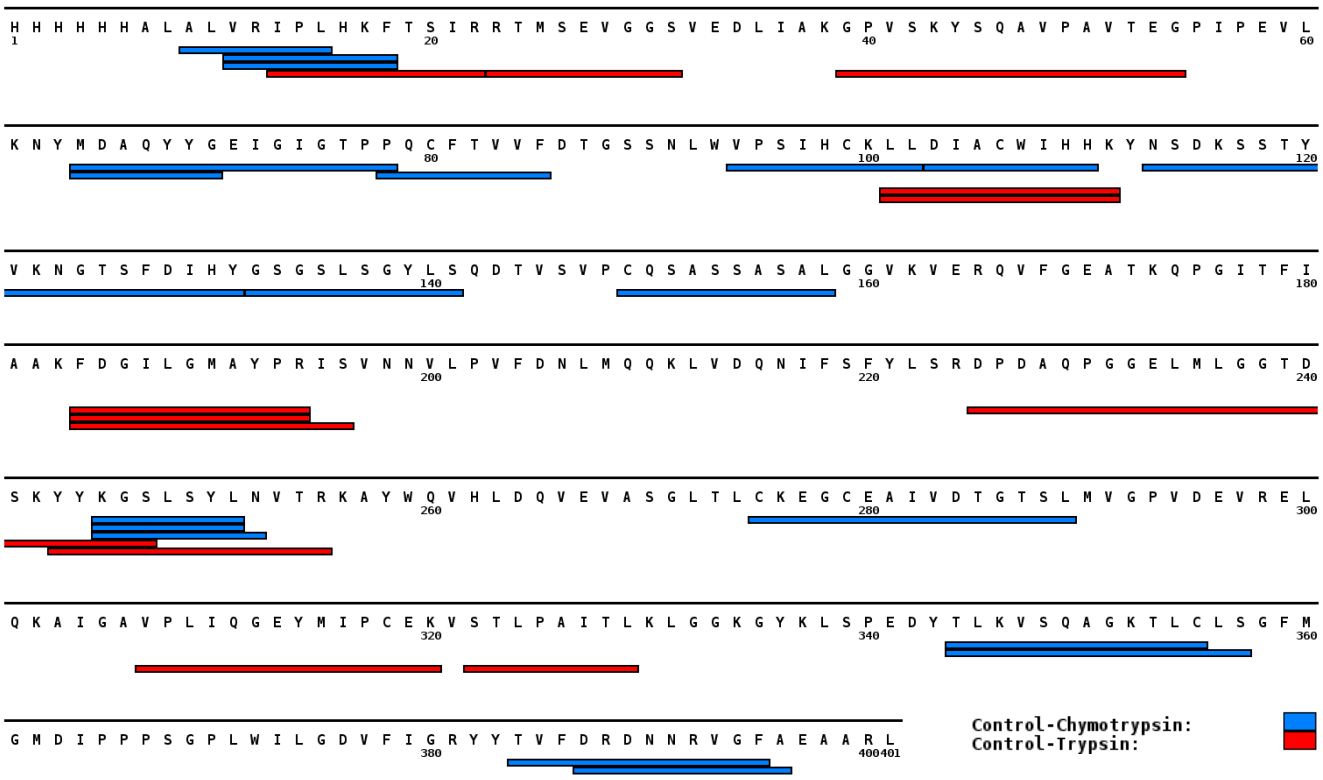

Figure 5.2.4: Protein Map of pCTSD with experimentally identified peptide sequences in the control experiments with tryptic and chymotryptic digestions of pCTSD and unmodified sepharose 4B.

Epitope extraction with the chymotryptic digestion of pCTSD and immobilized anti-CTSD antibody revealed a similar peak pattern than for the anti-pCTSD antibody epitope extraction with some differences (Figure 5.2.6; Table 8.1.9; Figure 8.2.19). The peptides [55-60], [266-272], [333-338], and [367-372] were identified again. Therefore, both antibodies produced in rabbits seemed to have the same binding capabilities to those sequence regions. However, multiple peptides from the sequence region [214-244], which had not been observed before, were identified. The peptides originating from [214-244] overlap partially with peptides from the control experiments but could form an epitope, which binds from [214-224] specifically to the anti-CTSD antibody, and without considering the control experiments with trypsin, the potential epitope sequence region would be extended to [214-233]. Furthermore, the peptide [175-188] was only identified in the epitope extraction with anit-CTSD antibody and partially in the control experiment with trypsin, making it another candidate for binding the anti-CTSD antibody more specifically than other protein regions.

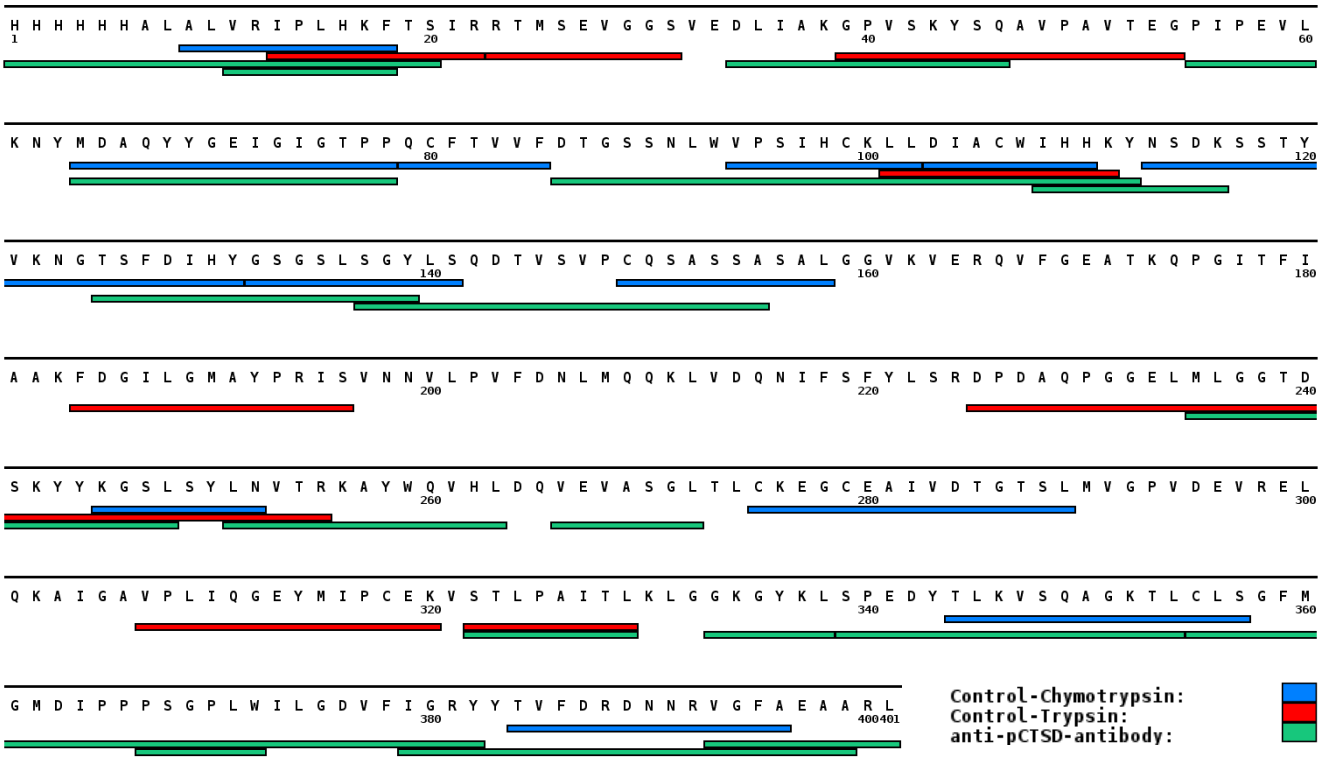

Figure 5.2.5: Protein Map of pCTSD with experimentally identified peptide sequences from the epitope extraction with anti-pCTSD antibody and the digestion of pCTSD with chymotrypsin. The protein regions in the control experiments with tryptic and chymotryptic digestions of pCTSD and unmodified sepharose 4B are also shown.

The protein regions or peptides from [34-46], [55-60], [266-272], [322-329], [333-338], and [367-372] seemed to bind both antibodies more specifically than others. They are highlighted in the CTSD crystal structure together with the peptide sequences, which were partially found in the control experiments ([86-112], [137-155], [235-263], and [339-354]) and with the peptide sequences ([214-224] and [175-188]), which were suggested to bind the anti-CTSD antibody specifically (Figure 5.2.7). The region [34-46] was left out because it was absent in the available crystal structure. The sequence regions [55-60], [86-97], [214-224], [137-155], and [367-372] are not accessible on the protein surface and can be excluded as epitopes for the anti-CTSD antibody. The sequence [175-188] was the most specific epitope for the anti-CTSD antibody, and the three regions [266-272], [322-329], and [333-338] are all on one side of the protein and could form a discontinuous binding site to the anti-CSTD and anti-pCTSD antibody. Furthermore, the protein sides [98-112], [235-263], and [339-354] are also potential epitopes. However, other experiments would be needed to identify or confirm one or more of the identified epitope candidates because the anti-CTSD antibody is a polyclonal antibody; multiple epitopes should exist.

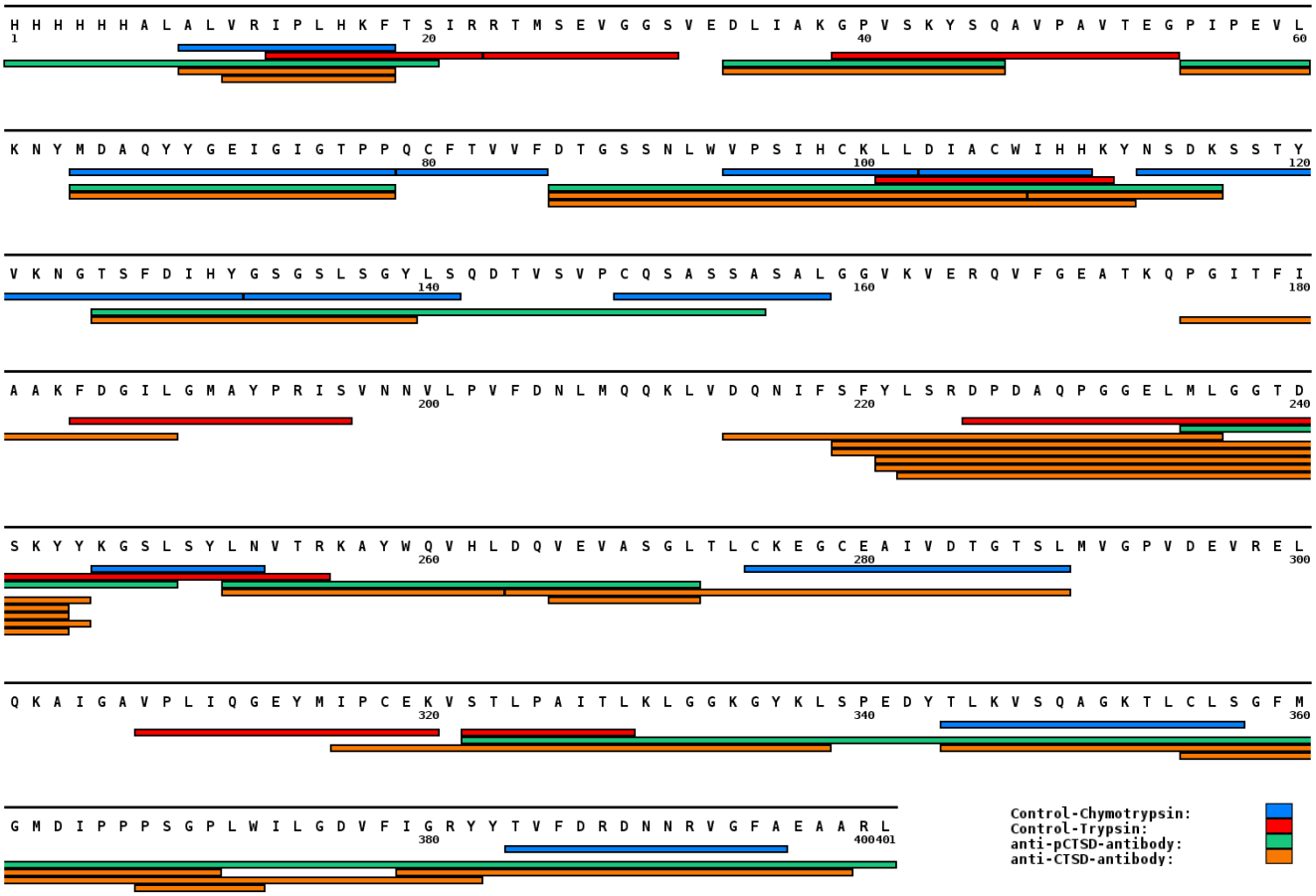

Figure 5.2.6: Protein Map of pCTSD with experimentally identified peptide sequences in the epitope extraction with anti-CTSD antibody and the chymotryptic digestion of pCTSD. The protein regions identified in the epitope extraction with anti-pCTSD antibody and control experiments with tryptic and chymotryptic digestions of pCTSD (with unmodified sepharose) are also shown.

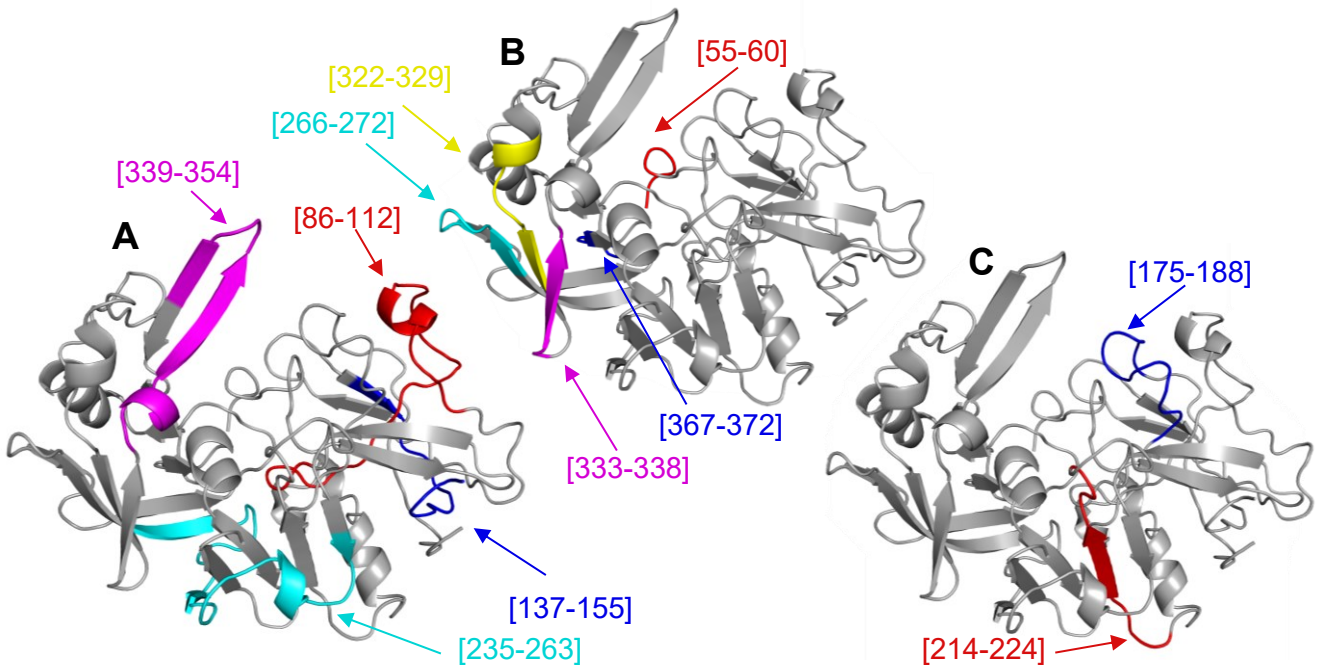

Figure 5.2.7: The identified protein patches from the different epitope extraction experiments are highlighted in the crystal structure of mature CTSD (PDB: 1LYW; images were created with PyMOL.[25]). (**A**) Peptide sequences found in the epitope extractions with anti-pCTSD and anti-CTSD antibodies, which overlap partly with peptide sequences found in the control experiments. (**B**) Peptide sequences were found in the epitope extractions with anti-pCTSD and anti-CTSD antibodies, which showed no overlap with the peptide sequences found in the control experiments. (**C**) Sequences in the protein identified only in the epitope extraction with the anti-CTSD antibody.

The epitope extraction experiments with the CTSD-aptamer were executed in analogy to the previous extractions with the antibodies. The acidic elution from the experiments with tryptic and chymotryptic pCTSD showed similar peaks/peptides compared to the control experiment with unmodified sepharose 4B (Figure 8.2.20; Figure 8.2.21; Table 8.1.10). The high-intensity signals in the control experiments with tryptic-digested pCTSD (m/z = 1845.1) and chymotryptic-digested pCTSD (m/z = 1009.6) made subsequent analysis challenging. The identified peptides for epitope extractions for pCTSD digested with trypsin and chymotrypsin are summarized in the protein map (Figure 5.2.8). The CTSD-aptamer was developed against the mature CTSD. Therefore, the pro-peptide (pCTSD[1-53]) should not be part of the binding site. Focusing on peptides, which show no overlap with the control experiments, pCTSD[212-224], pCTSD[257-261], and pCTSD[360-371] seem to be the best candidates for its binding site on pCTSD. More amino acid sequences were specifically identified in the CTSD-aptamer extraction experiments, but the corresponding peptides overlap with peptides from the control experiments. These protein sites are found in the peptides pCTSD[44-60] pCTSD[70-93], pCTSD[270-276] and pCTSD[379-399]. At this analysis stage, they cannot be excluded as potential binding sites with absolute certainty. Considering the crystal structure for binding site evaluation (Figure 5.2.9), at least four potential binding sites seem possible. Two potential binding sites could consist of multiple sequence parts from CTSD, pCTSD[55-60]/[257-261]/[360-371] and pCTSD[379-383]/[397-399]. The other two would be short linear binding sites around pCSTD[270-276] or pCTSD[214-224].

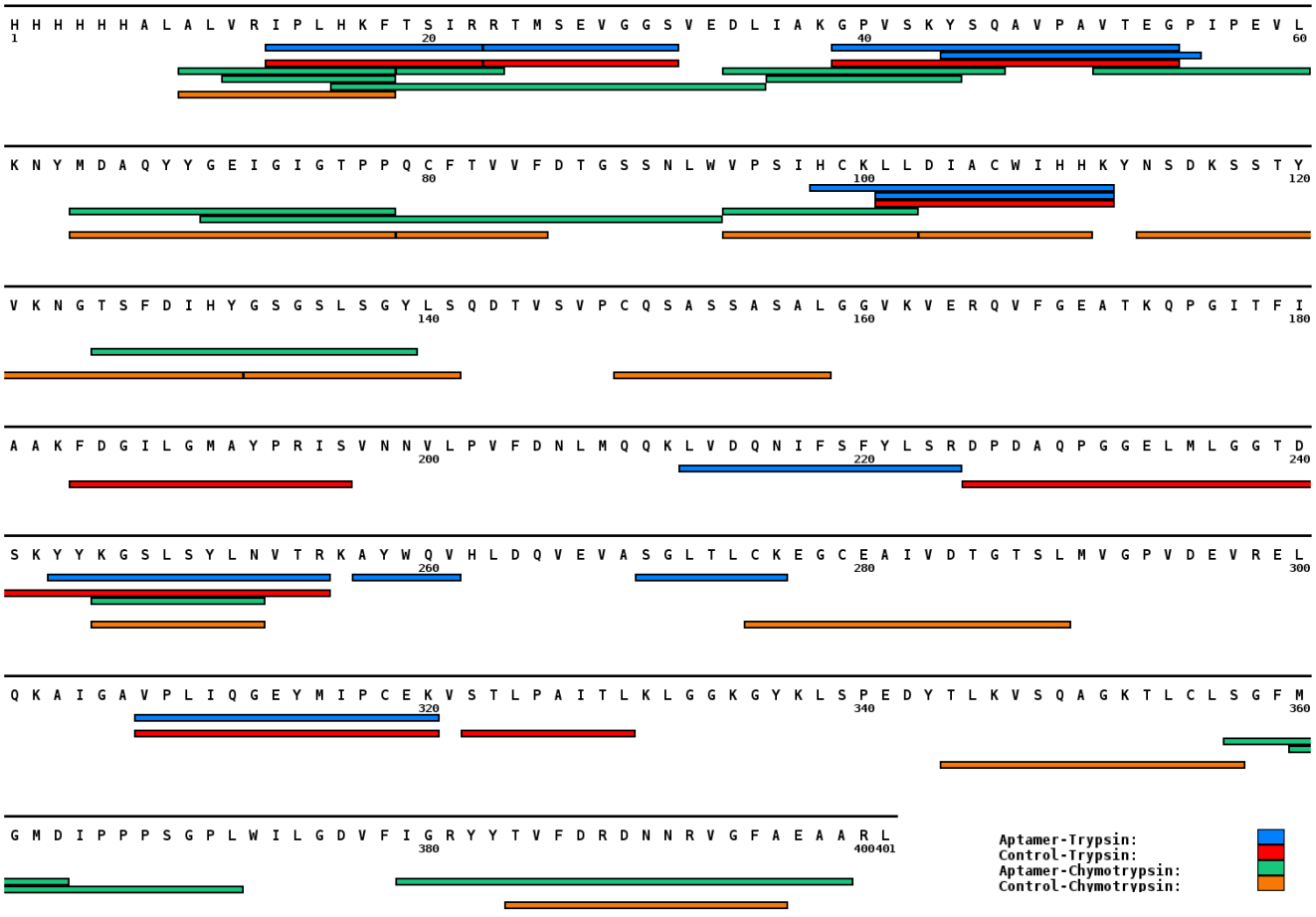

Figure 5.2.8: Protein Map of pCTSD with experimentally identified peptide sequences in the CTSD-Aptamer and the control experiments with unmodified sepharose 4B (digestions of pCTSD with trypsin and chymotrypsin).

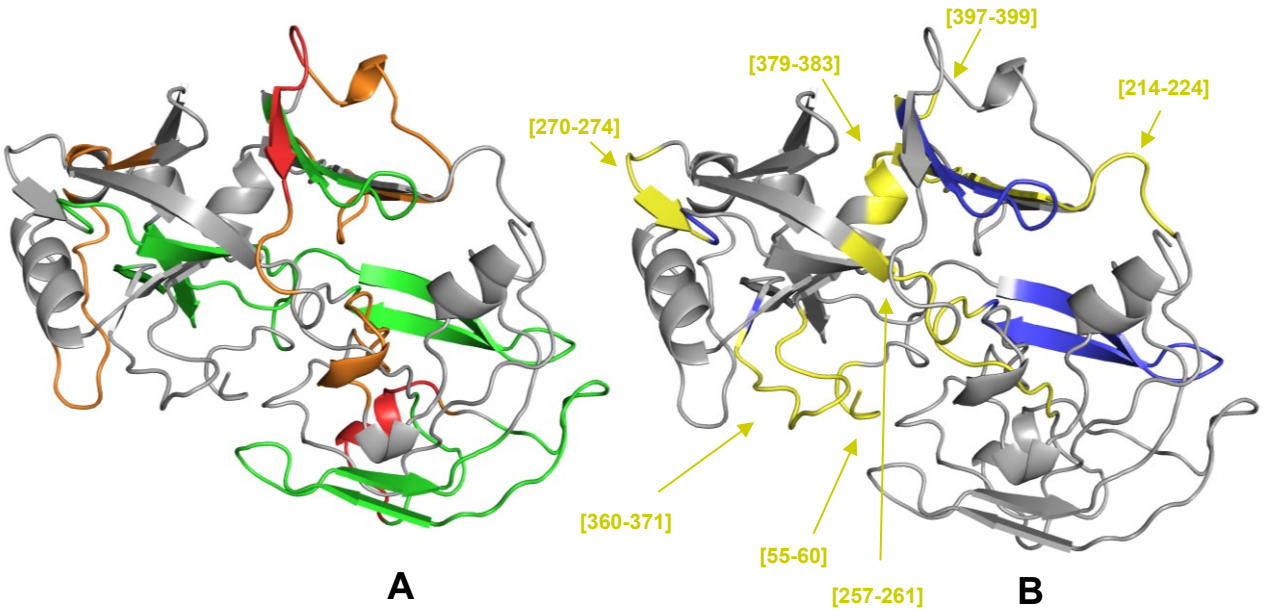

Figure 5.2.9: Crystal structure of matured CTSD (PDB: 1LYW) for epitope discussion of the CTSD-aptamer on CTSD. (**A**) Protein sequence parts were identified in the control experiments with trypsin (orange) and chymotrypsin (green) for the digestion of pCTSD. The overlapping regions for both control experiments are highlighted in red. (**B**) Sequence parts identified explicitly in the aptamer binding-site extraction experiments (yellow) and overlapping peptide sequences with the control experiments (blue). (The protein images were created with PyMOL.[25])

The epitope extraction experiments with pCTSD did not lead to the antibody or aptamer's precise epitope or binding sites. The massive amount of recovered peptides in the control experiments and their high signal intensities in the MS measurements distorted all obtained results via epitope extraction. Of course, one could speculate that the low affinities of the binding site-presenting peptides from the digestions indicate a complex, discontinuous epitope with multiple protein sites involved. However, another method would be needed to confirm this hypothesis. As previously seen, peptides with high surface-binding capabilities were challenging to analyze by the SPR biosensor. Therefore, another method would be necessary to confirm or dismiss the identified epitope peptide candidates. The presented epitope/peptide-binding-site extraction approach turned out to be problematic for CTSD binders due to the high amount of unspecific column binders identified. No linear epitope with highly preserved affinity could be found, which made the tested ligands and their potential epitopes unsuitable as biomarkers for CTSD in a diagnostic assay. Furthermore, the comparison of the epitope composition between the presented antibody and aptamer was impossible on the presented data set.

5.2.3 In-silico analysis of CTSD antibody epitopes

Epitope predictions with DiscoTope-2.0, BepiPRed-2.0, SEPPA-3.0, and BCEPS were compared in their capability of identifying an epitope on pCTSD or CTSD (Figure 5.2.10). The protein sites that formed the consensus of all prediction tools were defined as highly immunogenic, and the consensus of at least three tools was defined as protein sites with medium immunogenicity. The consensus of fewer than three tools is neglected because those protein sites are considered to exhibit low immunogenicity. The consensus of all prediction tools for immunogenic sites on CTSD consists of amino acids D115, S118, T119, V121, K122, N123, G124, T125, P226, D227, and P367. Of the studied peptide fragments, only pCTSD[214-244] contained two (P226, D227) of the highly immunogenic amino acids. According to the set analysis criteria applied here, the other potential antibody epitopes at pCTSD[251-289] and pCTSD[316-338] identified during epitope extraction showed low immunogenicity and pCTSD[175-183] medium immunogenicity. Therefore, pCTSD[214-244] could be considered the most likely candidate for the epitope of the anti-CTSD antibody. However, the sequence [214-224] was

identified to be inaccessible on the protein surface, leaving the protein region [225-244] as a potential epitope. The illustration of the consensus prediction and experimentally identified epitope candidates in the crystal structure shows apparent differences (Figure 5.2.11). Interestingly, the protein site pCTSD[107-132] might represent the highest immunogenicity of all protein sites in CTSD, which was detected in nearly all control experiments. Therefore, it could be part of an epitope, which remained unproven because of the high extent of unspecific binding events.

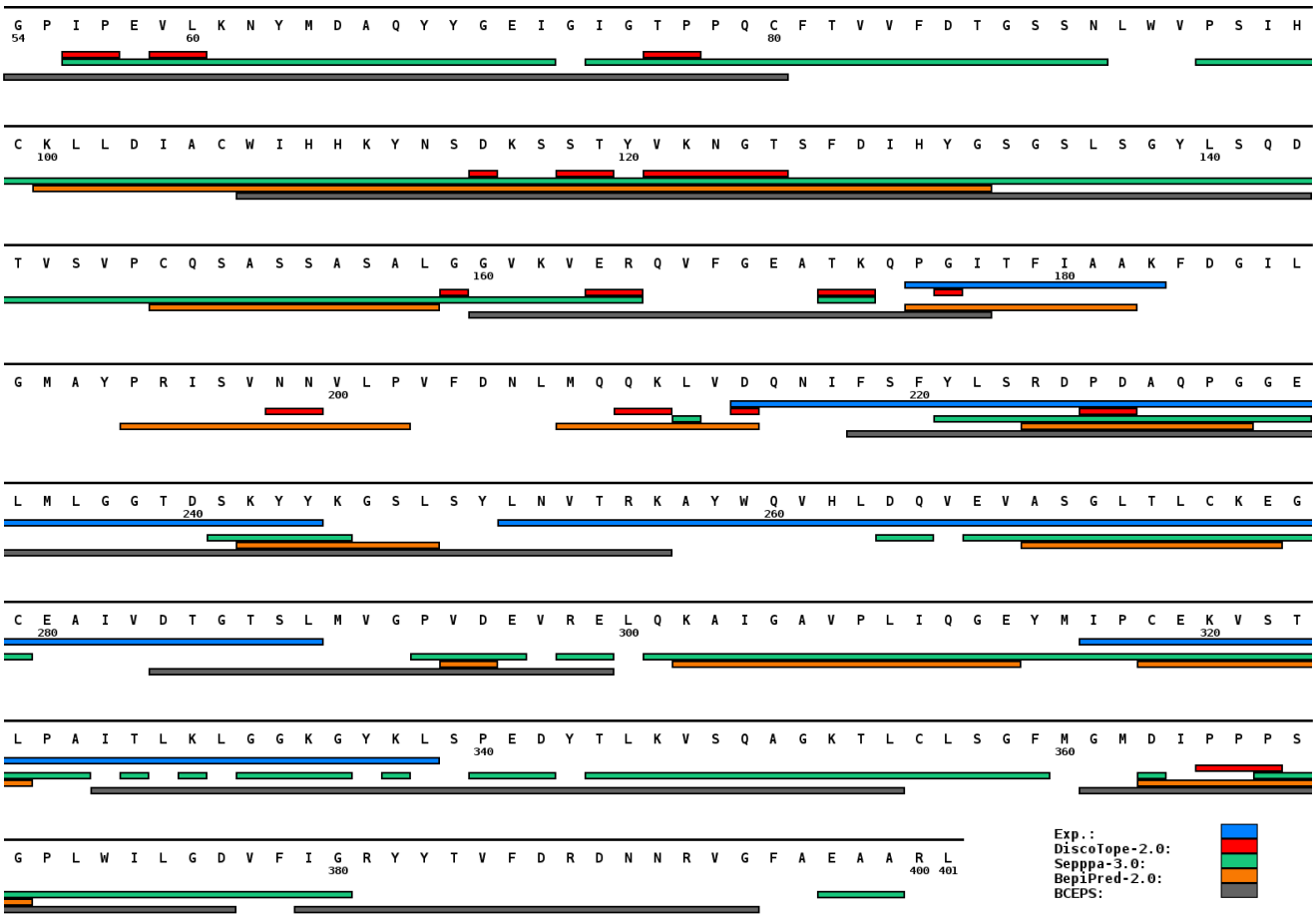

Figure 5.2.10: Protein map of CTSD with experimentally determined epitopes and epitope predictions with DiscoTope-2.0, Seppa-3.0, Bepipred-2.0, and BCEPS. The crystal structure in the PDB data bank entries used for the prediction did not contain any pro-peptides, which is why the N-terminal sequence part differs from the previous CTSD map, but the numbering is adjusted to the previous analysis.

The question posed at the beginning, "whether epitope prediction would show any benefit for the experimental design of epitope extraction," can be answered here with a yes. The predicted epitope peptides contain cleavage sites for trypsin and chymotrypsin. Therefore, another enzyme would have been needed. However, the epitope predictions were made after the experiments were executed, and there was no chance to test other enzymes for digestion. Moreover, it could not be answered if a linear or discontinuous epitope was more likely to be found.

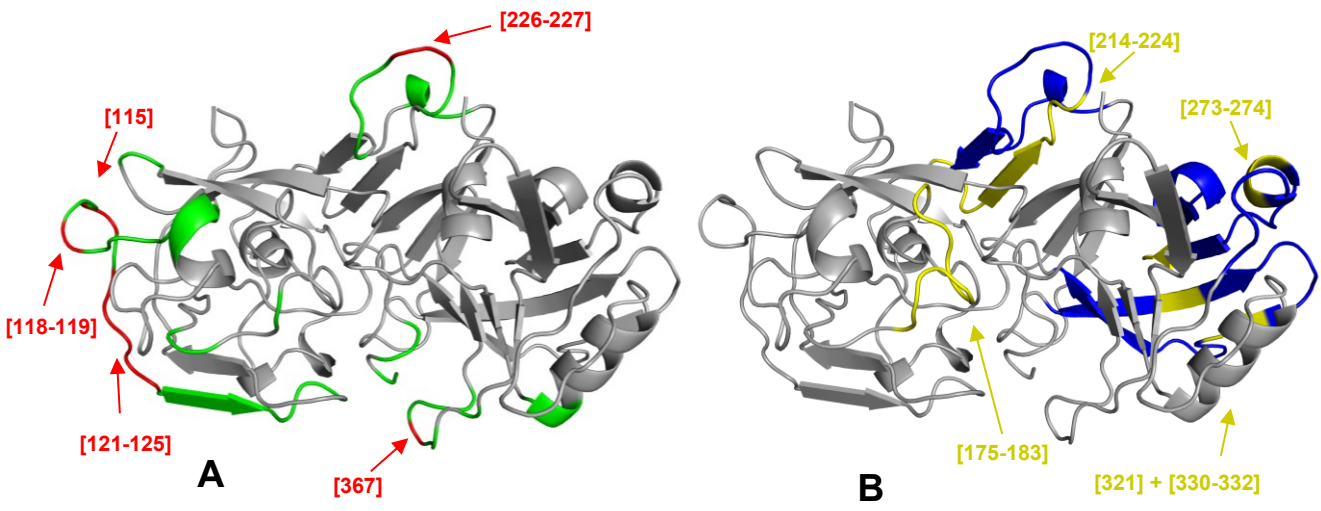

Figure 5.2.11: Crystal structure of CSTD (PDB: 1LYW) with (**A**) consensus of all four prediction tools (red) and consensus of three prediction tools (green). (**B**) experimentally identified epitope candidate regions (yellow and blue) with sites identified in the control experiments highlighted in blue. (The protein images were created with PyMOL.[25])

5.3 Research of an alpha-glucosidase A - antibody complex

Myozyme, the therapeutic drug for Pompe disease, was used in the third project presented in this work. This α-glucosidase A variant (GAA) was produced in CHO cells to produce all PTMs and glycosylations from natural human GAA for better tolerability. The protein was prepared by Sanofi. The protein sequence used for analysis was obtained from the drugbank-website.[196] A deglycosylation test with PNGF and subsequent SDS-PAGE and MALDI-tof MS of corresponding enzymatic digestions were carried out. An epitope extraction was performed with the commercially available monoclonal anti-GAA antibody (mAB-43G7) to identify binding peptides, which could be used in apheresis of patients under ERT to remove the autoimmune antibodies formed against the drug. The epitope extraction experiments were executed by Till Scheider and were reanalyzed by myself for the presented figures and tables. Moreover, Till Schneider repeated the digestions of GAA for his master's thesis, “Antibody Epitope Identification of Alpha-Glucosidase by Affinity Mass Spectrometry,” and obtained similar results.[249]

When the presented dissertation was about to be printed, there was a notification that the GAA used in this work did not match the sequence on the drugbank website. The sequence was extended by 13 amino acids on the N-terminus. This can explain some unidentified peaks in the data shown below. However, it should not significantly impact the overall analysis. The corrected data of the GAA digestions will be part of a publication, which is currently under review.

5.3.1 Protein characterization by enzymatic digestion, MALDI-MS, and SDS-PAGE

The reported mass for GAA or Myozyme was 105 kDa, including glycosylations and PTMs.[196] The SDS-PAGE (Figure 5.3.1) showed a mass slightly above 100 kDa for GAA. The GAA band was broadened at high concentrations with the highest density below 100 kDa. At lower concentrations, the band was narrower. The 1 µg aliquot of GAA digestions showed no residual GAA. Several bands at higher masses were detected for the intact GAA. Those bands disappear at lower concentrations, indicating concentration-dependent GAA oligomers and aggregates. For the digestion experiments and MALDI-tof MS analysis, removing the polysorbate 80 from the drug formulation was necessary, which would have otherwise interfered with the measurements. Therefore, the buffer was exchanged to 100 mM ammonium bicarbonate and MQ with spin-filters of 10 kDa MWCO. As shown in Figure 5.3.2, the buffer exchange B1 to MQ water led to stable protein aggregates, and buffer

exchange B2 against 100 mM ammonium bicarbonate buffer did not show those aggregates. Alkylated protein samples from B1 and B2 (alk-1 = B1; alk-2 = B2) also did not show the aggregates, making both buffer-exchanged fractions suitable for enzymatic digestions. However, the investigated protein digestions were prepared from the dialyzed samples against 100 mM ammonium bicarbonate buffer. Moreover, GAA treated with PNGF to remove glycosylations showed a slight shift of its band to lower masses, compared to alkylated and native GAA, indicating a successful deglycosylation. The digestion of GAA with trypsin showed no intact GAA protein and was expected to be sufficiently digested for subsequent MS analysis. Corresponding aliquotes of the digested GAA were analyzed by MALDI-tof MS.

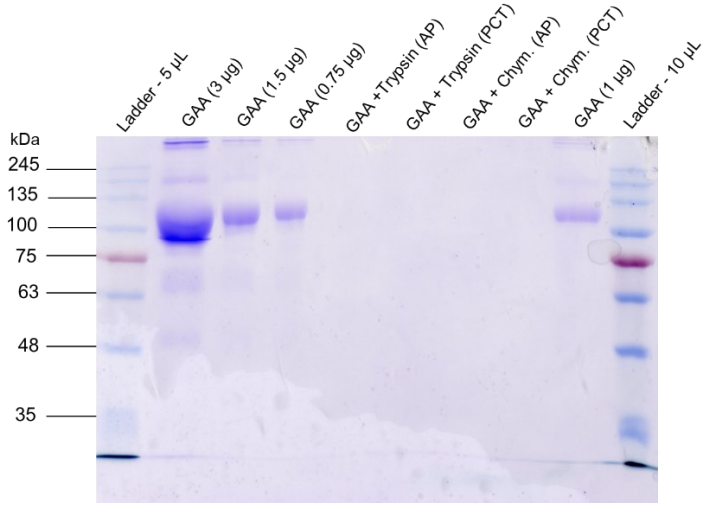

Figure 5.3.1: Tris-SDS-PAGE of GAA at different amounts (0.75 - 1.5 µg) loaded onto a 12 % acrylamide/bisacrylamide gel. 1 µg tryptic and chymotryptic GAA treated under atmospheric (AP) and high pressure (HP) conditions were loaded into the middle lanes. The first and last columns contained 5 µL (left) and 10 µL (right) of protein standard.

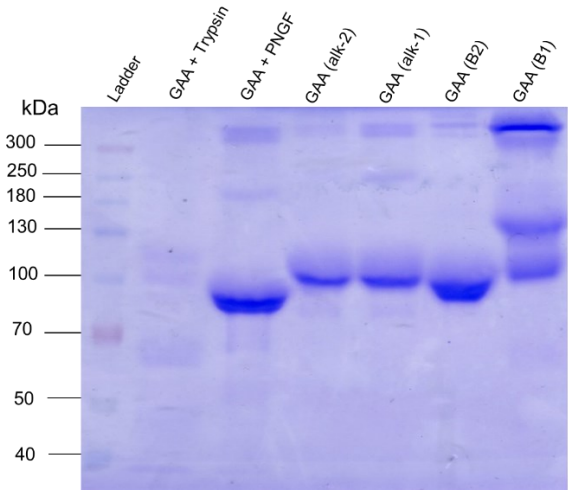

Figure 5.3.2: SDS-PAGE with differently treated samples of GAA on an 11 % acrylamide gel. 5 µg of trypsin-digested GA, 5 µg of PNGF-treated GAA, 5 µg of buffer exchanged GAA dialyzed against water (B1) and 100 mM ammonium bicarbonate (B2). Both buffer-exchanged fractions were alkylated (alk-1 from B1 and alk-2 from B2). 6 µL of the protein marker was loaded into the first lane.

The native MALDI-tof MS measurements of undigested GAA showed no signal for the intact protein. Therefore, it seemed to have very poor ionizability in the positive mode because of its glycosylations, which include phosphate and sialic acid modifications. The GAA digestion with trypsin (Figure 8.2.25; Figure 8.2.22; Table 8.1.12; Table 8.1.13) had a sequence coverage of 81 %, with several sequence regions remaining unidentified (Figure 5.3.3). Reasons for unidentified sequences in the MALDI-tof MS analysis were most likely related to the large number of peptide signals leading to ion suppression and glycosylated peptides that were difficult to ionize and identify. Therefore, the GAA glycosylation sites at N71, N164, N321, N401, N583, N813, and N856 were reviewed (Figure 5.3.3). In the MS analysis, the peptides from glycosylation sites containing N164, N321, N401,

and N813 were missing in the analysis of the tryptic digestion , most likely because of their poor ionizabilty, which arises from the glycosylations. Therefore, those positions seem to be always glycosylated, whereas the others are not glycosylated in all protein molecules.

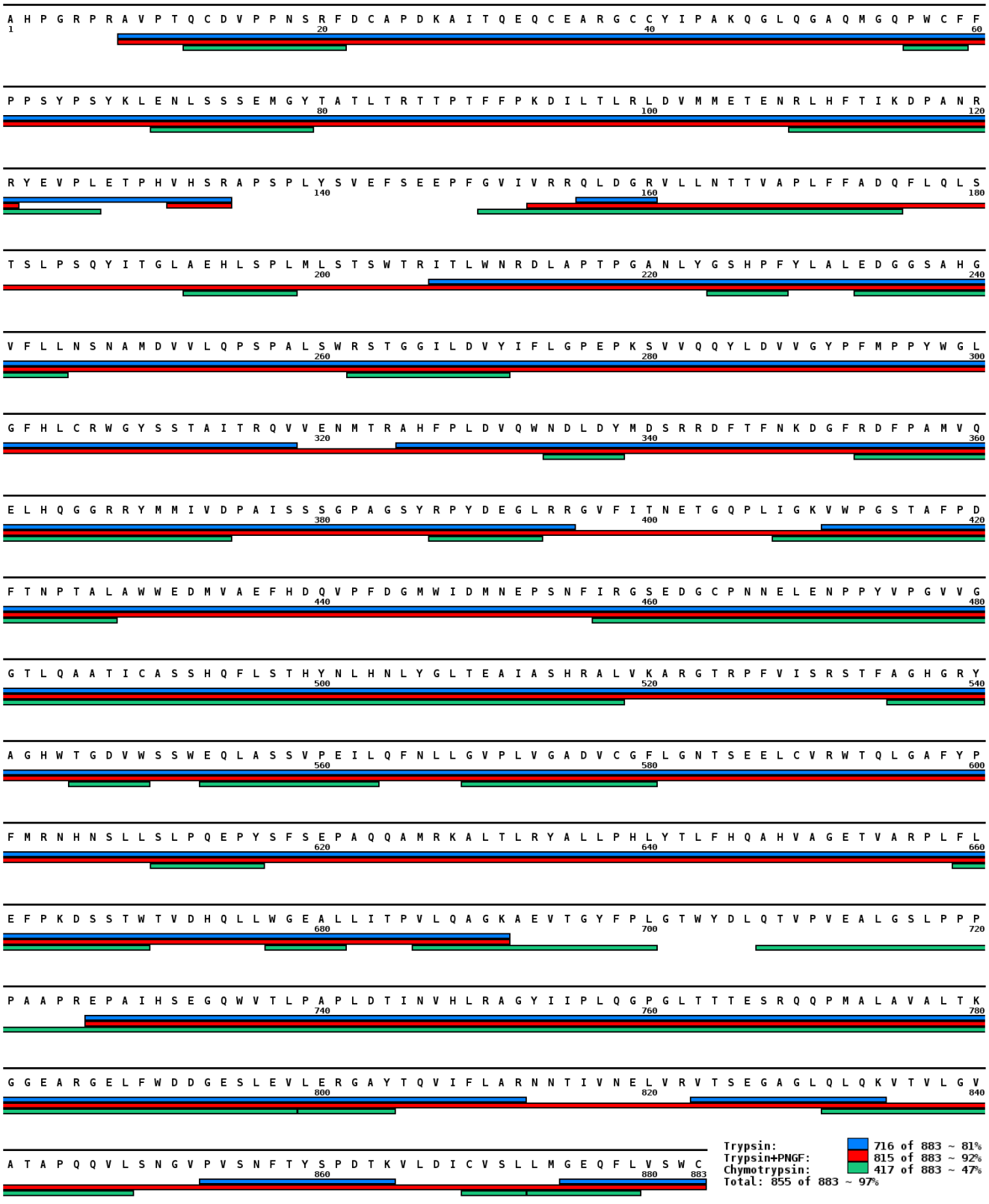

Figure 5.3.3: Summary of GAA digestions with trypsin, trpysin with PNGF and chymotrypsin. The identified sequence regions for each digestion are shown and at the positions N71, N164, N321, N401, N583, N813, and N856 glycosylations were expected.

The protein map of the chymotryptic digestion (Figure 8.2.26; Figure 8.2.23; Table 8.1.14; Table 8.1.15) displayed a low sequence coverage of only 47 %. The digestion of GAA with chymotrypsin led to many very small peptides that cannot be unambiguously identified from a single mixture by MALDI-tof MS. In combination with the results from the digestion with trypsin, a sequence coverage of 90 % was obtained (Figure 5.3.3). Moreover, chymotrypsin seemed to over-digest GAA quite rapidly, which made it challenging to identify the whole protein from the digestion. Of the peptide fragments from the glycosylation sites, the peptides with N321, N401, N583, N813, and N856 were absent. Therefore, peptides with glycosylations at N321, N401, and N813 were absent in both digestions. The analysis of a trypsin-digested GAA-aliquot previously treated with PNGF showed peptides for all glycosylation sites, including N321, N401, and N813 (Figure 8.2.27; Figure 8.2.24; Table 8.1.16; Table 8.1.17). Deglycoslyted peptides were recognized by a deamidation modification on the asparagine residue due to the deglycosylation via PNGF. All possible N-glycosylation sites were present in different peptides from the tryptic digestion. Therefore, a sequence coverage of 92 % was found, and combined with the chymotryptic digestion of GAA, a sequence coverage of 97 % was obtained, summarized in Figure 5.3.3. The detailed analysis of the glycosylation pattern is very important for determining protein functions, interactions, and structures, but for the epitope extraction, a relatively low impact was expected. During an immune response, N-glycosylations are often removed from peptides, or they block peptide cleavage sites in the proteasome while preparing for the MHC-I and MHC-II complexes.[250] Moreover, the sugar-antibody interactions have lower affinities ($K_D = 10^{-5} - 10^{-6}$) than protein-antibody interactions ($K_D > 10^{-9}$).[251–253] Therefore, glycosylated peptides seemed less relevant than non-glycosylated peptides for epitope extraction, and the non-PNGF digestions will be tested first for the epitope identifications. However, glycosylated peptides could form an epitope, as previously shown, and in general, glycosylated proteins are important for immune responses and cause strong immune responses.[250,251]

Finally, tryptic digestions of GAA under AP- and PCT conditions were compared (Table 5.3.1; Figure 8.2.28). The critical parameters, i.e., peak amount, missed cleavage sites, and sequence coverage, were similar for both digestions. As described for the other proteins, the semi-specific cleavage products for the enzymes were included in the analysis to see if they would differ for both procedures as proof of trypsin specificity. The corresponding peptide fragments were similar for the different digestion conditions, and the trypsin-specific peptides were dominant. Therefore, PCT digestion did not lead to an improvement under the tested conditions. Moreover, the digestion for 120 minutes at atmospheric pressure had the highest sequence coverage of 87 %, indicating an over-digestion for the digestion at AP1080 and the PCT-120. In further experiments, shorter digestion times should be tested.

Table 5.3.1: Comparison of tryptic digestion characteristics obtained under AP and PCT conditions for GA. Incubation time was 18 h for AP-digestion and 2 h for PCT-digestion. MSC = missed cleavage site; SQ = sequence coverage; TS = trypsin-specific peptides.

Digestion	Peaks (No.)	Amount TS (%)	Relative Intensity TS (%)	MSC = 0	MSC ≥ 1	SQ (%)
AP-1080	80	74	91	47	33	81
AP-120	78	83	86	40	38	87
PCT-120	80	74	86	41	39	81

5.3.2 Epitope Identification of GAA and mAB-43G7

The tryptic and chymotryptic digestions of GAA were used in the epitope extraction experiments with mAB-43G7. Till Schneider executed the epitope identification experiments during his master's thesis[249] stay at the Steinbeis Center, and the reanalyzed data for the epitope extraction from myself are shown.

The control experiments with sepharose beads without immobilized antibodies revealed several sepharose binders for the tryptic digestion of GAA (Figure 8.2.29; Table 8.1.18). The GAA-sequence regions identified were [110-136], [263-306], [350-364], [523-539], [634-664], [823-848]. Those sequences form 18 % of the total protein sequence and indicate a challenging epitope identification with the tryptic digestion of GAA. In contrast,

no sepharose binders were identified from the chymotryptic digestion of GAA, for which a much lower overall sequence coverage had been obtained for the digestion. The epitope extraction with the chymotryptic digestion and immobilized mAB-43G7 on preactivated sepharose 4B revealed no binding peptides either. Therefore, the peptides obtained by the chymotryptic digestion did not seem to include the epitope peptides for the mAB-43G7. The epitope extraction with the tryptic digestion of GAA was also executed with immobilized mAB-43G7 on preactivated sepharose 4B. In the acidic elutions, a cluster of signals was repeatedly recorded around a mass of 5700 Da (Figure 7.2.29). Not all signals could be annotated to tryptic GAA peptides, and the glycosylated peptides should not suddenly ionize that well. Therefore, it seemed more likely that the antibody was partly digested by the trypsin, which was still present in the digestion mixture. This could not be further investigated because of the unknown sequence of the mAB-43G7. The identified peaks from the acidic elutions (Figure 8.2.31; Table 8.1.19) were compared to those found in the corresponding control experiments (Figure 5.3.5). The protein regions [21-68], [317-324], [411-458], and [802-812] showed no overlap with the control experiment and [80-115], [304-349], [823-881] were partly overlapping with peptides from the control experiments. Therefore, these GAA sequences could contain the actual epitope. However, the IL8 experiments showed that the epitope peptides could also bind to the sepharose. However, including findings from previous studies, the epitope should be found in the 70 kDa GAA-fragment,[206] which covers the sequence [196-706] and would leave [317-324], [304-349], and [411-458], as best candidates for the epitope. The potential epitope regions for mAB-43G7 on GAA appeared to be scattered over the whole protein (Figure 5.3.4), rendering a definite epitope identification challenging based on the presented data set. However, the sequence regions [317-324], [304-349], and [411-458] sit on one side of the protein and could form a complex, discontinuous epitope. Additional experiments were needed to verify one or some of the identified peptides as the epitope or parts of it.

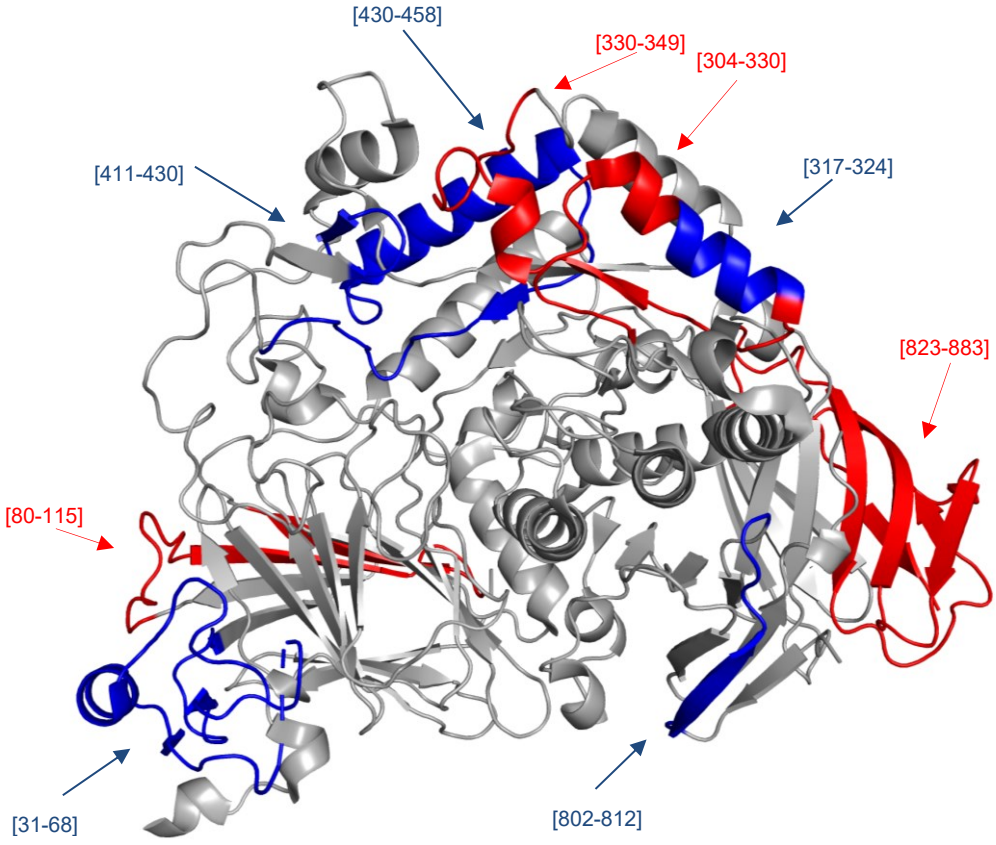

Figure 5.3.4: Potential epitope sites of mAB-43G7 on GAA. Sequence parts only found in the epitope extraction experiments are highlighted in blue, and sequences that overlap partly with the control experiment's peptides are highlighted in red. (PDB-ID: 5KZW. The protein image was created with PyMOL.[25])

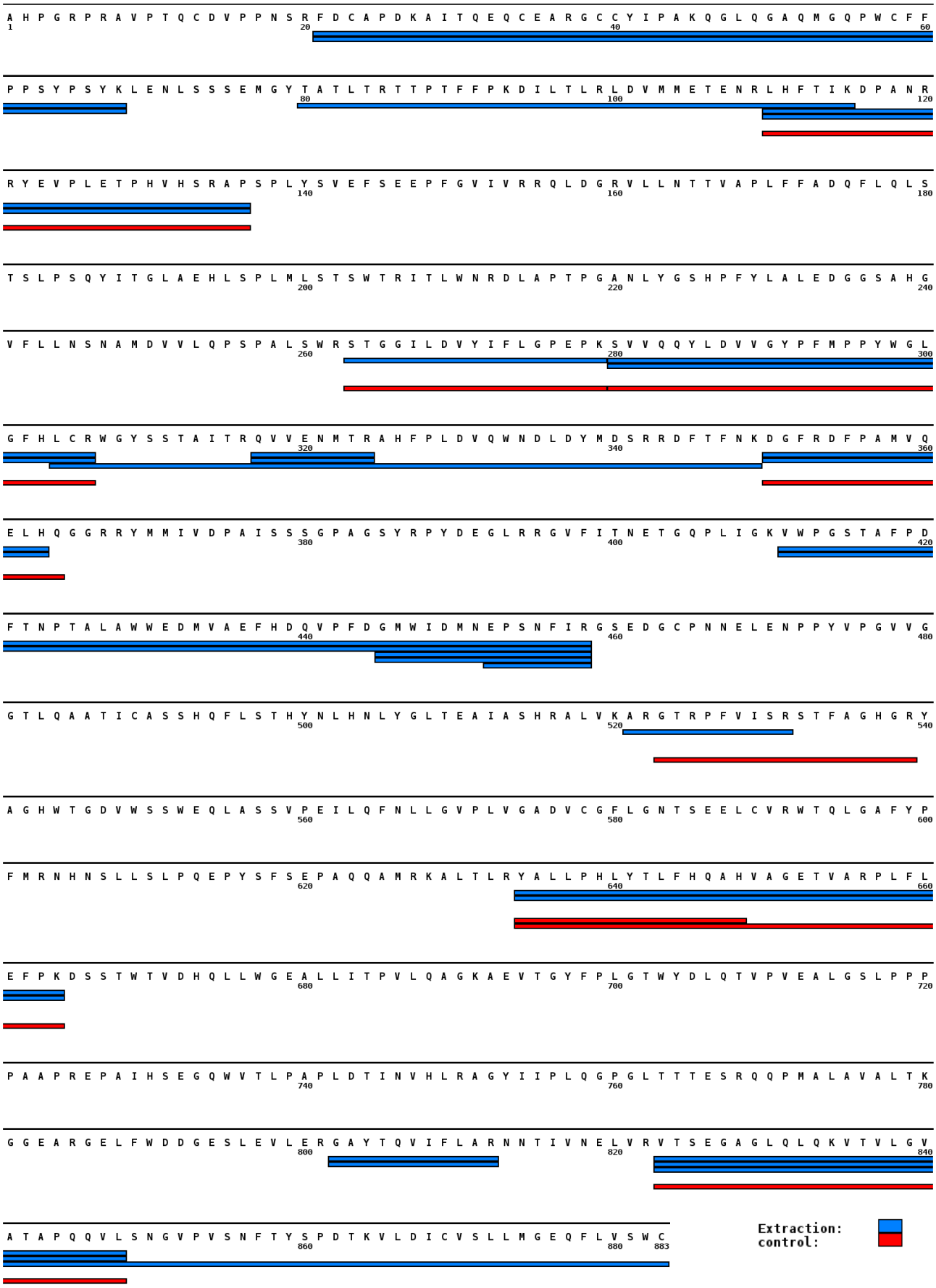

Figure 5.3.5: Protein map of the epitope extraction for the antibody and control experiments with tryptic GAA. The results of two independent epitope extractions with the mAB-43G7 column are shown. Experiments were executed by Till Schneider, and data were reprocessed by myself.

As described above, the epitope extraction with chymotryptic digestion of GAA and the mAB-43G7 antibody column yielded no peptides in the acidic elution. This suggests that the epitope binding site includes cleavage sites for chymotrypsin. This protease cleaves on the C-terminal site of Y, W, F, and L with high activity and with low cleavage activity on the C-terminal site of M, A, D, and E. In the previously identified peptides from the tryptic digest, chymotryptic cleavage sites are highly abundant (Figure 5.3.6). The resulting small peptide fragments retain little affinity to the antibody and do not even bind to sepharose 4B, so that no peptides were extracted in the corresponding experiments. Moreover, the sequence regions identified in the epitope extractions with the tryptic digestions of GAA were not found in those with chymotrypsin. Taken together, based on the experiments with the chymotryptic digestion, none of the identified tryptic peptides could be excluded as epitope-originating sequences.

For a final epitope peptide confirmation, peptides corresponding to the identified binding regions need to be synthesized to characterize their affinity to mAB-43G7. However, the potential binding sites are large, and reconstructing the potential discontinuous epitopes as synthetic peptides that bind similarly to the epitope on GAA is challenging. The high extent of unspecific surface binding of the tryptic GAA-peptides could also make the SPR-based measurements challenging. Moreover, it might not be easy to utilize one of those epitope peptides for any apheresis experiments, as proposed in the initial aim of this study. The epitope was only further investigated by in-silico experiments, and no further lab work was done.

[21-68]:	FDCAPDKAITQEQCEARGCCYIPAKQGLQGAQMGQPWCFFPPSYPSYK
[80-136]:	TATLTRTTPTFFPKDILTLRLDVMMETENRLHFTIKDPANRRYEVPLETPHVHSRAP
[263-324]:	STGGILDVYIFLGPEPKSVVQQYLDVVGYPFMPPYWGLGFHLCRWGYSSTAITRQVVENMTR
[350-363]:	DGFRDFPAMVQELH
[411-458]:	VWPGSTAFPDFTNPTALAWWEDMVAEFHDQVPFDGMWIDMNEPSNFIR
[521-531]:	ARGTRPFVISR
[634-664]:	YALLPHLYTLFHQAHVAGETVARPLFLEFPK
[802-812]:	GAYTQVIFLAR
[823-883]:	VTSEGAGLQLQKVTVLGVATAPQQVLSNGVPVSNFTYSPDTKVLDICVSLLMGEQFLVSWC

Figure 5.3.6: All potential epitope peptide sequences with chymotrypsin cleavage sites. The main cleavage sites of chymotrypsin are highlighted in red, and the amino acids with low enzyme activity are in yellow.

5.3.3 In-silico analysis of GAA antibody epitopes

As in the previous sections, GAA-epitope predictions were made with BepiPred-2.0, DiscoTope-2.0, SEPPA-3.0, and BCEPS. The crystal structure with the PDB-ID of 5KZW was used for predictions with the discontinuous predictors. The results from the predictions and experimentally identified epitope candidate peptides were compared in the GAA protein map and on the corresponding crystal structure (Figure 5.3.7, Figure 8.2.32). The experimentally identified epitope peptides were identified in at least one prediction, and the highest immunogenic sites in the protein, as supposed by the consensus of all four prediction tools, were amino acids K45, Q46, D340, S341, S380, G382, P383, and A384. The consensus of at least three tools suggests the N-terminal protein site is highly immunogenic, corresponding to the experimentally found sequence [21-68]. Peptide [304-349] also contains the predicted highly immunogenic amino acids D340 and S341. The experiments and predictions suggest a discontinuous epitope for mAB-43G7 around GAA[304-349]. This protein site could be synthesized first to validate it as an epitope-derived peptide. Furthermore, peptides from [317-324] and [411-458] could be synthesized next for affinity measurements with mAB-43G7. Regarding the experimental design and enzyme choice, trypsin was suggested because it generated larger peptide fragments from GAA. In general, for a first epitope extraction, an enzyme that cleaves only after one specific amino acid, like Lys-C, Glu-C, or Arg-C, might be beneficial to scout for an epitope region as it leads to even larger fragments that have a higher

chance to contain the full epitope and exhibit high affinity. This would facilitate epitope extraction in future experiments.

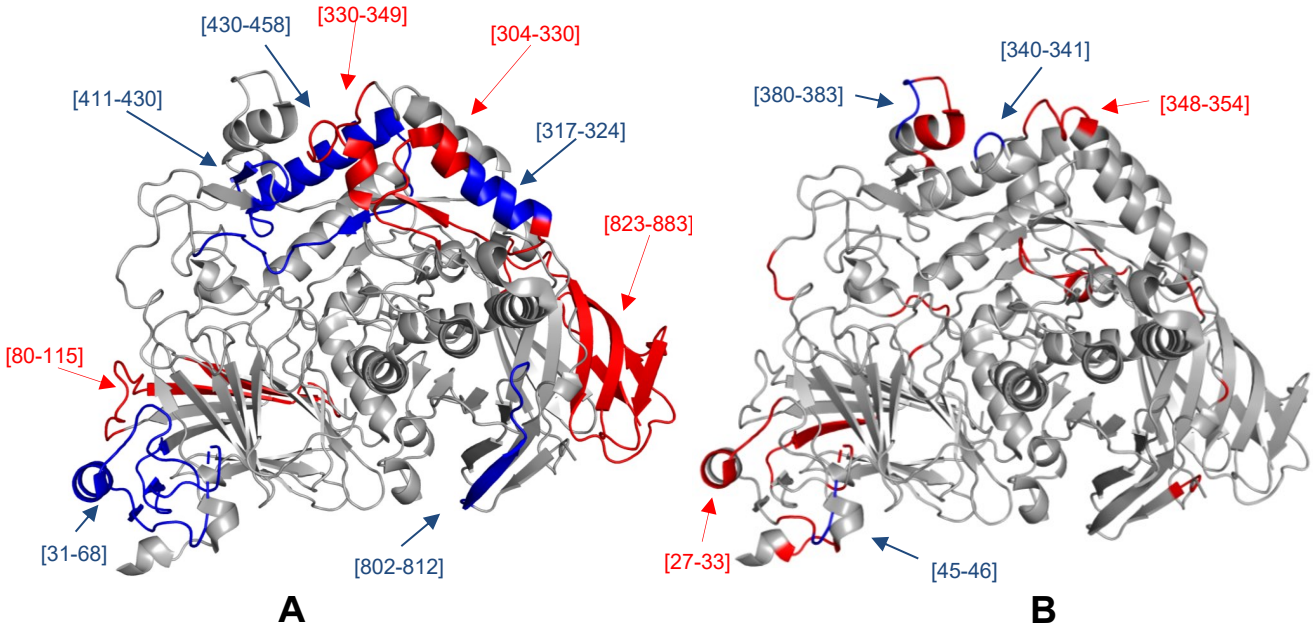

Figure 5.3.7: Crystal structure of GAA (PDB: 5KZW) with (A) experimental epitopes (red), (B) predicted epitope sites with the consensus of four (red) and three (blue) different tools. (The protein images were created with PyMOL.[25])

5.4 Assay development for survival motor neuron protein (SMN) quantification

The recombinant in *E.coli* expressed SMN protein (rSMN) and its monoclonal antibody mAB-7B10 (chapter 2.2.4) were characterized with the standard methods. In binding assays, like dot-blot and SPR biosensor analysis, the SMN protein was tested with the mAB-7B10 (epitope: rSMN[40-57]) and newly produced polyclonal antibodies pAB-IG1106 and pAB-IG1107 against a C-terminal SMN peptide (epitope: rSMN[279-294]). Furthermore, the mAB-7B10 and its epitope peptide were evaluated for a quantification assay of SMN protein via epitope extraction combined with MALDI-tof MS measurements. Since it was known that a linear epitope existed, it was necessary to demonstrate identifiability by epitope extraction and perform detailed affinity characterization. Then, the quantification assay was tested with synthetic epitope peptides. Tamsila Khan executed some of the epitope extraction experiments, prepared dilutions for the quantification tests, and assisted with the peptide synthesis.[254] The corresponding experiments were flagged, and the shown images are from myself with reanalyzed datasets.

5.4.1 Protein characterization by enzymatic digestion, MALDI-MS, and SDS-PAGE

Initial analysis of rSMN and its tryptic digestion under AP and PCT digestions by SDS-PAGE met the expectations (Figure 3.1.13). The rSMN appeared to be pure, and the protein was detectable down to 63 ng, the lowest loaded amount, and no band was seen for the digested rSMN samples. Therefore, the digestion efficiency was suitable for further experiments. The exact mass of rSMN, 35537.4 Da, was recorded in the corresponding MALDI-tof MS measurements as singly and doubly charged ions (Figure 8.2.30). The tryptic digestion of rSMN under atmospheric pressure was analyzed by MALDI-tof MS (Figure 8.2.34; Table 8.1.20; Table 8.1.21). Particular interest was laid on the epitope peptide of mAB-7B10, which should be represented by peptide rSMN[34-57].

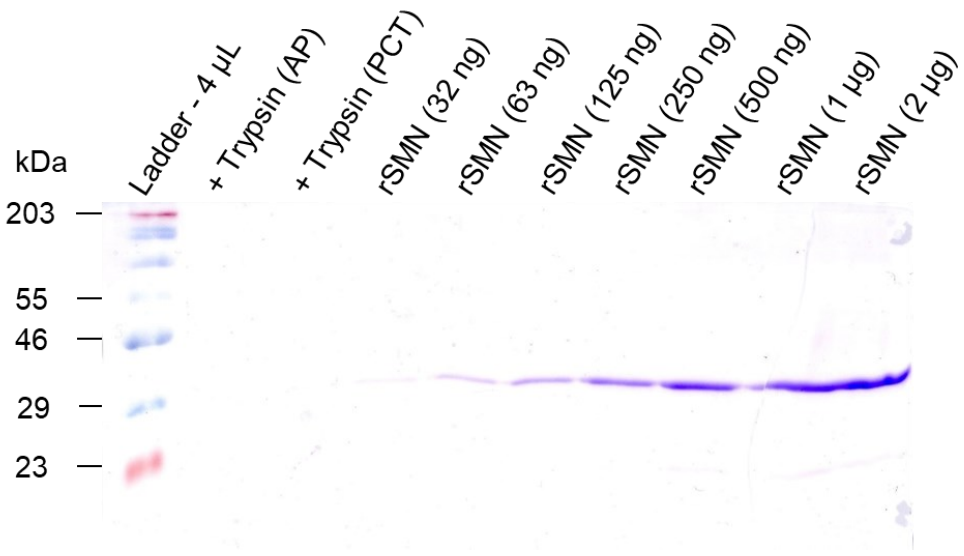

Figure 5.4.1: SDS-PAGE of rSMN1 at different amounts (0.032 - 2 µg) spotted on a 16 % acrylamide/bisacrylamide gel. 1 µg tryptic digestion of rSMN digested under atmospheric (AP) and high-pressure cycling (PCT) was loaded on the gel. 4 µL protein standard was loaded in the first lane.

Indeed, the peptide rSMN[34-57] was present in the digestion map, but truncated peptides from the epitope region were also seen (Figure 5.4.2). Therefore, it might be necessary to reduce the digestion time to avoid over-digestion of the N-terminal sequence of rSMN. However, the digestion had a complete sequence coverage of 100 %. The proline-rich C-terminal site of rSMN was detected in a few large peptides like rSMN[249-316] and rSMN[169-209] because of the lack of lysine and arginine residues. Moreover, the rSMN had some lysine-rich patches like rSMN[100-120], which created many peptides for these sequence regions with many semi-specific tryptic peptide fragments. Therefore, lowering the digestion time could prevent these events.

The digestion patterns for digestions of rSMN with trypsin under AP and PCT conditions looked very similar, and most of the identified peptides were identical or similar (Table 5.4.1; Figure 8.2.33). The high amount of semi-specific tryptic peptide fragments was still seen under both conditions, which indicated an over-digestion of rSMN, and actually, a much shorter digestion time could be sufficient for optimal digestion. The lower peak count for the 120-minute digestion under atmospheric pressure points to the over-digestion for AP-1080 and PCT-120 digestions. Therefore, 30-60 minutes of digestion under atmospheric pressure might be enough, and even shorter times for PCT digestion to generate reasonable digestion for further experiments.

Table 5.4.1: Comparison of tryptic digestion characteristics obtained under AP and PCT conditions for rSMN. Incubation time was 18 h for AP-digestion and 2 h for PCT-digestion. MSC = missed cleavage site; SQ = sequence coverage; TS = trypsin-specific peptides

Digestion	Peaks (No.)	Amount TS (%)	Relative Intensity TS (%)	MSC = 0	MSC ≥ 1	SQ (%)
AP-1080	65	48	76	30	35	100
AP-120	58	60	77	18	40	100
PCT-120	67	57	79	30	37	100

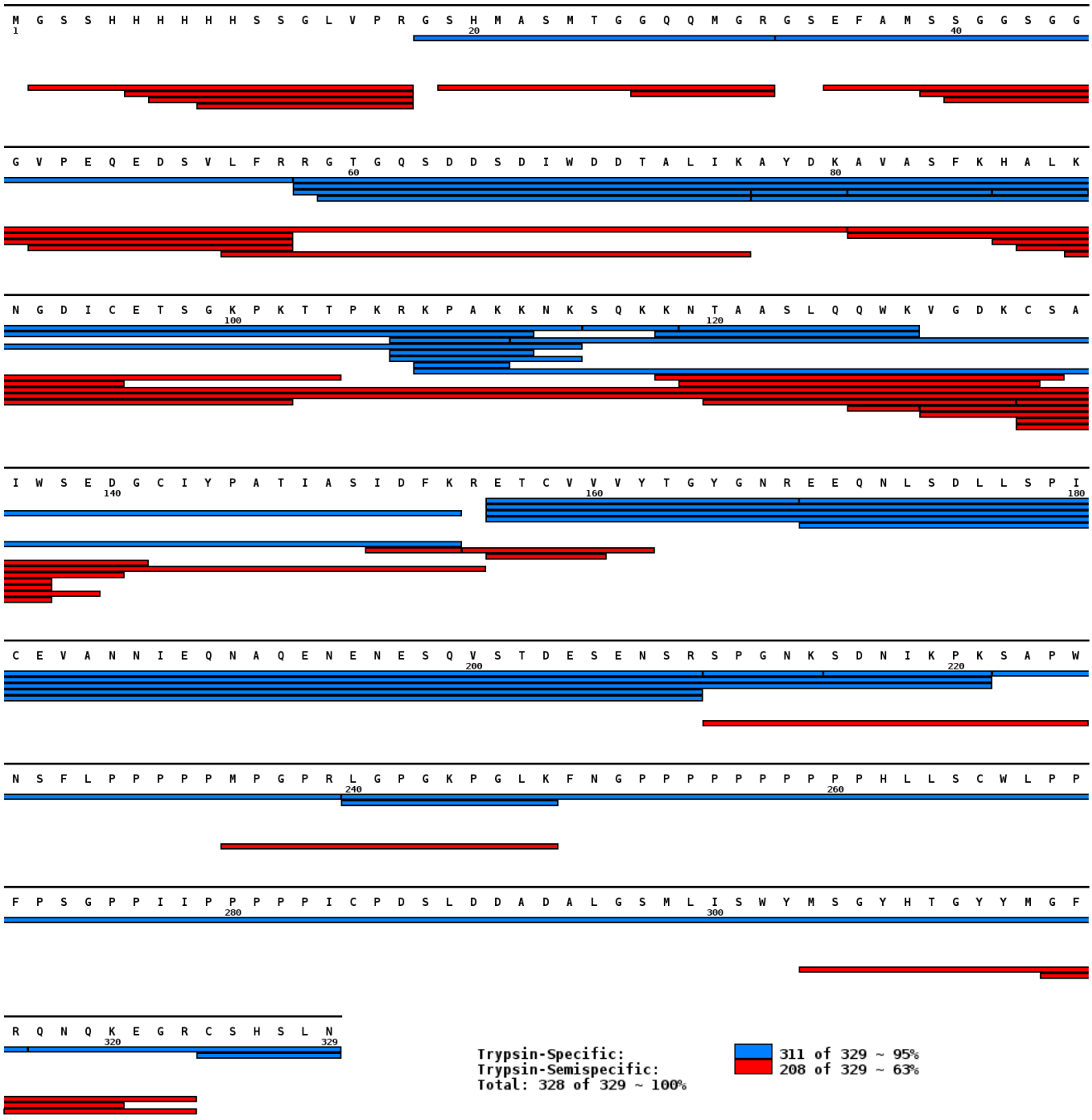

Figure 5.4.2: Protein Map of the analyzed tryptic rSMN digestion following the AP protocol. The trypsin-specific and semi-specific peptide fragments are highlighted, resulting in a sequence coverage of 100 %. (The protein image was created with PyMOL.[25])

5.4.2 Epitope verification of rSMN and mAB-7B10

The known antibody mAB-7B10 epitope should be used to quantify the SMN protein from biological samples. Therefore, several assay tests were executed for a corresponding quantification assay. The experimental setup included epitope extraction from an affinity column or chip and MALDI-tof MS measurements. The approach by epitope extraction via affinity chromatography was tested first. The known epitope rSMN[46-57] (key sequence for antibody binding rSMN[40-57]) for the mAB-7B10 was present in the tryptic digestion as rSMN[33-57] and

should be identified in different epitope extraction experiments. The epitope extraction from an affinity column (control and antibody experiment) was executed by Tamsila Khan during her bachelor thesis.

An initial control experiment with sepharose 4B without immobilized mAB-7B10 and 1 µg tryptic rSMN revealed no column-binding peptides in the tryptic rSMN digestion (Figure 8.2.50). Additionally, no peptides were seen after the 5th washing fraction, and rSMN[33-57] was seen until the 3rd washing fraction. The epitope extraction with immobilized mAB-7B10 on CNBr-activated Sepharose 4B and 1 µg tryptic rSMN diluted to 200 µL with PBS from digestion buffer showed the epitope peptide rSMN[33-57] in the acidic elution (Figure 5.4.3; Table 8.1.23).

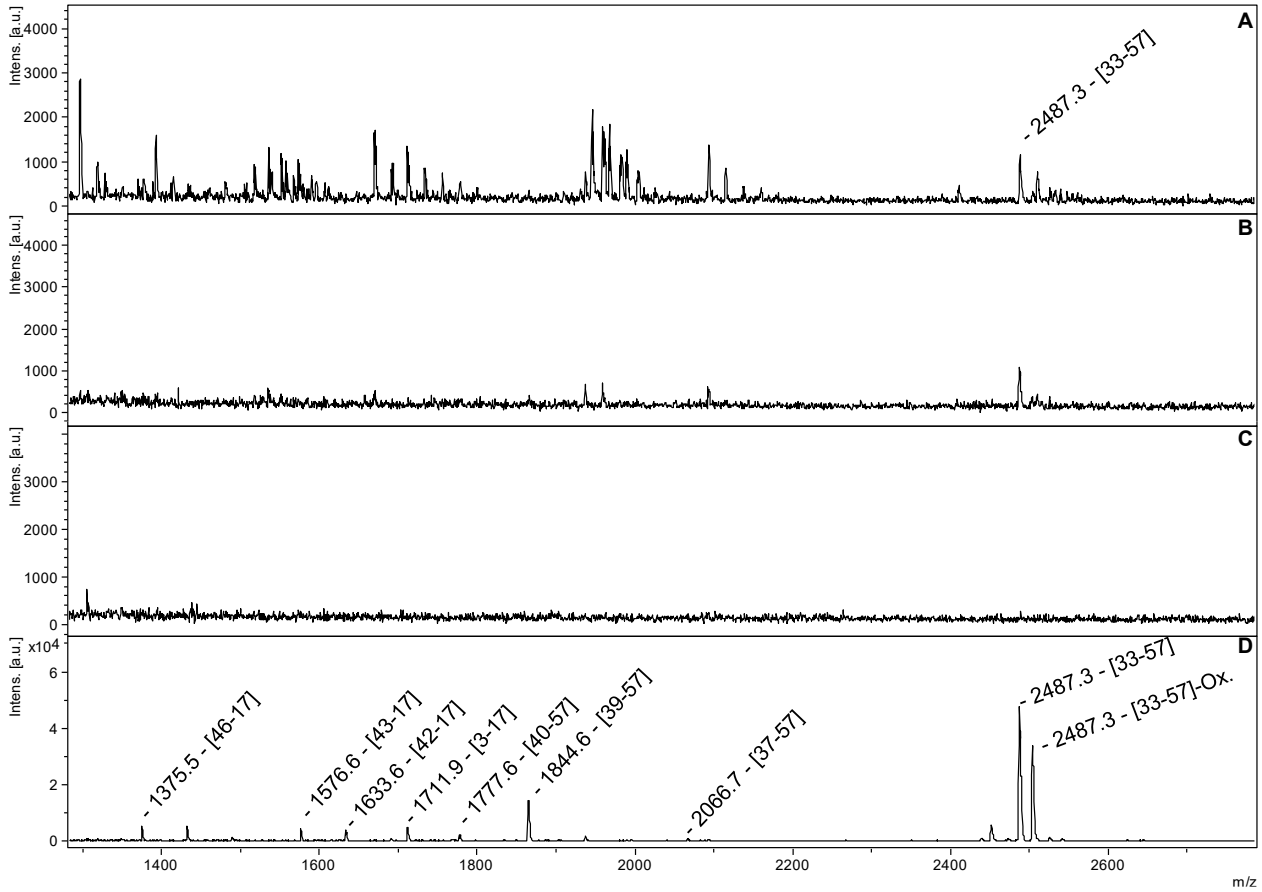

Figure 5.4.3: MALDI-tof MS measurements of selected fractions from the mAB-7B10 column and injected tryptic rSMN: (A) Injection fraction; (B) 3rd washing fraction; (C) 5th washing fraction; (D) acidic elution with 0.1 %TFA in MQ. The experiment was executed by Tamsila Khan and reprocessed data are shwon. (Method: RP; Matrix: DHB)

Moreover, the acidic elution showed additional peaks for truncated peptides from rSMN[33-57], corresponding to semi-tryptic peptide fragments, which were not detected in the initial digestion analysis. Most likely, they were enriched during the extraction, which is why they were undetected in the digestion analysis. The linear epitope showed excellent recovery via affinity chromatography, which indicates a well-conserved affinity in the linear epitope peptide. A good epitope peptide recovery was essential for the planned semi-quantification of SMN via tryptic digestion and MALDI-tof MS. Nevertheless, compared to the previous epitope extractions of IL8, CTSD, and GAA, no column-binding peptides were identified in the control experiments. Therefore, the absence of column binders and the linear (semi-structural) epitope made the corresponding data analysis much easier and faster.

The second step for the epitope peptide validation was the previously described epitope extraction from an SPR biosensor chip. The chip was functionalized with MHDA-PG, and the mAB-7B10 was crosslinked via DMP for covalent immobilization (Figure 8.2.38). The corresponding sensorgram for the injected tryptic rSMN showed a significant difference for reference and sample channel, which indicated a well-preserved affinity of the linear

epitope peptide to the mAB-7B10 (Figure 8.2.38, Figure 8.2.29). The collected fractions for the executed epitope extraction showed results similar to those of the column experiments (Figure 5.4.4). The tryptic peptide rSMN[33-57] was found in the first washing solution and the acidic elution. The epitope extraction with the SPR chip seemed less efficient than with the affinity column. Therefore, the quantification of rSMN by epitope extraction and MALDI-tof MS was further investigated. The synthetic peptides rSMN[37-57] and rSMN[38-57] were used in the following chapters to establish a quantification assay.

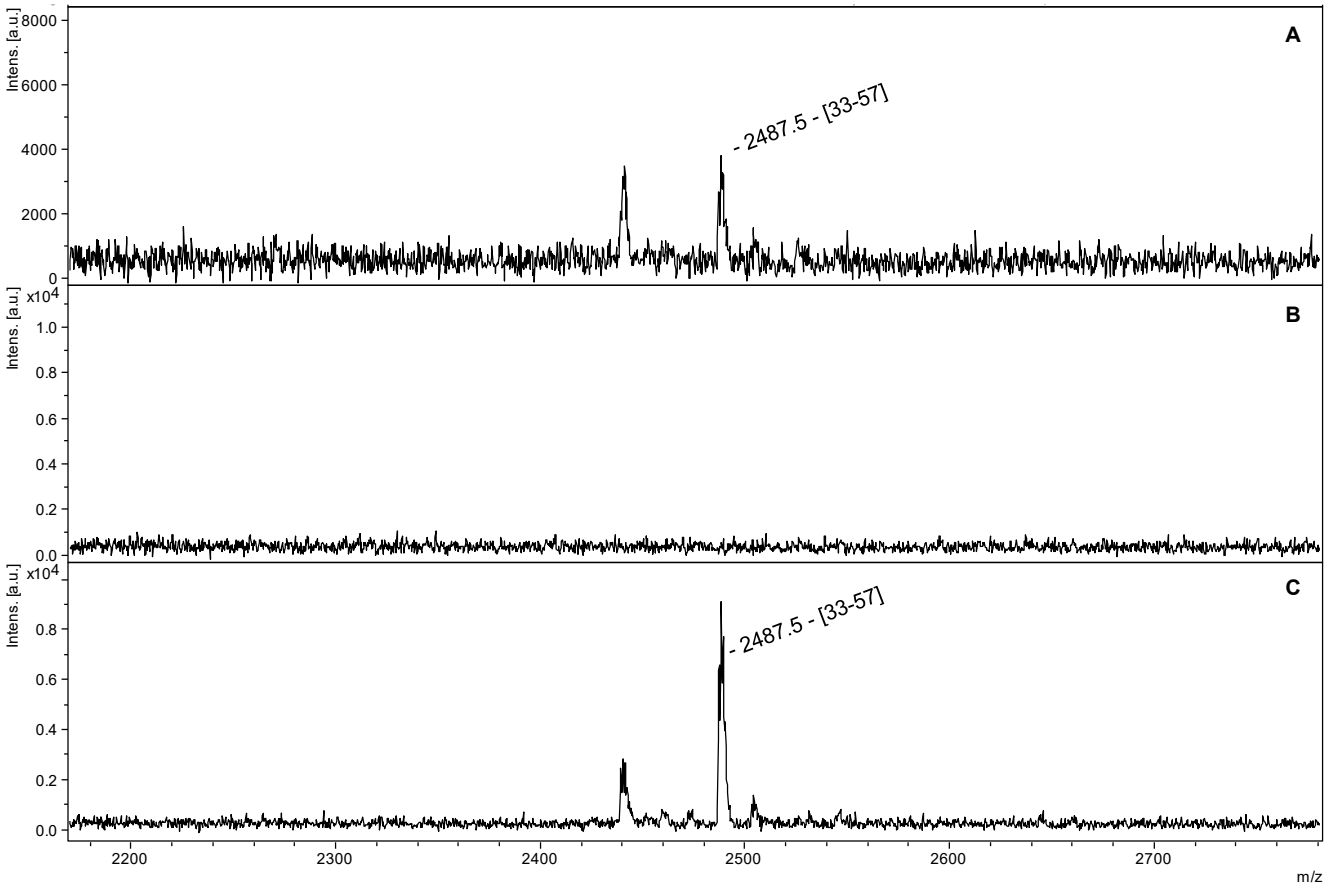

Figure 5.4.4: MALDI-tof MS measurements of selected fractions from the mAB-7B10 functionalized biosensor chip injected tryptic rSMN. The flow rate was 5 µL/min, and PBS was used as a running buffer. Before MALDI-tof MS measurements, the collected fractions were desalted via C18-ZipTip. (A) First washing fraction; (B) 7th washing fraction; (C) acidic elution with 0.1 %TFA in MQ. (Method: RP; Matrix: DHB)

5.4.3 In-silico analysis of SMN antibody epitopes

The epitope of mAB-7B10 on the SMN protein was known and extensively studied before (chapter 1.2.4). No experimental crystal structure of SMN was available on the PDB-databank when this study was executed. Therefore, predictions were only possible with tools that needed the amino acid sequence as input, i.e., BepiPred-2.0 and BCEPS. Predictions are compared to the known epitope rSMN[46-57] and experimentally validated tryptic epitope-peptide rSMN[33-57]. The corresponding protein map of rSMN (Figure 5.4.5) showed that the predictions include the identified epitope, but many more protein sites seem to be immunogenic and could be part of an epitope if the complete protein was used to raise an antibody. The simplicity of the linear epitope predictions seemed not very helpful for distinguishing more or less immunogenic sites from each other in the SMN sequence. However, the predictions indicated SMN as a highly immunogenic protein.

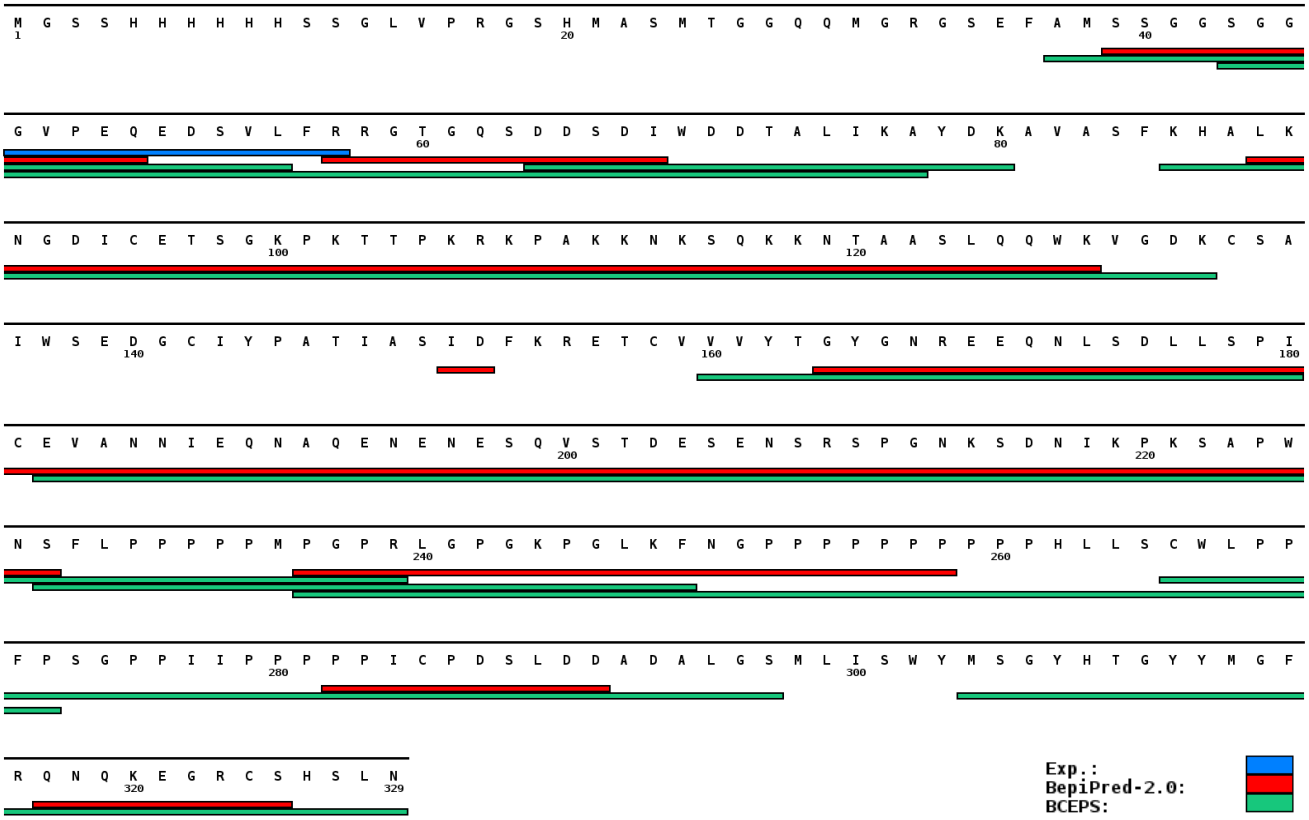

Figure 5.4.5: Protein map of rSMN with experimentally determined epitope results and predictions from Bepipred-2.0 and BCEPS.

5.4.4 Epitope peptide synthesis by FSPPS

Similar to the previous peptide synthesis were the peptides rSMN[37-57] (sequence: AMSSGGSGGGVPEQEDSVLFR) and rSMN[38-57] (sequence: MSSGGSGGGVPEQEDSVLFR) synthesized by FSPPS on a 1 mmol scale. Both peptides were synthesized in one batch, and before coupling the last amino acid (alanine), roughly half of the resin was taken out of the reaction chamber to get rSMN[38-57]. Reaction monitoring diagrams and chromatograms can be reviewed in Tamsila Khan's bachelor thesis.[254] Chromatograms of purified fractions and corresponding MALDI-tof MS analysis are in the appendix (Figure 8.2.52; Figure 8.2.53; Figure 8.2.51). The coupling of the last two serine residues was noticeable, which showed decreased absorption maxima. Therefore, a double coupling for those amino acids might increase the product yield if the synthesis has to be repeated. Overall, the synthesis seemed reasonable for further characterization of the crude peptides by HPLC and MALDI-tof MS. The purified peptides had purities between 97 and 99 %, which was perfectly suitable for the aimed semi-quantification tests (Table 5.4.2). Moreover, the MALDI-tof MS analysis showed the expected masses and confirmed the collected fraction's identity (Figure 8.2.51).

Table 5.4.2: Summary of the SMN peptide synthesis. Chromatograms and mass spectra are in the appendix. GT = gradient time frame; RT = retention time.

Name	Gradient (% Solvent A)	GT (min.)	RT (min.)	Purity (%)	Calc. Mass ([M+H]⁺)	Exp. Mass ([M+H]⁺)
rSMN[38-57]	80 to 74	20	9.5	97.6	1995.9	1996.2
rSMN[37-57]	80 to 70	20	8.9	98.6	2066.6	2066.9

5.4.5 Qualitative binding assay for rSMN-antibody complexes

A qualitative binding assay for rSMN binding to a monoclonal antibody (mAB-7B10; N-terminal epitope) and two affinity-purified, polyclonal antibodies (IG-1106 and IG-1107; C-terminal epitope) should indicate the relative strength of the interactions. As previously described, the polyclonal antibodies had been produced in rabbits by vaccination with a C-terminally modified peptide. After three vaccinations, bleeding and affinity purification of the antibody yielded the first antibody fractions, IG-1106-1 and IG-1107-1, which were used for affinity comparison. The dot blot with different rSMN concentrations spotted on a PVDF membrane should first compare the antibody performances (Figure 5.4.6). Using antibody mAB-7B10, SMN quantities between 10 and 400 ng were detectable.

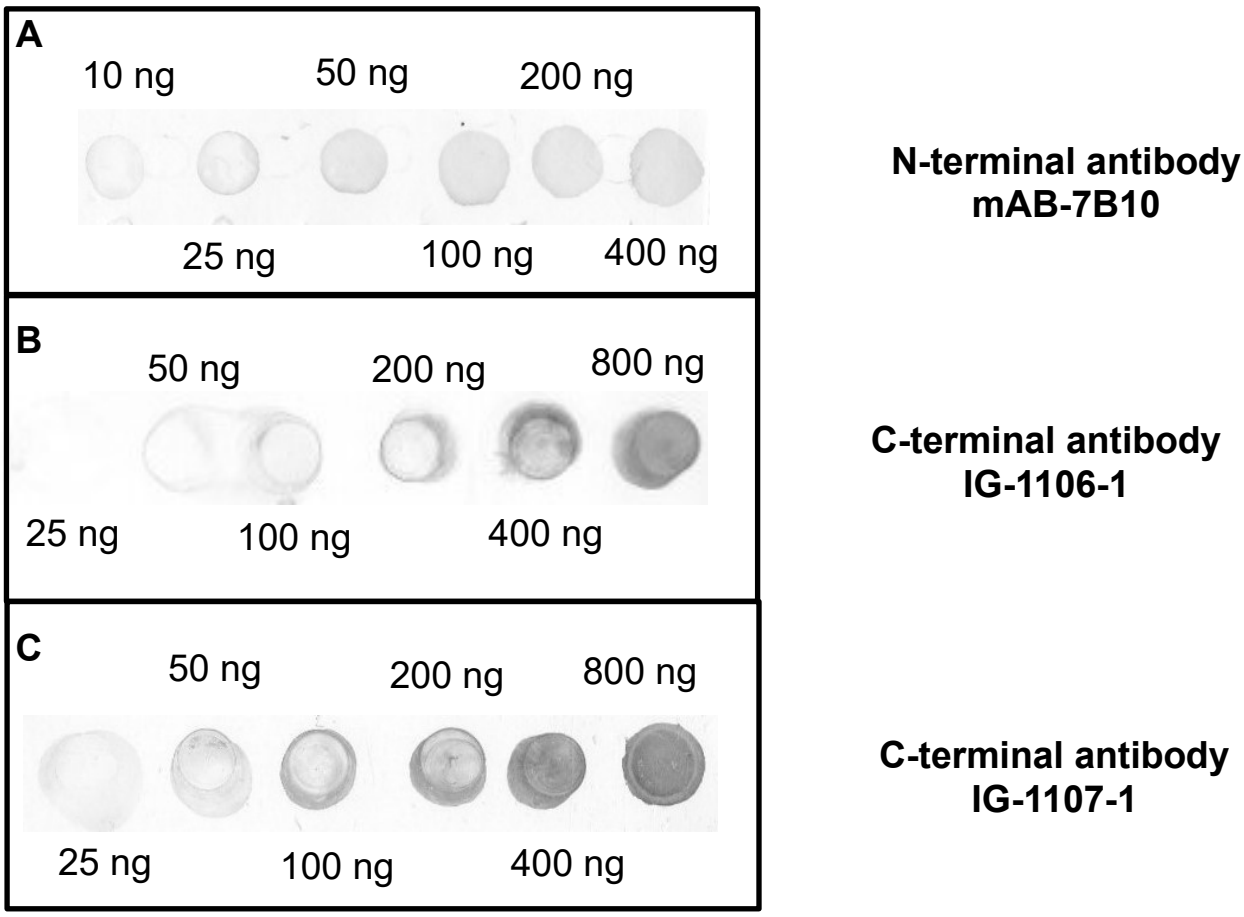

Figure 5.4.6: Dot blot experiments with immobilized rSMN on PVDF membrane at different amounts. Primary antibody concentrations were 1.8 µg/mL, and secondary antibodies (anti-mouse-HRP antibody and anti-rabbit-HRP antibody) were used in a 1:1000 dilution. Staining was achieved with 4-chloronaphtol/hydrogen peroxide incubation for (A) 5 minutes and (B)/(C) 10 minutes.

IG-1106-1 and IG-1107-1 were tested with rSMN quantities between 25 - 800 ng, where IG-1107-1 could detect the full detection range, whereas IG-1106-1 failed to detect the lowest concentration. The expected SMN protein levels for SMA patients were found to be 5 - 20 ng/mL whole blood and for healthy individuals to be 30 - 70 ng/mL whole blood.[215,217] Therefore, at least one milliliter of whole blood would be necessary for this assay to distinguish diseased from non-diseased individuals, neglecting dilutions and processing of the whole blood samples. However, there would be more sensitive detection setups, like luminescence-based substrates, for the dot-blot if used for a first assessment of sample concentrations. Moreover, the mAB-7B10 showed the best sensitivity in the dot-blot experiment compared to the polyclonal antibodies, but all antibodies seemed to exhibit reasonable affinities to the rSMN protein. Therefore, a more sensitive method could utilize these antibodies for reliable SMN protein quantifications. This hypothesis will be further investigated by SPR and MS analysis.

5.4.6 Affinity determination of rSMN-antibody complexes via SPR measurements

The performance of the introduced rSMN binding antibodies was examined for the SPR-based biosensor analysis to attempt to estimate their performance in an SMN detection and quantification assay. The affinity of the rSMN-antibody complexes (mAB-7B10, IG-1106-1, IG-1106-2, IG-1107-1, and IG-1107-2) was determined with immobilized rSMN on an MHDA-chip (Figure 5.4.7, Figure 8.2.40). A stable rSMN immobilization of 1172 µRIU was achieved. The antibodies were injected separately in a nanomolar concentration range in PBS-BSA buffer at 50 µL/min flow rate, and 50 mM glycine in 40 mM HCl was used as a regeneration solution.

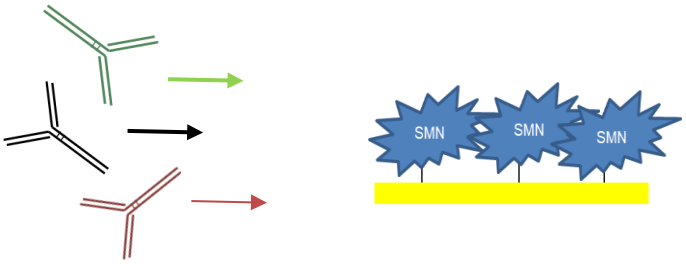

Figure 5.4.7: Experimental setup for anti-SMN antibody (mAB-7B10; IG-1106; IG-1107) comparison regarding binding kinetics and affinities.

The sensorgrams for the rSMN-antibody interactions revealed differences between the tested antibodies (Figure 5.4.8; Figure 8.2.41; Table 5.4.3). The mAB-7B10 had the fastest ka, slowest kd, and overall the lowest K_D with 0.25 nM of all rSMN antibodies tested with this experimental setup. IG-1106-1 (K_D =38 nM) and IG-1107-1 (K_D = 12.1 nM) showed significantly lower affinities. SPR data for the antibody extracts obtained after two additional vaccinations (IG-1107-2 and IG-1106-2) showed similar K_D values compared to IG-1106-1 and IG-1107-1. K_D values were slightly higher, but fit qualities (Chi^2) differed, especially for the IG-1106-1 and IG-1106-2. For those antibodies, the 1:1 binding model seemed far from optimal, which was to be expected because of the polyclonality of the antibodies. An explanation of the poor fit for the binding curves of IG-1106 could be a higher heterogeneity in this polyclonal antibody's composition than in that of IG-1107, which did not significantly change after additional vaccinations. Association rates of rSMN-IG-complexes were similar, but the small differences led to a Bmax of 600 µRIU for IG-1106 and a Bmax of 200 µRIU for IG-1107 at the same concentration. This result indicated that the sensitivity for SMN that can be reached with IG-1106 was 2 to 3 times higher than with IG-1107. The higher signal intensity might be beneficial for a quantification assay, even due to the faster dissociation of the rSMN-IG-1106 than the IG-1107 complex. Therefore, IG-1107 was expected to perform better in a corresponding quantification assay than IG-1106.

Table 5.4.3: Kinetic and affinity constants for the rSMN-antibody complexes determined via SPR-based measurements and a 1:1 binding model.

Curve name	ka (1/(M*s))	est. error	kd (1/s)	est. error	KD (nM)	est. error	Chi^2 ([Signal (uRIU)]^2)
mAB-7B10	2.08×10^{5}	$\pm 4.42 \times 10^{1}$	5.23×10^{-5}	$\pm 3.17 \times 10^{-6}$	0.25	±0.02	81.0
IG-1106-1	3.06×10^{4}	$\pm 0.92 \times 10^{1}$	1.16×10^{-3}	$\pm 1.13 \times 10^{-6}$	38.0	±0.05	292.4
IG-1106-2	2.20×10^{4}	$\pm 0.55 \times 10^{1}$	1.08×10^{-3}	$\pm 1.38 \times 10^{-6}$	48.9	±0.07	171.0
IG-1107-1	3.52×10^{4}	$\pm 2.69 \times 10^{1}$	4.26×10^{-4}	$\pm 5.21 \times 10^{-6}$	12.1	±0.16	16.6
IG-1107-2	4.31×10^{4}	$\pm 2.83 \times 10^{1}$	6.09×10^{-4}	$\pm 0.81 \times 10^{-6}$	14.1	±0.03	20.7

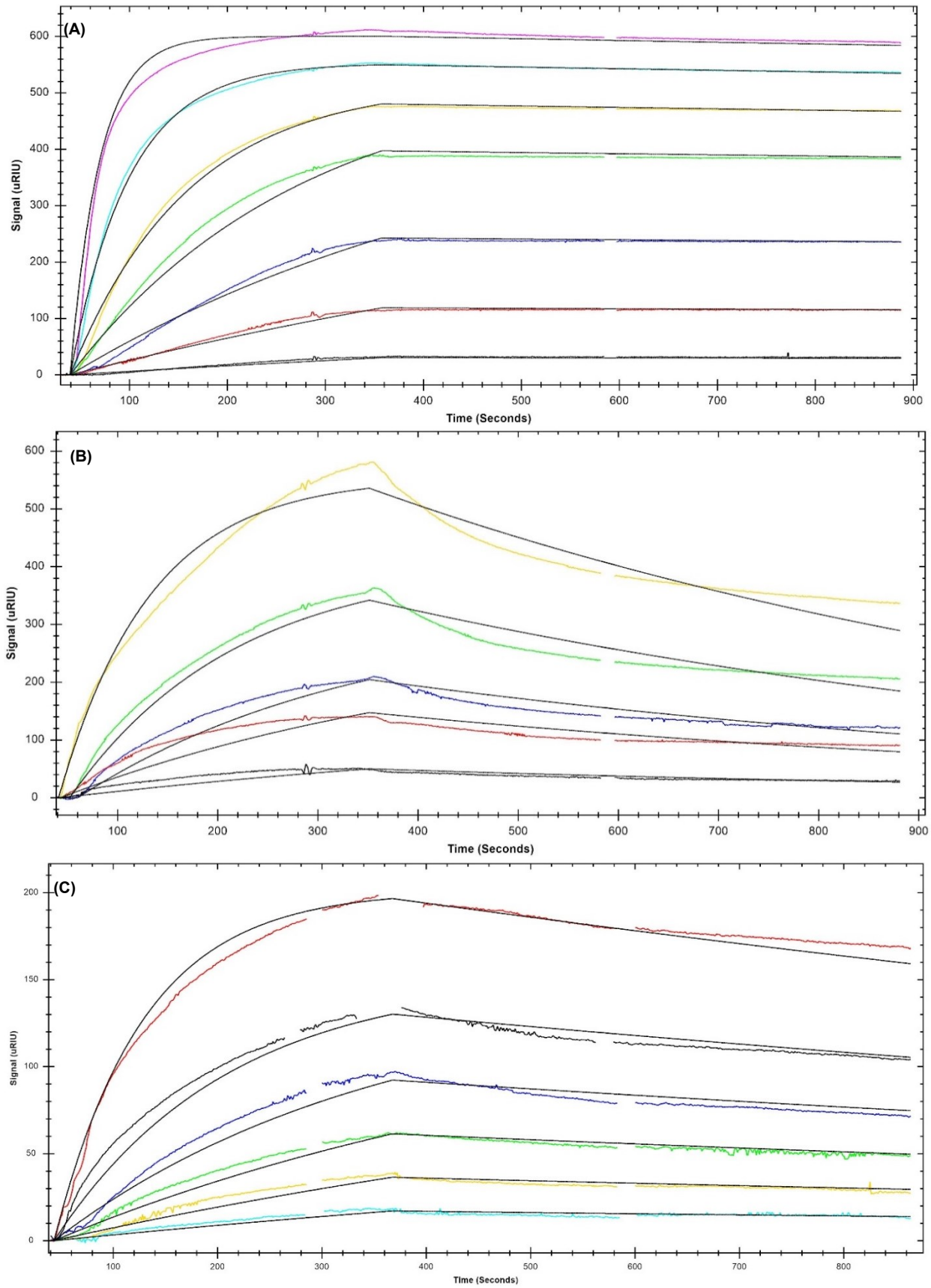

Figure 5.4.8: Senosorgrams for double-referenced curves for the sample and reference channel with buffer and anti-SMN antibody injections over immobilized rSMN. 1:2 dilutions of the antibodies with (A) 5-320 nM mAB-7B10, (B) 10-320 nM IG-1106-1, and (C) 10-320 nM IG-1107-1 were injected. Colored lines represent the measured curves, and black lines represent the 1:1 binding fit. Buffer spikes were cut out of the curves for better fitting, which led to holes in the curves.

Based on these results, the SMN quantification assay will be based on immobilized mAB-7B10 to capture SMN as the primary antibody for detection. Therefore, the mAB-7B10-SMN binding was further characterized after immobilization of mAB-7B10 via PG on an MHDA-gold chip (Figure 5.4.9; Figure 8.2.38; Figure 8.2.42).

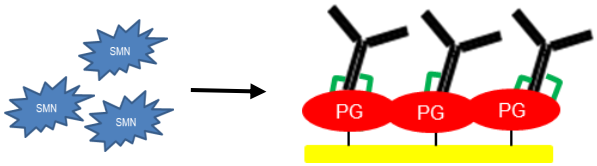

Figure 5.4.9: Experimental setup to analyze the interaction of soluble rSMN and mAB-7B10 immobilized via protein G.

The antibody mAB-7B10 was immobilized at 8 and 60 µg/mL concentrations and tested for interaction with rSMN at different concentrations. The SPR-chips with different amounts of immobilized mAB-7B10 showed similar kinetics and affinities for rSMN binding (Table 5.4.4; Figure 5.4.11). For 8 µg/mL and 60 µg/mL immobilized mAB-7B10, a K_D of 0.69 nM and 0.79 nM was determined, respectively. The sensorgrams showed a very slow dissociation of the rSMN-mAB-7B10 complex. Buffer jumps at the higher rSMN concentrations and the slow dissociating complex made accurate data fitting more challenging. Overall, the affinity (KD) determined for the rSMN - mAB-7B10 interaction was between 0.25 and 0.79 nM.

Table 5.4.4: Kinetic and affinity constants for the rSMN-antibody complexes determined via SPR-based measurements and a 1:1 binding model for different amounts of immobilized mAB-7B10.

Chip Preparation	ka (1/(M*s))	est. error	kd (1/s)	est. error	KD (nM)	est. error	Chi² ([Signal (uRIU)]²)
8 µg/mL mAB-7B10	1.39×10^{5}	$\pm 5.85 \times 10^{1}$	9.60×10^{-5}	$\pm 3.67 \times 10^{-5}$	0.69	±0.26	21.58
60 µg/mL mAB-7B10	0.96×10^{5}	$\pm 8.12 \times 10^{1}$	7.63×10^{-5}	$\pm 0.17 \times 10^{-5}$	0.79	±0.02	58.02

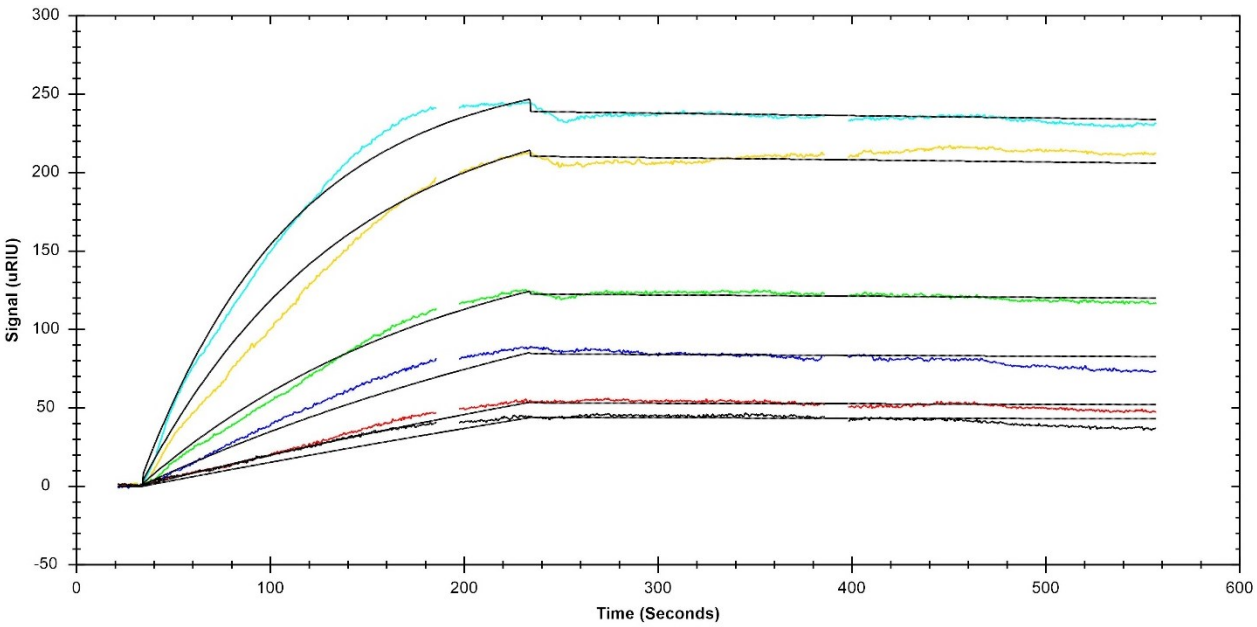

Figure 5.4.10: Sensorgrams for double-referenced curves for the sample and reference channel with buffer and rSMN injections in PBS at 75 µL/min. Injections of 5, 10, 20, 40, 60, 80 nM rSMN over mAB-7B10 (immobilization with 8 µg/mL mAB-7B109). Colored lines represent measurements. Black lines represent a 1:1 binding fit with buffer jumps at the beginning and end of the association phase.

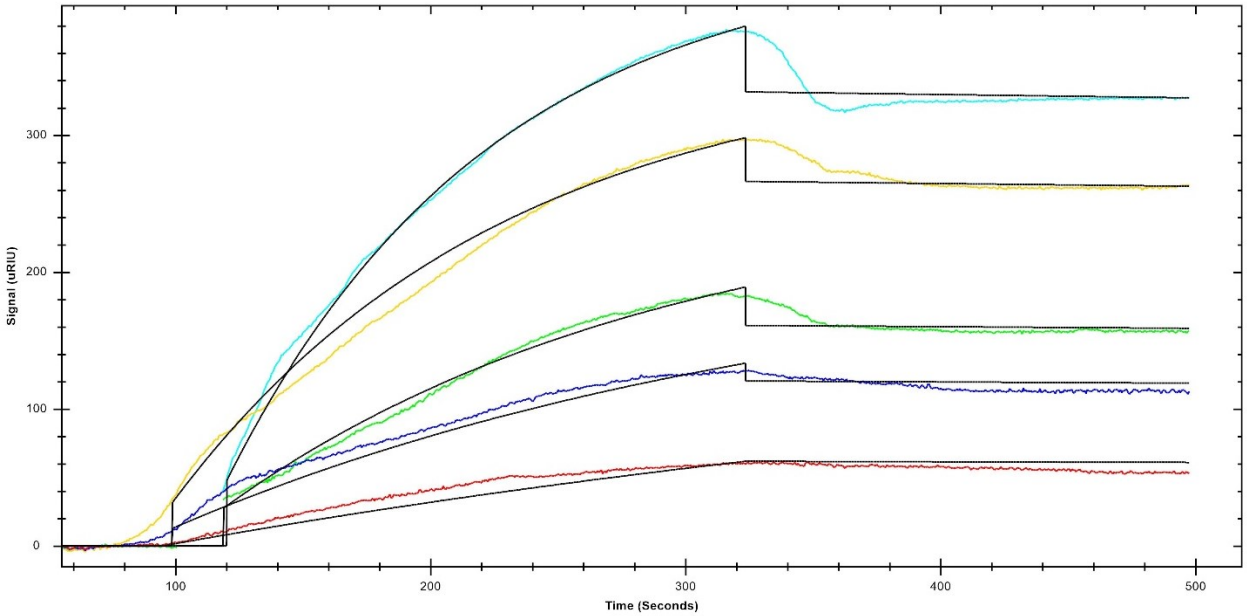

Figure 5.4.11: Sensorgrams for double-referenced curves for the sample and reference channel with buffer and rSMN injections in PBS at 75 µL/min. Injections of 10, 20, 40, 60, and 80 nM rSMN over mAB-7B10 (immobilization with 60 µg/mL mAB-7B109). Colored lines represent measurements. Black lines represent a 1:1 binding fit with buffer jumps at the beginning and end of the association phase.

How well the affinity was preserved in the epitope peptides (chapter 5.4.4) was tested on the prepared SPR-biosensor chips of mAB-7B10 (60 µg/mL mAB-7B10). For this purpose, injections of the synthesized epitope peptides rSMN[37-57], rSMN[38-57], and the tryptic digestion of rSMN over the immobilized mAB-7B10 were compared (Table 5.4.5; Figure 5.4.12). As expected, the peptide variants have nearly identical K_D values of 3.13 and 3.17 nM with small estimated errors and a good fit. The tryptic digestion of rSMN showed a similar K_D of 6.71 nM under the same experimental conditions with a larger error and lower maximum response. The SPR response was lower for the peptides, leading to worse signal-to-noise ratios and showing that detecting smaller peptides was more challenging. Comparison to the intact rSMN protein reveals 5 times higher K_D values for the peptides corresponding to the expected mAB-7B10 epitope (rSMN[40-57]), which can be considered as a well-preserved affinity in the peptides. Therefore, these peptides are well suited for the semi-quantification assay via epitope extraction and MALDI-tof MS. Moreover, it was possible to detect the N-terminal epitope peptide from the digestion of rSMN with trypsin in the SPR-based measurements, confirming that the SPR biosensor can be used as a platform for the assay with the generation of additional information about the affinity.

Table 5.4.5: Kinetics and affinities of rSMN[37-57], rSMN[38-57], and the tryptic digestion of rSMN to the immobilized mAB-7B10 and

Curve name	ka (1/(M*s))	est. error	kd (1/s)	est. error	KD (nM)	est. error	Chi2 ([Signal (uRIU)]^2)
rSMN[37-57]	2.15×10^5	$\pm 1.13 \times 10^3$	6.71×10^{-4}	$\pm 6.96 \times 10^{-6}$	3.13	±0.05	2.52
rSMN[38-57]	1.82×10^5	$\pm 0.46 \times 10^3$	5.76×10^{-4}	$\pm 9.44 \times 10^{-6}$	3.17	±0.06	3.03
Tryptic rSMN	1.32×10^5	$\pm 2.58 \times 10^3$	8.84×10^{-4}	$\pm 6.38 \times 10^{-4}$	6.71	±4.98	4.57

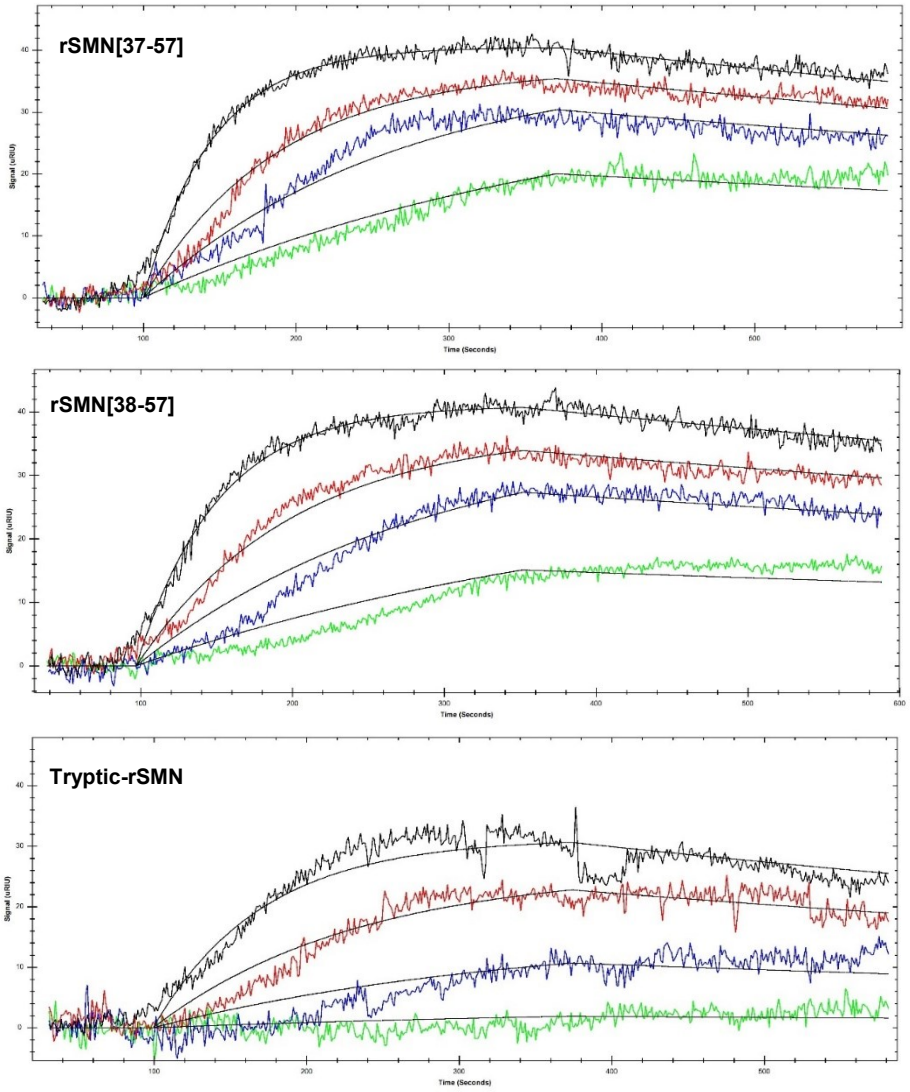

Figure 5.4.12: Sensorgrams for the interaction of 12.5, 25, 50, and 100 nM rSMN[37-57], rSMN[38-57], and tryptic rSMN with immobilized mAB-7B10 on a PG-functionalized gold chip.

Finally, the signal amplification on the SPR via the simultaneous usage of two anti-SMN antibodies was tested. In the setup, mAB-7B10 was immobilized on MHDA to provide a stable antibody surface. 250 µL 80 µg/mL were immobilized on an MHDA chip (Figure 8.2.43). The first injection of rSMN was followed by the IG-1106 injection for signal enhancement (Figure 5.4.13).

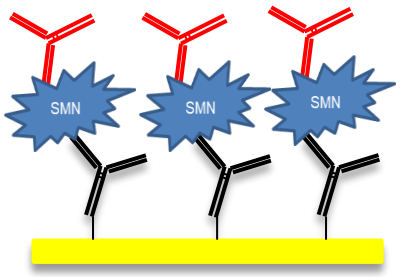

Figure 5.4.13: Scheme of the sandwich SPR-assay for SMN detection. mAB-7B10 (black) was immobilized on MHDA, and consecutive injections of rSMN and IG-1106 (red) were used for signal amplification for SMN detection.

In the first test, 50 nM rSMN was injected, followed by IG-1106 injection at a 6 times higher concentration (Figure 5.4.14). A 2.5-fold signal amplification was achieved. Therefore, the signal amplification with IG-1106 was possible, but the direct antibody immobilization on MHDA showed several drawbacks.

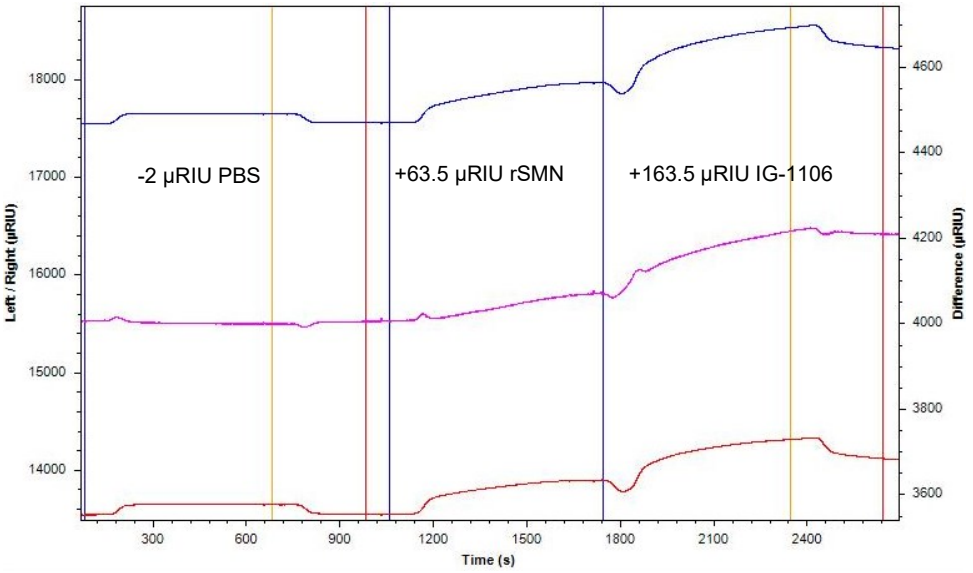

Figure 5.4.14: Sensorgram with sample (blue; left) and reference (red, right) signal and the difference (pink). A PBS-BSA buffer injection was followed by 50 nM rSMN and 300 nM IG-1106 injections. Injections were done at 25 µL/min with PBS-BSA as running and sample buffer. Vertical lines: blue marks the start of injection; yellow marks the dissociation start; red indicates the end of the dissociation phase; black shows a stop of recording. Horizontal lines: blue is the signal from the sample channel; red is the signal from the reference channel.

The antibody did not seem to remain highly active on the surface, and each regeneration cycle led to significantly reduced responses (Figure 5.4.15). The second set of response curves was recorded after 4 regeneration cycles (50 mM glycine in 40 mM HCl). Besides the reduced responses, a 4.7-fold signal amplification was observed for the shown injection. Therefore, the regeneration conditions might not be enough to dissolve the rSMN protein from the antibody fully, and it needs to be optimized.

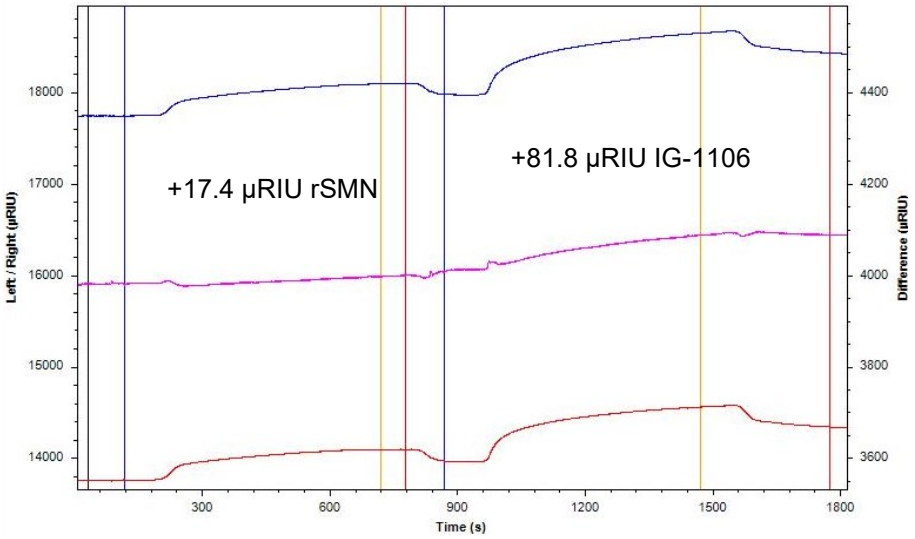

Figure 5.4.15: Sensorgram with sample (blue; left) and reference (red, right) signal and the difference (pink). Injections were done at 25 µL/min with PBS-BSA as running and sample buffer. A 50 nM rSMN injection was followed by 300 nM IG-1106 injections after several injections of 50 mM glycine in 40 mM HCl for surface regeneration. Vertical lines: blue marks the start of injection; yellow marks the dissociation start; red indicates the end of the dissociation phase; black shows a stop of recording. Horizontal lines: blue is the signal from the sample channel; red is the signal from the reference channel.

The tested experimental setup led to poorly reproducible results, and optimization would be necessary to use the setup as a diagnostic tool. The immobilization of the first antibody by PG could lead to interactions of the second antibody with the PG and falsify the results. However, if the PG is fully saturated with antibodies, it should be possible to exploit the advanced performance of those chips for further assay validations. Another alternative would be using a dextran functionalized gold chip in which the dextran surface prevents non-specific interactions. In principle, the sandwich assay for analyzing SMN and its antibodies was possible, but several modifications are necessary to improve its performance. Previous work on SPR-based sandwich assays showed up to a 10-fold increase in sensitivities.[255,256] To further increase the sensitivity of SPR-based sandwich assays, antibodies conjugated with gold nanoparticles were used to push sensitivity even further and suggest possible detection ranges from ng/mL to fg/mL.[257,258] The presented SPR biosensor could be used similarly to increase sensitivity and optimize the presented setup.

5.4.7 SMN quantification assay development based on epitope peptide rSMN[37-57]

An MS-based assay with rSMN[38-57] as reference peptide (RP) to quantify the epitope peptide rSMN[37-57] (EP) from a given sample was to be developed. After biological sample preparation, protein extraction, and pre-purification, the protein mixture could be directly digested and used for epitope extraction with mAB-7B10. The eluted fraction with the EP will be spiked with RP at a defined concentration for quantification by MALDI-tof MS. The concentration will be calculated with a calibration curve and the relative intensities of EP to RP. Another variant for the assay might be an initial SMN protein extraction from the affinity column with follow-up digestion, RP spiking, MS measurement, and concentration calculation. A simultaneous SPR measurement with the eluted protein fractions could cross-validate the determined concentration (chapter 5.4.5). Tamsila Khan assisted in the peptide purification and executed parts of the MALDI-tof MS measurements for establishing calibration curves, and she assisted with initial extraction experiments during her bachelor thesis stay at the Steinbeis Center.

At first, the reproducibility and linearity of the calibration curve with both synthetic peptides were tested. The first tests had a constant RP concentration at 500 µM and EP concentrations from 15.6 to 500 µM. 0.5 µL mixed RP and EP sample was spotted with DHB-matrix (Figure 5.4.16). Linear regression with intersection through the zero value of the Y-axis was done.

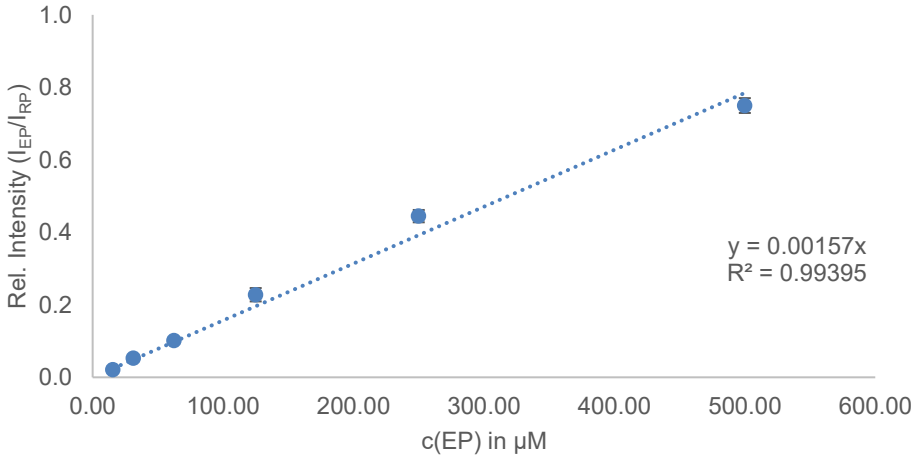

Figure 5.4.16: Linear regression of measured and calculated relative peptide peak intensities against the spotted concentration of peptide EP and regular 500 µM RP. Error bars represent the standard deviation from three technical replicates. The dotted line corresponds to linear regression with intersection through the zero value of the Y-axis. The experiments were executed by Tamsila Kahn, and the reprocessed data are shown.

The calibration curve for peptide (indirectly protein) concentration determination seemed well reproducible (small error bars), and linear regression showed a good fit to the measured values (R^2 = 0.994). Meeting a coefficient of determination higher than 0.99 was the first important quality criterion for developing the assay based on epitope extraction and MALDI-tof MS. The corresponding MALDI-tof MS spectra (Figure 5.4.17) show that the absolute intensities vary considerably between measurements and cannot be used on their own for the quantification, which illustrates the necessity of a calibrator substance for MS measurements. It is known that, especially, MALDI-tof MS analysis can struggle in absolute experimental reproducibility because of the sample-matrix crystallization and sample-to-matrix ratios (and applied laser frequencies, number of laser shots, laser intensity, and other instrumental parameters).[259,260] Therefore, an internal standard in the form of a well-defined peptide was necessary.[261–263]

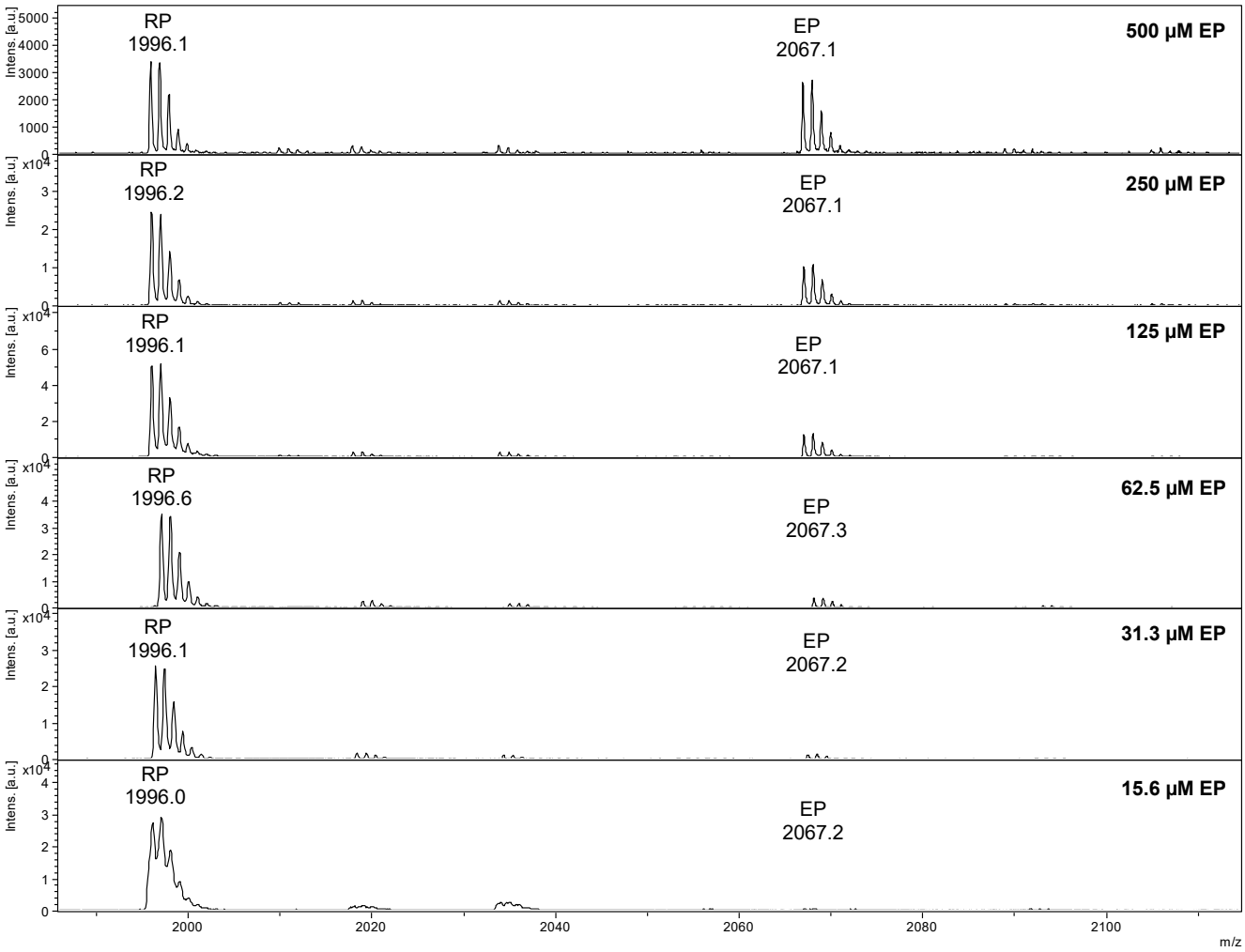

Figure 5.4.17: Example for the MALDI-tof MS measurements with a constant concentration of peptide RP (rSMN[38-57]; $[M_{theo.}+H]^+$ = 1995.9) at 500 µM and a 1:2 dilution series of peptide EP (rSMN[37-57]; $[M_{theo.}+H]^+$ = 2066.9) starting with 500 µM. The experiments were executed by Tamsila Kahn, and the reprocessed data are shown. (Method: RP; Matrix: DHB)

The concentration range of SMN protein in different biological samples was expected to be much lower than 500 µM; therefore, a calibration series from 30 - 210 nM EP was also prepared and evaluated (Figure 5.4.18). The concentration of RP was set constant at 100 nM. The coefficient of determination of the linear regression was slightly inferior to that of the previous calibration series but still reasonable for later tests (R^2 > 0.99). The lower concentrations and higher sample-to-matrix ratios most likely led to the deviations. The sample-to-matrix ratios for optimal sample signals were not optimized at this stage but would be necessary for the final assay to optimize the assay sensitivity. Considering general ICH guidelines for quantification assays, an S/N of 3:1 to 2:1 is considered the limit of detection (LOD), and an S/N of 10:1 is the limit of quantification (LOQ).[264] The lowest

measured concentration in the tests, 30 nM of EP, had an average S/N of 17:1, being so far the LOQ of the calibration. Alternatively, the LOD is defined as the average background noise multiplied by 3 standard deviations or multiplied by 10 for the LOQ, resulting in an LOD for the EP-peak intensity of 400 and an LOQ for the EP-peak intensity of 1200. For comparison, the average peak intensity for the measurement of 30 nM EP was 1700, which indicated an LOQ of 21 nM of EP. However, there would be potential for optimizing the LOD and LOQ by altering the instrumental settings of the MALDI-tof MS, i.e., increasing laser intensity or number of laser shots.

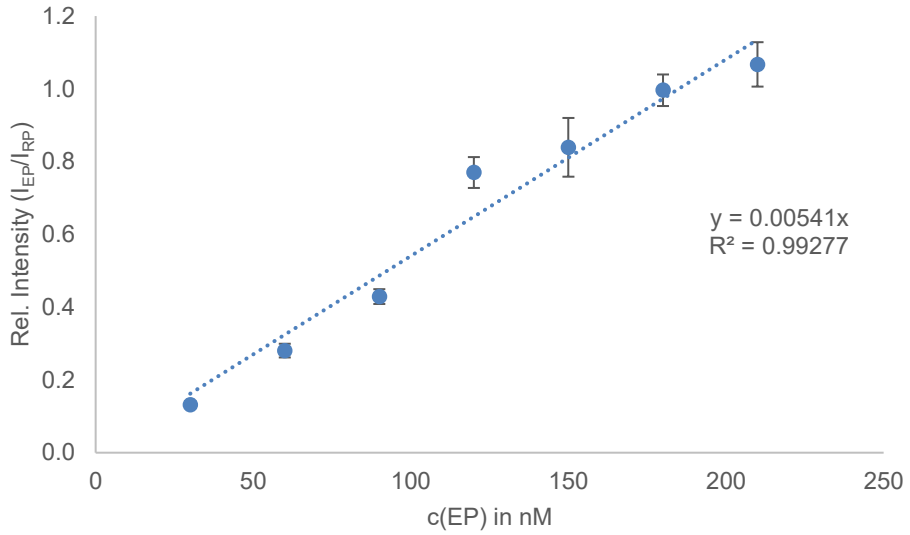

Figure 5.4.18: Linear regression of measured and calculated relative peptide peak intensities against the spotted concentration of peptide EP (30-210 nM) and constant 100 nM RP. Each sample was spotted twice, and each spot was measured 3 times. The experiments were executed by Tamsila Kahn, and the reprocessed data are shown.

In the next test, the calibration series was measured in the presence of 1 µM tryptic digestion of rSMN. Here, the matrix effects of a more complex background matrix were evaluated (Figure 5.4.19). A linear dependence was observed in the selected concentration range, albeit with a lower coefficient of determination ($R^2 < 0.99$), failing to meet essential quality criteria. Therefore, a suitable dilution of the final sample would be necessary to reproduce the result consistently.

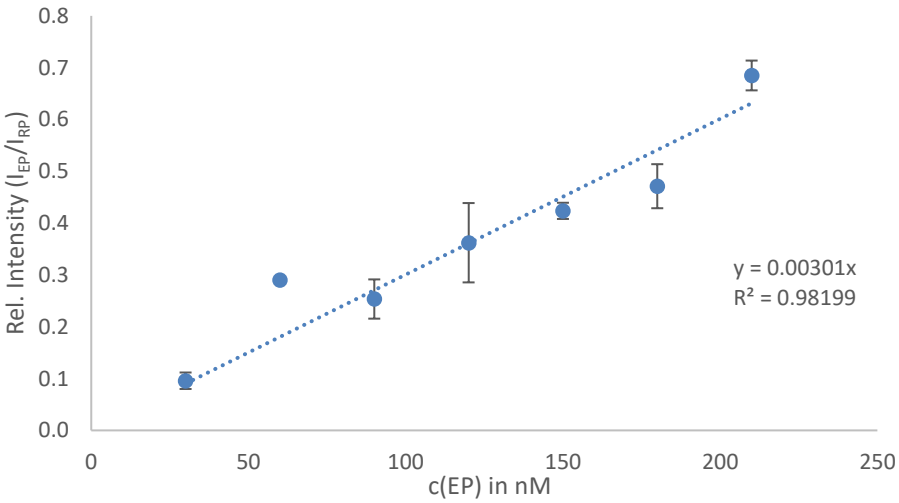

Figure 5.4.19: Linear regression of measured and calculated relative peptide peak intensities against the spotted concentration of peptide EP (30-210 nM) and constant 100 nM RP and tryptic rSMN digestion. Each sample was spotted twice, and each spot was measured 3 times. The experiments were executed by Tamsila Kahn, and the reprocessed data are shown.

The linearity of the calibrator (rSMN[38-57] = RP) was also tested for the tryptic epitope peptide from the recombinant SMN (rSMN[33-57] = EP2). For this purpose, the tryptic digestion of rSMN (rSMN[33-57] = EP1) and the synthetic rSMN[37-57] (= EP2) were spotted separately with a constant concentration of 50 nM RP (Figure 5.4.20). Triplicates of the measured samples showed good determination coefficients; this time, the diluted digestion mixture did not significantly influence the calibration curves.

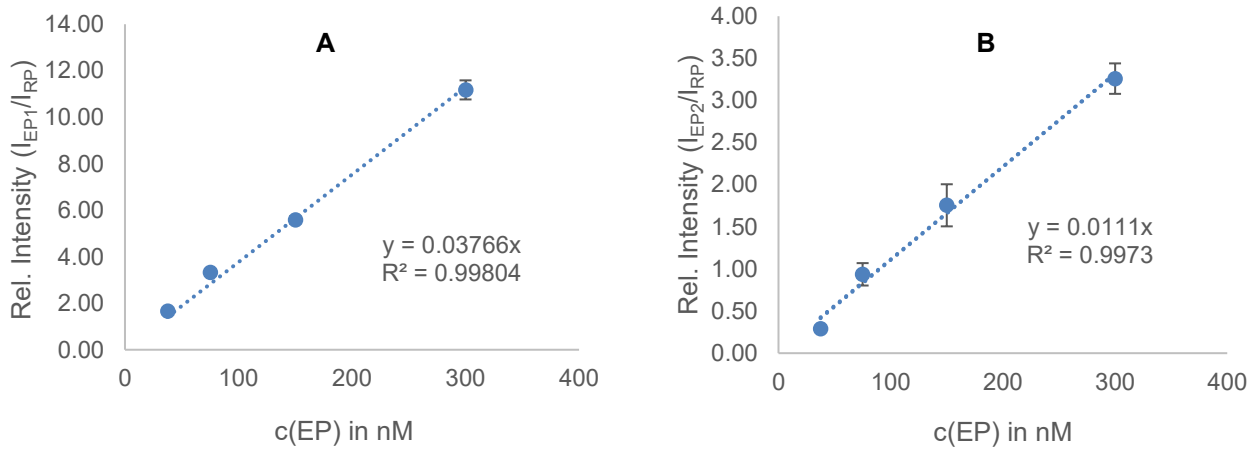

Figure 5.4.20: Linear regression of measured and calculated relative peptide peak intensities against the spotted concentration of (A) peptide EP (37.5 - 300 nM) and (B) tryptic rSMN digestion (37.5 - 300 nM) with a constant concentration of RP at 50 nM. Each sample was spotted twice, and each spot was measured 3 times. The experiments were executed by Tamsila Kahn, and the reprocessed data are shown.

The next step was to verify the reproducibility of the epitope peptide extraction from a prepared mAB-7B10 column. For this purpose, the extraction was repeated three times with the same amount of rSMN[37-57], and prior to the MALDI-tof MS measurement, the elution was spiked with the reference peptide rSMN[38-57] (measurement of triplicates). Additionally, several fractions were collected after incubating and washing the column to investigate the elution profile for the epitope peptide from the antibody (Figure 5.4.21). As expected, the peptide rSMN[37-57] was detected in all fractions (except pre- and post-experiment column washing fractions) but with very low signal intensity ratios from fractions 7 to 10.

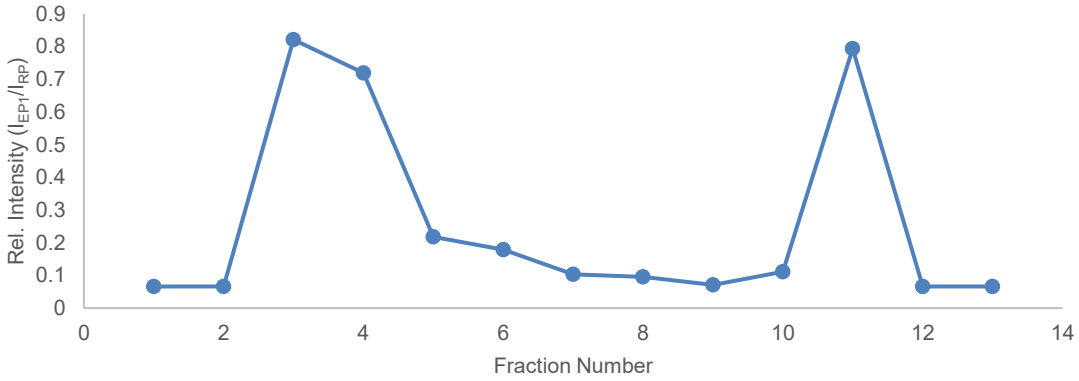

Figure 5.4.21: Elution profile of rSMN[37-57] from the mAB-7B10 column. Incubation of 200 µL 500 nM rSMN[37-57] and collection of fractions and elution with 0.1 % TFA in water. Factions of 1.5 mL were collected, lyophilized, and resuspended in 100 µL MQ for the MALDI-tof MS measurements.

The three independent tests on the same column revealed well-reproducible recovery rates (Table 5.4.6), demonstrating the mAB-7B10 to be very stable even under the harsh acidic elution conditions. The determined

concentrations are all in the range of +/- 5 %, demonstrating the suitability of the experimental setup as an assay for the semi-quantification of the epitope peptide and SMN protein via epitope extraction and MALDI-tof MS analysis. For the calculation, the calibration curve with 30 - 210 nM epitope peptide and constant 100 nM reference peptide were used (Figure 5.4.18).

Table 5.4.6: Results for the MALDI-tof MS semi-quantification of the epitope peptide extraction rSMN[37-57] from the same mAB-7B10 column. The standard deviation was calculated from triplicates.

Sample	Mean value (Rel-Intensity)	SD (Rel. Intensity)	Conc. (nM)	STABW (nM)
Test-1	0.794	0.03	143.5	5.4
Test-2	0.843	0.03	152.5	4.1
Test-3	0.774	0.04	139.9	5.8

Two experiments were carried out with human serum and whole blood cell lysate. At first, the tryptic digestion of rSMN was spiked to a control serum sample, followed by epitope extraction. The fraction analysis by MALDI-tof MS (Figure 5.4.22) showed no signals in the washing fractions, but the acidic elution fractions showed the epitope peptide. Therefore, in case of sufficient SMN digestion, it should be possible to extract the epitope peptide. Collected fractions were not pre-concentrated or desalted prior to the MALDI-tof MS measurements, which is why the incubation fraction F1 did not show detectable amounts of the epitope peptide.

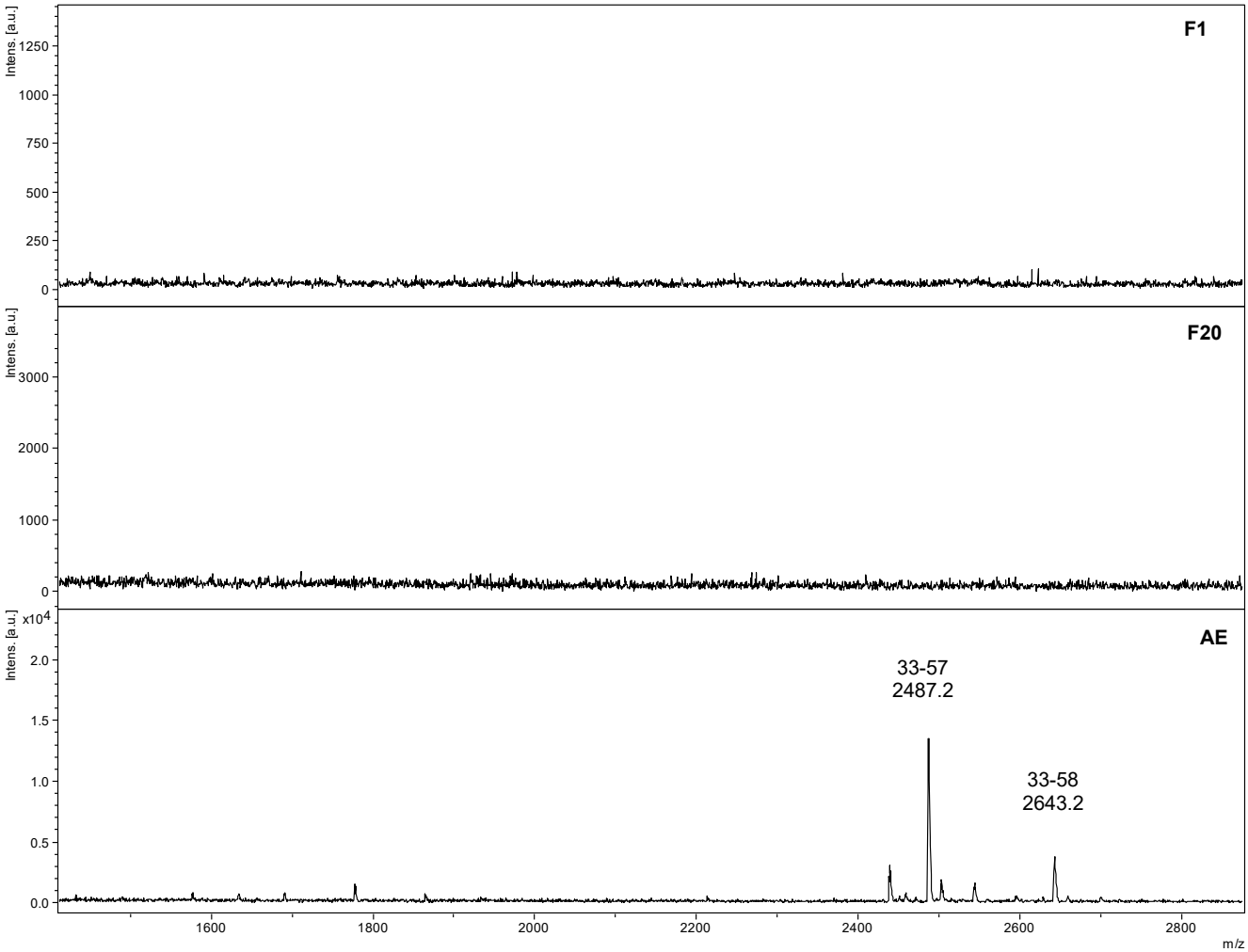

Figure 5.4.22: MALDI-tof MS spectra for the epitope extraction fractions from an mAB-7B10 sepharose column and tryptic rSMN digestion spiked to a serum sample. (F1) Injected tryptic digestion with serum, (F20) last washing step with 10 mM AmBic, and (AE) acidic elution with 0.1 % TFA in MQ. (Method: RP; Matrix: DHB)

The second and most crucial test was the identification of the epitope peptide from a biological sample with subsequent quantification. To this end, a healthy individual's whole blood cell lysate (WBCL) sample was investigated. After sample preparation and digestion, the digest was used in the epitope extraction with MALDI-tof MS measurements. The acidic elution revealed the epitope peptide rSMN[37-57] (Figure 5.4.23). The concentration of the epitope peptide rSMN[37-57] would be 15.6 nM. The volume of the elution fraction was 100 µL (= 1.56 pmol), and 0.5 mL of WBCL was processed. 2 mL of WBCL was generated from 6 mL of whole blood (WB). This means that a concentration of 1.04 nM of SMN had been present in the collected WB. However, the previous elution profile suggested an under-determined concentration because of the continuous elution of the epitope peptide. Therefore, the actual concentration should be higher. The determined 1.04 nM SMN concentration, together with the unknown correction coefficient for the actual concentration, seemed to be in the range of the previously described SMN levels in healthy individuals of 0.95 - 2.22 nM SMN (30 - 70 ng SMN / mL whole blood).[215,217] Moreover, distinguishing between SMA patients and healthy individuals is more important than determining the exact concentration. For this purpose, the chosen experimental conditions and precisely the chosen concentration of the reference peptide seemed too high compared to the measured rMSN[37-57] intensity, and the rSMN[38-57] concentration should be adjusted to lower concentrations for better determinations. The determined concentration of 15.6 nM was lower than the lowest tested concentration and should be seen as a first estimation of assay capabilities. Therefore, the calibration curve needed further optimization. The range of other MALDI-tof MS quantification assays was in the nmol- or fmol-range, depending on the experimental setup, target, and used instruments.[261,262,265] The reached concentration range was in there and could be further expanded. Finally, these preliminary results indicated a functional semi-quantification assay for the SMN protein, so that the proof-of-concept seemed successful. However, in-depth validation and verification of these results will be needed before it can be put into clinical practice.

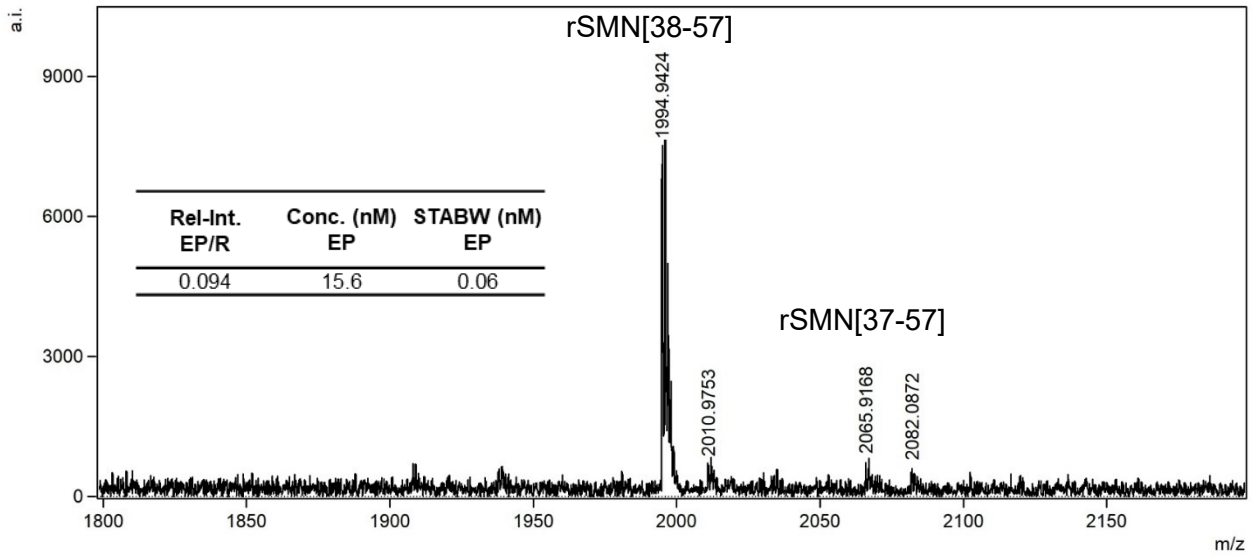

Figure 5.4.23: MALDI-tof MS spectrum of the elution fraction from the WBCL experiment with immobilized mAB-7B10. The reference peptide rSMN[38-57] was mixed with the column elution before the MS measurement. The relative intensity of EP (rSMN[37-57]) and R (rSMN[38-57]) leads to a concentration determination of 15.6 nM (+/- 0.06 nM). (Method: RP; Matrix: DHB)

For additional optimization, an important observation was the methionine oxidization of EP to different extents for older stock solutions, which were stored for at least one month in the fridge instead of the freezer, for the epitope peptides rSMN[37-57] and rSMN[38-57] (Figure 5.4.24). The storage and digestion conditions can lead to methionine oxidations and should be monitored throughout the experiments for proper concentration determinations. The fully-oxidized peptide could be used instead of the unoxidized peptide for the measurements. However, the reference peptide should be free of any oxidization to avoid errors in the concentration determination, and it could be good advice to resynthesize the reference peptide without

methionine, which should not exhibit a significant impact on the quantification experiments. Alternatively, the reference peptide must be handled carefully and always stored at - 20 °C.

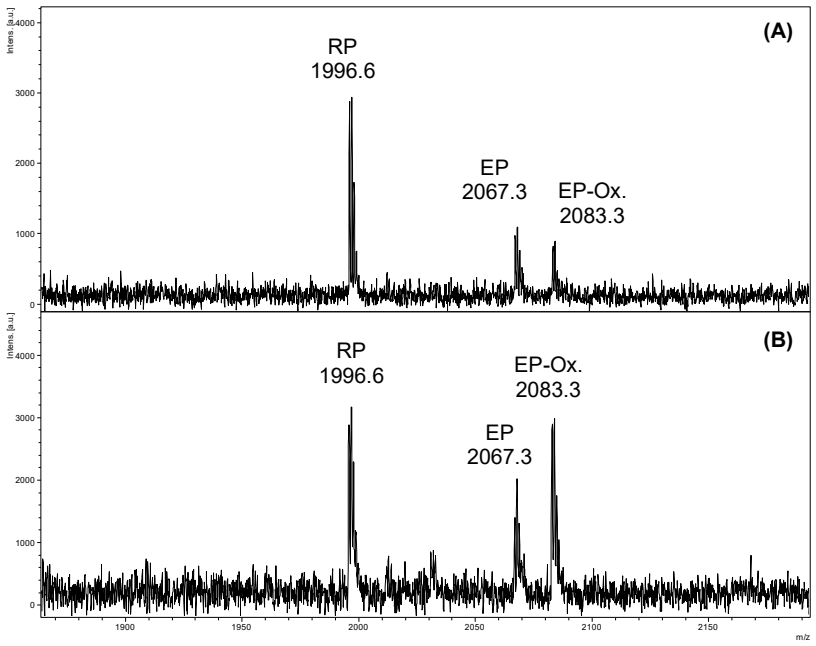

Figure 5.4.24: Examples of the MALDI-tof MS measurements for different stock solutions of the epitope peptides. The stock solutions were stored in the fridge (A) and at room temperature (B). The experiments were executed by Tamsila Kahn, and the reprocessed data are shown. (Method: RP; Matrix: DHB)

6 Conclusion and Outlook

The epitope identification of antibodies on its antigens via epitope extraction was the main focus of the presented work. The method was evaluated and modified to attempt to improve the epitope identification. The investigated proteins were interleukin-8 (IL8), cathepsin D (CTSD), alpha-glucosidase A (GAA), and survival motor neuron protein (SMN) and their antibody and aptamer ligands.

While an affinity column is traditionally used as an extraction platform in this work, a chip-based system with several modifications was tested for antibody immobilization. For this purpose, the respective antibody for epitope extraction was immobilized on a sepharose column, on a 16-MHDA modified gold chip, and the same chip with additional protein G modification. The focus was on improving the detectability of specific protein/peptide interactions and minimizing non-specific surface binding of peptides resulting from digestions of the protein antigens. A pressure cycling technology (PCT) was applied to accelerate the digestion, and the corresponding digestions were compared to a standard procedure under atmospheric pressure. Moreover, in-silico analysis with B-cell epitope predictors was done to evaluate if they could generate a first estimate of the epitope type and complexity of the corresponding analysis (the presented in-sillico analysis was done retro-perspective). Therefore, the experimental data obtained by epitope extraction was compared to the results of different B-cell epitope predictors. In epitope extraction, the complexity of analysis is low for linear epitopes and gets higher for discontinuous epitopes. For discontinuous epitopes, the more different protein sites contribute to the binding, the more intricate the successful epitope identification becomes because less affinity will be retained in resulting epitope-originating peptides. Moreover, the enzyme should not cleave the primary sequence of a protein in the epitope, which would lead to the loss of the affinity in the resulting peptides.

Therefore, the analyzed proteins and corresponding antibodies were categorized into different difficulty levels for successful epitope identification by epitope extraction. In principle, they could be defined as “straightforward”, “challenging”, and “seemingly impossible” epitope identification by epitope extraction.

An example of a “straightforward” epitope identification was the SMN protein and its antibody mAB-7B10. The epitope had been reported before and was confirmed during the presented work.[227,228] It illustrated the ease of analyzing a linear epitope by the epitope extraction. The reported epitope peptide rSMN[46-57] (^{46}GVPEQEDSVLFR^{57}) was well preserved in the tryptic peptide rSMN[33-57] (^{33}GSEFAMSS GGSGGGVPEQEDSVLFR^{57}) and easily isolated by epitope extraction. Without knowledge of the actual epitope, a nine amino acid (^{37}AMSSGGSGG^{44}) prolonged epitope would have been reported, neglecting the attached part of the T7-tag sequence (^{33}GSEF^{36}), which should not be part of the epitope. Additional methods like peptide mapping[1,106,107] would have been needed to narrow down the epitope to its essential amino acids. However, the absence of any sepharose and surface-binding peptides made the identification straightforward. For the binding verification by SPR, a gold chip functionalized with 16-MHDA, protein G, and the antibody mAB-7B10 was necessary to generate reasonable binding curves for the peptides. These measurements revealed a KD for the rSMN protein between 0.25 - 0.69 nM and for the synthetic epitope peptide rSMN[37-57] at 3.2 nM, which confirmed the high retained affinity. Therefore, the SMN protein and mAB-7B10 met all prerequisites to be further investigated as components of a diagnostic assay to quantify SMN via epitope extraction and MALDI-tof MS analysis. The C-terminal antibodies tested in this work could be used to perform an SPR-sandwich assay with the mAB 7B10 (N-terminal epitope on SMN protein) and one of the IG-1106/7 antibodies. The principle experimental setup was tested in this work and gave promising results, which should be further investigated. The first test for the epitope extraction from serum with spiked digestion of the SMN protein demonstrated the suitability of the assay. The successful extraction of the tryptic epitope peptide of SMN from a healthy individual's whole blood cell lysate sample was the final evidence that the experimental setup was functional. Calibration curves with synthetic peptides in buffer met quality criteria of $R^2 > 0.99$, and the lowest tested concentration of 30 nM could be enough with a slightly modified procedure because the epitope extraction would enrich the respective peptides from the whole blood cell lysate digest. Modifications of the procedure could include the sample resuspension in 20 - 50 µL MQ instead of 100 µL MQ, which would drastically increase

the sample concentration prior to the MS analysis, or a ZipTip could be used for concentrating the sample. Moreover, the MS analysis could be further optimized, and lower concentrations of the synthetic peptides for the calibration should be tested to obtain a lower limit of quantification to gain more flexibility for investigated sample concentrations. Another parameter that needs to be investigated is the continuous bleeding of epitope peptide from the sepharose column, which reduces final concentration estimations but does not seem too problematic. Therefore, the antibody mAB-7B10 showed high stability in repeated experiments with excellent elution profiles and recovery rates. In future work, the next step in establishing the SMN protein semi-quantification by epitope extraction and MALDI-tof MS would be the optimization of the MALDI-tof MS measurements (matrix composition, instrumental fine-tuning) and optimization of the biofluid sample preparation for the assay (volume, buffer, preparation procedure). Another important step would be to increase the assay's throughput, for which different strategies seem possible. The tested SPR-based biosensor could be coupled to an automated MS target plate spotter. The additional information from the SPR measurements would make the results more robust and reliable. Another strategy would be the sepharose-based approach, which could facilitate 96-well filter plates,[266,267] which have sepharose beads for antibody immobilization at the tips, and the elution could be directly spotted on a 96-well MALDI target plate. These 96-well filter plates were often used for LC-MS analysis of proteins and peptides and could also be used for epitope extraction. Alternatively, the sepharose beads, used for capturing the epitope peptide, could be spotted directly on the MALDI target plate for the analysis, which was demonstrated before as feasible.[268]

A “challenging epitope” identification was encountered for IL8/CXCL8 and its antibody mAB-I2519. The identified discontinuous epitope of IL8[12-20] and IL8[55-60] needed many control and validation experiments to confirm the epitope-forming peptides. Epitope extractions with immobilized antibody mAB-I2519 on a sepharose column and 16-MHDA functionalized SPR gold chip both showed that the tryptic peptides IL8[12 20] and IL8[55-60] bind to the carrier material and the antibody leaving the question open if they were epitope-originating or not. Additional experiments with chymotrypsin that cleaves at several sites within the epitope peptides found by tryptic digest revealed no binding peptides, adding to the evidence that both identified tryptic peptides are indeed epitope-originating. Follow-up experiments with antibody immobilization via protein G pointed further to the fact that both peptides bind the carrier material and the antibody. The SPR-based affinity determination for IL8 and its antibody was challenging. Neither a dextran nor a 16-MHDA carrier layer on the SPR gold chip led to reasonable binding curves. However, oriented antibody immobilization with protein G, first successfully tested on the model protein myoglobin and its antibody, could be used for mAB-I2519 - IL8 interaction analysis, resulting in a KD of 7.4 nM. As expected, the synthetic peptides from the discontinuous epitope had lower affinities: the KD for IL8[12-20] was 75.1 µM, and for IL8[55-60] 0.98 mM. Simultaneous injection of both peptides over the immobilized antibody led to an increased response, further supporting the hypothesis of a discontinuous epitope. The in-silico analysis with B-cell epitope predictors also pointed to a possible discontinuous epitope of IL8[12-20] and IL8[55-60], further supporting these peptides to be originating from the mAB-I2519 epitope.

The well-known inhibitory effect of the antibody on the interaction of IL8 and its natural receptor CXCR1 can be explained with the found epitope. [169–172] IL8[12-20] is part of the receptor-binding domain, so high-affinity binding of mAB I2519 will hinder receptor-binding. Moreover, the interaction of IL8 and CXCR1 comprises at least three binding sites on IL8, mainly flexible loops. By binding the discontinuous epitope, the antibody might stabilize the IL8 structure, and without the necessary structural flexibility, it is nearly impossible to bind the receptor. IL8[55-60] is part of the α-helix on the C-terminal site of IL8, which is necessary for the gradient formation of IL8 in the blood vessels and is essential for leukocyte recruitment. Therefore, the antibody inhibits the IL8 receptor binding and binding to cell surfaces, which is essential for the gradient formation, and both together inhibit the biological function of IL8 in vivo.

The “seemingly impossible” epitope identification of CTSD and GAA with their corresponding antibodies and aptamers showed the limits of epitope extraction. For both proteins and ligands, several peptides from digestions with trypsin and chymotrypsin could originate from an epitope. However, multiple sepharose binding peptides combined with seemingly complex discontinuous epitopes, which could consist of multiple protein

sites, made successful epitope identification even more challenging than before. Most likely, many peptide fragments would need to be combined to prove that they could exhibit high affinities in highly ordered structures. Many epitope peptide candidates would have needed to be synthesized and evaluated via SPR measurements and could be necessary to synthesize hybrid peptides of many tryptic peptides for generating detectable affinities. Therefore, the approach would nearly lead to the same experimental effort as an epitope peptide mapping experiment, and these seemingly complex, discontinuous epitopes might be difficult to identify with other methods, too. However, for the mAB-43G7 epitope, the sequence regions 317-324], [304-349], and [411-458] seemed the best guess for a discontinuous epitope because they are on one side of the protein. Moreover, they are all positioned in the 70 kDa GAA fragment, which was previously reported to bind to the antibody.[206] As the epitopes for the anti-CTSD antibodies and aptamers and the anti-GAA-antibodies appear to be non-linear and the retained affinity of the epitope-containing peptides from tryptic and chymotryptic digest is very low, none of the antibodies and aptamers was suitable for a semi-quantification assay. To identify the epitopes, another method, which does not rely on antibody immobilization, seems preferable in those cases. Although complex experimental data require more extensive analysis, methods like HDX-MS[109,110] or CC-MS[111,112] could deliver more reliable results. The potential apheresis for removing GAA antibodies from patients under ERT, which renders the GAA drug (myozyme) ineffective, could be done with in-silico identified epitope peptides. However, no further investigation for this kind of apheresis was done.

The changed and improved antibody immobilization via protein G enables the straightforward setup of the scouting experiments, improves the quality of the SPR data, and should be exploited in the column experiments. The unspecific surface interaction of IL8 with the 16-MHDA and dextran chip surfaces made its analysis very challenging. Switching to the different setup with protein G as an additional layer for oriented immobilization of the antibody created surfaces with much higher antibody activity and reduced unspecific binding effects. Therefore, more reliable affinities were determined for the IL8 and its antibody mAB-I2519. Moreover, it was possible to determine kinetic and affinity parameters for epitope peptides, which was impossible with the other tested surfaces. The higher activity of the oriented antibody with protein G made it easier to control the amount of immobilized antibody, and the experimental setup is more flexible for specific adjustments to new protein systems. These findings were confirmed by the analysis of rSMN, its epitope peptide, and antibody mAB-7B10. Moreover, the protein G could also be used in future column experiments to improve the epitope extraction and potentially mitigate the influence of unspecific peptide binders on the experimental outcome.

The different complexities for epitope identification by epitope extraction seen for the four model systems investigated in this work show how the unspecific binding of peptides to the used carrier material makes epitope extraction a challenging task. The variation of an epitope excision experiment was previously done in the Steibeis laboratory.[132,136,269] However, for IL8, CTSD, and GAA, the epitope excision was attempted but did not lead to any meaningful results, and no corresponding data are shown for it in the presented work. A scouting experiment for the expected epitope complexity and carrier material binding capacity would be beneficial. The presented epitope extraction with covalently immobilized antibody on an SPR-gold chip with 16-MHDA protein G surface seems suitable. For scouting multiple protein systems, it would be beneficial to use non-covalently immobilized antibodies, which would enable consecutive tests on one chip, and the experiments would be independent of the antibody stability under regeneration conditions. Two injections of digestion with and without immobilized antibodies and subsequent analysis of collected fractions could give an idea about the conserved affinity, potential epitope sequence, and the number of carrier material binding peptides. This setup was tested for the IL8 and SMN protein with promising results and should be applied in future scouting experiments. An advantage of the suggested scouting experiment is the independence of antibody stability after regeneration and that several control experiments can be run simultaneously. Furthermore, the scouting setup would not need to produce high-quality sensorgrams for affinity determinations, and much higher antibody surface concentrations could be utilized to generate qualitative statements about specific binding events.

Complementary to the extraction platform, the other important part of the experimental setup is the enzymatic protein digestion. This can be very challenging, depending on the protein stability. Furthermore, batch-to-batch variability of the digestions seen in several epitope extraction experiments made the subsequent analysis more

challenging. Therefore, the PCT digestion was compared to the standard digestion of cysteine-rich proteins under atmospheric pressure. For the direct application of the digested proteins in the epitope extraction experiments, most of the chemicals or organic solvents for protein denaturation were avoided because they are often incompatible with MALDI-tof MS measurements (e.g., urea) or following epitope extraction experiments (e.g., ACN). The tested proteins IL8, rSMN, CSTD, and GAA contained disulfide bonds of their cysteine residues, and after reduction and alkylation of those, they were digested under standard AP (37 °C, atmospheric pressure) and PCT (37 °C, high-pressure cycling) conditions. For the SMN protein, the AP and PCT digestion for 120 min resulted in sequence coverages of 100 % and similar specificity for trypsin cleavage products. A similar result was observed for the pCTSD digestion with trypsin, AP, and PCT digestion for 120 minutes, leading to sequence coverages of 97 % with similar trypsin specificities. A slightly different result was obtained for GAA: the AP digestion for 120 minutes led to a sequence coverage of 87 %, and the PCT digestion for 120 minutes led to 81 % with 11 % less trypsin-specific peptide fragments. A similar digestion pattern was observed for the overnight digestion of GAA, indicating an over-digestion of GAA after 120 minutes of PCT treatment. Shorter time frames would most likely produce more similar results to the digestion for 120 minutes at AP conditions. There are differences in the peaks obtained in the SMN, CTSD, and GAA digestions under AP and PCT digestion with trypsin. However, the differing peaks have relatively low intensities in the mass spectra, and the highest intensive peaks stayed the same for each protein for AP and PCT digestion. A shorter digestion time paired with lower amounts of the enzyme could reveal the full potential of PCT digestion. Therefore, the PCT digestion was investigated in more detail with IL8. Here, a 90-minute PCT digestion generated results similar to a 180-minute AP digestion. With both procedures, even the shortest tested digestion time of 30 minutes generated sufficiently digested IL8 protein for any epitope extraction experiment. The differences might get more significant at even higher enzyme-to-protein ratios than 1:100 and shorter time frames. Furthermore, a larger protein could make detecting differences in the digestion procedure easier. A detailed reproducibility should be carried out in future work to evaluate batch-to-batch variability. It is important to note that disulfide bond-containing proteins generally lose stability after reduction and alkylation, which makes it challenging to see a clear improvement in PCT digestion compared to AP digestion.

The in-silico B-cell epitope predictions for IL8, rSMN, CTSD, and GAA showed potential for epitope evaluation prior to any experiment and could influence future experimental setups for the epitope extraction. The presented in-silico predictions performed here were done after experiments, and to predict their impact on future epitope extractions were attempted. Moreover, the predictions should show if the experimentally identified epitopes are included in the predictions. In the case of IL8, the consent of all four used predictors, DiscoTope 2.0, Seppa 3.0, BepiPred 2.0, and BCEPS, and the consensus of at least three predictors resulted in an epitope map that overlapped with the experimental epitope. According to the prediction, the epitope could be extended by several amino acids on both experimental epitope sites, IL8[12-20] and IL8[55-60]. However, the digestion also contained longer peptides, including the identified peptides, but none of these were recovered in the extraction experiments. The affinity of those peptides might not be higher, and they were less abundant in digestion, as indicated by their low peak intensities in the MS measurements. At the time of the experimental work, no crystal structure was available for the SMN protein, and predictions with the two linear predictors, BepiPred 2.0 and BCEPS, could be made. The epitope was known for the interaction of mAB-7B10 and SMN protein. The predictions included the sequence rSMN[46-57], and the linear predictors indicated most of the protein sites as immunogenic. Therefore, poor discrimination between immunogenic and non-immunogenic protein sites was seen because, from the in-silico analysis, nearly 80 percent of SMN protein is immunogenic. The epitope identifications for CTSD, GAA, and their antibodies stayed incomplete. The large protein size made evaluations more challenging, but many overlapping regions were found in the experiments and predictions. As the IL8 experiments showed, the sepharose-binding peptides could also bind to the antibodies, many of which were included in the predictions. Therefore, the epitope peptides could be found in any of the extracted peptides, and additional experiments are necessary to find the corresponding epitopes.

In all cases, the predictions overlap with the peptides from the epitope extraction experiments, but what can they indicate for experimental changes and the use of specific enzymes? In the case of IL8, the predictions suggest using another enzyme to generate longer protein fragments for the epitope extraction because trypsin

would more often cleave after a lysine or arginine residue in the middle of an epitope. Commercially available enzymes are Arg-C, Lys-C, Lys-N, Glu-C, and Asp-N, which cleave after the corresponding amino acid either on the amino acid residue's C-terminal (C) or N-terminal (N) site.[141] Arg-C and Lys-C could be used in separate experiments, generating similar but longer peptides from the corresponding epitope regions. Alternatively, IL8 could be incubated with trypsin for shorter times, like 5 and 15 minutes, to preserve larger protein fragments without needing other enzymes that would require further optimization. The optimal enzyme seems to be Glu-C, which would generate longer peptides from the epitope regions. For chymotrypsin, B-cell epitope digestions would have indicated from the beginning that the epitope would most likely be cleaved in crucial positions for antibody binding, making the extraction of epitope peptides from the chymotryptic digestion of IL8 highly unlikely, which was confirmed by the corresponding experiment: no peptides were extracted and identified. Therefore, the predictions would have indicated an enzyme other than trypsin as the optimal enzyme for the epitope analysis of IL8.

Similarly, the incomplete epitope identifications for CTSD and GAA could have benefited from initial epitope prediction experiments. In both proteins, lysine, and arginine residues lay within the potential epitope sites, making trypsin semi-optimal for digestion and subsequent epitope extraction. Likewise, several chymotrypsin cleavage sites were also located within the immunogenic regions. It could have been possible to identify binding peptides if they had been enriched by the epitope extraction to an extent where their intensities in the MS analysis would have surpassed all others. However, as indicated by the prediction, crucial amino acids for antibody binding could be missing in the resulting enzymatic peptides, and there would be no enrichment of those peptides. Therefore, the predictions suggested a challenging epitope extraction, but the unspecific binding peptides were the real issue for the inconclusive epitope identifications. The predictions would not have identified the unspecific binding peptides, and for both proteins, a challenging epitope identification could still have been encountered despite changing to a more favorable enzyme. However, the unspecific peptides from experiments with digestions of trypsin and chymotrypsin were not identical, and other enzymes could produce peptides, which show less unspecific binding to the column medium. This hypothesis would need to be experimentally proven.

The use of several B-cell epitope prediction tools and their consensus of highly immunogenic protein sites seem very promising in assisting experimental setup for epitope extraction and evaluating the outcomes of the experiments. However, depending on the degree of unspecific peptide binders, the experiment should be repeated with another set of enzymes or digestion conditions because any related analysis will be questionable. In some cases, epitope prediction may even identify the epitope extraction method as unsuitable for the analysis of a given protein-antibody pair. Therefore, the experimental design could have significantly benefited from the predictions.

7 References

(1) Opuni, K. F. M.; Al-Majdoub, M.; Yefremova, Y.; El-Kased, R. F.; Koy, C.; Glocker, M. O. Mass spectrometric epitope mapping. *Mass spectrometry reviews* **2018**, *37*, 229–241.

(2) Israr, M. Z.; Bernieh, D.; Salzano, A.; Cassambai, S.; Yazaki, Y.; Suzuki, T. Matrix-assisted laser desorption ionisation (MALDI) mass spectrometry (MS): basics and clinical applications. *Clinical chemistry and laboratory medicine* **2020**, *58*, 883–896.

(3) Pandey, P. S.; Raghuwanshi, S. K.; Kumar, S. Recent Advances in Two-Dimensional Materials-Based Kretschmann Configuration for SPR Sensors: A Review. *IEEE Sensors J.* **2022**, *22*, 1069–1080.

(4) Kukacka, Z.; Iurascu, M.; Lupu, L.; Rusche, H.; Murphy, M.; Altamore, L.; Borri, F.; Maeser, S.; Papini, A. M.; Hennermann, J.*; et al.* Antibody Epitope of Human α-Galactosidase A Revealed by Affinity Mass Spectrometry: A Basis for Reversing Immunoreactivity in Enzyme Replacement Therapy of Fabry Disease. *ChemMedChem* **2018**, *13*, 909–915.

(5) Seppe Cambier; Mieke Gouwy; Paul Proost. The chemokines CXCL8 and CXCL12: molecular and functional properties, role in disease and efforts towards pharmacological intervention. *Cellular & Molecular Immunology* **2023**, 217–251.

(6) Wirth, B.; Karakaya, M.; Kye, M. J.; Mendoza-Ferreira, N. Twenty-Five Years of Spinal Muscular Atrophy Research: From Phenotype to Genotype to Therapy, and What Comes Next. *Annual review of genomics and human genetics* **2020**, *21*, 231–261.

(7) Benes, P.; Vetvicka, V.; Fusek, M. Cathepsin D--many functions of one aspartic protease. *Critical reviews in oncology/hematology* **2008**, *68*, 12–28.

(8) Peruzzo, P.; Pavan, E.; Dardis, A. Molecular genetics of Pompe disease: a comprehensive overview. *Annals of translational medicine* **2019**, *7*, 278.

(9) Kringelum, J. V.; Lundegaard, C.; Lund, O.; Nielsen, M. Reliable B cell epitope predictions: impacts of method development and improved benchmarking. *PLoS computational biology* **2012**, *8*, e1002829.

(10) Zhou, C.; Chen, Z.; Zhang, L.; Yan, D.; Mao, T.; Tang, K.; Qiu, T.; Cao, Z. SEPPA 3.0-enhanced spatial epitope prediction enabling glycoprotein antigens. *Nucleic acids research* **2019**, *47*, W388-W394.

(11) Jespersen, M. C.; Peters, B.; Nielsen, M.; Marcatili, P. BepiPred-2.0: improving sequence-based B-cell epitope prediction using conformational epitopes. *Nucleic acids research* **2017**, *45*, W24-W29.

(12) Ras-Carmona, A.; Pelaez-Prestel, H. F.; Lafuente, E. M.; Reche, P. A. BCEPS: A Web Server to Predict Linear B Cell Epitopes with Enhanced Immunogenicity and Cross-Reactivity. *Cells* **2021**, *10*.

(13) Jiang, P.; Li, F.; Ding, J. Development of an efficient LC-MS peptide mapping method using accelerated sample preparation for monoclonal antibodies. *Journal of chromatography. B, Analytical technologies in the biomedical and life sciences* **2020**, *1137*, 121895.

(14) Barh, D.; Azevedo, V. *Omics technologies and bio-engineering: Towards improving quality of life*; Emerging fields, animal and medical biotechnologies volume 1; Academic Press, 2018.

(15) Zaia, J. Mass spectrometry and glycomics. *Omics : a journal of integrative biology* **2010**, *14*, 401–418.

(16) Courant, F.; Antignac, J.-P.; Dervilly-Pinel, G.; Le Bizec, B. Basics of mass spectrometry based metabolomics. *PROTEOMICS* **2014**, *14*, 2369–2388.

(17) Lowe, R.; Shirley, N.; Bleackley, M.; Dolan, S.; Shafee, T. Transcriptomics technologies. *PLoS computational biology* **2017**, *13*, e1005457.

(18) Wu, C.; Zhou, F.; Ren, J.; Li, X.; Jiang, Y.; Ma, S. A Selective Review of Multi-Level Omics Data Integration Using Variable Selection. *High-throughput* **2019**, *8*.

(19) Caldera, M.; Buphamalai, P.; Müller, F.; Menche, J. Interactome-based approaches to human disease. *Current Opinion in Systems Biology* **2017**, *3*, 88–94.

(20) Imming, P.; Sinning, C.; Meyer, A. Drugs, their targets and the nature and number of drug targets. *Nature reviews. Drug discovery* **2006**, *5*, 821–834.

(21) Poluri, K. M.; Gulati, K.; Sarkar, S. *Protein-Protein Interactions*; Springer Singapore, 2021.

(22) Gerardo, N. M.; Hoang, K. L.; Stoy, K. S. Evolution of animal immunity in the light of beneficial symbioses. *Philosophical transactions of the Royal Society of London. Series B, Biological sciences* **2020**, *375*, 20190601.

(23) Berg, J. M.; Tymoczko, J. L.; Gatto, G. J.; Stryer, L. *Stryer Biochemie*; Springer Berlin Heidelberg: Berlin, Heidelberg, 2018.
(24) Chiu, M. L.; Goulet, D. R.; Teplyakov, A.; Gilliland, G. L. Antibody Structure and Function: The Basis for Engineering Therapeutics. *Antibodies* **2019**, *8*.
(25) Schrödinger, L. L. *The PyMOL Molecular Graphics System, Version 1.8*, 2015.
(26) Akbar, R.; Robert, P. A.; Pavlović, M.; Jeliazkov, J. R.; Snapkov, I.; Slabodkin, A.; Weber, C. R.; Scheffer, L.; Miho, E.; Haff, I. H.*; et al.* A compact vocabulary of paratope-epitope interactions enables predictability of antibody-antigen binding. *Cell reports* **2021**, *34*, 108856.
(27) Martini, S.; Nielsen, M.; Peters, B.; Sette, A. The Immune Epitope Database and Analysis Resource Program 2003-2018: reflections and outlook. *Immunogenetics* **2020**, *72*, 57–76.
(28) Vita, R.; Mahajan, S.; Overton, J. A.; Dhanda, S. K.; Martini, S.; Cantrell, J. R.; Wheeler, D. K.; Sette, A.; Peters, B. The Immune Epitope Database (IEDB): 2018 update. *Nucleic acids research* **2019**, *47*, D339-D343.
(29) Kastritis, P. L.; Bonvin, A. M. J. J. On the binding affinity of macromolecular interactions: daring to ask why proteins interact. *Journal of the Royal Society, Interface* **2013**, *10*, 20120835.
(30) Mattes, M. J. Binding parameters of antibodies: pseudo-affinity and other misconceptions. *Cancer immunology, immunotherapy : CII* **2005**, *54*, 513–516.
(31) Erlendsson, S.; Teilum, K. Binding Revisited-Avidity in Cellular Function and Signaling. *Frontiers in molecular biosciences* **2020**, *7*, 615565.
(32) van Regenmortel, M. H. Mapping Epitope Structure and Activity: From One-Dimensional Prediction to Four-Dimensional Description of Antigenic Specificity. *Methods (San Diego, Calif.)* **1996**, *9*, 465–472.
(33) Nimjee, S. M.; White, R. R.; Becker, R. C.; Sullenger, B. A. Aptamers as Therapeutics. *Annual review of pharmacology and toxicology* **2017**, *57*, 61–79.
(34) Arepalli, S.; Kaiser, P. K. Pipeline therapies for neovascular age related macular degeneration. *International journal of retina and vitreous* **2021**, *7*, 55.
(35) Arshavsky-Graham, S.; Urmann, K.; Salama, R.; Massad-Ivanir, N.; Walter, J.-G.; Scheper, T.; Segal, E. Aptamers vs. antibodies as capture probes in optical porous silicon biosensors. *The Analyst* **2020**, *145*, 4991–5003.
(36) Bauer, M.; Strom, M.; Hammond, D. S.; Shigdar, S. Anything You Can Do, I Can Do Better: Can Aptamers Replace Antibodies in Clinical Diagnostic Applications? *Molecules (Basel, Switzerland)* **2019**, *24*.
(37) Rabiee, N.; Ahmadi, S.; Arab, Z.; Bagherzadeh, M.; Safarkhani, M.; Nasseri, B.; Rabiee, M.; Tahriri, M.; Webster, T. J.; Tayebi, L. Aptamer Hybrid Nanocomplexes as Targeting Components for Antibiotic/Gene Delivery Systems and Diagnostics: A Review. *International journal of nanomedicine* **2020**, *15*, 4237–4256.
(38) Fesseha, H. Aptamers: Diagnostic and Therapeutic Applications. *BJSTR* **2020**, *28*.
(39) Baker, M. Reproducibility crisis: Blame it on the antibodies. *Nature* **2015**, *521*, 274–276.
(40) Darmostuk, M.; Rimpelova, S.; Gbelcova, H.; Ruml, T. Current approaches in SELEX: An update to aptamer selection technology. *Biotechnology advances* **2015**, *33*, 1141–1161.
(41) Zhuo, Z.; Yu, Y.; Wang, M.; Li, J.; Zhang, Z.; Liu, J.; Wu, X.; Lu, A.; Zhang, G.; Zhang, B. Recent Advances in SELEX Technology and Aptamer Applications in Biomedicine. *International journal of molecular sciences* **2017**, *18*, 2142.
(42) Xie, S.; Ai, L.; Cui, C.; Fu, T.; Cheng, X.; Qu, F.; Tan, W. Functional Aptamer-Embedded Nanomaterials for Diagnostics and Therapeutics. *ACS applied materials & interfaces* **2021**, *13*, 9542–9560.
(43) Jarczewska, M.; Malinowska, E. The application of antibody-aptamer hybrid biosensors in clinical diagnostics and environmental analysis. *Analytical methods : advancing methods and applications* **2020**, *12*, 3183–3199.
(44) Ng, E. W. M.; Shima, D. T.; Calias, P.; Cunningham, E. T.; Guyer, D. R.; Adamis, A. P. Pegaptanib, a targeted anti-VEGF aptamer for ocular vascular disease. *Nature reviews. Drug discovery* **2006**, *5*, 123–132.
(45) Yeo, N. J. Y.; Chan, E. J. J.; Cheung, C. Choroidal Neovascularization: Mechanisms of Endothelial Dysfunction. *Front. Pharmacol.* **2019**, *10*, 1363.
(46) Bukhari, S. N. H.; Jain, A.; Haq, E.; Mehbodniya, A.; Webber, J. Machine Learning Techniques for the Prediction of B-Cell and T-Cell Epitopes as Potential Vaccine Targets with a Specific Focus on SARS-CoV-2 Pathogen: A Review. *Pathogens (Basel, Switzerland)* **2022**, *11*.

(47) Yurina, V.; Adianingsih, O. R. Predicting epitopes for vaccine development using bioinformatics tools. *Therapeutic advances in vaccines and immunotherapy* **2022**, *10*, 25151355221100218.
(48) Galanis, K. A.; Nastou, K. C.; Papandreou, N. C.; Petichakis, G. N.; Pigis, D. G.; Iconomidou, V. A. Linear B-Cell Epitope Prediction for In Silico Vaccine Design: A Performance Review of Methods Available via Command-Line Interface. *International journal of molecular sciences* **2021**, *22*.
(49) Saha, S.; Raghava, G. P. S. Prediction of continuous B-cell epitopes in an antigen using recurrent neural network. *Proteins* **2006**, *65*, 40–48.
(50) Singh, H.; Ansari, H. R.; Raghava, G. P. S. Improved method for linear B-cell epitope prediction using antigen's primary sequence. *PloS one* **2013**, *8*, e62216.
(51) Yao, B.; Zhang, L.; Liang, S.; Zhang, C. SVMTriP: a method to predict antigenic epitopes using support vector machine to integrate tri-peptide similarity and propensity. *PloS one* **2012**, *7*, e45152.
(52) Manavalan, B.; Govindaraj, R. G.; Shin, T. H.; Kim, M. O.; Lee, G. iBCE-EL: A New Ensemble Learning Framework for Improved Linear B-Cell Epitope Prediction. *Frontiers in immunology* **2018**, *9*, 1695.
(53) Rubinstein, N. D.; Mayrose, I.; Martz, E.; Pupko, T. Epitopia: a web-server for predicting B-cell epitopes. *BMC bioinformatics* **2009**, *10*, 287.
(54) Ansari, H. R.; Raghava, G. P. Identification of conformational B-cell Epitopes in an antigen from its primary sequence. *Immunome research* **2010**, *6*, 6.
(55) Liang, S.; Zheng, D.; Standley, D. M.; Yao, B.; Zacharias, M.; Zhang, C. EPSVR and EPMeta: prediction of antigenic epitopes using support vector regression and multiple server results. *BMC bioinformatics* **2010**, *11*, 381.
(56) Ponomarenko, J.; Bui, H.-H.; Li, W.; Fusseder, N.; Bourne, P. E.; Sette, A.; Peters, B. ElliPro: a new structure-based tool for the prediction of antibody epitopes. *BMC bioinformatics* **2008**, *9*, 514.
(57) John A. Swets. Measuring the Accuracy of Diagnostic Systems. *Science* **1988**, 1285–1293.
(58) Chicco, D.; Jurman, G. The advantages of the Matthews correlation coefficient (MCC) over F1 score and accuracy in binary classification evaluation. *BMC Genomics* **2020**, *21*.
(59) Haste Andersen, P.; Nielsen, M.; Lund, O. Prediction of residues in discontinuous B-cell epitopes using protein 3D structures. *Protein science : a publication of the Protein Society* **2006**, *15*, 2558–2567.
(60) Hooshmand, N.; Fayazi, J.; Tabatabaei, S.; Ghaleh Golab Behbahan, N. Prediction of B cell and T-helper cell epitopes candidates of bovine leukaemia virus (BLV) by in silico approach. *Veterinary medicine and science* **2020**, *6*, 730–739.
(61) Li, W.; Li, L.; Sun, T.; He, Y.; Liu, G.; Xiao, Z.; Fan, Y.; Zhang, J. Spike protein-based epitopes predicted against SARS-CoV-2 through literature mining. *Medicine in novel technology and devices* **2020**, *8*, 100048.
(62) Torrisi, M.; Pollastri, G.; Le, Q. Deep learning methods in protein structure prediction. *Computational and structural biotechnology journal* **2020**, *18*, 1301–1310.
(63) Kuhlman, B.; Bradley, P. Advances in protein structure prediction and design. *Nature reviews. Molecular cell biology* **2019**, *20*, 681–697.
(64) Loeffler, F. F.; Viana, I. F. T.; Fischer, N.; Coêlho, D. F.; Silva, C. S.; Purificação, A. F.; Araújo, C. M. C. S.; Leite, B. H. S.; Durães-Carvalho, R.; Magalhães, T.*; et al.* Identification of a Zika NS2B epitope as a biomarker for severe clinical phenotypes. *RSC medicinal chemistry* **2021**, *12*, 1525–1539.
(65) Weaver, E.; Uddin, S.; Cole, D. K.; Hooker, A.; Lamprou, D. A. The Present and Future Role of Microfluidics for Protein and Peptide-Based Therapeutics and Diagnostics. *Applied Sciences* **2021**, *11*, 4109.
(66) Cheng, P.; Wang, L.; Gong, W. In silico Analysis of Peptide-Based Biomarkers for the Diagnosis and Prevention of Latent Tuberculosis Infection. *Frontiers in microbiology* **2022**, *13*, 947852.
(67) Heinrich, L.; Tissot, N.; Hartmann, D. J.; Cohen, R. Comparison of the results obtained by ELISA and surface plasmon resonance for the determination of antibody affinity. *Journal of Immunological Methods* **2010**, *352*, 13–22.
(68) Rossi, A. M.; Taylor, C. W. Analysis of protein-ligand interactions by fluorescence polarization. *Nature protocols* **2011**, *6*, 365–387.
(69) Zhang, F.; Xue, J.; Shao, J.; Jia, L. Compilation of 222 drugs' plasma protein binding data and guidance for study designs. *Drug Discovery Today* **2012**, *17*, 475–485.
(70) Prozeller, D.; Morsbach, S.; Landfester, K. Isothermal titration calorimetry as a complementary method for investigating nanoparticle-protein interactions. *Nanoscale* **2019**, *11*, 19265–19273.

(71) Duff, M. R.; Grubbs, J.; Howell, E. E. Isothermal titration calorimetry for measuring macromolecule-ligand affinity. *Journal of visualized experiments : JoVE* [Online early access]. DOI: 10.3791/2796. Published Online: Sep. 7, 2011.
(72) Petersen, R. L. Strategies Using Bio-Layer Interferometry Biosensor Technology for Vaccine Research and Development. *Biosensors* **2017**, *7*, 49.
(73) Singh, P. SPR Biosensors: Historical Perspectives and Current Challenges. *Sensors and Actuators B: Chemical* **2016**, *229*, 110–130.
(74) Li, X.; Song, S.; Shuai, Q.; Pei, Y.; Aastrup, T.; Pei, Y.; Pei, Z. Real-time and label-free analysis of binding thermodynamics of carbohydrate-protein interactions on unfixed cancer cell surfaces using a QCM biosensor. *Scientific reports* **2015**, *5*, 14066.
(75) Vuignier, K.; Schappler, J.; Veuthey, J.-L.; Carrupt, P.-A.; Martel, S. Drug-protein binding: a critical review of analytical tools. *Analytical and bioanalytical chemistry* **2010**, *398*, 53–66.
(76) Di Trani, J. M.; Cesco, S. de; O'Leary, R.; Plescia, J.; do Nascimento, C. J.; Moitessier, N.; Mittermaier, A. K. Rapid measurement of inhibitor binding kinetics by isothermal titration calorimetry. *Nature communications* **2018**, *9*, 893.
(77) Patris, S.; Vandeput, M.; Kauffmann, J.-M. Antibodies as target for affinity biosensors. *TrAC Trends in Analytical Chemistry* **2016**, *79*, 239–246.
(78) Dufour, C.; Dangles, O. Flavonoid-serum albumin complexation: determination of binding constants and binding sites by fluorescence spectroscopy. *Biochimica et biophysica acta* **2005**, *1721*, 164–173.
(79) Gaus, H. J.; Gupta, R.; Chappell, A. E.; Østergaard, M. E.; Swayze, E. E.; Seth, P. P. Characterization of the interactions of chemically-modified therapeutic nucleic acids with plasma proteins using a fluorescence polarization assay. *Nucleic acids research* **2019**, *47*, 1110–1122.
(80) Swenson, H.; Stadie, N. P. Langmuir's Theory of Adsorption: A Centennial Review. *Langmuir* **2019**, *35*, 5409–5426.
(81) Nehra, M.; Lettieri, M.; Dilbaghi, N.; Kumar, S.; Marrazza, G. Nano-Biosensing Platforms for Detection of Cow's Milk Allergens: An Overview. *Sensors* **2019**, *20*.
(82) Masson, J.-F. Surface Plasmon Resonance Clinical Biosensors for Medical Diagnostics. *ACS sensors* **2017**, *2*, 16–30.
(83) Qu, J.-H.; Dillen, A.; Saeys, W.; Lammertyn, J.; Spasic, D. Advancements in SPR biosensing technology: An overview of recent trends in smart layers design, multiplexing concepts, continuous monitoring and in vivo sensing. *Analytica chimica acta* **2020**, *1104*, 10–27.
(84) Schasfoort, R. B. M., Ed. *Handbook of Surface Plasmon Resonance*; Royal Society of Chemistry: Cambridge, 2017.
(85) Nurrohman, D. T.; Chiu, N.-F. A Review of Graphene-Based Surface Plasmon Resonance and Surface-Enhanced Raman Scattering Biosensors: Current Status and Future Prospects. *Nanomaterials* **2021**, *11*.
(86) Kumar, R.; Kushwaha, A. S.; Srivastava, M.; Mishra, H.; Srivastava, S. K. Enhancement in sensitivity of graphene-based zinc oxide assisted bimetallic surface plasmon resonance (SPR) biosensor. *Applied Physics A* **2018**, *124*.
(87) Xue, Y.; Li, X.; Li, H.; Zhang, W. Quantifying thiol-gold interactions towards the efficient strength control. *Nature communications* **2014**, *5*, 4348.
(88) Mauriz, E.; García-Fernández, M. C.; Lechuga, L. M. Towards the design of universal immunosurfaces for SPR-based assays: A review. *TrAC Trends in Analytical Chemistry* **2016**, *79*, 191–198.
(89) Drozd, M.; Karoń, S.; Malinowska, E. Recent Advancements in Receptor Layer Engineering for Applications in SPR-Based Immunodiagnostics. *Sensors* **2021**, *21*, 3781.
(90) Silin; Weetall; Vanderah. SPR Studies of the Nonspecific Adsorption Kinetics of Human IgG and BSA on Gold Surfaces Modified by Self-Assembled Monolayers (SAMs). *Journal of Colloid and Interface Science* **1997**, *185*, 94–103.
(91) Zhao, H.; Gorshkova, I. I.; Fu, G. L.; Schuck, P. A comparison of binding surfaces for SPR biosensing using an antibody-antigen system and affinity distribution analysis. *Methods (San Diego, Calif.)* **2013**, *59*, 328–335.
(92) user. Contents. *Polymer Contents* **1998**, *15*, i–ii.

(93) Vashist, S. K. Comparison of 1-Ethyl-3-(3-Dimethylaminopropyl) Carbodiimide Based Strategies to Crosslink Antibodies on Amine-Functionalized Platforms for Immunodiagnostic Applications. *Diagnostics (Basel, Switzerland)* **2012**, *2*, 23–33.
(94) Makaraviciute, A.; Ramanavicius, A.; Ramanaviciene, A. Development of a reusable protein G based SPR immunosensor for direct human growth hormone detection in real samples. *Analytical Methods* **2015**, *7*, 9875–9884.
(95) Caminha, M. A.; Lorena, V. M. B. de; Oliveira Júnior, W. de; Perales, J.; Carvalho, P. C.; Lima, D. B.; Da Cavalcanti, M. G. A. M.; Martins, S. M.; Valente, R. H.; Menna-Barreto, R. F. S. Data on antigen recognition hindrance by antibodies covalently immobilized to Protein G magnetic beads by dimethyl pimelimidate (DMP) cross-linking. *Data in brief* **2019**, *22*, 516–521.
(96) Bergström, G.; Mandenius, C.-F. Orientation and capturing of antibody affinity ligands: Applications to surface plasmon resonance biochips. *Sensors and Actuators B: Chemical* **2011**, *158*, 265–270.
(97) Kausaite-Minkstimiene, A.; Ramanaviciene, A.; Kirlyte, J.; Ramanavicius, A. Comparative study of random and oriented antibody immobilization techniques on the binding capacity of immunosensor. *Analytical chemistry* **2010**, *82*, 6401–6408.
(98) Teplyakov, A.; Obmolova, G.; Wu, S.-J.; Luo, J.; Kang, J.; O'Neil, K.; Gilliland, G. L. Epitope mapping of anti-interleukin-13 neutralizing antibody CNTO607. *Journal of molecular biology* **2009**, *389*, 115–123.
(99) Abbott, W. M.; Damschroder, M. M.; Lowe, D. C. Current approaches to fine mapping of antigen-antibody interactions. *Immunology* **2014**, *142*, 526–535.
(100) Toride King, M.; Brooks, C. L. Epitope Mapping of Antibody-Antigen Interactions with X-Ray Crystallography. *Methods in molecular biology (Clifton, N.J.)* **2018**, *1785*, 13–27.
(101) Bardelli, M.; Livoti, E.; Simonelli, L.; Pedotti, M.; Moraes, A.; Valente, A. P.; Varani, L. Epitope mapping by solution NMR spectroscopy. *Journal of molecular recognition : JMR* **2015**, *28*, 393–400.
(102) Rosen, O.; Anglister, J. Epitope mapping of antibody-antigen complexes by nuclear magnetic resonance spectroscopy. *Methods in molecular biology (Clifton, N.J.)* **2009**, *524*, 37–57.
(103) Szymczak, L. C.; Kuo, H.-Y.; Mrksich, M. Peptide Arrays: Development and Application. *Analytical chemistry* **2018**, *90*, 266–282.
(104) Long, F.; Fong, R. H.; Austin, S. K.; Chen, Z.; Klose, T.; Fokine, A.; Liu, Y.; Porta, J.; Sapparapu, G.; Akahata, W.*; et al.* Cryo-EM structures elucidate neutralizing mechanisms of anti-chikungunya human monoclonal antibodies with therapeutic activity. *Proceedings of the National Academy of Sciences of the United States of America* **2015**, *112*, 13898–13903.
(105) Bianchi, M.; Turner, H. L.; Nogal, B.; Cottrell, C. A.; Oyen, D.; Pauthner, M.; Bastidas, R.; Nedellec, R.; McCoy, L. E.; Wilson, I. A.*; et al.* Electron-Microscopy-Based Epitope Mapping Defines Specificities of Polyclonal Antibodies Elicited during HIV-1 BG505 Envelope Trimer Immunization. *Immunity* **2018**, *49*, 288-300.e8.
(106) Takei, J.; Asano, T.; Suzuki, H.; Kaneko, M. K.; Kato, Y. Epitope Mapping of the Anti-CD44 Monoclonal Antibody (C44Mab-46) Using Alanine-Scanning Mutagenesis and Surface Plasmon Resonance. *Monoclonal antibodies in immunodiagnosis and immunotherapy* **2021**, *40*, 219–226.
(107) Morrison, K. L.; Weiss, G. A. Combinatorial alanine-scanning. *Current Opinion in Chemical Biology* **2001**, *5*, 302–307.
(108) Gershoni, J. M.; Roitburd-Berman, A.; Siman-Tov, D. D.; Tarnovitski Freund, N.; Weiss, Y. Epitope mapping: the first step in developing epitope-based vaccines. *BioDrugs : clinical immunotherapeutics, biopharmaceuticals and gene therapy* **2007**, *21*, 145–156.
(109) Marciano, D. P.; Dharmarajan, V.; Griffin, P. R. HDX-MS guided drug discovery: small molecules and biopharmaceuticals. *Current opinion in structural biology* **2014**, *28*, 105–111.
(110) Masson, G. R.; Burke, J. E.; Ahn, N. G.; Anand, G. S.; Borchers, C.; Brier, S.; Bou-Assaf, G. M.; Engen, J. R.; Englander, S. W.; Faber, J.*; et al.* Recommendations for performing, interpreting and reporting hydrogen deuterium exchange mass spectrometry (HDX-MS) experiments. *Nature methods* **2019**, *16*, 595–602.
(111) Leitner, A.; Faini, M.; Stengel, F.; Aebersold, R. Crosslinking and Mass Spectrometry: An Integrated Technology to Understand the Structure and Function of Molecular Machines. *Trends in biochemical sciences* **2016**, *41*, 20–32.

(112) Leitner, A.; Walzthoeni, T.; Aebersold, R. Lysine-specific chemical cross-linking of protein complexes and identification of cross-linking sites using LC-MS/MS and the xQuest/xProphet software pipeline. *Nature protocols* **2014**, *9*, 120–137.
(113) Nilvebrant, J.; Rockberg, J. An Introduction to Epitope Mapping. *Methods in molecular biology (Clifton, N.J.)* **2018**, *1785*, 1–10.
(114) Yamauchi, O. Noncovalent interactions in biocomplexes. *Physical Sciences Reviews* **2016**, *1*.
(115) Levernæs, M.; Farhat, B.; Oulie, I.; Abdullah, S. S.; Paus, E.; Reubsaet, L.; Halvorsen, T. G. *Exploring peptide capture by anti-protein antibodies for LC-MS-based biomarker determination*, 2018.
(116) Huse, K.; Böhme, H.-J.; Scholz, G. H. Purification of antibodies by affinity chromatography. *Journal of Biochemical and Biophysical Methods* **2002**, *51*, 217–231.
(117) Suckau, D.; Köhl, J.; Karwath, G.; Schneider, K.; Casaretto, M.; Bitter-Suermann, D.; Przybylski, M. Molecular epitope identification by limited proteolysis of an immobilized antigen-antibody complex and mass spectrometric peptide mapping. *Proceedings of the National Academy of Sciences of the United States of America* **1990**, *87*, 9848–9852.
(118) Neagu, A.-N.; Jayathirtha, M.; Baxter, E.; Donnelly, M.; Petre, B. A.; Darie, C. C. Applications of Tandem Mass Spectrometry (MS/MS) in Protein Analysis for Biomedical Research. *Molecules* **2022**, *27*, 2411.
(119) Gross, J. H. *Massenspektrometrie: Spektroskopiekurs kompakt*, 1. Aufl. 2019; Springer Berlin Heidelberg: Berlin, Heidelberg, 2019.
(120) El-Aneed, A.; Cohen, A.; Banoub, J. Mass Spectrometry, Review of the Basics: Electrospray, MALDI, and Commonly Used Mass Analyzers. *Applied Spectroscopy Reviews* **2009**, *44*, 210–230.
(121) Wilm, M. Principles of electrospray ionization. *Molecular & cellular proteomics : MCP* **2011**, *10*, M111.009407.
(122) Hosseini, S.; Martinez-Chapa, S. O. Principles and Mechanism of MALDI-ToF-MS Analysis. *Fundamentals of MALDI-ToF-MS Analysis* **2017**, 1–19.
(123) Singhal, N.; Kumar, M.; Kanaujia, P. K.; Virdi, J. S. MALDI-TOF mass spectrometry: an emerging technology for microbial identification and diagnosis. *Frontiers in microbiology* **2015**, *6*, 791.
(124) Nguyen, H. P.; Schug, K. A. The advantages of ESI-MS detection in conjunction with HILIC mode separations: Fundamentals and applications. *Journal of Separation Science* **2008**, *31*, 1465–1480.
(125) Lupu, L.-M.; Wiegand, P.; Holdschick, D.; Mihoc, D.; Maeser, S.; Rawer, S.; Völklein, F.; Malek, E.; Barka, F.; Knauer, S.*; et al.* Identification and Affinity Determination of Protein-Antibody and Protein-Aptamer Epitopes by Biosensor-Mass Spectrometry Combination. *International journal of molecular sciences* **2021**, *22*.
(126) Slamnoiu, S.; Vlad, C.; Stumbaum, M.; Moise, A.; Lindner, K.; Engel, N.; Vilanova, M.; Diaz, M.; Karreman, C.; Leist, M.*; et al.* Identification and affinity-quantification of ß-amyloid and α-synuclein polypeptides using on-line SAW-biosensor-mass spectrometry. *Journal of the American Society for Mass Spectrometry* **2014**, *25*, 1472–1481.
(127) Dragusanu, M.; Petre, B.-A.; Slamnoiu, S.; Vlad, C.; Tu, T.; Przybylski, M. On-line bioaffinity-electrospray mass spectrometry for simultaneous detection, identification, and quantification of protein-ligand interactions. *Journal of the American Society for Mass Spectrometry* **2010**, *21*, 1643–1648.
(128) Mihoc, D.; Lupu, L.-M.; Wiegand, P.; Kleinekofort, W.; Müller, O.; Völklein, F.; Glocker, M. O.; Barka, F.; Barka, G.; Przybylski, M. Antibody Epitope and Affinity Determination of the Myocardial Infarction Marker Myoglobin by SPR-Biosensor Mass Spectrometry. *Journal of the American Society for Mass Spectrometry* **2021**, *32*, 106–113.
(129) Rinaldi, F.; Lupu, L.; Rusche, H.; Kukačka, Z.; Tengattini, S.; Bernardini, R.; Piubelli, L.; Bavaro, T.; Maeser, S.; Pollegioni, L.*; et al.* Epitope and affinity determination of recombinant Mycobacterium tuberculosis Ag85B antigen towards anti-Ag85 antibodies using proteolytic affinity-mass spectrometry and biosensor analysis. *Analytical and bioanalytical chemistry* **2019**, *411*, 439–448.
(130) Ștefănescu, R.; Lupu, L.; Manea, M.; Iacob, R. E.; Przybylski, M. Molecular characterization of the β-amyloid(4-10) epitope of plaque specific Aβ antibodies by affinity-mass spectrometry using alanine site mutation. *Journal of peptide science : an official publication of the European Peptide Society* **2018**, *24*.
(131) Iuraşcu, M.-I.; Marroquin Belaunzanar, O.; Cozma, C.; Petrausch, U.; Renner, C.; Przybylski, M. An HLA-B27 Homodimer Specific Antibody Recognizes a Discontinuous Mixed-Disulfide Epitope as Identified by Affinity-Mass Spectrometry. *Journal of the American Society for Mass Spectrometry* **2016**, *27*, 1105–1112.

(132) Pimenova, T.; Meier, L.; Roschitzki, B.; Paraschiv, G.; Przybylski, M.; Zenobi, R. Polystyrene beads as an alternative support material for epitope identification of a prion-antibody interaction using proteolytic excision-mass spectrometry. *Analytical and bioanalytical chemistry* **2009**, *395*, 1395–1401.
(133) Sladewska, A.; Szymańska, A.; Kordalska, M.; Lewandowska, A.; Kołodziejczyk, A. S.; Paraschiv, G.; Przybylski, M.; Czaplewska, P. Identification of the epitope for anti-cystatin C antibody. *Journal of molecular recognition : JMR* **2011**, *24*, 687–699.
(134) Tramarin, A.; Naldi, M.; Degani, G.; Lupu, L.; Wiegand, P.; Mazzolari, A.; Altomare, A.; Aldini, G.; Popolo, L.; Vistoli, G.*; et al.* Unveiling the molecular mechanisms underpinning biorecognition of early-glycated human serum albumin and receptor for advanced glycation end products. *Analytical and bioanalytical chemistry* **2020**, *412*, 4245–4259.
(135) Lupu, L.; Wiegand, P.; Hüttmann, N.; Rawer, S.; Kleinekofort, W.; Shugureva, I.; Kichkailo, A. S.; Tomilin, F. N.; Lazarev, A.; Berezovski, M. V.*; et al.* Molecular Epitope Determination of Aptamer Complexes of the Multidomain Protein C-Met by Proteolytic Affinity-Mass Spectrometry. *ChemMedChem* **2020**, *15*, 363–369.
(136) Baschung, Y.; Lupu, L.; Moise, A.; Glocker, M.; Rawer, S.; Lazarev, A.; Przybylski, M. Epitope Ligand Binding Sites of Blood Group Oligosaccharides in Lectins Revealed by Pressure-Assisted Proteolytic Excision Affinity Mass Spectrometry. *Journal of the American Society for Mass Spectrometry* **2018**, *29*, 1881–1891.
(137) Switzar, L.; Giera, M.; Niessen, W. M. A. Protein digestion: an overview of the available techniques and recent developments. *Journal of proteome research* **2013**, *12*, 1067–1077.
(138) Vandermarliere, E.; Mueller, M.; Martens, L. Getting intimate with trypsin, the leading protease in proteomics. *Mass spectrometry reviews* **2013**, *32*, 453–465.
(139) Heissel, S.; Frederiksen, S. J.; Bunkenborg, J.; Højrup, P. Enhanced trypsin on a budget: Stabilization, purification and high-temperature application of inexpensive commercial trypsin for proteomics applications. *PloS one* **2019**, *14*, e0218374.
(140) Burkhart, J. M.; Schumbrutzki, C.; Wortelkamp, S.; Sickmann, A.; Zahedi, R. P. Systematic and quantitative comparison of digest efficiency and specificity reveals the impact of trypsin quality on MS-based proteomics. *Journal of proteomics* **2012**, *75*, 1454–1462.
(141) Tsiatsiani, L.; Heck, A. J. R. Proteomics beyond trypsin. *The FEBS Journal* **2015**, *282*, 2612–2626.
(142) León, I. R.; Schwämmle, V.; Jensen, O. N.; Sprenger, R. R. Quantitative assessment of in-solution digestion efficiency identifies optimal protocols for unbiased protein analysis. *Molecular & cellular proteomics : MCP* **2013**, *12*, 2992–3005.
(143) Lakbub, J. C.; Shipman, J. T.; Desaire, H. Recent mass spectrometry-based techniques and considerations for disulfide bond characterization in proteins. *Analytical and bioanalytical chemistry* **2018**, *410*, 2467–2484.
(144) Monzo, A.; Sperling, E.; Guttman, A. Proteolytic enzyme-immobilization techniques for MS-based protein analysis. *TrAC Trends in Analytical Chemistry* **2009**, *28*, 854–864.
(145) Hedrick, V. E.; LaLand, M. N.; Nakayasu, E. S.; Paul, L. N. Digestion, Purification, and Enrichment of Protein Samples for Mass Spectrometry. *Current protocols in chemical biology* **2015**, *7*, 201–222.
(146) Eisenmenger, M. J.; Reyes-De-Corcuera, J. I. High pressure enhancement of enzymes: A review. *Enzyme and Microbial Technology* **2009**, *45*, 331–347.
(147) gross, v. PCT-HD for Tissue Biopsy Samples: Comparison to a Standard Method. Vera Gross1; Peter Hains3; Keith Ashman2; Val Valova3; Alexander Lazarev1; 1Pressure BioSciences, Inc., 14 Norfolk Ave., South Easton, MA 02375,United States; 2SCIEX, 500 Old Connecticut Path Framingham, MA 01701,United States; 3 Children's Medical Research Institute, 214 Hawkesbury Rd., Westmead NSW 2145, Australia.
(148) Lazarev; Alexander. PowerPoint Presentation.
(149) PBI-Website.
(150) Sallusto, F.; Baggiolini, M. Chemokines and leukocyte traffic. *Nature immunology* **2008**, *9*, 949–952.
(151) Rot, A.; Andrian, U. H. von. Chemokines in innate and adaptive host defense: basic chemokinese grammar for immune cells. *Annual review of immunology* **2004**, *22*, 891–928.
(152) Harada, A.; Sekido, N.; Akahoshi, T.; Wada, T.; Mukaida, N.; Matsushima, K. Essential involvement of interleukin-8 (IL-8) in acute inflammation. *Journal of leukocyte biology* **1994**, *56*, 559–564.
(153) Gordon, S. Phagocytosis: An Immunobiologic Process. *Immunity* **2016**, *44*, 463–475.
(154) Krishnamurthy, A.; Joshua, V.; Haj Hensvold, A.; Jin, T.; Sun, M.; Vivar, N.; Ytterberg, A. J.; Engström, M.; Fernandes-Cerqueira, C.; Amara, K.*; et al.* Identification of a novel chemokine-dependent molecular

mechanism underlying rheumatoid arthritis-associated autoantibody-mediated bone loss. *Annals of the rheumatic diseases* **2016**, *75*, 721–729.
(155) Lowes, M. A.; Bowcock, A. M.; Krueger, J. G. Pathogenesis and therapy of psoriasis. *Nature* **2007**, *445*, 866–873.
(156) Brat, D. J.; Bellail, A. C.; van Meir, E. G. The role of interleukin-8 and its receptors in gliomagenesis and tumoral angiogenesis. *Neuro-oncology* **2005**, *7*, 122–133.
(157) Waugh, D. J. J.; Wilson, C. The interleukin-8 pathway in cancer. *Clinical cancer research : an official journal of the American Association for Cancer Research* **2008**, *14*, 6735–6741.
(158) Viola, A.; Luster, A. D. Chemokines and their receptors: drug targets in immunity and inflammation. *Annual review of pharmacology and toxicology* **2008**, *48*, 171–197.
(159) Bilusic, M.; Heery, C. R.; Collins, J. M.; Donahue, R. N.; Palena, C.; Madan, R. A.; Karzai, F.; Marté, J. L.; Strauss, J.; Gatti-Mays, M. E.*; et al.* Phase I trial of HuMax-IL8 (BMS-986253), an anti-IL-8 monoclonal antibody, in patients with metastatic or unresectable solid tumors. *Journal for ImmunoTherapy of Cancer* **2019**, *7*, 240.
(160) Schalper, K. A.; Carleton, M.; Zhou, M.; Chen, T.; Feng, Y.; Huang, S.-P.; Walsh, A. M.; Baxi, V.; Pandya, D.; Baradet, T.*; et al.* Elevated serum interleukin-8 is associated with enhanced intratumor neutrophils and reduced clinical benefit of immune-checkpoint inhibitors. *Nature medicine* **2020**, *26*, 688–692.
(161) CXCL8 - Interleukin-8 precursor - Homo sapiens (Human) - CXCL8 gene & protein. https://www.uniprot.org/uniprot/P10145 (accessed June 1, 2022).
(162) van Damme, J.; van Beeumen, J.; Conings, R.; Decock, B.; Billiau, A. Purification of granulocyte chemotactic peptide/interleukin-8 reveals N-terminal sequence heterogeneity similar to that of beta-thromboglobulin. *European journal of biochemistry* **1989**, *181*, 337–344.
(163) Schutyser, E.; Struyf, S.; Proost, P.; Opdenakker, G.; Laureys, G.; Verhasselt, B.; Peperstraete, L.; van de Putte, I.; Saccani, A.; Allavena, P.*; et al.* Identification of biologically active chemokine isoforms from ascitic fluid and elevated levels of CCL18/pulmonary and activation-regulated chemokine in ovarian carcinoma. *Journal of Biological Chemistry* **2002**, *277*, 24584–24593.
(164) Hébert, C. A.; Baker, J. B. Interleukin-8: a review. *Cancer investigation* **1993**, *11*, 743–750.
(165) Luster, A. D. Chemokines--chemotactic cytokines that mediate inflammation. *The New England journal of medicine* **1998**, *338*, 436–445.
(166) Clore, G. M.; Appella, E.; Yamada, M.; Matsushima, K.; Gronenborn, A. M. Three-dimensional structure of interleukin 8 in solution. *Biochemistry* **1990**, *29*, 1689–1696.
(167) Lowman, H. B.; Fairbrother, W. J.; Slagle, P. H.; Kabakoff, R.; Liu, J.; Shire, S.; Hébert, C. A. Monomeric variants of IL-8: effects of side chain substitutions and solution conditions upon dimer formation. *Protein science : a publication of the Protein Society* **1997**, *6*, 598–608.
(168) Fernando, H.; Chin, C.; Rösgen, J.; Rajarathnam, K. Dimer dissociation is essential for interleukin-8 (IL-8) binding to CXCR1 receptor. *Journal of Biological Chemistry* **2004**, *279*, 36175–36178.
(169) Rajagopalan, L.; Rajarathnam, K. Ligand selectivity and affinity of chemokine receptor CXCR1. Role of N-terminal domain. *Journal of Biological Chemistry* **2004**, *279*, 30000–30008.
(170) Leong, S. R.; Kabakoff, R. C.; Hébert, C. A. Complete mutagenesis of the extracellular domain of interleukin-8 (IL-8) type A receptor identifies charged residues mediating IL-8 binding and signal transduction. *Journal of Biological Chemistry* **1994**, *269*, 19343–19348.
(171) Helmer, D.; Rink, I.; Dalton, J. A. R.; Brahm, K.; Jöst, M.; Nargang, T. M.; Blum, W.; Wadhwani, P.; Brenner-Weiss, G.; Rapp, B. E.*; et al.* Rational design of a peptide capture agent for CXCL8 based on a model of the CXCL8:CXCR1 complex. *RSC advances* **2015**, *5*, 25657–25668.
(172) Helmer, D.; Rink, I.; Dalton, J. A. R.; Brahm, K.; Jöst, M.; Nargang, T. M.; Blum, W.; Wadhwani, P.; Brenner-Weiss, G.; Rapp, B. E.*; et al.* Correction: Rational design of a peptide capture agent for CXCL8 based on a model of the CXCL8:CXCR1 complex. *RSC advances* **2018**, *8*, 16800–16801.
(173) Aitken, M. L.; Somayaji, R.; Hinds, T. R.; Pier, M.; Droguett, K.; Rios, M.; Skerrett, S. J.; Villalon, M. Glycated Albumin Triggers an Inflammatory Response in the Human Airway Epithelium and Causes an Increase in Ciliary Beat Frequency. *Frontiers in Physiology* **2021**, *12*, 653177.
(174) Kaiser, R.; Leunig, A.; Pekayvaz, K.; Popp, O.; Joppich, M.; Polewka, V.; Escaig, R.; Anjum, A.; Hoffknecht, M.-L.; Gold, C.*; et al.* Self-sustaining IL-8 loops drive a prothrombotic neutrophil phenotype in severe COVID-19. *JCI insight* **2021**, *6*.

(175) Mukaida, N.; Harada, A.; Yasumoto, K.; Matsushima, K. Properties of pro-inflammatory cell type-specific leukocyte chemotactic cytokines, interleukin 8 (IL-8) and monocyte chemotactic and activating factor (MCAF). *Microbiology and immunology* **1992**, *36*, 773–789.
(176) TEIZO YOSHIMURA, Kouji MATSUSHIMAt, SHUJI TANAKA, ELIZABETH A. ROBINSON, ETTORE APPELLA. Purification of a human monocyte-derived neutrophil chemotactic factor that has peptide sequence similarity to other host defense cytokines. **1987**, 9233–9237.
(177) Mijanovic, O.; Petushkova, A. I.; Brankovic, A.; Turk, B.; Solovieva, A. B.; Nikitkina, A. I.; Bolevich, S.; Timashev, P. S.; Parodi, A.; Zamyatnin, A. A. Cathepsin D-Managing the Delicate Balance. *Pharmaceutics* **2021**, *13*, 837.
(178) Trivedi, P. C.; Bartlett, J. J.; Pulinilkunnil, T. Lysosomal Biology and Function: Modern View of Cellular Debris Bin. *Cells* **2020**, *9*.
(179) Castino, R.; Davies, J.; Beaucourt, S.; Isidoro, C.; Murphy, D. Autophagy is a prosurvival mechanism in cells expressing an autosomal dominant familial neurohypophyseal diabetes insipidus mutant vasopressin transgene. *FASEB journal : official publication of the Federation of American Societies for Experimental Biology* **2005**, *19*, 1021–1023.
(180) Aufschnaiter, A.; Kohler, V.; Büttner, S. Taking out the garbage: cathepsin D and calcineurin in neurodegeneration. *Neural regeneration research* **2017**, *12*, 1776–1779.
(181) Alroy, J.; Lyons, J. A. Lysosomal Storage Diseases. *Journal of Inborn Errors of Metabolism and Screening* **2014**, *2*, 232640981351766.
(182) Steinfeld, R.; Reinhardt, K.; Schreiber, K.; Hillebrand, M.; Kraetzner, R.; Bruck, W.; Saftig, P.; Gartner, J. Cathepsin D deficiency is associated with a human neurodegenerative disorder. *American journal of human genetics* **2006**, *78*, 988–998.
(183) Marques, A. R. A.; Di Spiezio, A.; Thießen, N.; Schmidt, L.; Grötzinger, J.; Lüllmann-Rauch, R.; Damme, M.; Storck, S. E.; Pietrzik, C. U.; Fogh, J.*; et al.* Enzyme replacement therapy with recombinant pro-CTSD (cathepsin D) corrects defective proteolysis and autophagy in neuronal ceroid lipofuscinosis. *Autophagy* **2020**, *16*, 811–825.
(184) Ashraf, Y.; Mansouri, H.; Laurent-Matha, V.; Alcaraz, L. B.; Roger, P.; Guiu, S.; Derocq, D.; Robin, G.; Michaud, H.-A.; Delpech, H.*; et al.* Immunotherapy of triple-negative breast cancer with cathepsin D-targeting antibodies. *Journal for ImmunoTherapy of Cancer* **2019**, *7*, 29.
(185) Halim, A.; Rüetschi, U.; Larson, G.; Nilsson, J. LC-MS/MS characterization of O-glycosylation sites and glycan structures of human cerebrospinal fluid glycoproteins. *Journal of proteome research* **2013**, *12*, 573–584.
(186) Chen, R.; Jiang, X.; Sun, D.; Han, G.; Wang, F.; Ye, M.; Wang, L.; Zou, H. Glycoproteomics analysis of human liver tissue by combination of multiple enzyme digestion and hydrazide chemistry. *Journal of proteome research* **2009**, *8*, 651–661.
(187) André R. A. Marques; Alessandro Di Spiezio; Niklas Thießen; Lina Schmidt; Joachim Grötzinger; Renate Lüllmann-Rauch; Markus Damme; Steffen E. Storck; Claus U. Pietrzik; Jens Fogh*; et al.* Enzyme replacement therapy with recombinant pro-CTSD (cathepsin D) corrects defective proteolysis and autophagy in neuronal ceroid lipofuscinosis **2020**.
(188) Beck, M. Treatment strategies for lysosomal storage disorders. *Developmental medicine and child neurology* **2018**, *60*, 13–18.
(189) Hers, H. G. alpha-Glucosidase deficiency in generalized glycogenstorage disease (Pompe's disease). *Biochemical Journal* **1963**, *86*, 11–16.
(190) Kohler, L.; Puertollano, R.; Raben, N. Pompe Disease: From Basic Science to Therapy. *Neurotherapeutics : the journal of the American Society for Experimental NeuroTherapeutics* **2018**, *15*, 928–942.
(191) Roig-Zamboni, V.; Cobucci-Ponzano, B.; Iacono, R.; Ferrara, M. C.; Germany, S.; Bourne, Y.; Parenti, G.; Moracci, M.; Sulzenbacher, G. Structure of human lysosomal acid α-glucosidase-a guide for the treatment of Pompe disease. *Nature communications* **2017**, *8*, 1111.
(192) McVie-Wylie, A. J.; Lee, K. L.; Qiu, H.; Jin, X.; Do, H.; Gotschall, R.; Thurberg, B. L.; Rogers, C.; Raben, N.; O'Callaghan, M.*; et al.* Biochemical and pharmacological characterization of different recombinant acid alpha-glucosidase preparations evaluated for the treatment of Pompe disease. *Molecular genetics and metabolism* **2008**, *94*, 448–455.

(193) Moreland, R. J.; Jin, X.; Zhang, X. K.; Decker, R. W.; Albee, K. L.; Lee, K. L.; Cauthron, R. D.; Brewer, K.; Edmunds, T.; Canfield, W. M. Lysosomal acid alpha-glucosidase consists of four different peptides processed from a single chain precursor. *The Journal of biological chemistry* **2005**, *280*, 6780–6791.
(194) Alglucosidase alfa: Uses, Interactions, Mechanism of Action | DrugBank Online. https://go.drugbank.com/drugs/DB01272 (accessed June 29, 2022).
(195) Drug Approval Package: Myozyme (Alglucosidase Alfa) NDA #125141 (accessed June 30, 2022).
(196) Alglucosidase alfa: Uses, Interactions, Mechanism of Action | DrugBank Online. https://go.drugbank.com/drugs/DB01272 (accessed November 1, 2023).
(197) Hahn, A.; Schänzer, A. Long-term outcome and unmet needs in infantile-onset Pompe disease. *Annals of translational medicine* **2019**, *7*, 283.
(198) El Cheikh, K.; Basile, I.; Da Silva, A.; Bernon, C.; Cérutti, P.; Salgues, F.; Perez, M.; Maynadier, M.; Gary-Bobo, M.; Caillaud, C.*; et al.* Design of Potent Mannose 6-Phosphate Analogues for the Functionalization of Lysosomal Enzymes To Improve the Treatment of Pompe Disease. *Angewandte Chemie* **2016**, *128*, 14994–14997.
(199) Eggers, M.; Vannoy, C. H.; Huang, J.; Purushothaman, P.; Brassard, J.; Fonck, C.; Meng, H.; Prom, M. J.; Lawlor, M. W.; Cunningham, J.*; et al.* Muscle-directed gene therapy corrects Pompe disease and uncovers species-specific GAA immunogenicity. *EMBO molecular medicine* **2022**, *14*, e13968.
(200) Bellotti, A. S.; Andreoli, L.; Ronchi, D.; Bresolin, N.; Comi, G. P.; Corti, S. Molecular Approaches for the Treatment of Pompe Disease. *Molecular neurobiology* **2020**, *57*, 1259–1280.
(201) Doerfler, P. A.; Nayak, S.; Corti, M.; Morel, L.; Herzog, R. W.; Byrne, B. J. Targeted approaches to induce immune tolerance for Pompe disease therapy. *Molecular therapy. Methods & clinical development* **2016**, *3*, 15053.
(202) Bali, D. S.; Goldstein, J. L.; Banugaria, S.; Dai, J.; Mackey, J.; Rehder, C.; Kishnani, P. S. Predicting cross-reactive immunological material (CRIM) status in Pompe disease using GAA mutations: lessons learned from 10 years of clinical laboratory testing experience. *American journal of medical genetics. Part C, Seminars in medical genetics* **2012**, *160C*, 40–49.
(203) Bali, D. S.; Goldstein, J. L.; Rehder, C.; Kazi, Z. B.; Berrier, K. L.; Dai, J.; Kishnani, P. S. Clinical Laboratory Experience of Blood CRIM Testing in Infantile Pompe Disease. *Molecular genetics and metabolism reports* **2015**, *5*, 76–79.
(204) Wang, Z.; Okamoto, P.; Keutzer, J. A new assay for fast, reliable CRIM status determination in infantile-onset Pompe disease. *Molecular genetics and metabolism* **2014**, *111*, 92–100.
(205) Groot, A. S. de; Kazi, Z. B.; Martin, R. F.; Terry, F. E.; Desai, A. K.; Martin, W. D.; Kishnani, P. S. HLA- and genotype-based risk assessment model to identify infantile onset pompe disease patients at high-risk of developing significant anti-drug antibodies (ADA). *Clinical immunology (Orlando, Fla.)* **2019**, *200*, 66–70.
(206) Hilkens, J.; Tager, J. M.; Buijs, F.; Brouwer-Kelder, B.; van Thienen, G. M.; Tegelaers, F. P.; Hilgers, J. Monoclonal antibodies against human acid alpha-glucosidase. *Biochimica et biophysica acta* **1981**, *678*, 7–11.
(207) Singh, R. N.; Howell, M. D.; Ottesen, E. W.; Singh, N. N. Diverse role of survival motor neuron protein. *Biochimica et biophysica acta. Gene regulatory mechanisms* **2017**, *1860*, 299–315.
(208) Burghes, A. H. M.; Beattie, C. E. Spinal muscular atrophy: why do low levels of survival motor neuron protein make motor neurons sick? *Nature reviews. Neuroscience* **2009**, *10*, 597–609.
(209) Thelen, M. P.; Kye, M. J. The Role of RNA Binding Proteins for Local mRNA Translation: Implications in Neurological Disorders. *Frontiers in molecular biosciences* **2019**, *6*, 161.
(210) Saposnik, G.; Díaz-Abós, P.; Sánchez-Menéndez, V.; Álvarez, C.; Terzaghi, M.; Maurino, J.; Brañas-Pampillón, M.; Málaga, I. Therapeutic decisions under uncertainty for spinal muscular atrophy: The DECISIONS-SMA study protocol. *PloS one* **2022**, *17*, e0264006.
(211) Jablonka, S.; Hennlein, L.; Sendtner, M. Therapy development for spinal muscular atrophy: perspectives for muscular dystrophies and neurodegenerative disorders. *Neurological Research and Practice* **2022**, *4*, 2.
(212) López-Cortés, A.; Echeverría-Garcés, G.; Ramos-Medina, M. J. Molecular Pathogenesis and New Therapeutic Dimensions for Spinal Muscular Atrophy. *Biology* **2022**, *11*, 894.
(213) Czibere, L.; Burggraf, S.; Fleige, T.; Glück, B.; Keitel, L. M.; Landt, O.; Durner, J.; Röschinger, W.; Hohenfellner, K.; Wirth, B.*; et al.* High-throughput genetic newborn screening for spinal muscular atrophy by

rapid nucleic acid extraction from dried blood spots and 384-well qPCR. *European journal of human genetics : EJHG* **2020**, *28*, 23–30.
(214) Vill, K.; Kölbel, H.; Schwartz, O.; Blaschek, A.; Olgemöller, B.; Harms, E.; Burggraf, S.; Röschinger, W.; Durner, J.; Gläser, D.*; et al.* One Year of Newborn Screening for SMA - Results of a German Pilot Project. *Journal of neuromuscular diseases* **2019**, *6*, 503–515.
(215) Alves, C. R. R.; Zhang, R.; Johnstone, A. J.; Garner, R.; Eichelberger, E. J.; Da Lepez, S. S. D.; Yi, V.; Stevens, V.; Poxson, R.; Schwartz, R.*; et al.* Whole blood survival motor neuron protein levels correlate with severity of denervation in spinal muscular atrophy. *Muscle & nerve* **2020**, *62*, 351–357.
(216) Ramos, D. M.; d'Ydewalle, C.; Gabbeta, V.; Dakka, A.; Klein, S. K.; Norris, D. A.; Matson, J.; Taylor, S. J.; Zaworski, P. G.; Prior, T. W.*; et al.* Age-dependent SMN expression in disease-relevant tissue and implications for SMA treatment. *The Journal of clinical investigation* **2019**, *129*, 4817–4831.
(217) Zaworski, P.; Herrmann, K. M. von; Taylor, S.; Sunshine, S. S.; McCarthy, K.; Risher, N.; Newcomb, T.; Weetall, M.; Prior, T. W.; Swoboda, K. J.*; et al.* SMN Protein Can Be Reliably Measured in Whole Blood with an Electrochemiluminescence (ECL) Immunoassay: Implications for Clinical Trials. *PloS one* **2016**, *11*, e0150640.
(218) Calucho, M.; Bernal, S.; Alías, L.; March, F.; Venceslá, A.; Rodríguez-Álvarez, F. J.; Aller, E.; Fernández, R. M.; Borrego, S.; Millán, J. M.*; et al.* Correlation between SMA type and SMN2 copy number revisited: An analysis of 625 unrelated Spanish patients and a compilation of 2834 reported cases. *Neuromuscular disorders : NMD* **2018**, *28*, 208–215.
(219) Kobayashi, D. T.; Olson, R. J.; Sly, L.; Swanson, C. J.; Chung, B.; Naryshkin, N.; Narasimhan, J.; Bhattacharyya, A.; Mullenix, M.; Chen, K. S. Utility of survival motor neuron ELISA for spinal muscular atrophy clinical and preclinical analyses. *PloS one* **2011**, *6*, e24269.
(220) AB_2490283 Search - The Antibody Registry. https://antibodyregistry.org/search.php?q=AB_2490283 (accessed July 13, 2022).
(221) Meister, G.; Bühler, D.; Laggerbauer, B.; Zobawa, M.; Lottspeich, F.; Fischer, U. Characterization of a nuclear 20S complex containing the survival of motor neurons (SMN) protein and a specific subset of spliceosomal Sm proteins. *Human molecular genetics* **2000**, *9*, 1977–1986.
(222) Chen, T.; Zhang, B.; Ziegenhals, T.; Prusty, A. B.; Fröhler, S.; Grimm, C.; Hu, Y.; Schaefke, B.; Fang, L.; Zhang, M.*; et al.* A missense mutation in SNRPE linked to non-syndromal microcephaly interferes with U snRNP assembly and pre-mRNA splicing. *PLoS genetics* **2019**, *15*, e1008460.
(223) Neuenkirchen, N.; Englbrecht, C.; Ohmer, J.; Ziegenhals, T.; Chari, A.; Fischer, U. Reconstitution of the human U snRNP assembly machinery reveals stepwise Sm protein organization. *The EMBO Journal* **2015**, *34*, 1925–1941.
(224) Schilling, M.; Prusty, A. B.; Boysen, B.; Oppermann, F. S.; Riedel, Y. L.; Husedzinovic, A.; Rasouli, H.; König, A.; Ramanathan, P.; Reymann, J.*; et al.* TOR signaling regulates liquid phase separation of the SMN complex governing snRNP biogenesis. *Cell reports* **2021**, *35*, 109277.
(225) Meister, G.; Bühler, D.; Pillai, R.; Lottspeich, F.; Fischer, U. A multiprotein complex mediates the ATP-dependent assembly of spliceosomal U snRNPs. *Nature cell biology* **2001**, *3*, 945–949.
(226) Otter, S.; Grimmler, M.; Neuenkirchen, N.; Chari, A.; Sickmann, A.; Fischer, U. A comprehensive interaction map of the human survival of motor neuron (SMN) complex. *Journal of Biological Chemistry* **2007**, *282*, 5825–5833.
(227) Kroiss, M.; Brünger, K. M.; Wiesner, J.; Grimmler, M.; Sickmann, A.; Fischer, U. Native purification of protein and RNA-protein complexes using a novel affinity procedure. *Fly* **2009**, *3*, 223–231.
(228) High-Content Peptide Microarrays for Epitope Mapping and Serum Antibody Profiling. https:// www.pepperprint.com/fileadmin/user_upload/news/pepperchip_08_2013.html (accessed July 13, 2022).
(229) Lee, B.-S.; Huang, J.-S.; Jayathilaka, L. P.; Lee, J.; Gupta, S. Antibody Production with Synthetic Peptides. *Methods in molecular biology (Clifton, N.J.)* **2016**, *1474*, 25–47.
(230) Lateef, S. S.; Gupta, S.; Jayathilaka, L. P.; Krishnanchettiar, S.; Huang, J.-S.; Lee, B.-S. An improved protocol for coupling synthetic peptides to carrier proteins for antibody production using DMF to solubilize peptides. *Journal of Biomolecular Techniques : JBT* **2007**, *18*, 173–176.
(231) Strohalm, M.; Kavan, D.; Novák, P.; Volný, M.; Havlícek, V. mMass 3: a cross-platform software environment for precise analysis of mass spectrometric data. *Analytical chemistry* **2010**, *82*, 4648–4651.

(232) Strohalm, M.; Hassman, M.; Kosata, B.; Kodícek, M. mMass data miner: an open source alternative for mass spectrometric data analysis. *Rapid communications in mass spectrometry : RCM* **2008**, *22*, 905–908.
(233) Niedermeyer, T. H. J.; Strohalm, M. mMass as a software tool for the annotation of cyclic peptide tandem mass spectra. *PloS one* **2012**, *7*, e44913.
(234) Schneider, C. A.; Rasband, W. S.; Eliceiri, K. W. NIH Image to ImageJ: 25 years of image analysis. *Nature methods* **2012**, *9*, 671–675.
(235) Kavan, D.; Man, P. MSTools—Web based application for visualization and presentation of HXMS data. *International Journal of Mass Spectrometry* **2011**, *302*, 53–58.
(236) MS Tools. http://peterslab.org/MSTools/ (accessed November 25, 2023).
(237) Antibody Epitope Prediction. http://tools.iedb.org/bcell/ (accessed November 21, 2022).
(238) DiscoTope. http://tools.iedb.org/discotope/ (accessed November 21, 2022).
(239) SEPPA 3.0. http://www.badd-cao.net/seppa3/submission.html (accessed November 21, 2022).
(240) Immunomedicine Group: Tools BCEPS: B Cell Epitope Prediction Software. http://imbio.med.ucm.es/bceps/ (accessed November 21, 2022).
(241) Deng, Y.; van der Veer, F.; Sforza, S.; Gruppen, H.; Wierenga, P. A. Towards predicting protein hydrolysis by bovine trypsin. *Process Biochemistry* **2018**, *65*, 81–92.
(242) Corporation, P. Chymotrypsin, Sequencing Grade, Certificate of Analysis 9PIV106.
(243) Daria Holdschick. Myocardial Infarct Marker Myoglobin investigated by SPR-MS. *Master Thesis - Hochschule RheinMain Rüsselsheim & Steinbeis Center* **2021**.
(244) Loredana-Mirela Lupu; Pascal Wiegand; Daria Holdschick; Delia Mihoc; Stefan Maeser; Stephan Rawer; Friedemann Völklein; Ebrahim Malek; Frederik Barka; Sascha Knauer*; et al.* Identification and Affinity Determination of Protein-Antibody and Protein-Aptamer Epitopes by Biosensor-MassSpectrometry Combination "2279.
(245) Mihoc, D.; Lupu, L.-M.; Wiegand, P.; Kleinekofort, W.; Müller, O.; Völklein, F.; Glocker, M. O.; Barka, F.; Barka, G.; Przybylski, M. Antibody Epitope and Affinity Determination of the Myocardial Infarction Marker Myoglobin by SPR-Biosensor Mass Spectrometry. *Journal of the American Society for Mass Spectrometry* **2021**, *32*, 106–113.
(246) Heinz, H.; Farmer, B. L.; Pandey, R. B.; Slocik, J. M.; Patnaik, S. S.; Pachter, R.; Naik, R. R. Nature of molecular interactions of peptides with gold, palladium, and Pd-Au bimetal surfaces in aqueous solution. *Journal of the American Chemical Society* **2009**, *131*, 9704–9714.
(247) Breault-Turcot, J.; Chaurand, P.; Masson, J.-F. Unravelling nonspecific adsorption of complex protein mixture on surfaces with SPR and MS. *Analytical chemistry* **2014**, *86*, 9612–9619.
(248) Masson, J.-F.; Battaglia, T. M.; Cramer, J.; Beaudoin, S.; Sierks, M.; Booksh, K. S. Reduction of nonspecific protein binding on surface plasmon resonance biosensors. *Analytical and bioanalytical chemistry* **2006**, *386*, 1951–1959.
(249) Till Schneider. Antibody Epitope Identification of Alpha-Glucosidase by Affinity Mass Spectrometry. *Master Thesis - Hochschule RheinMain Rüsselsheim & Steinbeis Center* **2020**.
(250) Wolfert, M. A.; Boons, G.-J. Adaptive immune activation: glycosylation does matter. *Nature chemical biology* **2013**, *9*, 776–784.
(251) Amin, M. N.; McLellan, J. S.; Huang, W.; Orwenyo, J.; Burton, D. R.; Koff, W. C.; Kwong, P. D.; Wang, L.-X. Synthetic glycopeptides reveal the glycan specificity of HIV-neutralizing antibodies. *Nature chemical biology* **2013**, *9*, 521–526.
(252) Brooks, C. L.; Schietinger, A.; Borisova, S. N.; Kufer, P.; Okon, M.; Hirama, T.; MacKenzie, C. R.; Wang, L.-X.; Schreiber, H.; Evans, S. V. Antibody recognition of a unique tumor-specific glycopeptide antigen. *Proceedings of the National Academy of Sciences of the United States of America* **2010**, *107*, 10056–10061.
(253) MacKenzie, C. R.; Hirama, T.; Deng, S. J.; Bundle, D. R.; Narang, S. A.; Young, N. M. Analysis by surface plasmon resonance of the influence of valence on the ligand binding affinity and kinetics of an anti-carbohydrate antibody. *Journal of Biological Chemistry* **1996**, *271*, 1527–1533.
(254) Tamsila Khan. Entwicklung einer quantitativen Bestimmungsmethode für das Survival Motor Neuron-Protein SMN. *Bachelor Thesis - Hochschule RheinMain Rüsselsheim & Steinbeis Center* **2022**.

(255) Wei, J.; Mu, Y.; Song, D.; Fang, X.; Liu, X.; Bu, L.; Zhang, H.; Zhang, G.; Ding, J.; Wang, W.*; et al.* A novel sandwich immunosensing method for measuring cardiac troponin I in sera. *Analytical biochemistry* **2003**, *321*, 209–216.
(256) Jing, J.; Liu, K.; Jiang, J.; Xu, T.; Wang, S.; Ma, J.; Zhang, Z.; Zhang, W.; Liu, T. Double-Antibody Sandwich Immunoassay and Plasmonic Coupling Synergistically Improved Long-Range SPR Biosensor with Low Detection Limit. *Nanomaterials (Basel, Switzerland)* **2021**, *11*.
(257) Kim, H.-M.; Kim, H.-J.; Park, J.-H.; Lee, S.-K. High-performance biosensor using a sandwich assay via antibody-conjugated gold nanoparticles and fiber-optic localized surface plasmon resonance. *Analytica chimica acta* **2022**, *1213*, 339960.
(258) Gnedenko, O. V.; Mezentsev, Y. V.; Molnar, A. A.; Lisitsa, A. V.; Ivanov, A. S.; Archakov, A. I. Highly sensitive detection of human cardiac myoglobin using a reverse sandwich immunoassay with a gold nanoparticle-enhanced surface plasmon resonance biosensor. *Analytica chimica acta* **2013**, *759*, 105–109.
(259) O'Rourke, M. B.; Djordjevic, S. P.; Padula, M. P. The quest for improved reproducibility in MALDI mass spectrometry. *Mass spectrometry reviews* **2018**, *37*, 217–228.
(260) Oberle, M.; Wohlwend, N.; Jonas, D.; Maurer, F. P.; Jost, G.; Tschudin-Sutter, S.; Vranckx, K.; Egli, A. The Technical and Biological Reproducibility of Matrix-Assisted Laser Desorption Ionization-Time of Flight Mass Spectrometry (MALDI-TOF MS) Based Typing: Employment of Bioinformatics in a Multicenter Study. *PloS one* **2016**, *11*, e0164260.
(261) Popp, R.; Li, H.; LeBlanc, A.; Mohammed, Y.; Aguilar-Mahecha, A.; Chambers, A. G.; Lan, C.; Poetz, O.; Basik, M.; Batist, G.*; et al.* Immuno-Matrix-Assisted Laser Desorption/Ionization Assays for Quantifying AKT1 and AKT2 in Breast and Colorectal Cancer Cell Lines and Tumors. *Analytical chemistry* **2017**, *89*, 10592–10600.
(262) Anderson, N. L.; Razavi, M.; Pearson, T. W.; Kruppa, G.; Paape, R.; Suckau, D. Precision of heavy-light peptide ratios measured by maldi-tof mass spectrometry. *Journal of proteome research* **2012**, *11*, 1868–1878.
(263) Sherrod, S. D.; Myers, M. V.; Li, M.; Myers, J. S.; Carpenter, K. L.; MacLean, B.; MacCoss, M. J.; Liebler, D. C.; Ham, A.-J. L. Label-free quantitation of protein modifications by pseudo selected reaction monitoring with internal reference peptides. *Journal of proteome research* **2012**, *11*, 3467–3479.
(264) ICH Q2(R2) Validation of analytical procedures - Scientific guideline | European Medicines Agency. https://www.ema.europa.eu/en/ich-q2r2-validation-analytical-procedures-scientific-guideline (accessed December 6, 2023).
(265) Randolph, T. W.; Mitchell, B. L.; McLerran, D. F.; Lampe, P. D.; Feng, Z. Quantifying peptide signal in MALDI-TOF mass spectrometry data. *Molecular & cellular proteomics : MCP* **2005**, *4*, 1990–1999.
(266) Jeon, J.; Yang, J.; Park, J.-M.; Han, N.-Y.; Lee, Y.-B.; Lee, H. Development of an automated high-throughput sample preparation protocol for LC-MS/MS analysis of glycated peptides. *Journal of chromatography. B, Analytical technologies in the biomedical and life sciences* **2018**, *1092*, 88–94.
(267) Yu, Y.; Suh, M.-J.; Sikorski, P.; Kwon, K.; Nelson, K. E.; Pieper, R. Urine sample preparation in 96-well filter plates for quantitative clinical proteomics. *Analytical chemistry* **2014**, *86*, 5470–5477.
(268) Li, H.; Popp, R.; Borchers, C. H. Affinity-mass spectrometric technologies for quantitative proteomics in biological fluids. *TrAC Trends in Analytical Chemistry* **2017**, *90*, 80–88.
(269) Paraschiv, G.; Vincke, C.; Czaplewska, P.; Manea, M.; Muyldermans, S.; Przybylski, M. Epitope structure and binding affinity of single chain llama anti-β-amyloid antibodies revealed by proteolytic excision affinity-mass spectrometry. *Journal of molecular recognition : JMR* **2013**, *26*, 1–9.

8 Appendix

8.1 Tables

Table 8.1.1: Peak table of the identified tryptic IL8 peptides via MALDI-tof MS analysis for the atmospheric pressure digestion (Figure 8.2.1; Figure 5.1.3).

S/N	Meas. MS	Slice	Misc.	Theo. MS	Sequence	Error
230.3	407.5	[21-23]	0	407.3	k.FIK.e	0.2
230.3	407.5	[65-67]	0	407.3	k.FLK.r	0.2
377.0	417.5	[4-6]	0	417.2	k.ELR.c	0.3
377.0	417.5	[24-26]	0	417.2	k.ELR.v	0.3
40.4	466.8	[7-10]	0	466.2	r.CQCI.k	0.6
96.5	474.6	[61-64]	0	474.3	r.VVEK.f	0.3
11.4	489.5	[68-71]	1	489.2	k.RAEN.s	0.3
34.2	545.6	[3-6]	1	545.3	a.KELR.c	0.1
34.2	545.6	[23-26]	1	545.3	i.KELR.v	0.1
310.2	547.6	[43-47]	0	547.3	k.LSDGR.e	0.3
181.7	563.7	[65-68]	1	563.4	k.FLKR.a	0.3
287.9	576.6	[68-72]	1	576.3	k.RAENS.	0.3
10.8	625.6	[16-20]	0	625.3	k.PFHPK.f	0.3
136.4	691.6	[64-68]	2	691.5	e.KFLKR.a	0.1
62.1	708.6	[7-11]	0	708.3	r.CQCIK.t [2xCarbamidomethyl]	0.3
26.8	805.8	[21-26]	1	805.5	k.FIKELR.v	0.3
325.2	831.7	[55-60]	0	831.4	k.ENWVQR.v	0.3
151.8	874.7	[48-54]	0	874.4	r.ELCLDPK.e [1xCarbamidomethyl]	0.3
6.8	1056.8	[53-60]	1	1056.6	d.PKENWVQR.v	0.2
5.1	1083.8	[27-36]	0	1083.5	r.VIESGPHCAN.t [1xCarbamidomethyl]	0.3
14.0	1089.8	[61-69]	3	1089.7	r.VVEKFLKRA.e	0.1
337.0	1104.9	[12-20]	0	1104.6	k.TYSKPFHPK.f	0.3
77.0	1158.8	[55-63]	1	1158.6	k.ENWVQRVVE.k	0.2
4.7	1402.9	[43-54]	1	1402.7	k.LSDGRELCLDPK.e [1xCarbamidomethyl]	0.2
4.8	1493.0	[12-23]	1	1492.8	k.TYSKPFHPKFIK.e	0.2
93.7	1687.0	[48-60]	1	1686.8	r.ELCLDPKENWVQR.v [1xCarbamidomethyl]	0.2
355.5	1767.1	[27-42]	0	1766.9	r.VIESGPHCANTEIIVK.l [1xCarbamidomethyl]	0.2
6.0	1740.9	[51-64]	2	1739.9	c.LDPKENWVQRVVEK.f	-1
6.5	1874.9	[43-58]	2	1873.9	k.LSDGRELCLDPKENWV.q	1

Table 8.1.2: Peak table of the identified chymotryptic IL8 peptides via MALDI-tof MS analysis for the atmospheric pressure digestion (Figure 5.1.4).

S/N	Meas. MS	Slice	Misc.	Theo. MS	Sequence	Error
83.7	405.8	[49-51]	1	405.2	e.LCL.d [1xCarbamidomethyl]	0.6
32.2	478.2	[14-17]	0	478.3	y.SKPF.h	0
27.4	522.3	[62-65]	0	522.3	v.VEKF.l	0
18.4	528.3	[18-21]	0	528.3	f.HPKF.i	0
17.8	557.3	[30-34]	0	557.2	e.SGPHC.a [1xCarbamidomethyl]	-0.1
17.1	623.3	[6-9]	0	623.2	l.RCQC.i [2xCarbamidomethyl]	-0.1
10.3	649.4	[21-25]	2	649.4	k.FIKEL.r	0
133.3	676.5	[44-49]	2	676.3	l.SDGREL.c	0.1
11.5	730.6	[66-71]	3	730.4	f.LKRAEN.s	-0.2
8.3	812.1	[8-13]	1	812.4	c.QCIKTY.s [1xCarbamidomethyl]	0.3
18.4	874.7	[49-55]	2	874.4	e.LCLDPKE.n [1xCarbamidomethyl]	0.3
152.1	894.7	[26-33]	1	894.5	l.RVIESGPH.c	-0.2
117.5	916.7	[38-45]	2	916.5	t.EIIVKLSD.g	-0.2
230.0	1004.9	[50-57]	2	1004.5	l.CLDPKENW.v	0.4
41.0	1011.9	[18-25]	2	1011.6	f.HPKFIKEL.r	0.3
19.5	1044.8	[29-38]	2	1044.4	i.ESGPHCANTE.i	-0.4
99.0	1048.9	[3-10]	2	1049.5	a.KELRCQCI.k [1xCarbamidomethyl]	0.6
48.8	1061.9	[50-57]	2	1061.5	l.CLDPKENW.v [1xCarbamidomethyl]	0.4
42.9	1070.9	[6-13]	0	1071.5	l.RCQCIKTY.s [1xCarbamidomethyl]	-0.7
22.8	1110.7	[25-34]	1	1110.6	e.LRVIESGPHC.a	-0.1
108.2	1128.9	[6-13]	0	1128.5	l.RCQCIKTY.s [2xCarbamidomethyl]	0.3
35.4	1183.0	[26-36]	2	1182.6	l.RVIESGPHCAN.t	-0.4
7.8	1207.9	[1-10]	2	1207.6	.SAKELRCQCI.k [1xCarbamidomethyl]	-0.3
25.0	2036.6	[26-43]	3	2036.1	l.RVIESGPHCANTEIIVKL.s [1xCarbamidomethyl]	0.5
15.5	2058.6	[1-17]	4	2059	.SAKELRCQCIKTYSKPF.h [1xCarbamidomethyl]	-0.5

Table 8.1.3: Peak table of the identified tryptic pCTSD peptides via MALDI-tof MS analysis for the atmospheric pressure digestion (Figure 8.2.2; Figure 8.2.12; Figure 8.2.14). Identified peaks in the mass range between 300 and 4000 m/z were analyzed for their monoisotopic mass.

S/N	Meas. MS	Slice	Misc.	Theo. MS	Sequence	Error
147.7	374.6	[331-334]	0	374.2	k.LGGK.g	0.4
43.1	388.6	[300-302]	0	388.3	e.LQK.a	-0.3
49.0	458.7	[9-12]	0	458.3	l.ALVR.i	-0.4
16.1	510.7	[119-122]	0	510.3	s.TYVK.n	-0.4
155.1	623.2	[18-22]	0	623.4	k.FTSIR.r	-0.2
13.1	684.2	[117-122]	0	684.4	k.SSTYVK.n	-0.1
452.7	820.4	[393-400]	0	820.4	r.VGFAEAAR.l	0
30.2	862.4	[11-17]	1	862.6	l.VRIPLHK.f	0.2
42.3	879.4	[166-173]	0	879.5	r.QVFGEATK.q	0
124.6	963.5	[382-388]	0	963.5	r.YYTVFDR.d	0
24.2	1028.6	[109-116]	1	1028.5	i.HHKYNSDK.s	-0.1
33.5	1042.7	[321-330]	0	1042.7	k.VSTLPAITLK.l	0
62.6	1045.6	[174-183]	0	1045.6	k.QPGITFIAAK.f	0
24.0	1087.6	[28-38]	0	1087.6	e.VGGSVEDLIAK.g	0
36.5	1104.6	[166-175]	1	1104.6	r.QVFGEATKQP.g	0
36.8	1175.7	[372-381]	0	1175.7	l.WILGDVFIGR.y	0
442.5	1239.7	[184-194]	0	1239.6	k.FDGILGMAYPR.i	0.1
21.3	1283.7	[90-100]	0	1283.7	s.SNLWVPSIHCK.l	0
28.9	1348.8	[101-111]	0	1348.7	k.LLDIACWIHHK.y	0.1
43.4	1405.9	[101-111]	0	1405.7	k.LLDIACWIHHK.y [1xCarbamidomethyl]	0.1
24.1	1462.8	[382-392]	1	1462.7	r.YYTVFDRDNNR.v	0.1
12.9	1535.9	[24-38]	0	1535.8	r.TMSEVGGSVEDLIAK.g	0.1
463.8	1602.0	[212-224]	0	1601.8	k.LVDQNIFSFYLSR.d	0.1
10.0	1788.0	[225-242]	0	1787.8	r.DPDAQPGGELMLGGTDSK.y	0.2
52.8	1898.2	[44-61]	0	1898	k.YSQAVPAVTEGPIPEVLK.n	0.2
72.0	1959.2	[195-211]	0	1959	r.ISVNNVLPVFDNLMQQK.l	0.2
55.8	1981.2	[303-320]	0	1989	k.AIGAVPLIQGEYMIPCEK.v [1xCarbamidomethyl]	0.2
6.1	2025.2	[316-334]	2	2025.2	m.IPCEKVSTLPAITLKLGGK.g [1xCarbamidomethyl]	0
23.9	2141.2	[100-116]	2	2141.1	c.KLLDIACWIHHKYNSDK.s [1xCarbamidomethyl]	-0.1
4.2	2260.3	[257-276]	0	2260.1	k.AYWQVHLDQVEVASGLTLCK.e	0.2
5.7	2266.4	[174-194]	1	2266.2	k.QPGITFIAAKFDGILGMAYPR.i	0.2
5.0	2277.3	[277-298]	0	2277.1	k.EGCEAIVDTGTSLMVGPVDEVR.e	0.2
13.1	2317.4	[257-276]	0	2317.2	k.AYWQVHLDQVEVASGLTLCK.e [1xCarbamidomethyl]	0.2
15.1	2334.3	[277-298]	0	2334.1	k.EGCEAIVDTGTSLMVGPVDEVR.e [1xCarbamidomethyl]	0.2
12.4	2339.3	[331-352]	3	2339.3	k.LGGKGYKLSPEDYTLKVSQAGK.t	0.1
6.3	2390.4	[347-370]	1	2390.2	k.VSQAGKTLCLSGFMGMDIPPPSGP.l	-0.2
5.6	2445.4	[256-276]	1	2445.3	r.KAYWQVHLDQVEVASGLTLCK.e [1xCarbamidomethyl]	0.2
6.6	3038.2	[13-40]	4	3038.6	r.IPLHKFTSIRRTMSEVGGSVEDLIAKGP.v	0.4
9.5	3089.9	[353-381]	0	3089.6	k.TLCLSGFMGMDIPPPSGPLWILGDVFIGR.y	0.3
6.8	3127.0	[166-194]	2	3126.6	r.QVFGEATKQPGITFIAAKFDGILGMAYPR.i	0.4
24.1	3146.9	[353-381]	0	3146.6	k.TLCLSGFMGMDIPPPSGPLWILGDVFIGR.y [1xCarbamidomethyl]	0.4
6.3	3169.0	[299-327]	2	3168.7	r.ELQKAIGAVPLIQGEYMIPCEKVSTLPAI.t [1xCarbamidomethyl]	-0.3
37.7	3299.0	[195-222]	1	3298.7	r.ISVNNVLPVFDNLMQQKLVDQNIFSFYL.s	-0.3
4.1	3343.2	[95-122]	3	3343.7	v.PSIHCKLLDIACWIHHKYNSDKSSTYVK.n [1xCarbamidomethyl]	0.5

Table 8.1.4: Peak table of the identified tryptic pCTSD peptides via MALDI-tof MS analysis for the atmospheric pressure digestion (Figure 8.2.2; Figure 8.2.12; Figure 8.2.14). Identified peaks in the mass range 4000 - 9000 m/z were analyzed for their average mass.

S/N	Meas. MS	Slice	Misc.	Theo. MS	Sequence	Error
4.4	4592.5	[353-392]	2	4593.3	k.TLCLSGFMGMDIPPPSGPLWILGDVFIGRYYTVFDRDNNR.v [1xCarbamidomethyl]	-0.7
3.4	4629.4	[139-183]	3	4629.2	g.YLSQDTVSVPCQSASSASALGGVKVERQVFGEATKQPGITFIAAK.f	-0.2
1.8	4650.3	[256-298]	2	4649.3	r.KAYWQVHLDQVEVASGLTLCKEGCEAIVDTGTSLMVGPVDEVR.e	1
15.6	5070.5	[166-211]	3	5069.9	r.QVFGEATKQPGITFIAAKFDGILGMAYPRISVNNVLPVFDNLMQQK.l	0.7
2.3	5113.5	[335-381]	3	5114.9	k.GYKLSPEDYTLKVSQAGKTLCLSGFMGMDIPPPSGPLWILGDVFIGR.y [1xCarbamidomethyl]	-1.5
1.7	5181.8	[123-173]	2	5182.6	k.NGTSFDIHYGSGSLSGYLSQDTVSVPCQSASSASALGGVKVERQVFGEATK.q	-0.8
12.2	5314.9	[195-242]	2	5314	r.ISVNNVLPVFDNLMQQKLVDQNIFSFYLSRDPDAQPGGELMLGGTDSK.y	1
5.5	5394.4	[353-400]	3	5395.1	k.TLCLSGFMGMDIPPPSGPLWILGDVFIGRYYTVFDRDNNRVGFAEAAR.l [1xCarbamidomethyl]	-0.8
3.8	5546.4	[207-255]	4	5547.2	n.LMQQKLVDQNIFSFYLSRDPDAQPGGELMLGGTDSKYYKGSLSYLNVTR.k	0.8
3.5	6154.4	[338-392]	4	6154	k.LSPEDYTLKVSQAGKTLCLSGFMGMDIPPPSGPLWILGDVFIGRYYTVFDRDNNR.v	0.4
2.2	6184.2	[277-334]	4	6185.2	k.EGCEAIVDTGTSLMVGPVDEVRELQKAIGAVPLIQGEYMIPCEKVSTLPAITLKLGGK.g [2xCarbamidomethyl]	-1
10.9	6363.3	[257-315]	3	6363.3	k.AYWQVHLDQVEVASGLTLCKEGCEAIVDTGTSLMVGPVDEVRELQKAIGAVPLIQGEYM.i	0
4.3	6386.4	[190-245]	4	6387.2	g.MAYPRISVNNVLPVFDNLMQQKLVDQNIFSFYLSRDPDAQPGGELMLGGTDSKYYK.g	0.8
5.4	7013.1	[338-400]	5	7013	k.LSPEDYTLKVSQAGKTLCLSGFMGMDIPPPSGPLWILGDVFIGRYYTVFDRDNNRVGFAEAAR.l [1xCarbamidomethyl]	0.1
5.9	7163.1	[243-307]	5	7162.1	k.YYKGSLSYLNVTRKAYWQVHLDQVEVASGLTLCKEGCEAIVDTGTSLMVGPVDEVRELQKAIGAV.p [1xCarbamidomethyl]	-1
3.5	8406.4	[226-302]	6	8405.4	d.PDAQPGGELMLGGTDSKYYKGSLSYLNVTRKAYWQVHLDQVEVASGLTLCKEGCEAIVDTGTSLMVGPVDEVRELQK.a [1xCarbamidomethyl]	-1
7.7	8423.5	[166-242]	5	8423.6	r.QVFGEATKQPGITFIAAKFDGILGMAYPRISVNNVLPVFDNLMQQKLVDQNIFSFYLSRDPDAQPGGELMLGGTDSK.y	-0.1
4.5	8442.8	[256-334]	6	8441.8	r.KAYWQVHLDQVEVASGLTLCKEGCEAIVDTGTSLMVGPVDEVRELQKAIGAVPLIQGEYMIPCEKVSTLPAITLKLGGK.g	1

Table 8.1.5: Peak table of the identified chymotryptic pCTSD peptides via MALDI-tof MS analysis for the atmospheric pressure digestion (Figure 8.2.15). Identified peaks in the mass range of 300 - 4000 m/z were analyzed for their monoisotopic mass.

S/N	Meas. MS	Slice	Misc.	Theo. MS	Sequence	Error
17.4	567.0	[244-248]	1	567.3	y.YKGSL.s	-0.3
25.7	595.1	[249-253]	1	595.3	l.SYLNV.t	0.2
16.2	597.5	[11-15]	0	597.4	l.VRIPL.h	0.1
12.4	600.0	[229-234]	0	600.3	a.QPGGEL.m	0.3
16.5	609.4	[310-314]	0	609.3	l.IQGEY.m	0.1
132.0	630.5	[396-401]	0	630.4	f.AEAARL.	0.1
16.0	659.2	[65-69]	1	659.3	m.DAQYY.g	0.1
13.1	671.5	[379-383]	1	671.4	f.IGRYY.t	0.1
22.0	674.5	[266-272]	0	674.4	q.VEVASGL.t	-0.1
33.8	781.7	[9-15]	1	781.5	l.ALVRIPL.h	0.2
9.4	825.7	[82-89]	2	825.4	f.TVVFDTGS.s	-0.3
6.4	864.7	[19-25]	1	864.5	f.TSIRRTM.s	-0.2
14.0	923.6	[253-259]	2	923.5	n.VTRKAYW.q	-0.1
7.7	953.8	[94-101]	0	953.5	w.VPSIHCKL.l [1xCarbamidomethyl]	0.3
10.8	962.8	[36-44]	0	962.6	l.IAKGPVSKY.s	0.3
206.9	1009.9	[11-18]	1	1009.6	l.VRIPLHKF.t	0.3
10.8	1092.8	[387-395]	0	1092.5	f.DRDNNRVGF.a	0.3
18.0	1118.9	[159-168]	0	1118.6	l.GGVKVERQVF.g	0.3
10.8	1190.0	[364-374]	2	1189.7	d.IPPPSGPLWIL.g	-0.3
41.8	1194.1	[9-18]	2	1193.8	l.ALVRIPLHKF.t	0.3
16.1	1244.0	[290-300]	0	1243.6	l.MVGPVDEVREL.q	0.3
12.7	1348.0	[36-48]	1	1347.8	l.IAKGPVSKYSQAV.p	-0.2
16.1	1440.1	[384-395]	1	1439.7	y.TVFDRDNNRVGF.a	0.4
16.6	1485.1	[316-329]	2	1484.8	m.IPCEKVSTLPAITL.k	-0.3
11.3	1509.2	[219-232]	3	1509.7	f.SFYLSRDPDAQPGG.e	0.5
12.0	1581.1	[259-272]	2	1580.8	y.WQVHLDQVEVASGL.t	0.3
81.8	1612.2	[64-78]	3	1611.7	y.MDAQYYGEIGIGTPP.q	-0.5
15.9	1625.1	[141-157]	1	1624.7	l.SQDTVSVPCQSASSASA.l	-0.4
44.6	1634.2	[113-127]	1	1634.8	y.NSDKSSTYVKNGTSF.d	-0.6
5.8	1673.2	[315-329]	0	1672.9	y.MIPCEKVSTLPAITL.k [1xCarbamidomethyl]	0.3
8.4	1704.2	[387-401]	1	1703.9	f.DRDNNRVGFAEAARL.	0.4
7.2	1739.2	[273-289]	1	1739.8	l.TLCKEGCEAIVDTGTSL.m	-0.6
20.7	1837.3	[19-35]	0	1836.9	f.TSIRRTMSEVGGSVEDL.i	0.4
25.0	1847.3	[116-131]	3	1846.9	d.KSSTYVKNGTSFDIHY.g	-0.4
10.2	1881.3	[70-87]	4	1880.9	y.GEIGIGTPPQCFTVVFDT.g	-0.4
10.0	2051.5	[384-401]	2	2051	y.TVFDRDNNRVGFAEAARL.	0.4
11.3	2121.6	[290-309]	1	2121.2	l.MVGPVDEVRELQKAIGAVPL.i	0.4
10.1	2307.5	[222-243]	3	2307.1	y.LSRDPDAQPGGELMLGGTDSKY.y	0.4
5.3	2514.5	[252-273]	5	2514.3	l.NVTRKAYWQVHLDQVEVASGLT.l	-0.2
10.7	2781.0	[19-44]	1	2780.5	f.TSIRRTMSEVGGSVEDLIAKGPVSKY.s	0.5
5.6	2868.8	[264-291]	6	2868.4	l.DQVEVASGLTLCKEGCEAIVDTGTSLMV.g	-0.4

Table 8.1.6: Peak table of the identified chymotryptic pCTSD peptides via MALDI-tof MS analysis for the atmospheric pressure digestion (Figure 8.2.15). Identified peaks in the mass range of 4000 - 9000 m/z were analyzed for their average mass.

S/N	Meas. MS	Slice	Misc.	Theo. MS	Sequence	Error
3.9	4549.5	[273-314]	4	4549.2	l.TLCKEGCEAIVDTGTSLMVGPVDEVRELQKAIGAVPLIQGEY.m [2xCarbamidomethyl]	0.3
4.4	4683.2	[355-395]	9	4682.4	l.CLSGFMGMDIPPPSGPLWILGDVFIGRYYTVFDRDNNRVGF.a [1xCarbamidomethyl]	0.8
3.7	4729.3	[360-401]	8	4729.4	f.MGMDIPPPSGPLWILGDVFIGRYYTVFDRDNNRVGFAEAARL.	-0.1
4.5	4834.6	[273-317]	8	4833.6	l.TLCKEGCEAIVDTGTSLMVGPVDEVRELQKAIGAVPLIQGEYMIP.c [1xCarbamidomethyl]	-1
2.7	5021.2	[357-401]	9	5020.7	l.SGFMGMDIPPPSGPLWILGDVFIGRYYTVFDRDNNRVGFAEAARL.	0.5
2.7	5294.8	[355-401]	10	5294	l.CLSGFMGMDIPPPSGPLWILGDVFIGRYYTVFDRDNNRVGFAEAARL. [1xCarbamidomethyl]	0.8
3.3	5390.9	[264-314]	5	5391.1	l.DQVEVASGLTLCKEGCEAIVDTGTSLMVGPVDEVRELQKAIGAVPLIQGEY.m [1xCarbamidomethyl]	-0.2
1.9	5447.0	[264-314]	5	5448.2	l.DQVEVASGLTLCKEGCEAIVDTGTSLMVGPVDEVRELQKAIGAVPLIQGEY.m [2xCarbamidomethyl]	-1.1
3.4	6421.9	[344-401]	12	6421.4	y.TLKVSQAGKTLCLSGFMGMDIPPPSGPLWILGDVFIGRYYTVFDRDNNRVGFAEAARL. [1xCarbamidomethyl]	0.5
11.6	6626.3	[159-218]	7	6625.7	l.GGVKVERQVFGEATKQPGITFIAAKFDGILGMAYPRISVNNVLPVFDNLMQQKLVDQNIF.s	0.6
3.6	6667.8	[82-140]	12	6666.4	f.TVVFDTGSSNLWVPSIHCKLLDIACWIHHKYNSDKSSTYVKNGTSFDIHYGSGSLSGYL.s [2xCarbamidomethyl]	1.5
2.7	7197.3	[337-401]	14	7197.2	y.KLSPEDYTLKVSQAGKTLCLSGFMGMDIPPPSGPLWILGDVFIGRYYTVFDRDNNRVGFAEAARL.	0.1
5.8	7255.7	[337-401]	14	7254.3	y.KLSPEDYTLKVSQAGKTLCLSGFMGMDIPPPSGPLWILGDVFIGRYYTVFDRDNNRVGFAEAARL. [1xCarbamidomethyl]	1.4
4.0	7959.0	[330-401]	16	7958.1	l.KLGGKGYKLSPEDYTLKVSQAGKTLCLSGFMGMDIPPPSGPLWILGDVFIGRYYTVFDRDNNRVGFAEAARL. [1xCarbamidomethyl]	0.9
6.8	8517.1	[310-386]	16	8518	l.IQGEYMIPCEKVSTLPAITLKLGGKGYKLSPEDYTLKVSQAGKTLCLSGFMGMDIPPPSGPLWILGDVFIGRYYTVF.d [2xCarbamidomethyl]	-0.8

Table 8.1.7: Summary of identified pCTSD peptide fragments from the control epitope extraction with the digestion of pCTSD and chymotrypsin. If a peptide was identified in both experiments, the S/N, meas. mass and error are reported for experiment E1.

S/N	Meas. MS	Slice	Theo. MS	Error	Exp. No.
16.1	781.0	[9-15]	781.5	-0.6	E2
188.4	1009.8	[11-18]	1009.6	0.1	E1/E3
4.1	1612.0	[64-78]	1611.7	-0.3	E1
6.3	847.5	[64-70]	847.3	-0.2	E2
7.8	997.8	[78-85]	997.5	-0.3	E3
3.4	1066.8	[94-102]	1066.6	0.2	E1
6.9	995.0	[103-110]	994.5	-0.5	E2
6.1	2163.0	[113-131]	2163	0	E2
12.6	927.5	[132-141]	927.4	-0.1	E2
8.6	981.9	[149-158]	981.4	-0.5	E3
5.0	768.0	[245-251]	767.4	0.6	E1/E3
11.0	881.4	[245-252]	881.5	0.1	E1
72.8	1639.9	[275-289]	1639.7	0.2	E2
12.0	1305.7	[344-355]	1305.7	0	E2
6.5	1448.9	[344-357]	1448.8	-0.1	E2
6.7	1439.8	[384-395]	1439.7	0.1	E2
9.6	1163.6	[387-396]	1163.6	0	E2

Table 8.1.8: Summary of identified chymotryptic peptides in the acidic elution from anti-pCTSD antibody experiments.

S/N	Meas. MS	Slice	Theo. MS	Error	Exp. No.
46.7	2387.8	[1-20]	2388.3	0.5	E2
137.5	1009.7	[11-18]	1009.6	0.1	E1
44.8	1010.0	[11-18]	1009.6	0.3	E2
300.3	1406.2	[34-46]	1405.8	-0.4	E1
15.6	667.3	[55-60]	667.4	0.1	E1
64.1	1611.8	[64-78]	1611.7	-0.1	E1
6.1	3194.3	[86-112]	3193.6	0.7	E1
7.5	1141.6	[108-116]	1141.6	0	E1
125.9	1590.3	[125-139]	1590.7	0.4	E1
34.7	1943.7	[137-155]	1943.9	0.2	E2
46.1	1520.3	[235-248]	1519.7	0.6	E2
16.4	1627.8	[251-263]	1627.9	-0.1	E1
17.1	674.4	[266-272]	674.4	0	E1
9.1	815.4	[322-329]	815.5	0.1	E1
14.5	665.4	[333-338]	665.4	0	E1
80.7	1736.5	[339-354]	1736.9	-0.4	E2
12.2	3038.0	[355-382]	3038.5	-0.5	E1
83.6	3038.6	[355-382]	3038.5	0.1	E2
28.8	656.3	[367-372]	656.3	0	E1
24.5	933.6	[393-401]	933.5	-0.1	E1
76.9	2434.1	[379-399]	2434.2	0.1	E2

Table 8.1.9: Summary of identified chymotryptic peptides in the acidic elution from anti-CTSD antibody experiments.

S/N	Meas. MS	Slice	Theo. MS	Error	Exp. No.
42.8	1193.7	[9-18]	1193.8	0	E1
399.5	1009.6	[11-18]	1009.6	0	E1
1199.1	1009.7	[11-18]	1009.6	0.1	E2
647.2	1405.7	[34-46]	1405.8	-0.1	E2
9.2	667.3	[55-60]	667.4	0.1	E1
75.5	1611.8	[64-78]	1611.7	-0.1	E2
9.0	2515.3	[86-107]	2515.2	0.1	E3
5.4	3193.9	[86-112]	3193.6	0.3	E2
21.3	1141.6	[108-116]	1141.6	0	E2
733.2	1589.8	[125-139]	1590.7	0.9	E2
20.2	1462.7	[175-188]	1462.8	0.1	E2
2.3	2613.8	[214-236]	2613.2	-0.6	E1
3.0	2704.2	[219-243]	2704.3	-0.1	E2
7.0	2867.5	[219-244]	2867.3	0.2	E2
4.1	2470.2	[221-243]	2470.2	0	E1
20.4	2470.0	[221-243]	2470.2	-0.1	E2
7.0	2470.1	[221-243]	2470.2	0	E3
4.6	2632.7	[221-244]	2633.2	-0.5	E2
3.5	2307.1	[222-243]	2307.1	0	E1
13.6	2307.0	[222-243]	2307.1	-0.1	E2
74.9	1627.8	[251-263]	1627.9	-0.1	E2
3.0	2638.2	[264-289]	2638.3	0	E3
6.8	674.3	[266-272]	674.4	0.1	E1
3.9	2486.1	[316-338]	2486.4	0.3	E1
5.8	2732.6	[344-370]	2732.4	-0.2	E3
6.2	3037.7	[355-382]	3038.5	-0.7	E2
8.2	656.3	[367-372]	656.3	0	E1
2.4	2433.6	[379-399]	2434.2	0.4	E1

Table 8.1.10: Summary of identified tryptic peptides in the acidic elution from CTSD-aptamer experiments.

S/N	Meas. MS	Slice	Theo. MS	Error	Exp. No.
8.1	1211.8	[13-22]	1211.7	0.1	E2
26.6	1589.9	[39-54]	1589.8	0.1	E2
22.6	1218.6	[44-55]	1218.6	0	E1
67.0	1773.6	[98-111]	1773.9	0.3	E1
43.7	1405.5	[101-111]	1405.7	-0.3	E1
38.2	1405.8	[101-111]	1405.7	0.1	E2
60.3	1601.5	[212-224]	1601.8	-0.3	E1
15.2	1563.9	[243-255]	1563.8	0.1	E2
24.8	923.1	[23-31]	923.4	0.3	E2
13.1	666.7	[257-261]	666.3	-0.4	E2
91.8	778.3	[270-276]	778.4	0.1	E1
314.1	1676.6	[307-320]	1676.8	0.2	E1
82.5	1677.0	[307-320]	1676.8	-0.2	E2

Table 8.1.11: Summary of chymotryptic peptides identified in the acidic elution from CTSD-Aptamer experiments.

S/N	Meas. MS	Slice	Theo. MS	Error	Exp. No.
9.3	1193.7	[9-18]	1193.8	-0.1	E2
188.4	1009.8	[11-18]	1009.6	0.1	E1
1082.9	1009.6	[11-18]	1009.6	0	E2
4.0	2249.2	[16-35]	2249.1	0	E1
90.4	632.3	[19-23]	632.4	0.1	E2
11.4	1405.9	[34-46]	1405.8	-0.1	E1
18.3	962.5	[36-44]	962.6	0	E2
50.8	1053.6	[51-60]	1053.6	0	E2
4.1	1612.0	[64-78]	1611.7	-0.3	E1
6.9	1611.7	[64-78]	1611.7	0	E2
13.0	2581.7	[70-93]	2582.2	-0.6	E1
3.4	1066.8	[94-102]	1066.6	0.2	E1
14.5	1590.0	[125-139]	1590.7	0.7	E1
11.0	881.4	[245-252]	881.5	-0.1	E1
26.7	744.4	[357-363]	744.3	-0.1	E2
15.0	1211.7	[360-371]	1211.6	0.1	E2
11.5	2434.6	[379-399]	2434.2	-0.4	E1

Table 8.1.12: Peak table of the identified tryptic GAA peptides via MALDI-tof MS analysis for the atmospheric pressure digestion (Figure 8.2.22; Figure 8.2.25). Identified peaks in the mass range of 300 - 4000 m/z were analyzed for their monoisotopic mass.

S/N	Meas. MS	Slice	Misc.	Theo. MS	Sequence	Error
20.4	426.2	[536-539]	0	426.2	a.GHGR.y	0
11.0	430.3	[517-520]	0	430.3	r.ALVK.a	0
11.2	440.9	[21-23]	0	441.1	r.FDC.a [1xCarbamidomethyl]	0.2
106.3	489.2	[781-785]	0	489.2	k.GGEAR.g	0
128.8	494.2	[350-353]	0	494.2	k.DGFR.d	0
152.9	498.3	[131-134]	0	498.3	h.VHSR.a	0
121.2	573.4	[629-633]	0	573.4	k.ALTLR.y	0
37.9	577.3	[523-527]	0	577.3	r.GTRPF.v	0
118.0	588.3	[156-160]	0	588.3	r.QLDGR.v	0
34.9	629.3	[830-834]	0	629.4	g.LQLQK.v	0.1
97.9	701.5	[628-633]	1	701.5	r.KALTLR.y	0.1
15.2	728.5	[116-121]	1	728.4	k.DPANRR.y	0.1
265.4	730.5	[94-99]	0	730.4	k.DILTLR.l	0.1
24.5	758.5	[110-115]	0	758.5	r.LHFTIK.d	0.1
38.3	771.5	[344-349]	0	771.4	r.DFTFNK.d	0.1
304.9	802.6	[207-212]	0	802.5	r.ITLWNR.d	0.1
322.1	832.5	[532-539]	0	832.4	r.STFAGHGR.y	0.1
57.4	852.5	[21-27]	0	852.4	r.FDCAPDK.a [1xCarbamidomethyl]	0.1
70.8	854.5	[38-45]	0	854.4	r.GCCYIPAK.q	0.1
31.1	908.6	[389-395]	1	908.5	p.YDEGLRR.g	0.1
173.9	927.6	[343-349]	1	927.5	r.RDFTFNK.d	0.1
78.7	938.6	[86-93]	0	938.5	r.TTPTFFPK.d	0.1
29.5	968.6	[38-45]	0	968.4	r.GCCYIPAK.q [2xCarbamidomethyl]	0.1
239.1	1032.7	[523-531]	0	1032.6	r.GTRPFVISR.s	0.1
34.7	1058.6	[620-628]	1	1058.5	s.EPAQQAMRK.a	0.1
16.4	1125.7	[875-883]	0	1125.5	m.GEQFLVSWC. [1xCarbamidomethyl]	0.2
200.8	1141.7	[307-316]	0	1141.6	r.WGYSSTAITR.q	0.1
12.2	1148.7	[28-37]	0	1148.5	k.AITQEQCEAR.g	0.1
4.0	1179.6	[359-368]	1	1179.6	m.VQELHQGGRR.y	0
120.6	1205.7	[28-37]	0	1205.6	k.AITQEQCEAR.g [1xCarbamidomethyl]	0.1
13.9	1230.8	[823-834]	0	1230.7	r.VTSEGAGLQLQK.v	0.1
50.3	1237.7	[100-109]	0	1237.6	r.LDVMMETENR.l	0.1
9.1	1246.7	[344-353]	1	1246.6	r.DFTFNKDGFR.d	0.1
56.5	1259.8	[521-531]	1	1259.7	k.ARGTRPFVISR.s	0.1
11.4	1270.9	[769-780]	0	1270.7	r.QQPMALAVALTK.g	0.1
69.5	1311.8	[110-120]	1	1311.7	r.LHFTIKDPANR.r	0.1
3.3	1355.8	[853-864]	0	1355.6	v.PVSNFTYSPDTK.v	-0.2
2.2	1368.9	[307-318]	1	1368.7	r.WGYSSTAITRQV.v	-0.2
14.4	1402.8	[343-353]	2	1402.7	r.RDFTFNKDGFR.d	0.1
171.8	1440.8	[8-20]	0	1440.7	r.AVPTQCDVPPNSR.f [1xCarbamidomethyl]	0.1
29.8	1467.9	[110-121]	2	1467.8	r.LHFTIKDPANRR.y	0.1
8.9	1478.8	[356-368]	1	1478.8	f.PAMVQELHQGGRR.y	0
208.5	1516.9	[592-603]	0	1516.7	r.WTQLGAFYPFMR.n	0.1

222.2	1584.9	[354-367]	0	1584.8	r.DFPAMVQELHQGGR.r	0.1
38.8	1806.1	[263-279]	0	1806	r.STGGILDVYIFLGPEPK.s	0.1
197.0	1874.1	[751-768]	0	1874	r.AGYIIPLQGPGLTTTESR.q	0.1
163.9	1894.0	[786-801]	0	1893.9	r.GELFWDDGESLEVLER.g	0.1
45.8	2060.1	[350-367]	1	2060	k.DGFRDFPAMVQELHQGGR.r	0.1
66.4	2222.1	[325-342]	0	2222	r.AHFPLDVQWNDLDYMDSR.r	0.1
6.3	2378.3	[325-343]	1	2378.1	r.AHFPLDVQWNDLDYMDSRR.d	0.2
19.9	2382.4	[665-685]	0	2382.2	k.DSSTWTVDHQLLWGEALLITP.v	0.2
4.1	2674.5	[46-68]	0	2674.2	k.QGLQGAQMGQPWCFFPPSYPSYK.l [1xCarbamidomethyl]	0.2
4.8	2679.5	[70-93]	1	2679.3	l.ENLSSSEMGYTATLTRTTPTFFPK.d	-0.2
22.0	2744.6	[604-627]	0	2744.3	r.NHNSLLSLPQEPYSFSEPAQQAMR.k	0.3
29.8	2793.7	[726-750]	0	2793.5	r.EPAIHSEGQWVTLPAPLDTINVHLR.a	0.2
7.7	2832.6	[369-394]	0	2832.3	r.YMMIVDPAISSSGPAGSYRPYDEGLR.r	0.3
5.1	2979.0	[665-691]	0	2978.6	k.DSSTWTVDHQLLWGEALLITPVLQAGK.a	0.4
6.3	3001.0	[292-316]	1	3000.4	y.PFMPPYWGLGFHLCRWGYSSTAITR.q [1xCarbamidomethyl]	-0.6
3.3	3090.8	[38-64]	1	3091.4	r.GCCYIPAKQGLQGAQMGQPWCFFPPSY.p [2xCarbamidomethyl]	-0.6
4.3	3113.0	[786-812]	1	3113.6	r.GELFWDDGESLEVLERGAYTQVIFLAR.n	-0.5
10.7	3229.0	[280-306]	0	3228.6	k.SVVQQYLDVVGYPFMPPYWGLGFHLCR.w [1xCarbamidomethyl]	0.4

Table 8.1.13: Peak table of the identified tryptic GAA peptides via MALDI-tof MS analysis for the atmospheric pressure digestion (Figure 8.2.22; Figure 8.2.25). Identified peaks in the mass range of 4000 - 9000 m/z were analyzed for their average mass.

S/N	Meas. MS	Slice	Misc.	Theo. MS	Sequence	Error
3.6	3253.2	[263-292]	1	3253.7	r.STGGILDVYIFLGPEPKSVVQQYLDVVGYP.f	0.5
4.8	3579.5	[634-664]	0	3578.9	r.YALLPHLYTLFHQAHVAGETVARPLFLEFPK.d	0.6
16.0	3624.5	[500-531]	4	3624	h.YNLHNLYGLTEAIASHRALVKARGTRPFVISR.s	-0.5
6.2	3523.2	[726-757]	1	3523	r.EPAIHSEGQWVTLPAPLDTINVHLRAGYIIPL.q	0.2
25.2	3580.7	[634-664]	0	3581.2	r.YALLPHLYTLFHQAHVAGETVARPLFLEFPK.d	-0.4
80.2	3625.7	[38-68]	1	3626.2	r.GCCYIPAKQGLQGAQMGQPWCFFPPSYPSYK.l [3xCarbamidomethyl]	-0.4
7.5	4163.4	[86-120]	4	4163.8	r.TTPTFFPKDILTLRLDVMMETENRLHFTIKDPANR.r	-0.4
3.3	4185.9	[8-45]	3	4184.7	r.AVPTQCDVPPNSRFDCAPDKAITQEQCEARGCCYIPAK.q [1xCarbamidomethyl]	1.2
5.0	4320.0	[86-121]	5	4320	r.TTPTFFPKDILTLRLDVMMETENRLHFTIKDPANRR.y	0
22.7	5269.3	[213-262]	0	5268.9	r.DLAPTPGANLYGSHPFYLALEDGGSAHGVFLLNSNAMDV VLQPSPALSWR.s	0.4
46.1	5618.7	[411-458]	0	5618.2	k.VWPGSTAFPDFTNPTALAWWEDMVAEFHDQVPFDGM WIDMNEPSNFIR.g	0.5
7.4	5663.9	[88-134]	6	5663.5	t.PTFFPKDILTLRLDVMMETENRLHFTIKDPANRRYEVPLE TPHVHSR.a	-0.4
1.7	6211.8	[459-516]	0	6210.7	r.GSEDGCPNNELENPPYVPGVVGGTLQAATICASSHQFLS THYNLHNLYGLTEAIASHR.a [1xCarbamidomethyl]	1.1
2.8	6313.3	[30-85]	3	6313.1	i.TQEQCEARGCCYIPAKQGLQGAQMGQPWCFFPPSYPS YKLENLSSSEMGYTATLTR.t [1xCarbamidomethyl]	-0.2
5.4	6490.8	[46-102]	4	6490.3	k.QGLQGAQMGQPWCFFPPSYPSYKLENLSSSEMGYTAT LTRTTPTFFPKDILTLRLDV.m [1xCarbamidomethyl]	-0.5
9.7	6543.5	[634-691]	1	6542.5	r.YALLPHLYTLFHQAHVAGETVARPLFLEFPKDSSTWTVD HQLLWGEALLITPVLQAGK.a	1
3.5	6566.1	[459-520]	1	6565.2	r.GSEDGCPNNELENPPYVPGVVGGTLQAATICASSHQFLS THYNLHNLYGLTEAIASHRALVK.a	0.8
2.2	7537.4	[523-591]	2	7538.4	r.GTRPFVISRSTFAGHGRYAGHWTGDVWSSWEQLASSV PEILQFNLLGVPLVGADVCGFLGNTSEELCVR.w [1xCarbamidomethyl]	-1
1.0	8121.9	[46-115]	5	8122.3	k.QGLQGAQMGQPWCFFPPSYPSYKLENLSSSEMGYTAT LTRTTPTFFPKDILTLRLDVMMETENRLHFTIK.d [1xCarbamidomethyl]	-0.3

Table 8.1.14: Peak table of the identified chymotryptic GAA peptides via MALDI-tof MS analysis for the atmospheric pressure digestion (Figure 8.2.26). Identified peaks in the mass range of 300 - 4000 m/z were analyzed for their monoisotopic mass.

S/N	Meas. MS	Slice	Misc.	Theo. MS	Sequence	Error
5.0	420.9	[869-872]	0	421.2	i.CVSL.l	0.3
6.6	435.1	[387-389]	0	435.2	y.RPY.d	-0.1
9.8	468.9	[192-195]	0	469.2	l.AEHL.s	-0.3
5.3	484.9	[569-573]	1	484.3	l.GVPLV.g	-0.6
13.0	544.2	[224-228]	0	544.3	y.GSHPF.y	0
11.7	575.2	[677-681]	1	575.3	l.WGEAL.l	-0.1
18.9	577.2	[545-549]	0	577.3	w.TGDVW.s	0
45.5	609.3	[56-59]	1	609.2	q.PWCF.f [1xCarbamidomethyl]	-0.1
22.5	639.3	[334-338]	1	639.3	w.NDLDY.m	0
15.9	660.3	[535-540]	0	660.3	f.AGHGRY.a	0
23.5	695.3	[193-198]	1	695.4	a.EHLSPL.m	0.1
12.2	811.4	[743-749]	0	811.4	l.DTINVHL.r	-0.1
46.5	824.4	[573-580]	0	824.4	l.VGADVCGF.l [1xCarbamidomethyl]	0.1
16.3	833.3	[610-616]	0	833.4	l.SLPQEPY.s	-0.1
14.0	837.3	[873-879]	2	837.4	l.LMGEQFL.v	-0.1
14.1	849.3	[387-393]	1	849.4	y.RPYDEGL.r	-0.1
8.0	931.4	[14-21]	0	931.5	c.DVPPNSRF.d	0.1
25.1	1080.5	[262-271]	1	1080.6	w.RSTGGILDVY.i	0
15.7	1116.4	[70-79]	1	1116.5	l.ENLSSSEMGY.t	0
20.7	1122.5	[163-172]	3	1122.6	l.LNTTVAPLFF.a	-0.1
16.2	1129.5	[775-786]	1	1129.6	l.AVALTKGGEARG.e	0.1
10.1	1185.4	[553-563]	1	1185.6	w.EQLASSVPEIL.q	-0.3
8.0	1201.3	[233-244]	2	1201.6	l.EDGGSAHGVFLL.n	-0.3
30.4	1205.5	[353-362]	0	1205.6	f.RDFPAMVQEL.h	-0.1
11.6	1219.5	[12-21]	0	1219.6	t.QCDVPPNSRF.d [1xCarbamidomethyl]	0.1
7.0	1323.4	[164-175]	3	1323.7	l.NTTVAPLFFADQ.f	0.3
7.3	1356.6	[659-669]	2	1356.6	l.FLEFPKDSSTW.t	-0.1
13.0	1462.6	[363-374]	1	1462.7	l.HQGGRRYMMIVD.p	0.1
7.5	1592.6	[686-700]	4	1592.9	p.VLQAGKAEVTGYFPL.g	0.3
9.3	1594.6	[150-163]	2	1594	f.GVIVRRQLDGRVLL.n	0.6
3.4	1600.6	[475-491]	1	1600.8	y.VPGVVGGTLQAATICAS.s [1xCarbamidomethyl]	0.2
4.2	1662.7	[158-172]	4	1662.9	l.DGRVLLNTTVAPLFF.a	-0.2
3.9	1696.7	[163-177]	5	1696.9	l.LNTTVAPLFFADQFL.q	-0.2
8.1	1738.8	[790-804]	3	1738.8	f.WDDGESLEVLERGAY.t	0
17.4	1893.6	[831-848]	2	1893.1	l.QLQKVTVLGVATAPQQVL.s	0.5
10.7	2060.8	[457-474]	1	2060.9	f.IRGSEDGCPNNELENPPY.v [1xCarbamidomethyl]	-0.1
7.1	2119.0	[408-427]	1	2119.1	l.IGKVWPGSTAFPDFTNPTAL.a	-0.1
29.9	2193.9	[715-735]	0	2194.1	l.GSLPPPPAAPREPAIHSEGQW.v	-0.2
6.1	2224.8	[109-126]	3	2225.2	n.RLHFTIKDPANRRYEVPL.e	0.4
7.2	2840.4	[457-483]	2	2840.4	f.IRGSEDGCPNNELENPPYVPGVVGGTL.q [1xCarbamidomethyl]	0

Table 8.1.15: Peak table of the identified chymotryptic GAA peptides via MALDI-tof MS analysis for the atmospheric pressure digestion (Figure 8.2.22; Figure 8.2.25). Identified peaks in the mass range of 4000 - 9000 m/z were analyzed for their average mass.

S/N	Meas. MS	Slice	Misc.	Theo. MS	Sequence	Error
7.9	3400.2	[475-506]	6	3400.8	y.VPGVVGGTLQAATICASSHQFLSTHYNLHNLY.g	-0.6
69.0	4620.4	[475-518]	8	4621.2	y.VPGVVGGTLQAATICASSHQFLSTHYNLHNLYGLTEAIA SHRAL.v	-0.8
6.2	8552.0	[707-788]	9	8552.7	l.QTVPVEALGSLPPPPAAPREPAIHSEGQWVTLPAPLDTI NVHLRAGYIIPLQGPGLTTTESRQQPMALAVALTKGGEA RGEL.f	-0.7

Table 8.1.16: Peak table of the identified chymotryptic GAA(-PNGF) peptides via MALDI-tof MS analysis for the atmospheric pressure digestion (Figure 8.2.27; Figure 8.2.24). Identified peaks in the mass range of 4000 - 9000 m/z were analyzed for their average mass.

S/N	Meas. MS	Slice	Misc.	Theo. MS	Sequence	Error
14.2	4164.0	[86-120]	4	4163.8	r.TTPTFFPKDILTLRLDVMMETENRLHFTIKDPANR.r	0.2
4.2	4185.3	[8-45]	3	4184.7	r.AVPTQCDVPPNSRFDCAPDKAITQEQCEARGCCYIPAK.q [1xCarbamidomethyl]	0.6
9.1	4319.9	[86-121]	5	4320	r.TTPTFFPKDILTLRLDVMMETENRLHFTIKDPANRR.y	0
3.5	4486.6	[38-76]	2	4487	r.GCCYIPAKQGLQGAQMGQPWCFFPPSYPSYKLENLSSS E.m [3xCarbamidomethyl; 1xDeamidation]	0.4
34.0	4533.1	[46-85]	1	4532	k.QGLQGAQMGQPWCFFPPSYPSYKLENLSSSEMGYTAT LTR.t [1xCarbamidomethyl; 1xDeamidation]	1
4.5	5112.5	[161-206]	0	5111.9	r.VLLNTTVAPLFFADQFLQLSTSLPSQYITGLAEHLSPLMLS TSWTR.i [1xDeamidation]	0.6
9.2	5269.6	[213-262]	0	5268.9	r.DLAPTPGANLYGSHPFYLALEDGGSAHGVFLLNSNAMDV VLQPSPALSWR.s	0.7
6.1	5312.9	[280-324]	2	5313	k.SVVQQYLDVVGYPFMPPYWGLGFHLCRWGYSSTAITRQ VVENMTR.a [1xCarbamidomethyl; 1xDeamidation]	-0.2
22.2	5618.2	[411-458]	0	5618.2	k.VWPGSTAFPDFTNPTALAWWEDMVAEFHDQVPFDGM WIDMNEPSNFIR.g	0
14.2	5768.7	[540-591]	0	5768.4	r.YAGHWTGDVWSSWEQLASSVPEILQFNLLGVPLVGADV CGFLGNTSEELCVR.w [2xCarbamidomethyl; 1xDeamidation]	0.3
1.7	5834.8	[321-368]	7	5834.4	e.NMTRAHFPLDVQWNDLDYMDSRRDFTFNKDGFRDFPA MVQELHQGGRR.y [1xDeamidation]	-0.4
23.7	6268.5	[459-516]	0	6267.8	r.GSEDGCPNNELENPPYVPGVVGGTLQAATICASSHQFLS THYNLHNLYGLTEAIASHR.a [2xCarbamidomethyl]	0.7
15.2	6401.9	[38-93]	3	6402.2	r.GCCYIPAKQGLQGAQMGQPWCFFPPSYPSYKLENLSSS EMGYTATLTRTTPTFFPK.d [3xCarbamidomethyl; 1xDeamidation]	-0.3
13.3	6542.5	[634-691]	1	6542.5	r.YALLPHLYTLFHQAHVAGETVARPLFLEFPKDSSTWTVD HQLLWGEALLITPVLQAGK.a	0
5.8	7099.9	[263-324]	3	7101.1	r.STGGILDVYIFLGPEPKSVVQQYLDVVGYPFMPPYWGLG FHLCRWGYSSTAITRQVVENMTR.a [1xCarbamidomethyl; 1xDeamidation]	-1.2
5.9	7223.9	[628-691]	3	7225.3	r.KALTLRYALLPHLYTLFHQAHVAGETVARPLFLEFPKDSS TWTVDHQLLWGEALLITPVLQAGK.a	-1.5
12.2	7921.9	[459-531]	3	7920.8	r.GSEDGCPNNELENPPYVPGVVGGTLQAATICASSHQFLS THYNLHNLYGLTEAIASHRALVKARGTRPFVISR.s [2xCarbamidomethyl]	1.2
4.6	8932.3	[802-883]	4	8931.2	r.GAYTQVIFLARNNTIVNELVRVTSEGAGLQLQKVTVLGVA TAPQQVLSNGVPVSNFTYSPDTKVLDICVSLLMGEQFLVS WC. [2xCarbamidomethyl; 2xDeamidation]	1.1

Table 8.1.17: Peak table of the identified chymotryptic GAA(-PNGF) peptides via MALDI-tof MS analysis for the atmospheric pressure digestion (Figure 8.2.27; Figure 8.2.24). Identified peaks in the mass range 400 - 4000 m/z were analyzed for their average mass.

S/N	Meas. MS	Slice	Misc.	Theo. MS	Sequence	Error
80.4	489.2	[781-785]	0	489.2	k.GGEAR.g	-0.1
31.9	494.2	[350-353]	0	494.2	k.DGFR.d	0
106.9	498.2	[131-134]	0	498.3	h.VHSR.a	0.1
78.6	573.4	[629-633]	0	573.4	k.ALTLR.y	0
72.6	588.3	[156-160]	0	588.3	r.QLDGR.v	0
6.5	629.3	[830-834]	0	629.4	g.LQLQK.v	0.1
89.2	701.5	[628-633]	1	701.5	r.KALTLR.y	0
155.4	730.5	[94-99]	0	730.4	k.DILTLR.l	0
6.4	758.5	[110-115]	0	758.5	r.LHFTIK.d	0
47.2	771.4	[344-349]	0	771.4	r.DFTFNK.d	0
136.0	802.5	[207-212]	0	802.5	r.ITLWNR.d	0
207.2	832.4	[532-539]	0	832.4	r.STFAGHGR.y	0
27.2	852.4	[21-27]	0	852.4	r.FDCAPDK.a [1xCarbamidomethyl]	0
47.6	854.4	[38-45]	0	854.4	r.GCCYIPAK.q	0
31.1	908.5	[389-395]	1	908.5	p.YDEGLRR.g	0
107.8	927.5	[343-349]	1	927.5	r.RDFTFNK.d	0
50.7	938.5	[86-93]	0	938.5	r.TTPTFFPK.d	0
29.4	968.5	[38-45]	0	968.4	r.GCCYIPAK.q [2xCarbamidomethyl]	0
105.3	977.5	[317-324]	0	977.5	r.QVVENMTR.a [1xDeamidation]	0
18.2	999.5	[153-160]	2	999.6	i.VRRQLDGR.v	0.1
146.7	1032.6	[523-531]	0	1032.6	r.GTRPFVISR.s	0
46.0	1058.5	[620-628]	1	1058.5	s.EPAQQAMRK.a	0
15.9	1125.6	[875-883]	0	1125.5	m.GEQFLVSWC. [1xCarbamidomethyl]	-0.1
193.0	1141.6	[307-316]	0	1141.6	r.WGYSSTAITR.q	0
14.6	1148.6	[28-37]	0	1148.5	k.AITQEQCEAR.g	0
19.9	1172.7	[813-822]	0	1172.6	r.NNTIVNELVR.v [1xDeamidation]	0
95.9	1205.6	[28-37]	0	1205.6	k.AITQEQCEAR.g [1xCarbamidomethyl]	0
17.2	1230.7	[823-834]	0	1230.7	r.VTSEGAGLQLQK.v	0
43.9	1237.6	[100-109]	0	1237.6	r.LDVMMETENR.l	0
186.4	1238.7	[802-812]	0	1238.7	r.GAYTQVIFLAR.n	0
17.2	1246.6	[344-353]	1	1246.6	r.DFTFNKDGFR.d	0
125.1	1259.7	[521-531]	1	1259.7	k.ARGTRPFVISR.s	0
29.9	1270.7	[769-780]	0	1270.7	r.QQPMALAVALTK.g	0
43.3	1311.7	[110-120]	1	1311.7	r.LHFTIKDPANR.r	0
4.8	1369.7	[307-318]	1	1368.7	r.WGYSSTAITRQV.v	-0.2
9.2	1402.7	[343-353]	2	1402.7	r.RDFTFNKDGFR.d	0
168.9	1440.7	[8-20]	0	1440.7	r.AVPTQCDVPPNSR.f [1xCarbamidomethyl]	0
19.3	1467.8	[110-121]	2	1467.8	r.LHFTIKDPANRR.y	0
6.1	1478.7	[356-368]	1	1478.8	f.PAMVQELHQGGRR.y	0
259.7	1516.7	[592-603]	0	1516.7	r.WTQLGAFYPFMR.n	0
43.2	1574.8	[396-410]	0	1574.8	r.GVFITNETGQPLIGK.v [1xDeamidation]	0
39.4	1584.7	[354-367]	0	1584.8	r.DFPAMVQELHQGGR.r	0
13.6	1649.9	[86-99]	1	1649.9	r.TTPTFFPKDILTLR.l	0

27.3	1730.9	[395-410]	1	1730.9	r.RGVFITNETGQPLIGK.v [1xDeamidation]	-0.1
11.1	1805.9	[263-279]	0	1806	r.STGGILDVYIFLGPEPK.s	-0.1
175.6	1873.9	[751-768]	0	1874	r.AGYIIPLQGPGLTTTESR.q	-0.1
144.7	1893.8	[786-801]	0	1893.9	r.GELFWDDGESLEVLER.g	-0.1
39.1	2038.8	[21-37]	1	2038.9	r.FDCAPDKAITQEQCEAR.g [2xCarbamidomethyl]	-0.1
54.1	2059.9	[350-367]	1	2060	k.DGFRDFPAMVQELHQGGR.r	-0.1
20.3	2216.0	[350-368]	2	2216.1	k.DGFRDFPAMVQELHQGGRR.y	-0.1
58.1	2221.9	[325-342]	0	2222	r.AHFPLDVQWNDLDYMDSR.r	-0.1
4.1	2238.0	[325-343]	1	2378.1	r.AHFPLDVQWNDLDYMDSRR.d	-0.1
26.8	2378.0	[325-343]	1	2378.1	r.AHFPLDVQWNDLDYMDSRR.d	0.1
19.9	2382.1	[665-685]	0	2382.2	k.DSSTWTVDHQLLWGEALLITP.v	0.1
7.5	2674.2	[46-68]	0	2674.2	k.QGLQGAQMGQPWCFFPPSYPSYK.l [1xCarbamidomethyl]	0
37.2	2744.3	[604-627]	0	2744.3	r.NHNSLLSLPQEPYSFSEPAQQAMR.k	-0.1
28.1	2793.4	[726-750]	0	2793.5	r.EPAIHSEGQWVTLPAPLDTINVHLR.a	0
6.1	2832.3	[369-394]	0	2832.3	r.YMMIVDPAISSSGPAGSYRPYDEGLR.r	0
2.9	3090.7	[835-864]	0	3090.6	k.VTVLGVATAPQQVLSNGVPVSNFTYSPDTK.v [1xDeamidation]	0.1
2.5	3144.6	[368-395]	2	3144.5	r.RYMMIVDPAISSSGPAGSYRPYDEGLRR.g	0.1
4.3	3229.0	[280-306]	0	3228.6	k.SVVQQYLDVVGYPFMPPYWGLGFHLCR.w [1xCarbamidomethyl]	0.4
1.9	3579.3	[634-664]	0	3578.9	r.YALLPHLYTLFHQAHVAGETVARPLFLEFPK.d	0.4
12.6	3624.3	[38-68]	1	3623.6	r.GCCYIPAKQGLQGAQMGQPWCFFPPSYPSYK.l [3xCarbamidomethyl]	0.7

Table 8.1.18: Summary of identified tryptic GAA peptides in the acidic elution from the control experiment.

S/N	Meas. MS	Slice	Theo. MS	Error	Exp. No.
5.75	3180.40	[110-136]	3180.70	0.3	E1/E2
4.20	1806.03	[263-279]	1806.00	0.1	E1/E2
3.67	3228.58	[280-306]	3228.60	0.0	E1/E2
3.22	1790.08	[350-364]	1789.83	-0.3	E1/E2
3.82	1845.95	[523-539]	1845.98	0.0	E1/E2
6.45	1824.00	[634-648]	1823.96	0.0	E1/E2
23.44	3578.99	[634-664]	3578.90	0.1	E1/E2
39.04	2607.26	[823-848]	2607.47	0.2	E1/E2

Table 8.1.19: Summary of identified tryptic GAA peptides in the acidic elution from mAB-43G7 extraction experiments.

S/N	Meas. MS	Slice	Theo. MS	Error	Exp. No.
1.22	5475.78	[21-68]	5476.2	-0.42	E1
1.44	5476.38	[21-68]	5476.2	0.18	E2
2.83	4253.06	[80-115]	4253.97	0.91	E1
14.53	3182.92	[110-136]	3182.58	-0.34	E1
7.99	3182.38	[110-136]	3182.58	0.28	E2
5.83	1805.79	[263-279]	1805.97	-0.15	E2
2.66	3228.58	[280-306]	3228.58	0	E1
6.58	3229.93	[280-306]	3230.74	-0.81	E2
3.65	5586.81	[304-349]	5586.21	-0.6	E2
14.75	976.43	[317-324]	976.49	-0.06	E1
27.97	976.43	[317-324]	976.49	-0.27	E2
4.91	1661.62	[350-363]	1661.77	0.15	E1
4.30	1661.61	[350-363]	1661.77	-0.16	E2
2.59	5618.53	[411-458]	5618.2	0.33	E1
1.70	5617.18	[411-458]	5618.2	-1.02	E2
6.93	1709.62	[445-458]	1709.78	0.16	E1
5.52	1709.59	[445-458]	1709.78	-0.19	E2
4.66	862.38	[452-458]	862.44	0.06	E2
3.03	1260.52	[521-531]	1259.73	0.66	E2
9.35	3581.68	[634-664]	3581.16	0.52	E1
10.27	3580.52	[634-664]	3581.16	-0.64	E2
3.81	1238.60	[802-812]	1238.69	-0.09	E1
10.63	1238.60	[802-812]	1238.69	-0.23	E2
9.94	2607.21	[823-848]	2607.47	-0.01	E2
9.28	2607.18	[823-848]	2607.47	-0.29	E1
2.72	6442.48	[823-883]	6441.4	1.08	E2

Table 8.1.20: Peak table of the identified tryptic rSMN1 peptides via MALDI-tof MS analysis for the atmospheric pressure digestion (Figure 8.2.34Figure 5.4.2). Identified peaks in the mass range 300 - 4000 m/z were analyzed for their monoisotopic mass.

S/N	Meas. MS	Slice	Misc.	Theo. MS	Sequence	Error
175.0	442.9	[108-111]	0	443.3	r.KPAK.k	-0.4
7.8	460.9	[126-128]	0	461.3	q.QWK.v	0.4
38.8	468.2	[87-90]	0	468.3	k.HALK.n	-0.1
28.0	490.2	[115-118]	1	490.3	k.SQKK.n	-0.1
14.7	496.1	[77-80]	0	496.2	k.AYDK.a	-0.1
11.7	502.2	[210-214]	0	502.3	r.SPGNK.s	-0.1
36.5	522.2	[151-154]	0	522.3	s.IDFK.r	0.1
12.0	550.3	[156-160]	0	550.3	r.ETCVV.v	0
62.8	579.3	[133-137]	0	579.3	k.CSAIW.s	0
86.8	599.3	[107-111]	1	599.4	k.RKPAK.k	-0.1
43.0	622.3	[81-86]	0	622.4	k.AVASFK.h	0
20.8	676.4	[27-32]	0	676.32	g.GQQMGR.g	-0.1
11.3	717.3	[324-329]	0	717.3	r.CSHSLN. [1xCarbamidomethyl]	0
83.1	727.5	[107-112]	2	727.5	k.RKPAKK.n	0
82.8	795.4	[133-139]	0	795.3	k.CSAIWSE.d	-0.1
22.5	801.4	[215-221]	0	801.4	k.SDNIKPK.s	0
28.9	866.5	[240-248]	0	866.5	r.LGPGKPGLK.f	0
16.0	877.4	[314-320]	1	877.5	m.GFRQNQK.e	0.1
18.0	910.5	[133-140]	0	910.4	k.CSAIWSED.g	-0.1
7.7	968.5	[155-162]	1	968.5	k.RETCVVVY.t	0.0
17.9	969.5	[107-114]	3	969.6	k.RKPAKKNK.s	-0.2
11.8	978.5	[129-137]	1	978.5	k.VGDKCSAIW.s	0.0
47.5	989.5	[9-17]	0	989.5	h.HHSSGLVPR.g	0.0
77.2	1015.6	[316-323]	1	1015.5	f.RQNQKEGR.c	-0.1
15.1	1035.5	[129-137]	1	1035.5	k.VGDKCSAIW.s [1xCarbamidomethyl]	0.0
41.0	1146.6	[119-128]	0	1146.6	k.NTAASLQQWK.v	0
20.5	1263.7	[7-17]	0	1263.7	h.HHHHSSGLVPR.g	-0.1
23.0	1274.7	[118-128]	1	1274.7	k.KNTAASLQQWK.v	0
7.9	1318.7	[47-57]	0	1318.7	g.VPEQEDSVLFR.r	0.0
3.8	1400.7	[6-17]	0	1400.7	h.HHHHHSSGLVPR.g	0
4.5	1404.7	[235-248]	2	1404.8	p.MPGPRLGPGKPGLK.f	0.1
6.7	1431.7	[120-132]	1	1431.8	n.TAASLQQWKVGDK.c	0.1
8.5	1433.7	[90-102]	1	1433.7	l.KNGDICETSGKPK.t [1xCarbamidomethyl]	0
5.5	1478.6	[19-32]	0	1478.6	g.SHMASMTGGQQMGR.g	0
9.3	1517.7	[156-168]	0	1517.7	r.ETCVVVYTGYGNR.e [1xCarbamidomethyl]	0
60.5	1535.7	[18-32]	0	1535.7	r.GSHMASMTGGQQMGR.g	0
22.0	1557.7	[317-329]	2	1557.7	r.QNQKEGRCSHSLN. [1xCarbamidomethyl]	-0.1
8.2	1573.7	[81-95]	1	1573.8	k.AVASFKHALKNGDIC.e	0.1
19.2	1648.8	[119-133]	2	1648.8	k.NTAASLQQWKVGDKC.s	0.0
5.3	1726.1	[210-225]	2	1725.9	r.SPGNKSDNIKPKSAPW.n	-0.2
21.2	1768.9	[2-17]	0	1768.9	m.GSSHHHHHHSSGLVPR.g	-0.1
4.0	1777.9	[40-57]	0	1777.8	s.SGGSGGGVPEQEDSVLFR.r	-0.1
2.1	1864.9	[39-57]	0	1864.9	m.SSGGSGGGVPEQEDSVLFR.r	0

3.4	1921.0	[118-134]	3	1921	k.KNTAASLQQWKVGDKCS.a [1xCarbamidomethyl]	0
4.7	1937.0	[59-76]	0	1936.9	r.GTGQSDDSDIWDDTALIK.a	0.1
55.1	1945.1	[222-239]	0	1945	k.SAPWNSFLPPPPPMPGPR.l	0.1
42.5	2093.1	[58-76]	1	2093	r.RGTGQSDDSDIWDDTALIK.a	0.1
5.4	2410.3	[304-323]	2	2410.1	y.MSGYHTGYYMGFRQNQKEGR.c	-0.2
52.1	2487.3	[33-57]	0	2487.1	r.GSEFAMSSGGSGGGVPEQEDSVLFR.r	0.2
3.9	2503.4	[81-104]	4	2503.3	k.AVASFKHALKNGDICETSGKPKTT.p	-0.1
16.0	2509.3	[55-76]	2	2509.2	v.LFRRGTGQSDDSDIWDDTALIK.a	-0.1

Table 8.1.21: Peak table of the identified tryptic rSMN1 peptides via MALDI-tof MS analysis for the atmospheric pressure digestion (Figure 8.2.34; Figure 5.4.2). Identified peaks in the mass range 4000 - 9000 m/z were analyzed for their average mass.

S/N	Meas. MS	Slice	Misc.	Theo. MS	Sequence	Error
3.6	4215.7	[77-114]	8	4215.9	k.AYDKAVASFKHALKNGDICETSGKPKTTPKRKPAKKNK.s [1xCarbamidomethyl]	-0.2
3.9	4609.5	[169-209]	0	4608.7	r.EEQNLSDLLSPICEVANNIEQNAQENENESQVSTDESENSR.s	0.8
15.8	4666.4	[169-209]	0	4665.7	r.EEQNLSDLLSPICEVANNIEQNAQENENESQVSTDESENSR.s [1xCarbamidomethyl]	0.6
10.9	4818.6	[112-154]	6	4818.4	k.KNKSQKKNTAASLQQWKVGDKCSAIWSEDGCIYPATIASIDFK.r [1xCarbamidomethyl]	0.1
3.4	4896.8	[35-80]	3	4897.2	s.EFAMSSGGSGGGVPEQEDSVLFRRGTGQSDDSDIWDDTALIKAYDK.a	0.4
3.5	5299.9	[108-154]	7	5300	r.KPAKKNKSQKKNTAASLQQWKVGDKCSAIWSEDGCIYPATIASIDFK.r [2xCarbamidomethyl]	-0.1
3.0	6048.3	[58-112]	9	6048.7	r.RGTGQSDDSDIWDDTALIKAYDKAVASFKHALKNGDICETSGKPKTTPKRKPAKK.n [1xCarbamidomethyl]	-0.5
3.1	6139.6	[87-141]	11	6139.9	k.HALKNGDICETSGKPKTTPKRKPAKKNKSQKKNTAASLQQWKVGDKCSAIWSEDG.c [2xCarbamidomethyl]	0.3
7.1	6164.1	[156-209]	1	6165.4	r.ETCVVVYTGYGNREEQNLSDLLSPICEVANNIEQNAQENENESQVSTDESENSR.s [2xCarbamidomethyl]	-1.3
2.1	6291.7	[58-114]	10	6291	r.RGTGQSDDSDIWDDTALIKAYDKAVASFKHALKNGDICETSGKPKTTPKRKPAKKNK.s [1xCarbamidomethyl]	0.7
2.6	7316.9	[156-221]	3	7317.7	r.ETCVVVYTGYGNREEQNLSDLLSPICEVANNIEQNAQENENESQVSTDESENSRSPGNKSDNIKPK.s	-0.8
5.8	7432.7	[156-221]	3	7431.8	r.ETCVVVYTGYGNREEQNLSDLLSPICEVANNIEQNAQENENESQVSTDESENSRSPGNKSDNIKPK.s [2xCarbamidomethyl]	0.9
1.7	7582.1	[88-155]	12	7582.7	h.ALKNGDICETSGKPKTTPKRKPAKKNKSQKKNTAASLQQWKVGDKCSAIWSEDGCIYPATIASIDFKR.e [2xCarbamidomethyl]	0.6
2.8	8273.2	[240-316]	1	8274.6	r.LGPGKPGLKFNGPPPPPPPPPPHLLSCWLPPFPSGPPIIPPPPPICPDSLDDADALGSMLISWYMSGYHTGYYMGFR.q [1xCarbamidomethyl]	-1.4

Table 8.1.22: Peak table of the identified tryptic IL8 peptides via MALDI-tof MS analysis for the PCT-digestion (Figure 5.1.6; Figure 5.1.5;).

S/N	Meas. MS	Slice	Misc.	Theo. MS	Sequence	Error
33.0	402.0	[58-60]	0	402.2	w.VQR.v	0.2
149.5	407.1	[21-23]	0	407.3	k.FIK.e	-0.2
149.5	407.1	[65-67]	0	407.3	k.FLK.r	-0.2
373.5	417.1	[4-6]	0	417.2	k.ELR.c	-0.2
373.5	417.1	[24-26]	0	417.2	k.ELR.v	-0.2
72.2	474.1	[61-64]	0	474.3	r.VVEK.f	-0.2
7.4	489.1	[68-71]	1	489.2	k.RAEN.s	0.1
26.7	545.2	[3-6]	1	545.3	a.KELR.c	0.1
26.7	545.2	[23-26]	1	545.3	i.KELR.v	0.1
215.0	547.2	[43-47]	0	547.3	k.LSDGR.e	-0.1
142.9	563.3	[65-68]	1	563.4	k.FLKR.a	-0.1
195.2	576.2	[68-72]	1	576.3	k.RAENS.	-0.1
7.4	625.3	[16-20]	0	625.3	k.PFHPK.f	0
16.5	691.3	[64-68]	2	691.5	e.KFLKR.a	0.2
6.6	702.4	[37-42]	0	702.4	n.TEIIVK.l	0
6.6	702.4	[56-60]	0	702.4	e.NWVQR.v	0
20.3	708.3	[7-11]	0	708.3	r.CQCIK.t [2xCarbamidomethyl]	0
2.2	805.5	[21-26]	1	805.5	k.FIKELR.v	0
129.3	831.6	[55-60]	0	831.4	k.ENWVQR.v	0.1
14.9	857.5	[58-64]	1	857.5	w.VQRVVEK.f	0
24.9	874.5	[48-54]	0	874.4	r.ELCLDPK.e [1xCarbamidomethyl]	0.1
23.1	912.5	[27-35]	0	912.4	r.VIESGPHCA.n	-0.1
5.9	1056.6	[53-60]	1	1056.6	d.PKENWVQR.v	0
104.7	1104.7	[12-20]	0	1104.6	k.TYSKPFHPK.f	0.1
3.3	1158.6	[55-63]	1	1158.6	k.ENWVQRVVE.k	0
5.0	1218.7	[61-70]	3	1218.7	r.VVEKFLKRAE.n	0
2.6	1402.8	[43-54]	1	1402.7	k.LSDGRELCLDPK.e [1xCarbamidomethyl]	0.1
10.5	1686.9	[48-60]	1	1686.8	r.ELCLDPKENWVQR.v [1xCarbamidomethyl]	0
209.6	1767.0	[27-42]	0	1766.9	r.VIESGPHCANTEIIVK.l [1xCarbamidomethyl]	0.1

Table 8.1.23: Summary of acidic elution from the mAB-7B10 column measured by MALDI-tof MS. All identified peaks are highlighted in the related mass spectrum (Figure 5.4.3).

S/N	Meas. MS	Slice	Theo. MS	Error
28.3	1375.5	[46-57]	1375.7	0.2
28.7	1432.5	[45-57]	1432.7	0.2
27.5	1576.6	[43-57]	1576.8	0.2
21.8	1633.6	[42-57]	1633.8	0.2
26.5	1711.6	[3-17]	1711.8	0.2
4.3	1768.6	[2-17]	1768.8	0.2
14.1	1777.6	[40-57]	1777.8	0.2
80.7	1864.6	[39-57]	1864.9	0.3
6.0	2066.7	[37-57]	2066.9	0.2
106.0	2486.9	[33-57]	2487.1	-0.2
70.8	2502.9	[33-57] Ox.	2503.1	-0.2

8.2 Figures

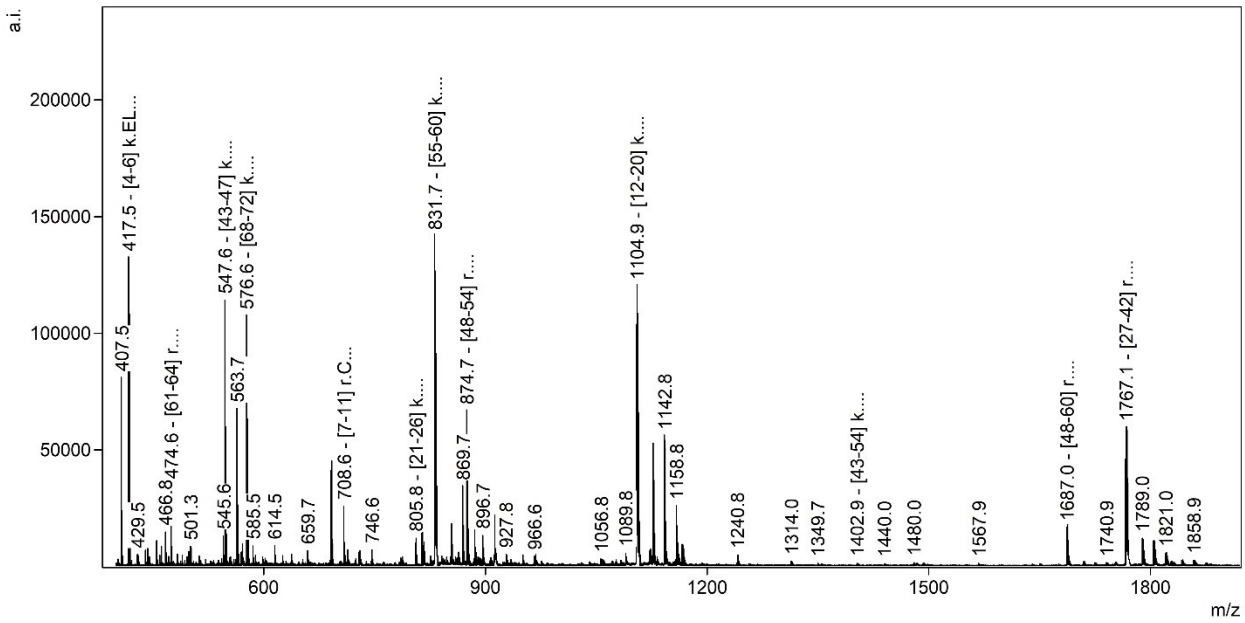

Figure 8.2.1: MALDI-tof mass spectrum of the tryptic digested IL8 under atmospheric pressure. Highlighted/annotated peaks correlate to fully tryptic peptide fragments. (Method: RP; Matrix: DHB).

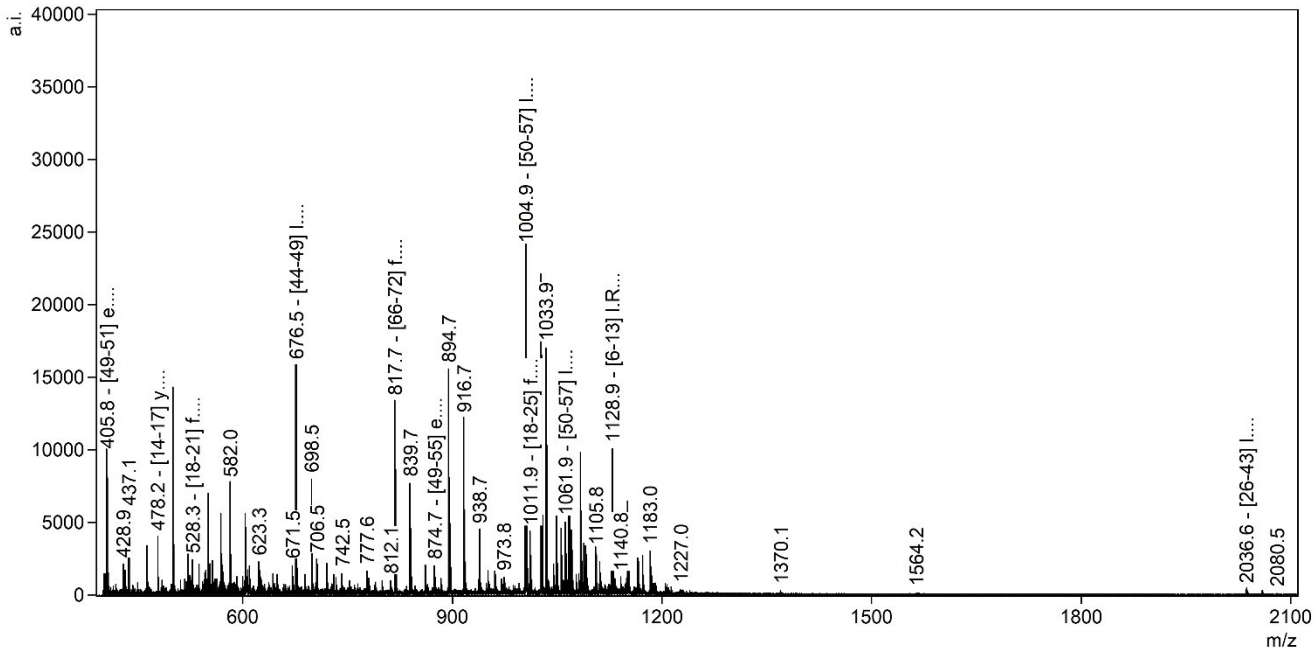

Figure 8.2.2: MALDI-tof mass spectrum of the chymotryptic digested IL8 under atmospheric pressure. Highlighted/annotated peaks correlate to fully tryptic peptide fragments. (Method: RP; Matrix: DHB).

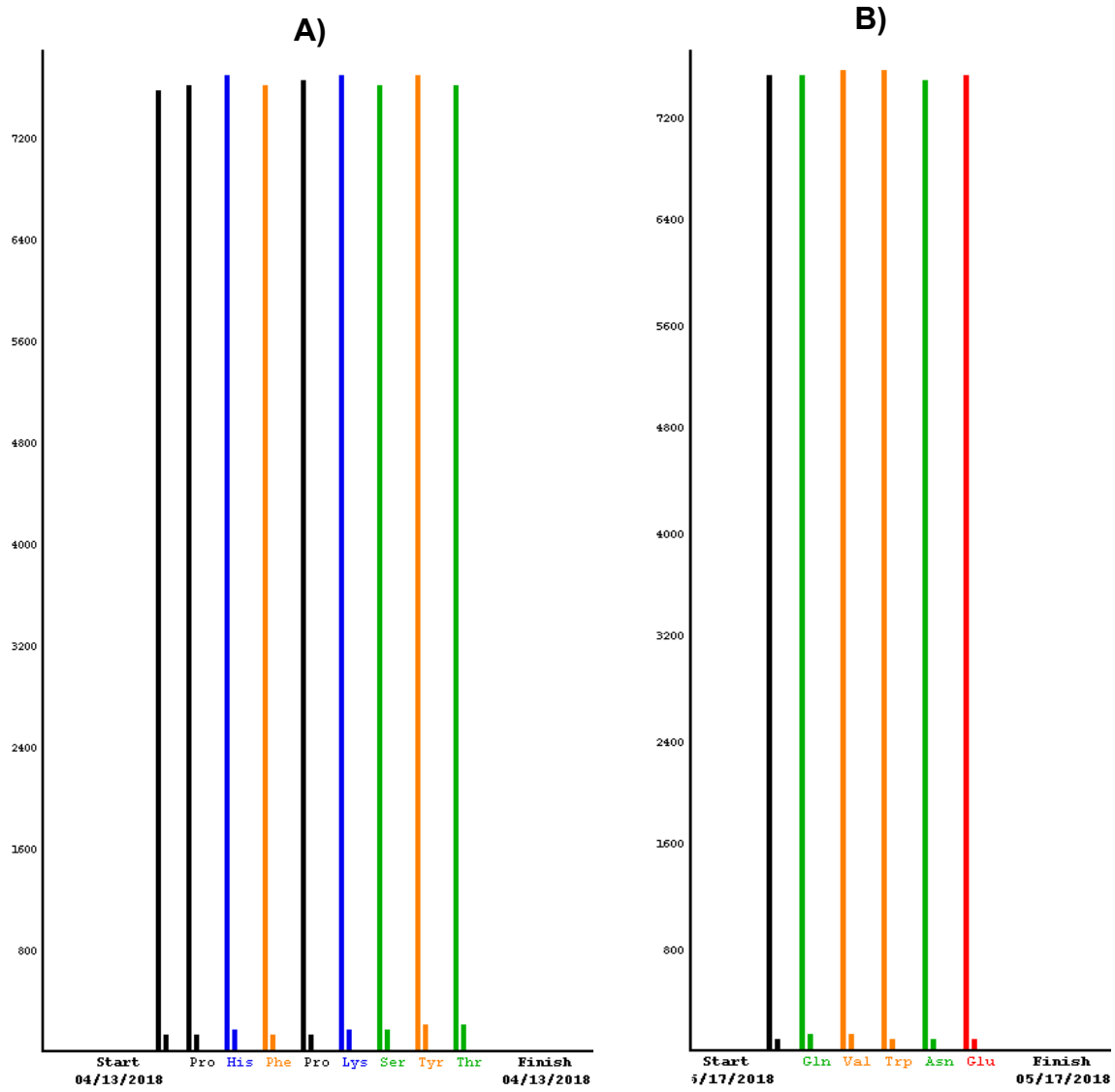

Figure 8.2.3: Deprotection monitoring with the UV detector of the ABI 433A peptide synthesizer measuring absorption at 301 nm after each deprotection step. A) Monitoring of the IL8[12-20] peptide synthesis and B) monitoring of the IL8[55-60] peptide synthesis.

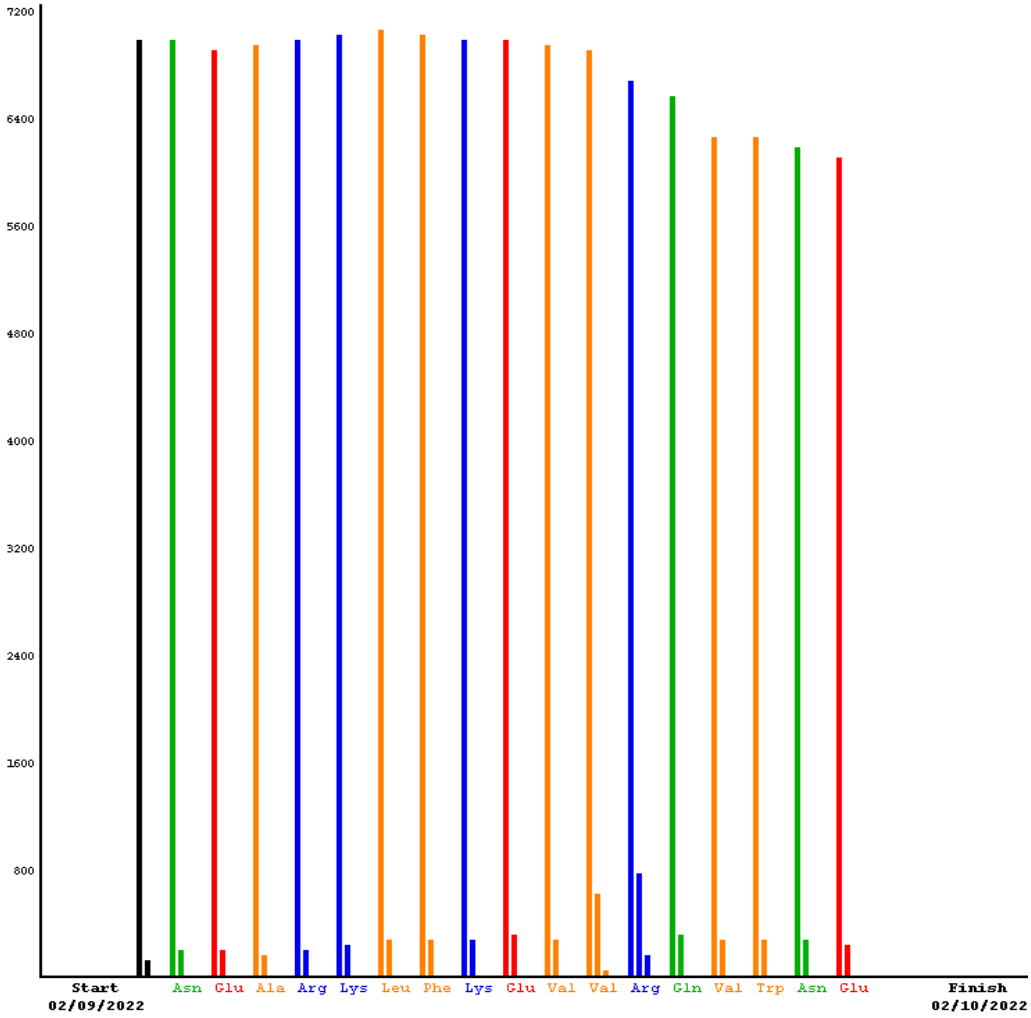

Figure 8.2.4: Deprotection monitoring of the IL8[55-72] peptide synthesis on the ABI 433 A peptide synthesizer. Absorption was measured at 301 nm after each deprotection step to estimate Fmoc-cleavage.

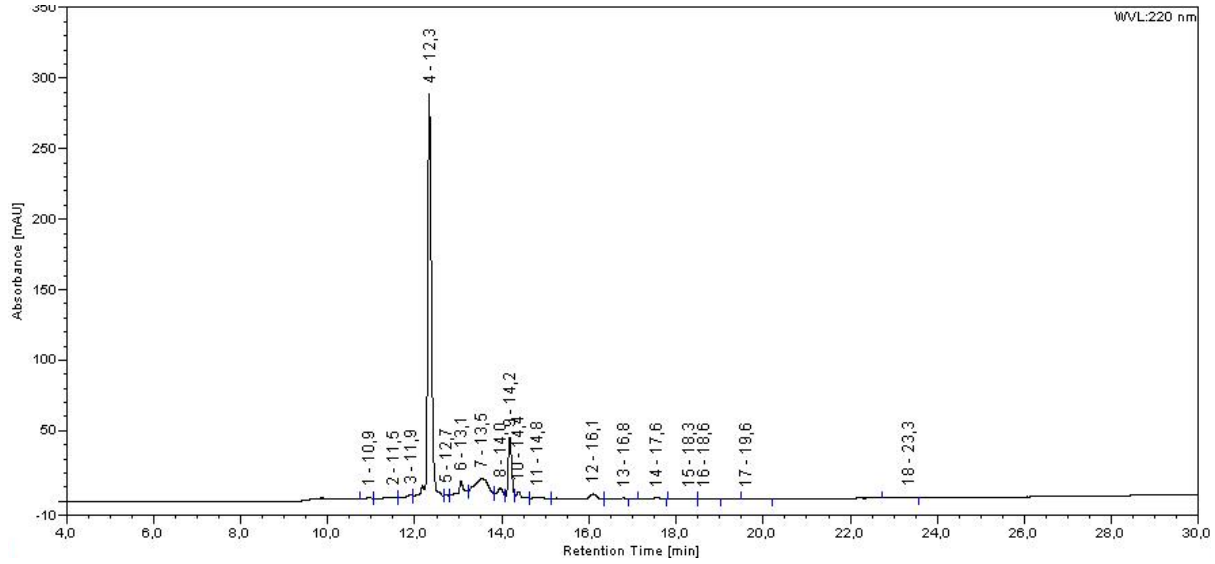

Figure 8.2.5: Chromatogram for the crude peptide IL8[12-20] eluted with a gradient of 90% to 70% solvent A from 5 - 25 minutes. Peak-4, with a retention time of 12.3 minutes, corresponds to the peptide IL[12-20] with a relative area of 72.5 %. HPLC was performed on the 2795 Alliance HT HPLC instrument (Waters, Massachusetts, USA) with the RP-C18 column from Interchim (Interchrom-KR5C18-25QK).

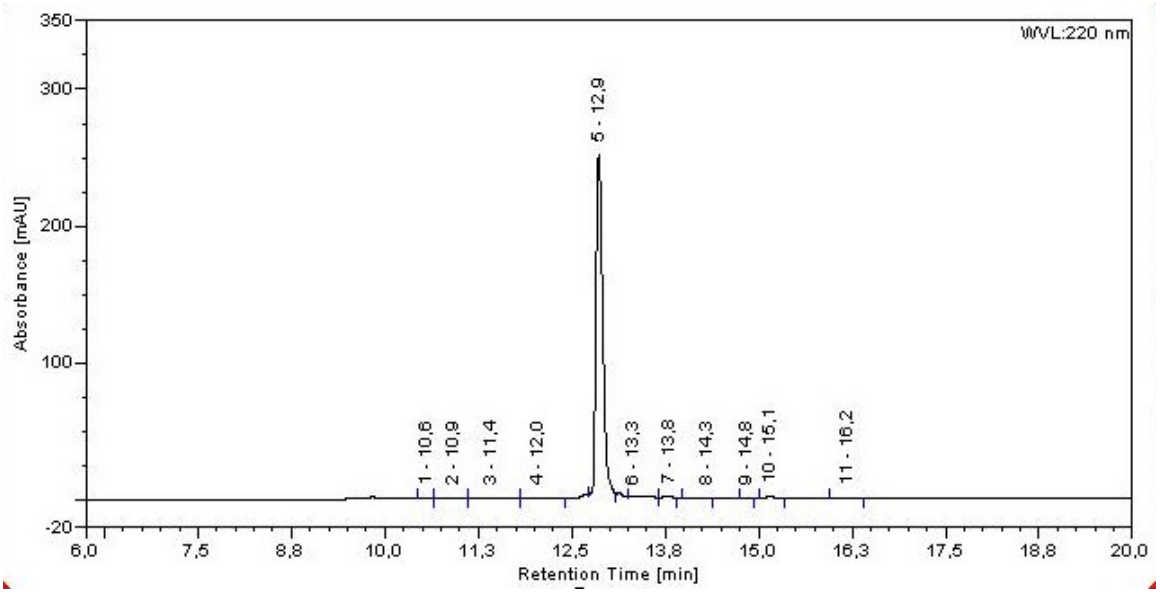

Figure 8.2.6: Chromatogram for the purified peptide IL8[12-20] eluted with a gradient of 90% to 70% solvent A from 5 - 25 minutes. Peak-5, with a retention time of 12.9 minutes, corresponds to the peptide IL[12-20] with a relative area of 97.2 %. HPLC was performed on the 2795 Alliance HT HPLC instrument (Waters, Massachusetts, USA) with the RP-C18 column from Interchim (Interchrom-KR5C18-25QK).

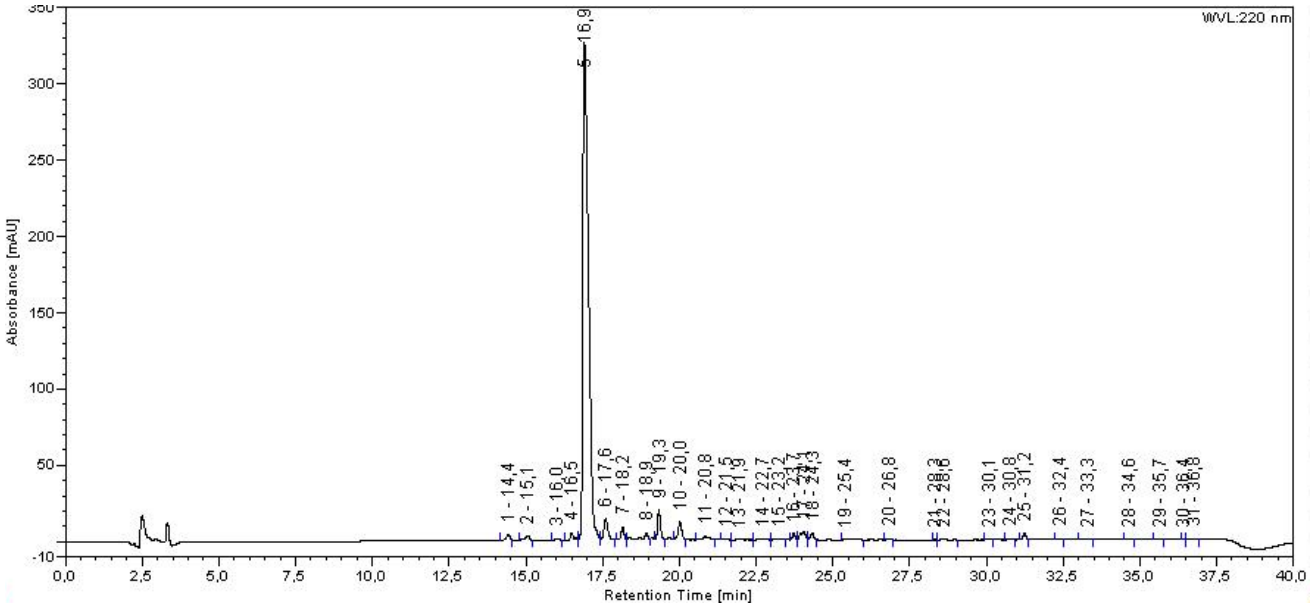

Figure 8.2.7: Chromatogram for the crude peptide IL8[55-60] eluted with a gradient of 90% to 80% solvent A from 5 - 35 minutes. Peak-5, with a retention time of 16.9 minutes, corresponds to the peptide IL[55-60] with a relative area of 84.5 %. HPLC was performed on the 2795 Alliance HT HPLC instrument (Waters, Massachusetts, USA) with the RP-C18 column from Interchim (Interchrom-KR5C18-25QK).

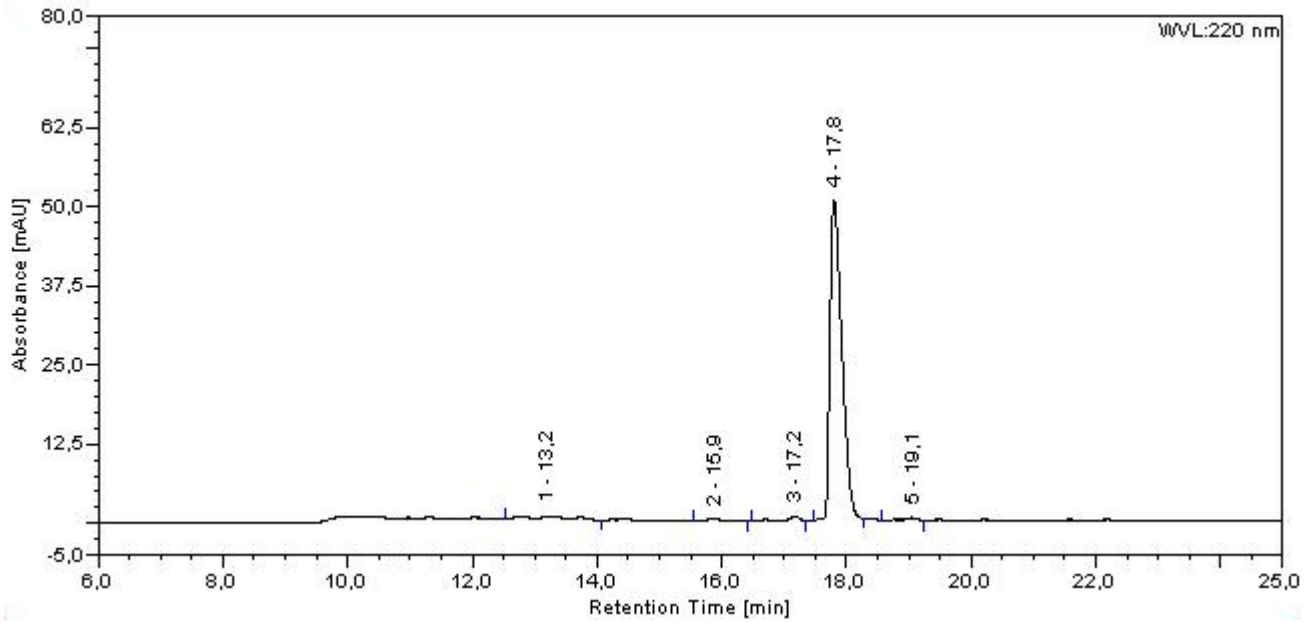

Figure 8.2.8: Chromatogram for the purified peptide IL8[55-60] eluted with a gradient of 90% to 80% solvent A from 5 - 30 minutes. Peak-4, with a retention time of 17.8 minutes, corresponds to the peptide IL[55-60] with a relative area of 94.1 %. HPLC was performed on the 2795 Alliance HT HPLC instrument (Waters, Massachusetts, USA) with the RP-C18 column from Interchim (Interchrom-KR5C18-25QK).

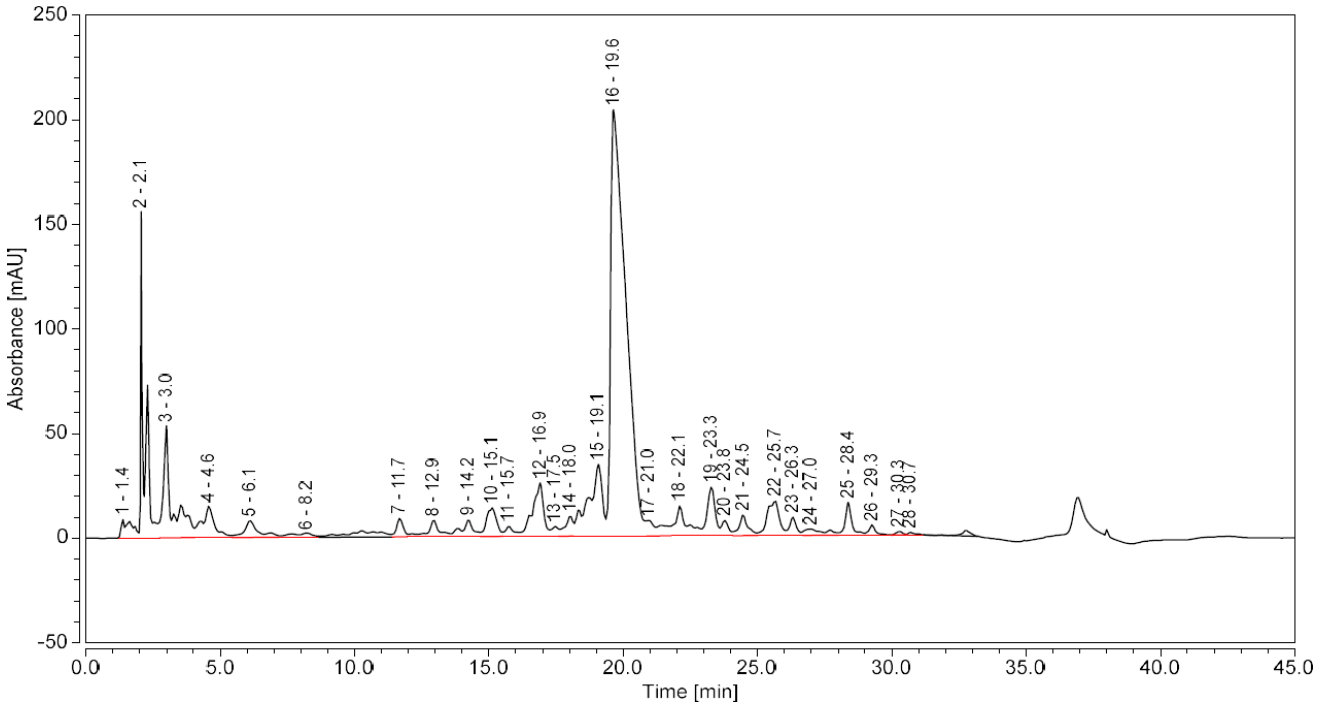

Figure 8.2.9: Chromatogram for the crude peptide IL8[55-72] eluted with a gradient of 75 % to 55% solvent A from 5 - 30 minutes. Peak-16, with a retention time of 19.6 minutes, corresponds to the peptide IL8[55-72] with a relative area of 44.9 %. HPLC was performed on the Vanquish HPLC System (ThermoFisher Scientific, Langerwehe, GER) with the RP-C18 column from Macherey-Nagel (Nucelosil 100-5 C18 Nautilus).

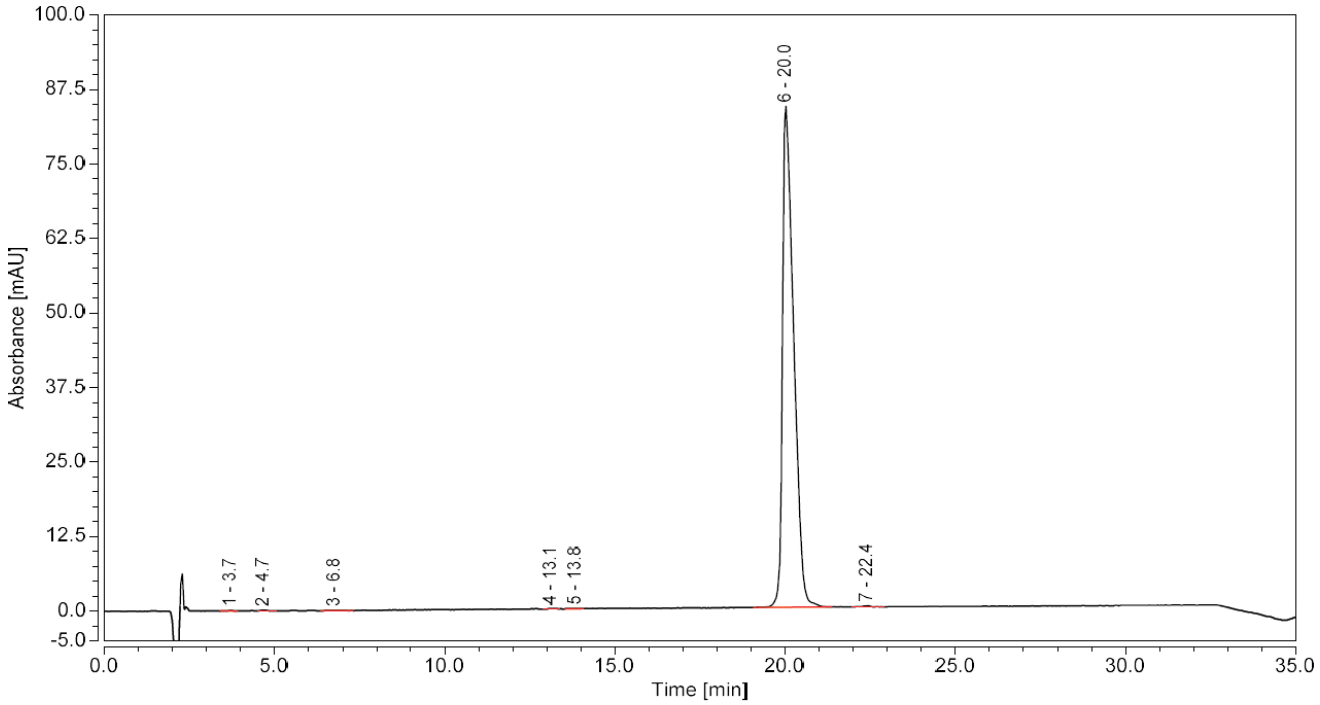

Figure 8.2.10: Chromatogram for the purified peptide IL8[55-72] eluted with a gradient of 75 % to 55% solvent A from 5 - 30 minutes. Peak-6, with a retention time of 20.0 minutes, corresponds to the peptide IL8[55-72] with a relative area of 99.6 %. HPLC was performed on the Vanquish HPLC System (ThermoFisher Scientific, Langerwehe, GER) with the RP-C18 column from Macherey-Nagel (Nucelosil 100-5 C18 Nautilus).

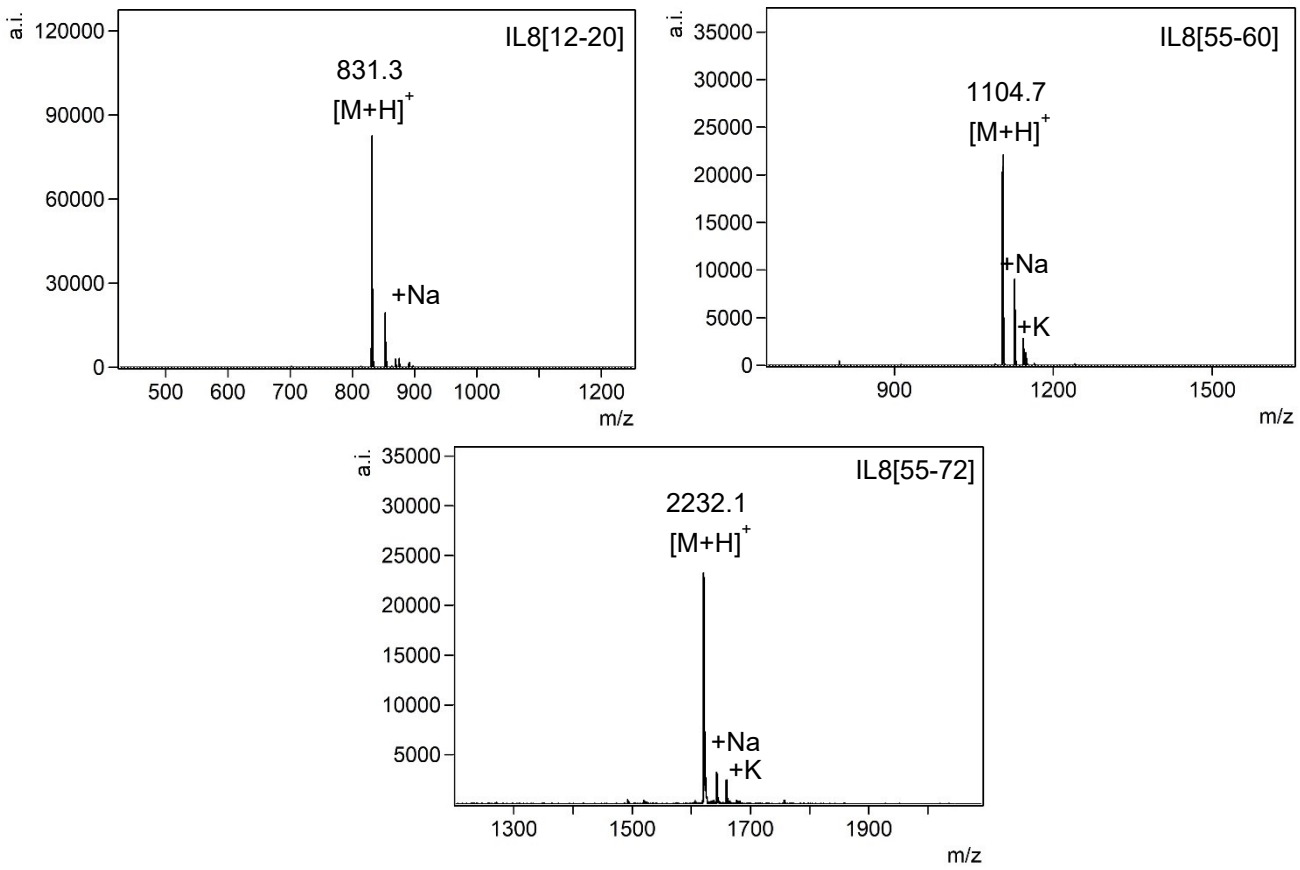

Figure 8.2.11: MALDI-tof MS measurements of the purified peptides and combined fractions for the IL8 peptides: IL8[12-20] ($[M_{theo.}+H]^+$ = 1104.6), IL8[55-60] ($[M_{theo.}+H]^+$ = 831.4), and IL8[55-72] ($[M_{theo.}+H]^+$ = 2231.2).

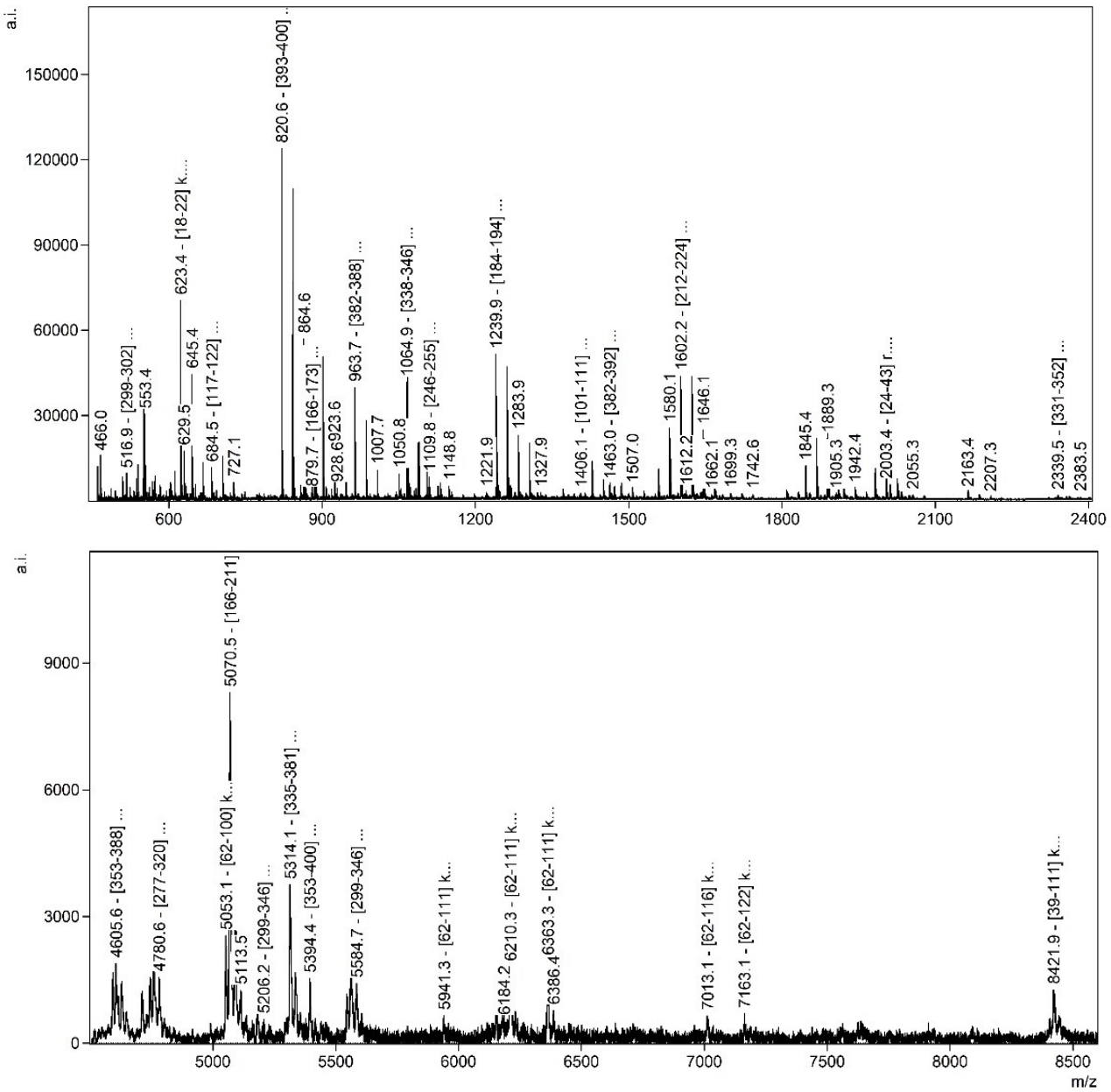

Figure 8.2.12: MALDI-tof mass spectra for smaller and larger tryptic pCTSD peptide fragments. Highlighted/annotated peaks correlate to fully tryptic peptide fragments. (Upper spectrum: Method: RP; Matrix: DHB) / (Lower spectrum: Method: LP; Matrix: SDHB)

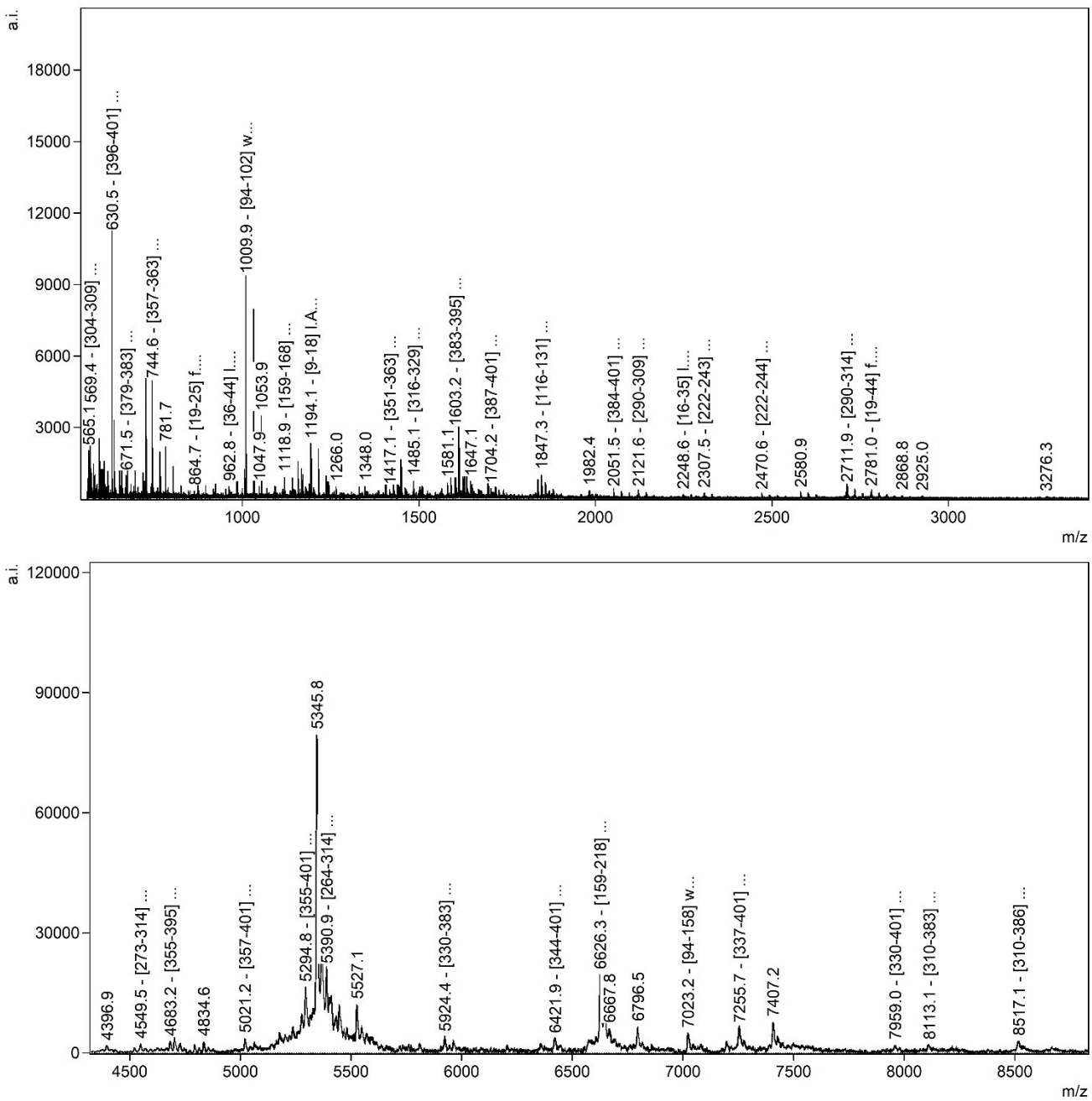

Figure 8.2.13: MALDI-tof mass spectra for smaller and larger chymotryptic pCTSD peptide fragments for the atmospheric pressure digestion. Highlighted/annotated peaks correlate to fully tryptic peptide fragments. (Upper spectrum: Method: RP; Matrix: DHB) / (Lower spectrum: Method: LP; Matrix: SDHB)

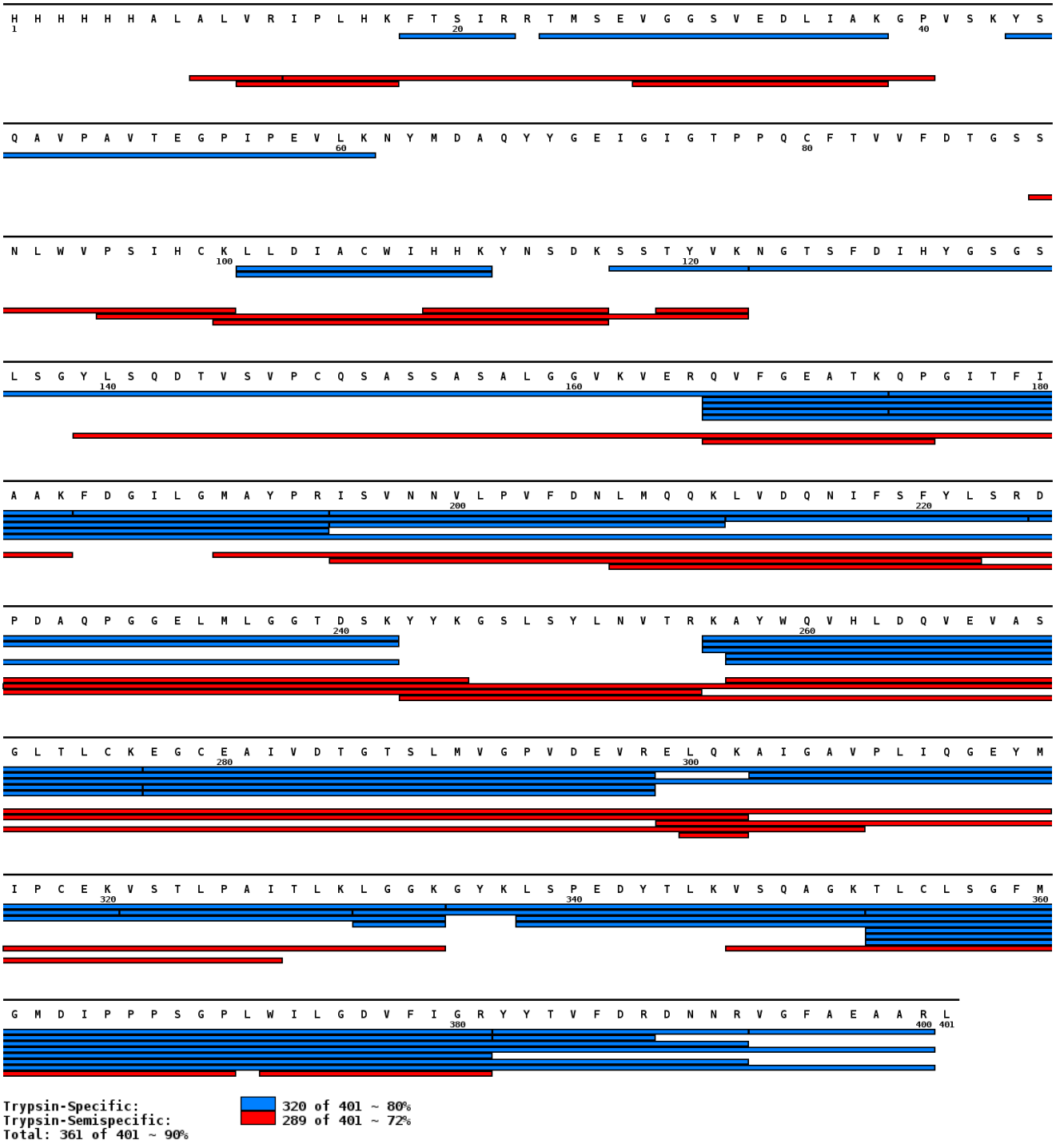

Figure 8.2.14: Protein Map of the analyzed tryptic pCTSD digestion following the AP protocol. The trypsin-specific and semi-specific peptide fragments are highlighted, resulting in a sequence coverage of 90 %.

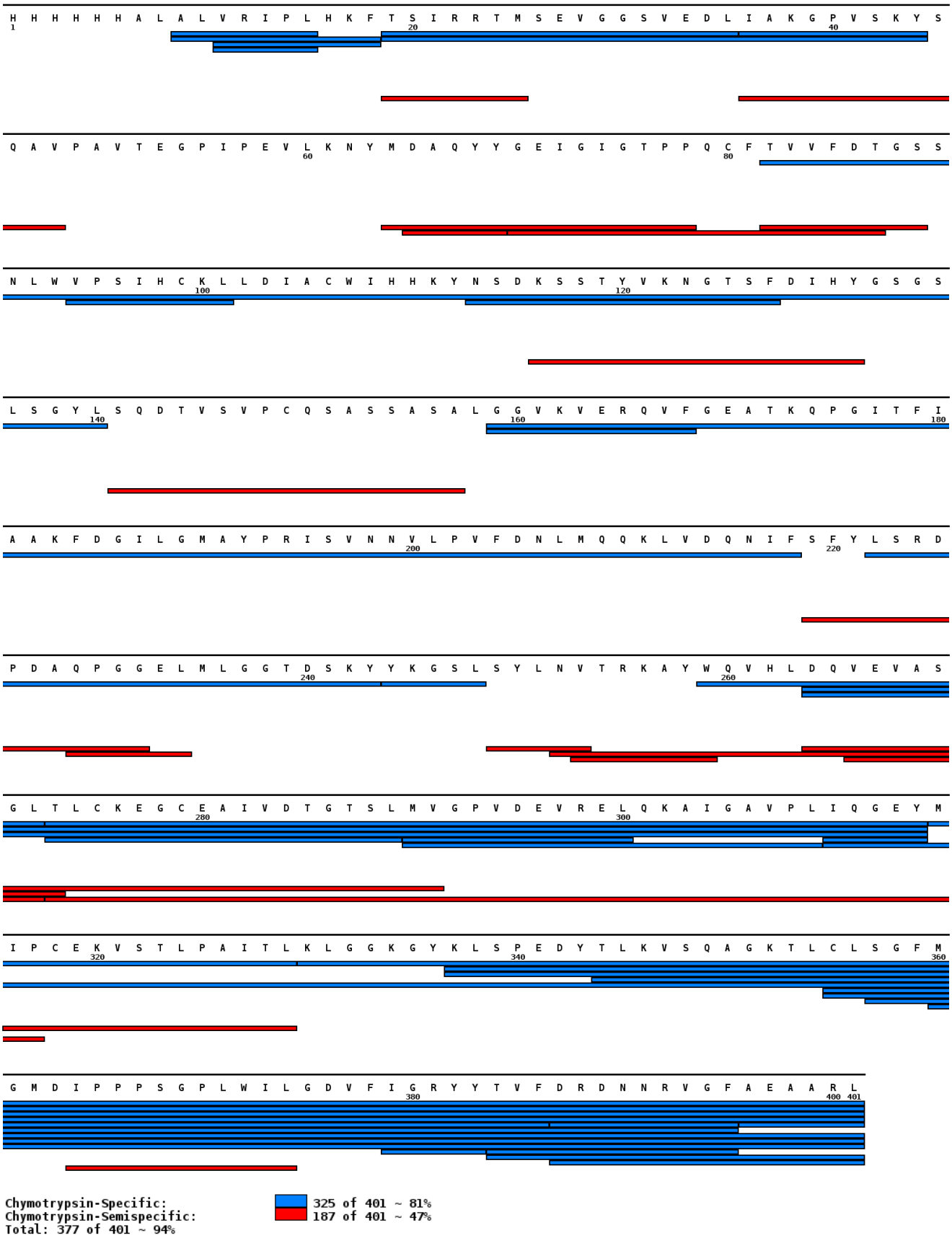

Figure 8.2.15: Protein Map of the analyzed chymotryptic pCTSD digestion following the AP protocol. Highlighted are the chymotrypsin-specific and semi-specific peptide fragments, resulting in a sequence coverage of 94 %.

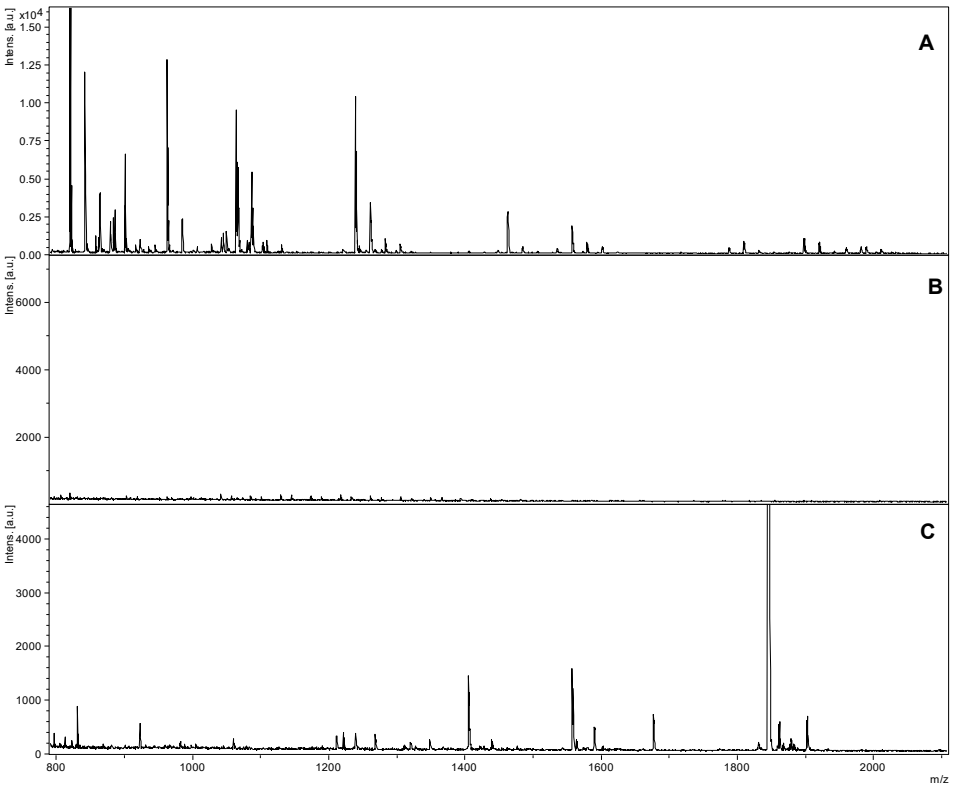

Figure 8.2.16: Mass spectra of selected fractions from the control experiments with the tryptic digestion of pCTSD and sepharose 4B. (A) Injection fraction with tryptic peptides. (B) Last washing fraction with no peaks for tryptic peptides. (C) Acidic elution with 0.1 % TFA with pCTSD-derived tryptic peptide fragments. Peak table for the elution fraction for E1 (see Table 5.2.2). (Method: RP; Matrix: DHB)

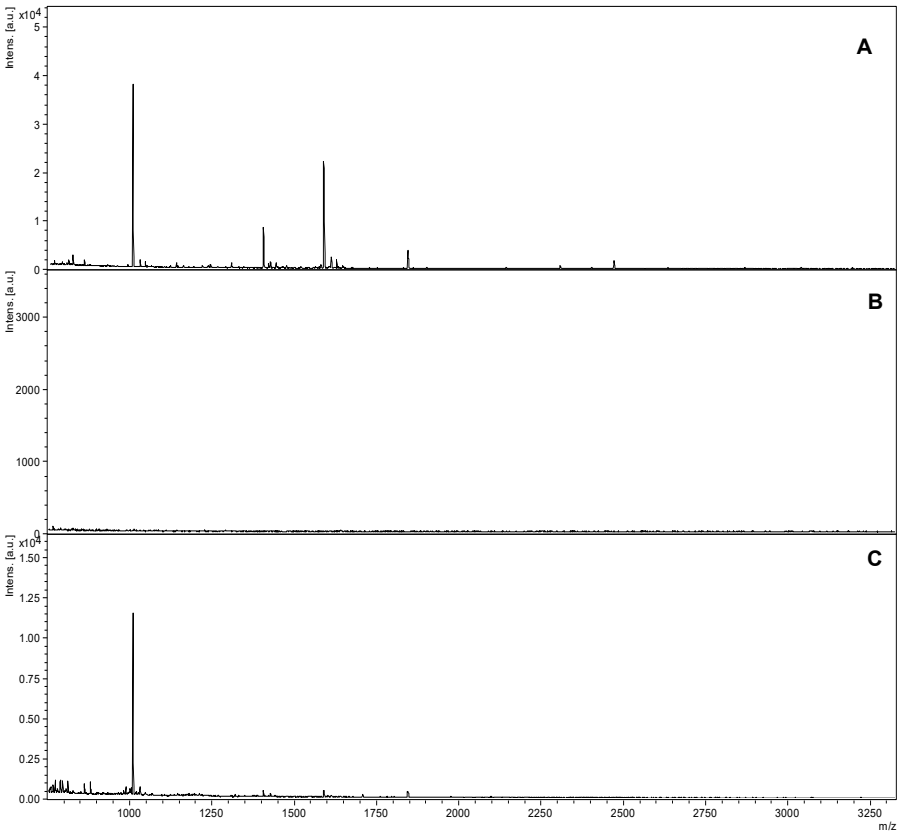

Figure 8.2.17: Mass spectra of chymotryptic digestion of pCTSD for extraction from a control experiment. (A) Mass spectrum of the injection fraction with present tryptic peptides. (B) The last washing fraction shows no peaks for tryptic peptides. (C) Acidic elution with 0.1 % TFA shows chymotryptic peptide peaks and unidentified peaks. The peak table for the elution fraction is in chapter 5.2.2. (Method: RP; Matrix: DHB)

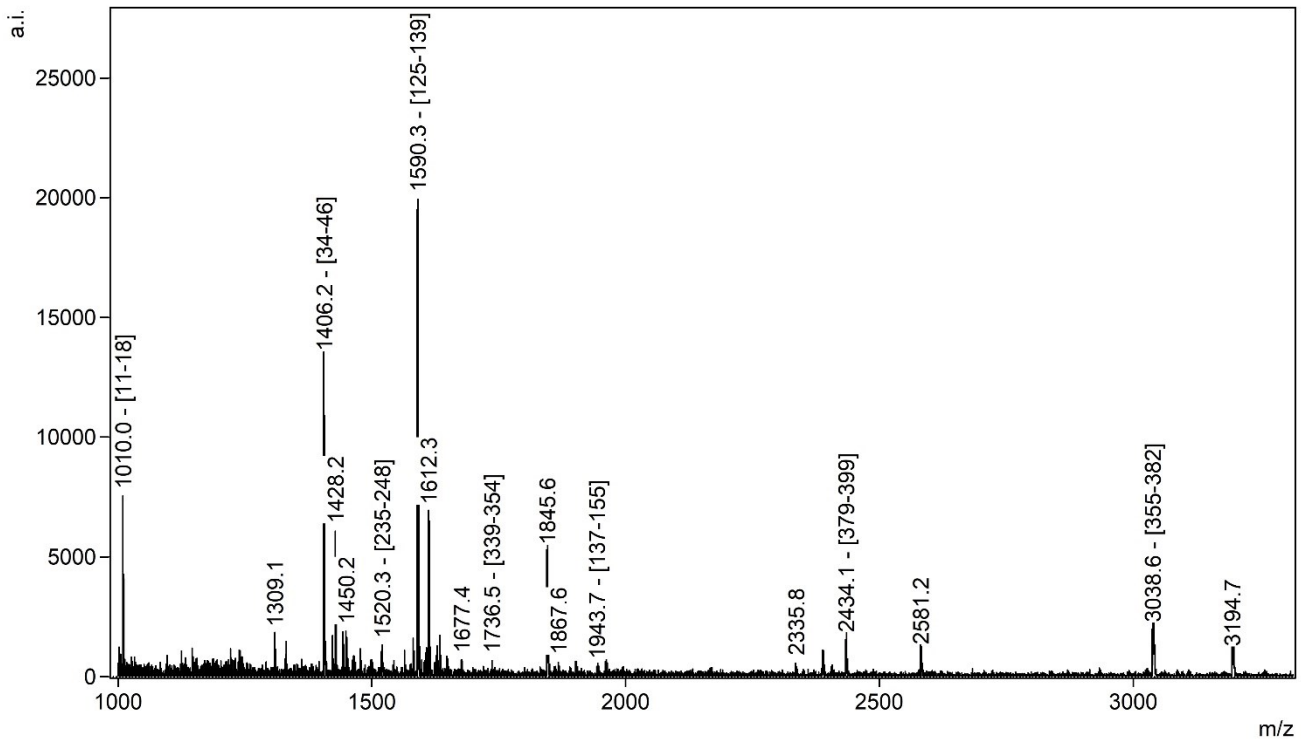

Figure 8.2.18: MLADI-tof mass spectrum of the acidic elution (E2) from immobilized anti-pCTSD and chymotryptic pCTSD. (Method: RP; Matrix: DHB)

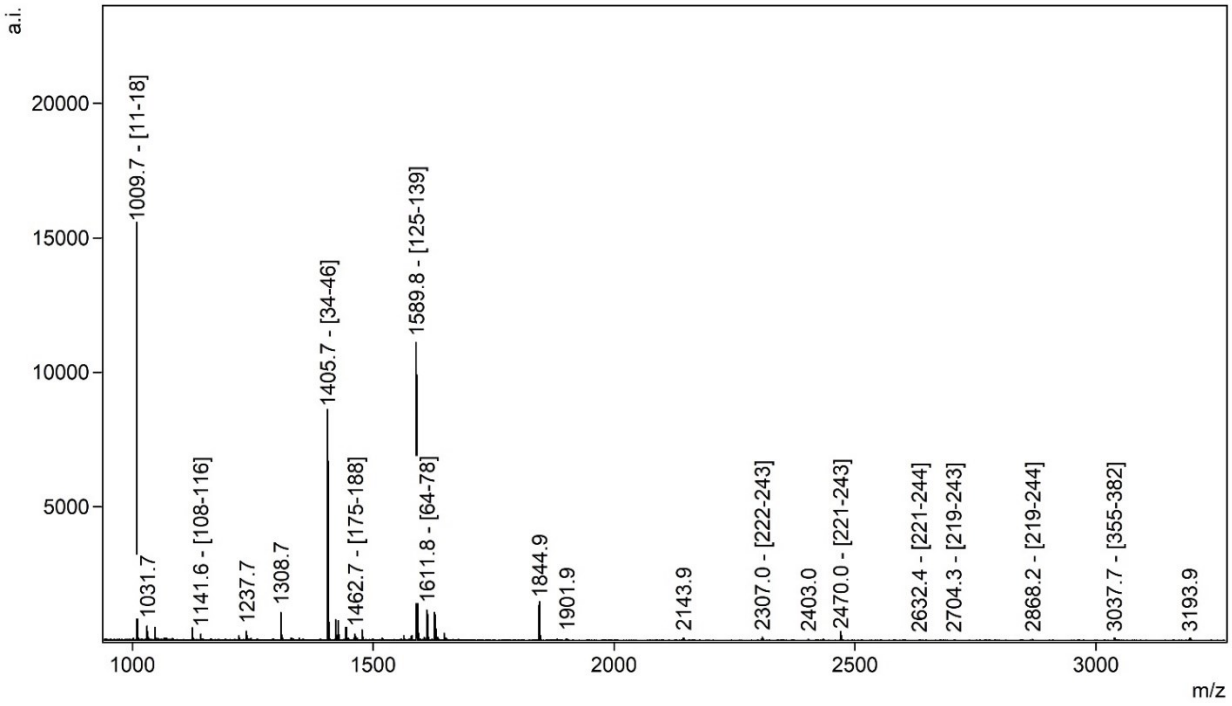

Figure 8.2.19: Exemplary MALDI-tof mass spectrum of the acidic elution (E2) from immobilized anti-CTSD and chymotryptic pCTSD. (Method: RP; Matrix: DHB)

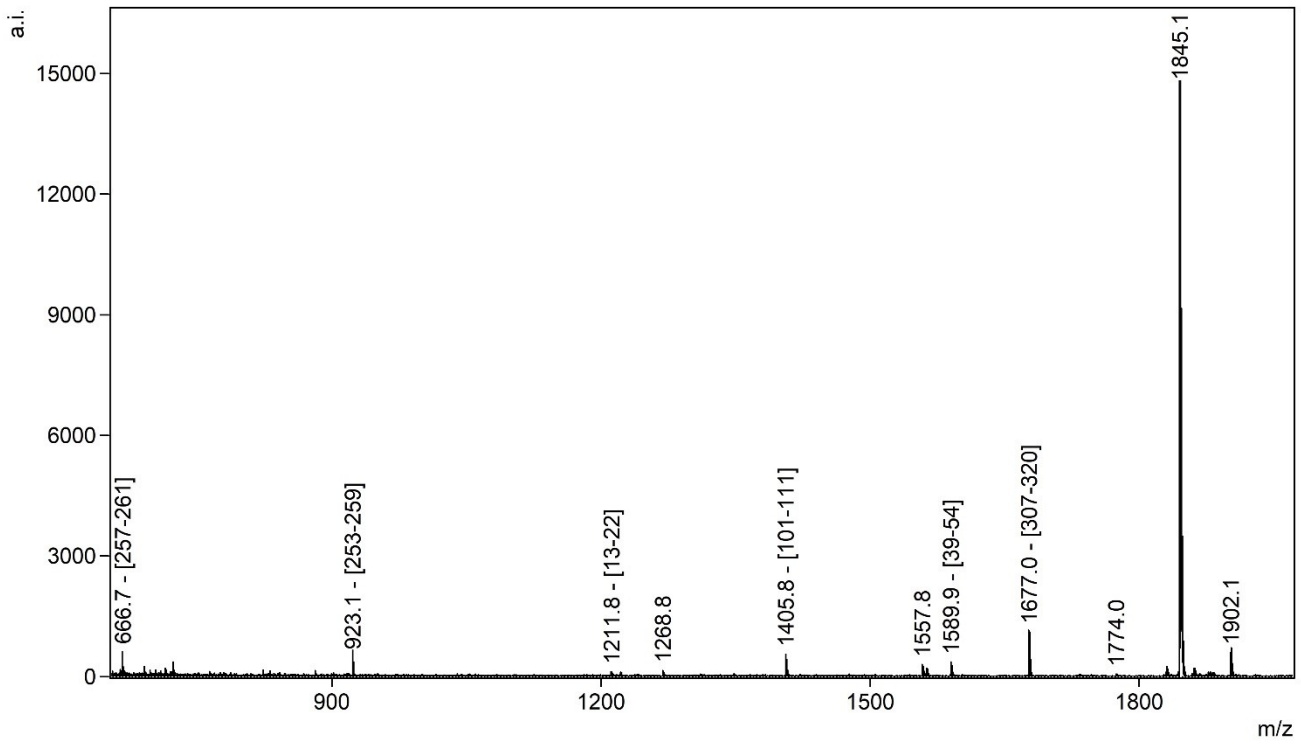

Figure 8.2.20: Exemplary MALDI-tof mass spectrum of the acidic elution (E2) from immobilized CTSD-Aptamer and tryptic pCTSD. (Method: RP; Matrix: DHB)

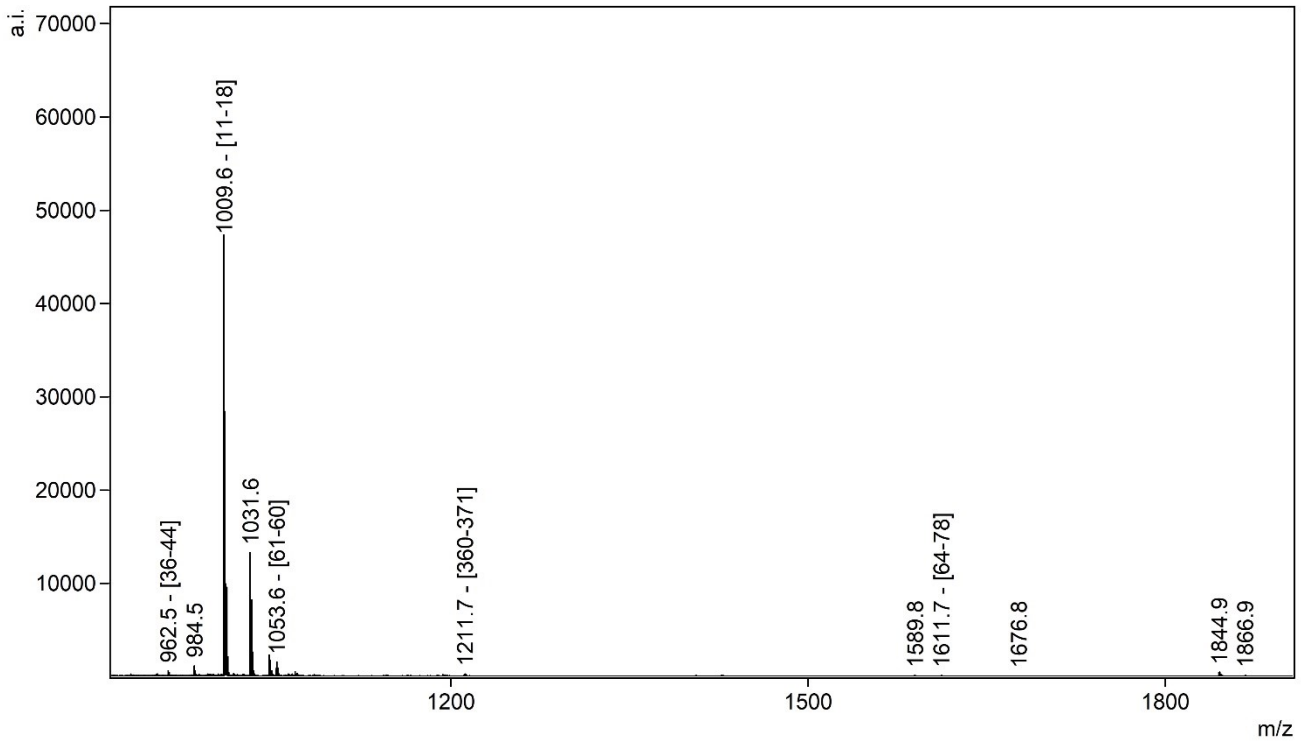

Figure 8.2.21: Exemplary MALDI-tof mass spectrum of the acidic elution (E2) from immobilized CTSD-Aptamer and chymotryptic pCTSD. (Method: RP; Matrix: DHB)

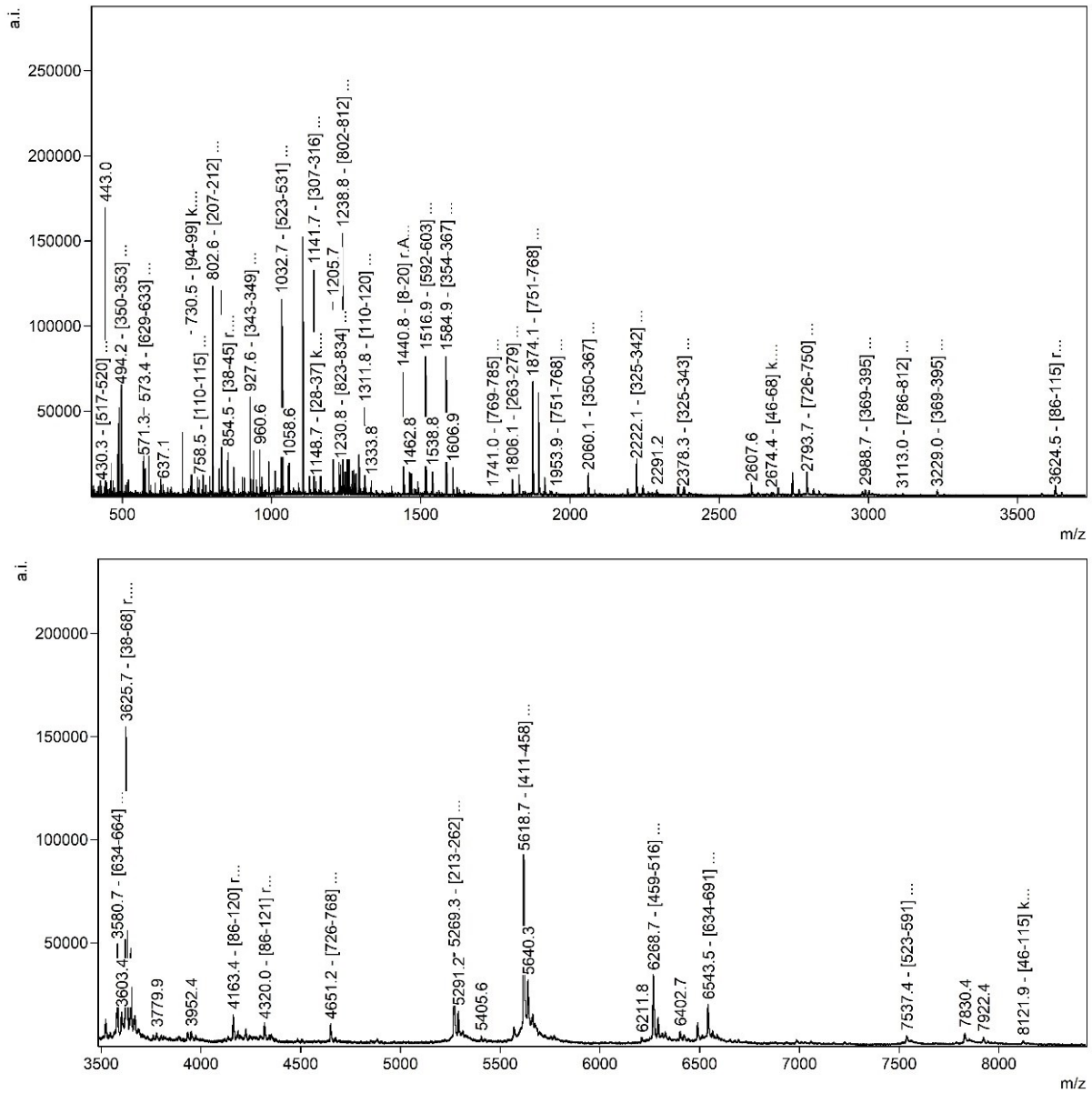

Figure 8.2.22: MALDI-tof mass spectra for smaller and larger tryptic GAA peptide fragments for digestion under atmospheric pressure. Highlighted/annotated peaks correlate to fully tryptic peptide fragments. (Upper spectrum: Method: RP; Matrix: DHB) / (Lower spectrum: Method: LP; Matrix: SDHB)

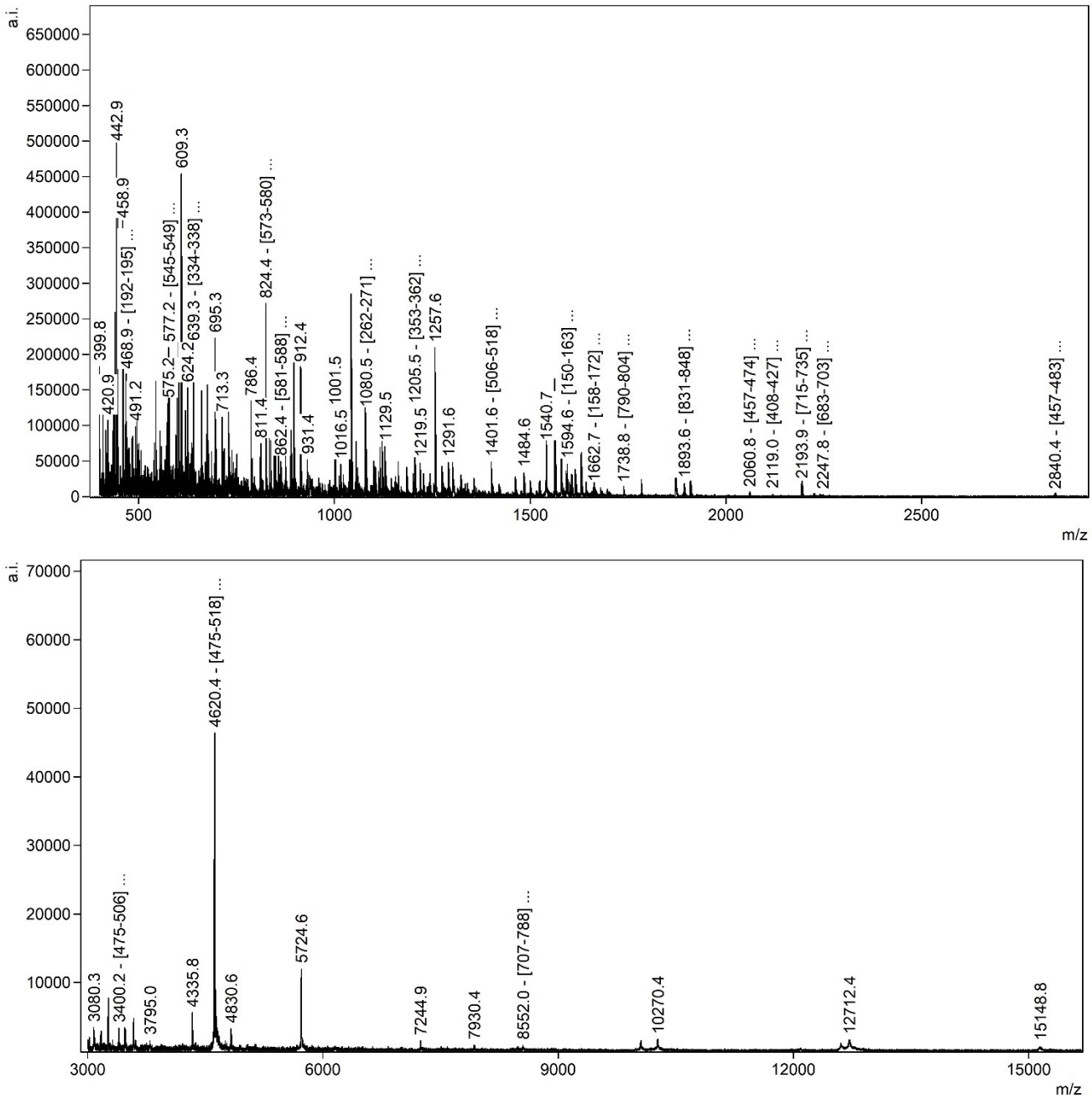

Figure 8.2.23: MALDI-tof mass spectra for smaller and larger chymotryptic GAA peptide fragments for digestion under atmospheric pressure. Highlighted/annotated peaks correlate to fully tryptic peptide fragments. (Upper spectrum: Method: RP; Matrix: DHB) / (Lower spectrum: Method: LP; Matrix: SDHB)

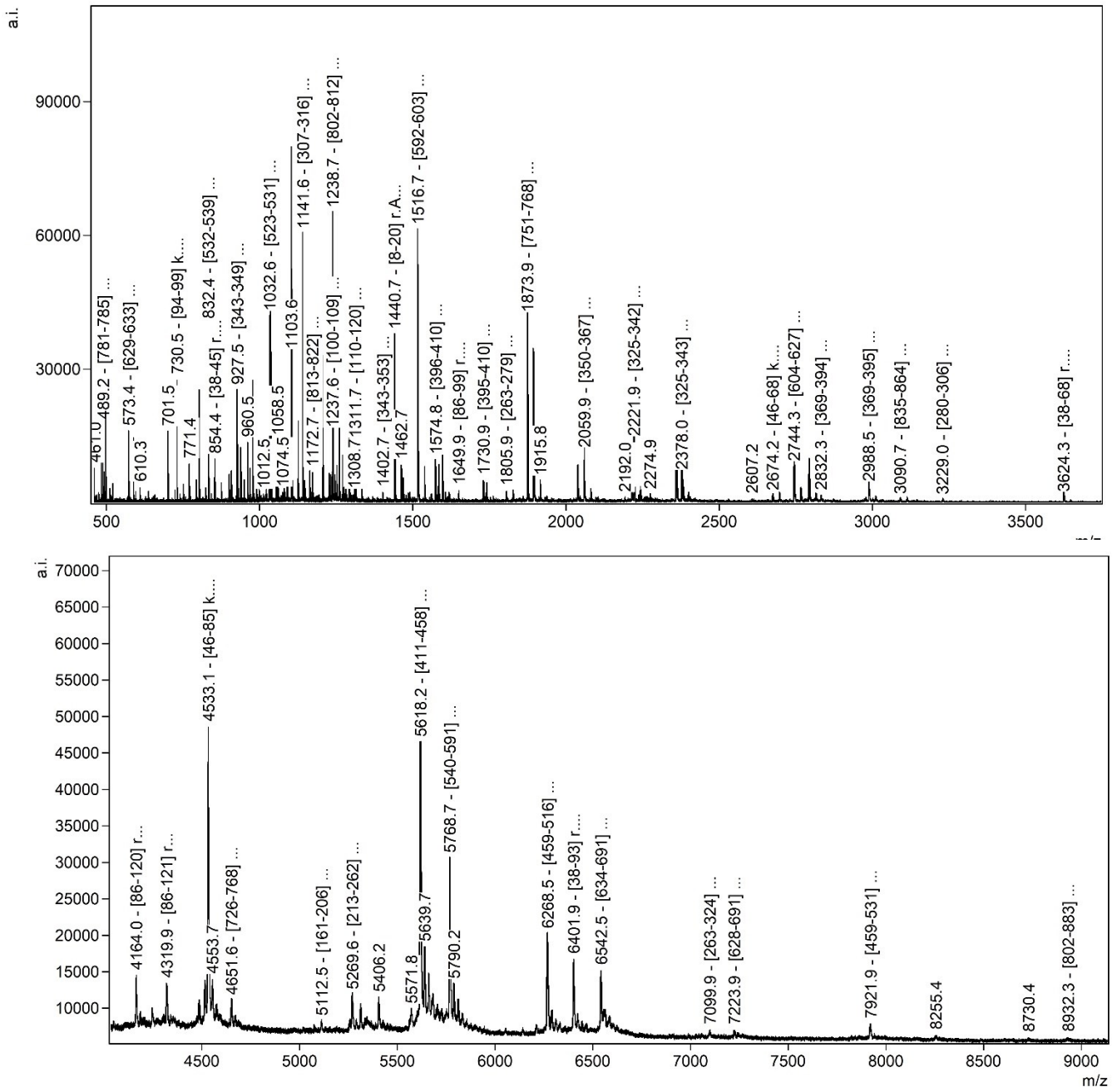

Figure 8.2.24: MALDI-tof mass spectra for smaller and larger tryptic GAA(-PNGF) peptide fragments for digestion under atmospheric pressure. Highlighted/annotated peaks correlate to fully tryptic peptide fragments. (Upper spectrum: Method: RP; Matrix: DHB) / (Lower spectrum: Method: LP; Matrix: SDHB)

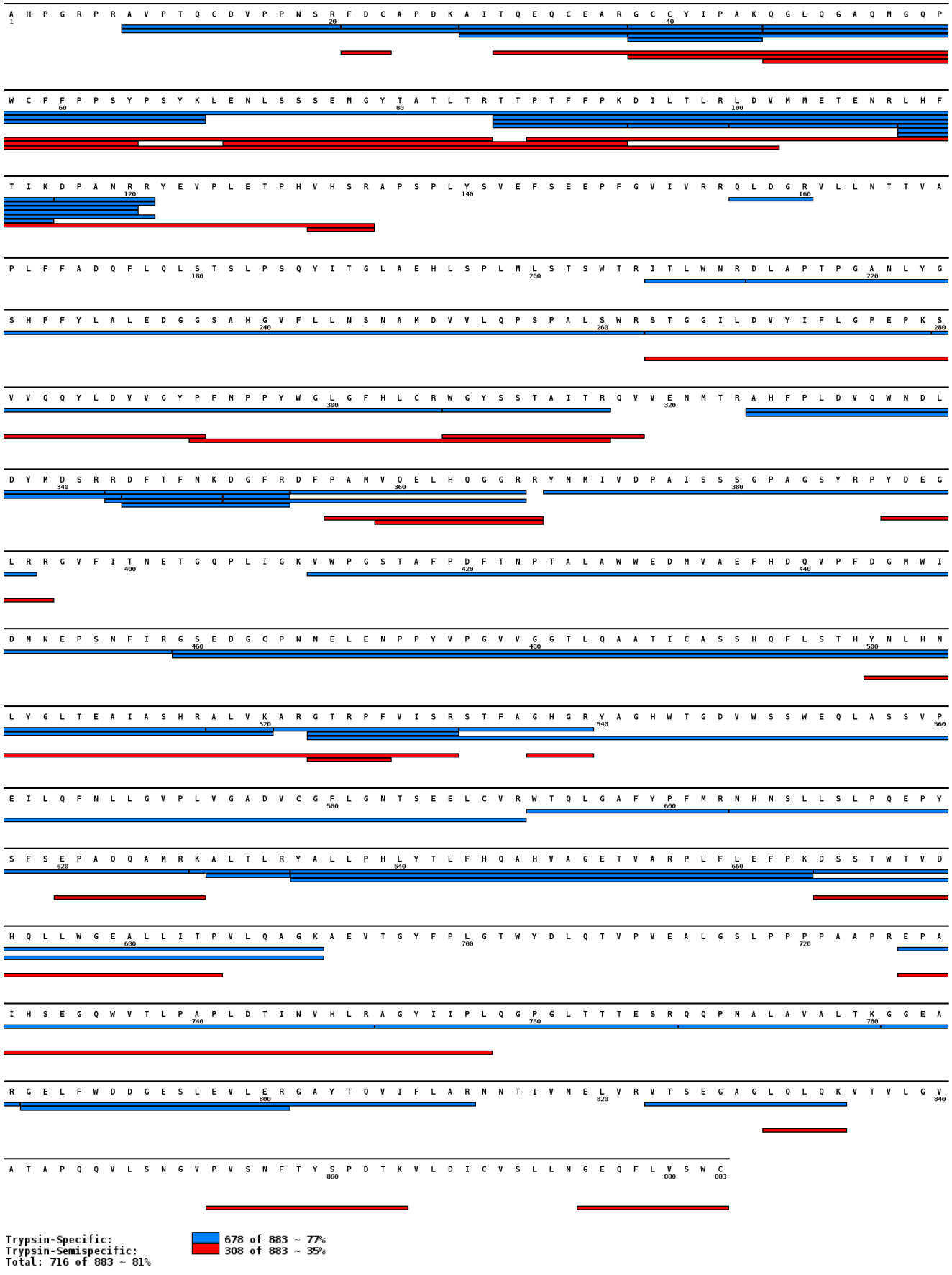

Figure 8.2.25: Protein map of the tryptic digestion of GAA following the AP protocol. The trypsin-specific and semi-specific peptide fragments are highlighted in blue and red. The resulting sequence coverage is 81 %.

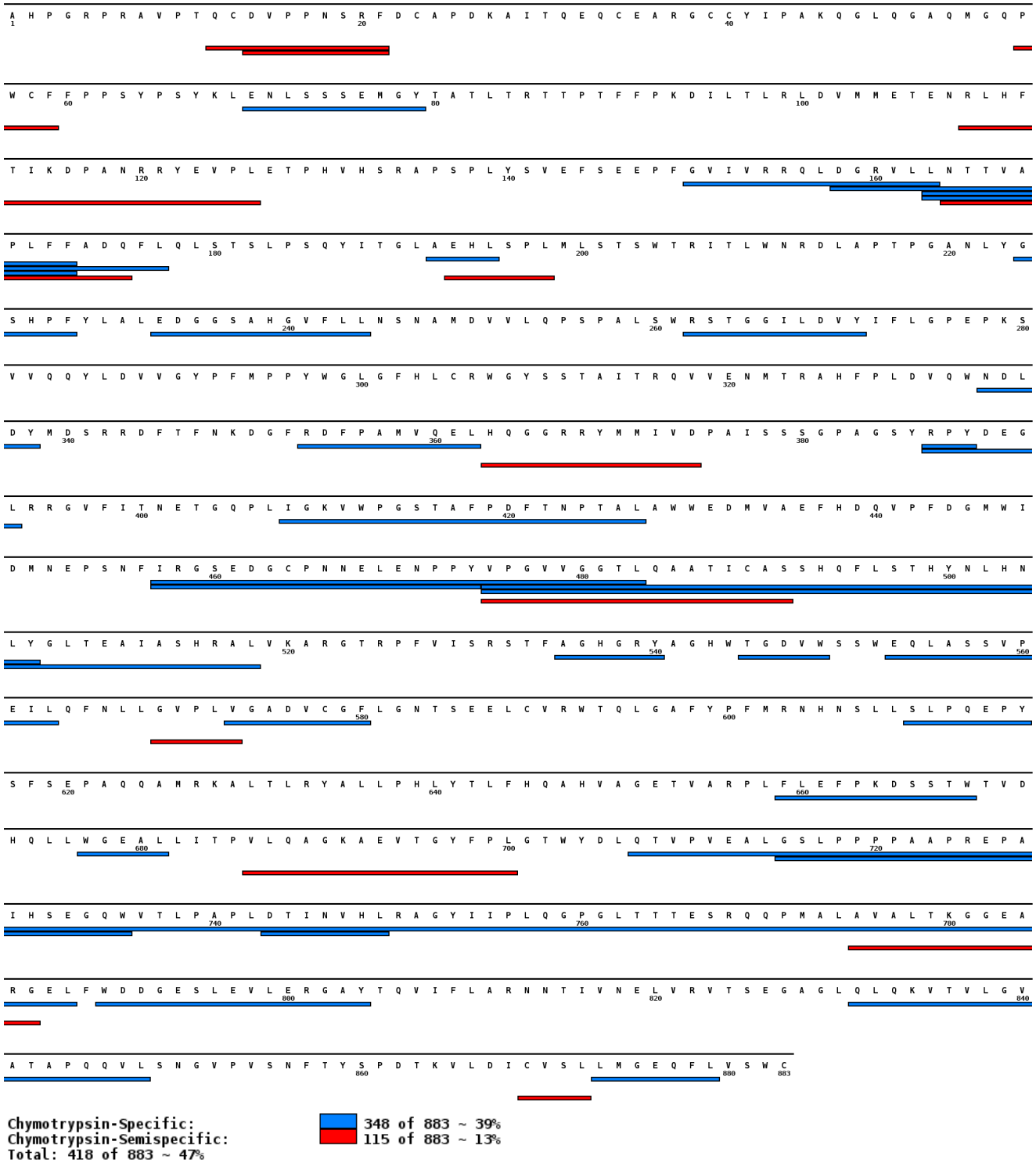

Figure 8.2.26: Protein map of the chymotryptic digestion of GAA following the AP protocol. The trypsin-specific and semi-specific peptide fragments are highlighted in blue and red, respectively. The resulting sequence coverage is 47 %.

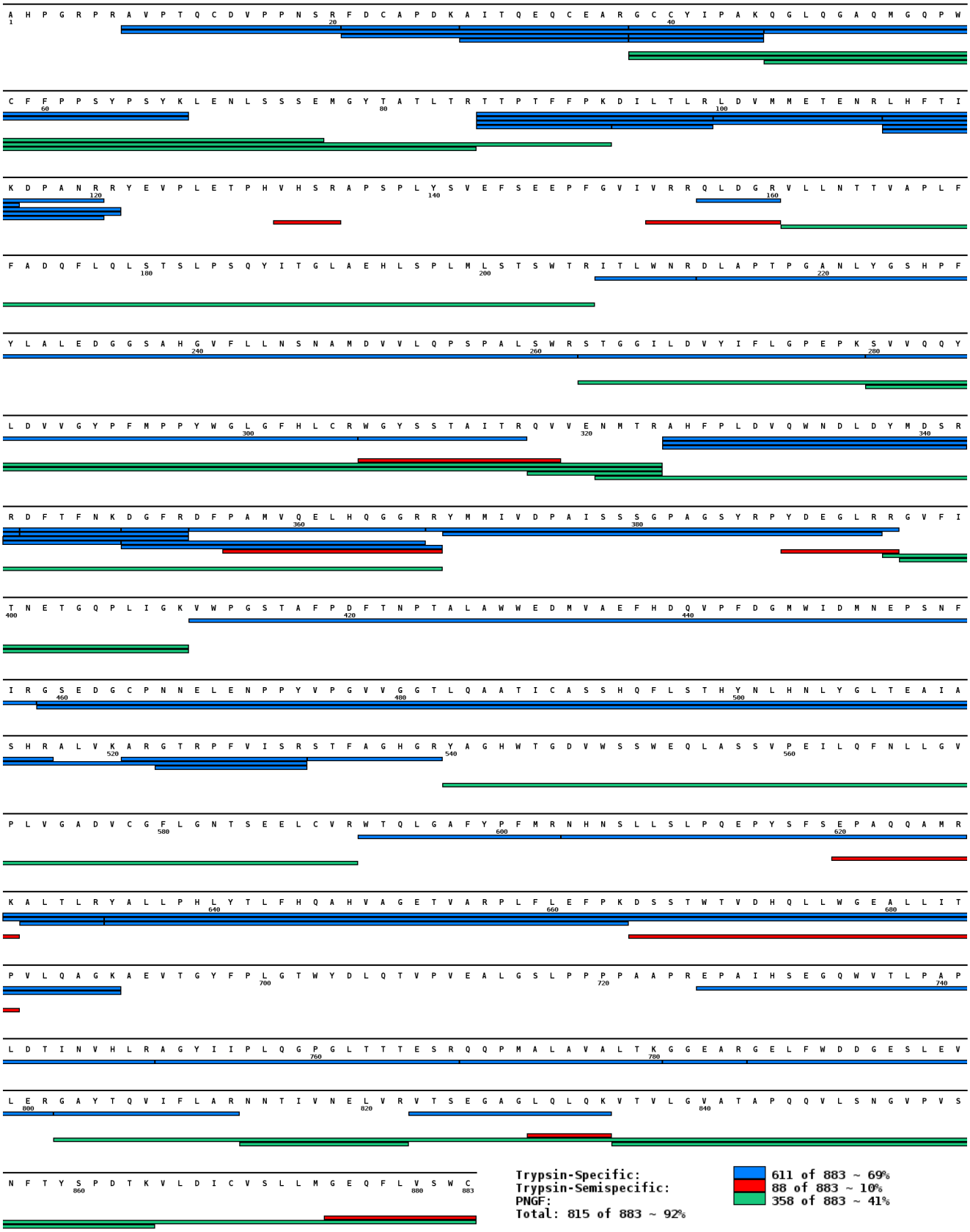

Figure 8.2.27: Protein map of the tryptic digestion of PNGF-treated GAA following the AP protocol. Highlighted are the trypsin-specific (blue), semi-specific (red), and PNGF-specific (green) peptide fragments from the digestion. The resulting sequence coverage is 92 %.

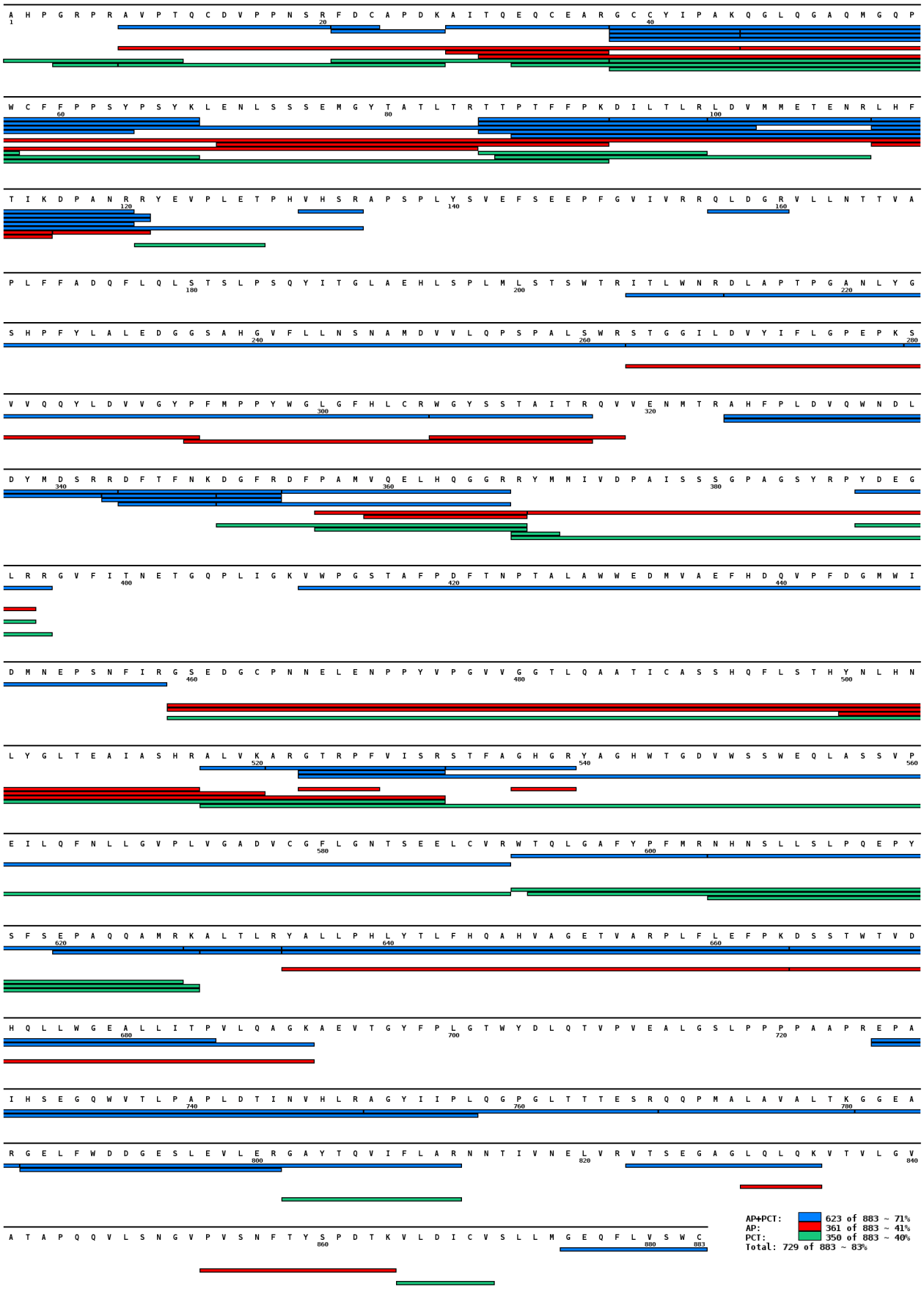

Figure 8.2.28: Protein map of the tryptic digestion of GAA under AP and PCT conditions. Identical peptide fragments in AP and PCT digestion are shown in blue bars, red bars are peptide fragments only identified in the AP digestion, and green bars are peptide fragments only identified in the PCT digestion.

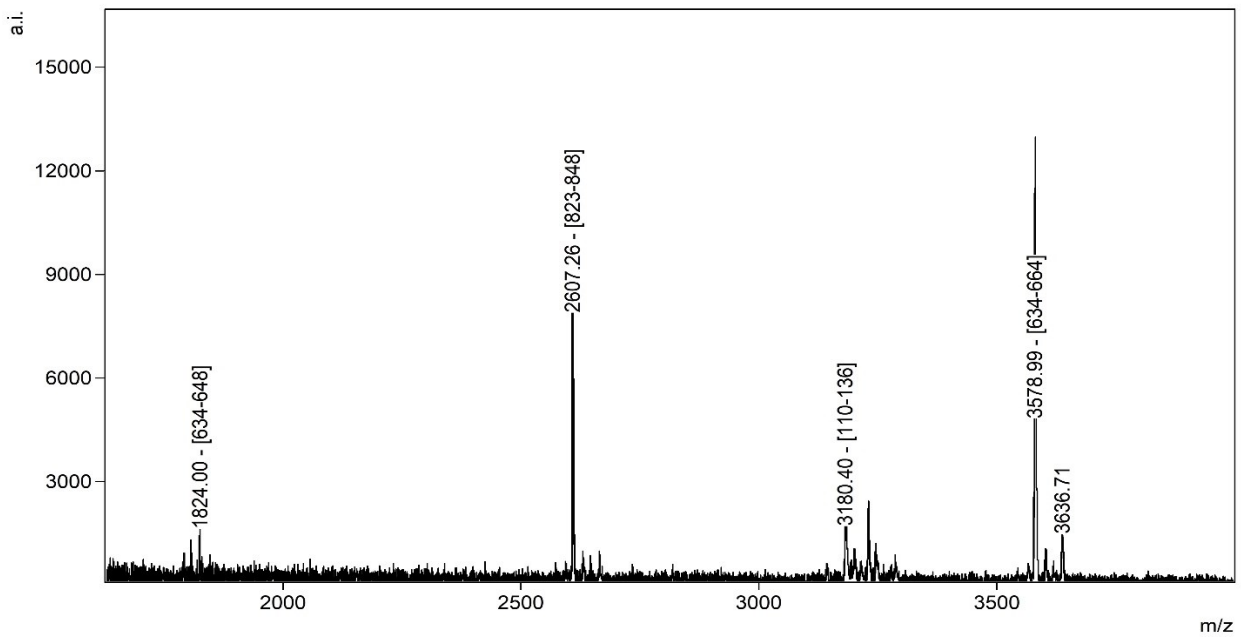

Figure 8.2.29: MALDI-tof MS measurement of the acidic elution from a control sepharose column incubated with trypsin-digested GAA. (Method: RP; Matrix: DHB)

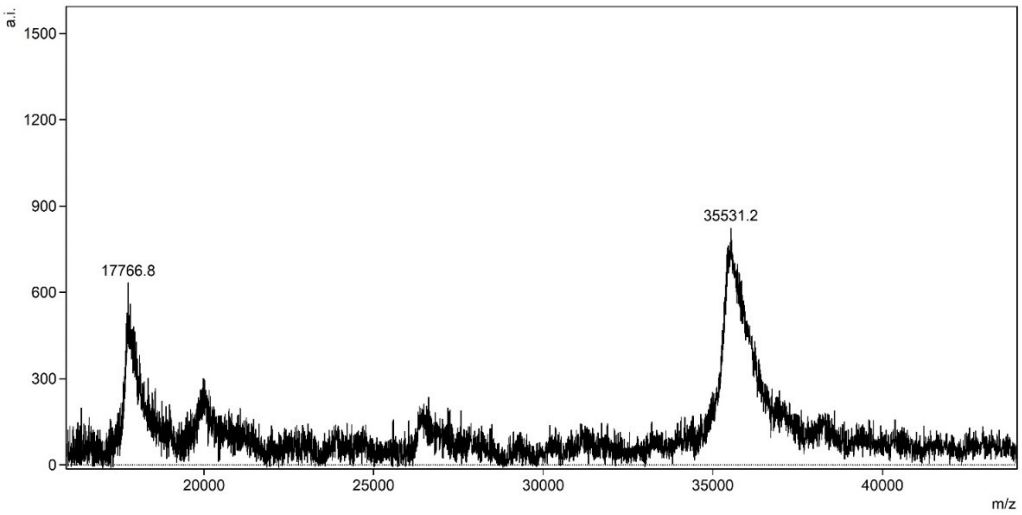

Figure 8.2.30: Native MALDI-tof MS of rSMN for protein identification. Expected value for $[M_{theo.} + H]^{1+}$ = 35538.4 and $[M_{theo.} + 2H]^{2+}$ = 17765.7. (Method: LP; Matrix: SDHB)

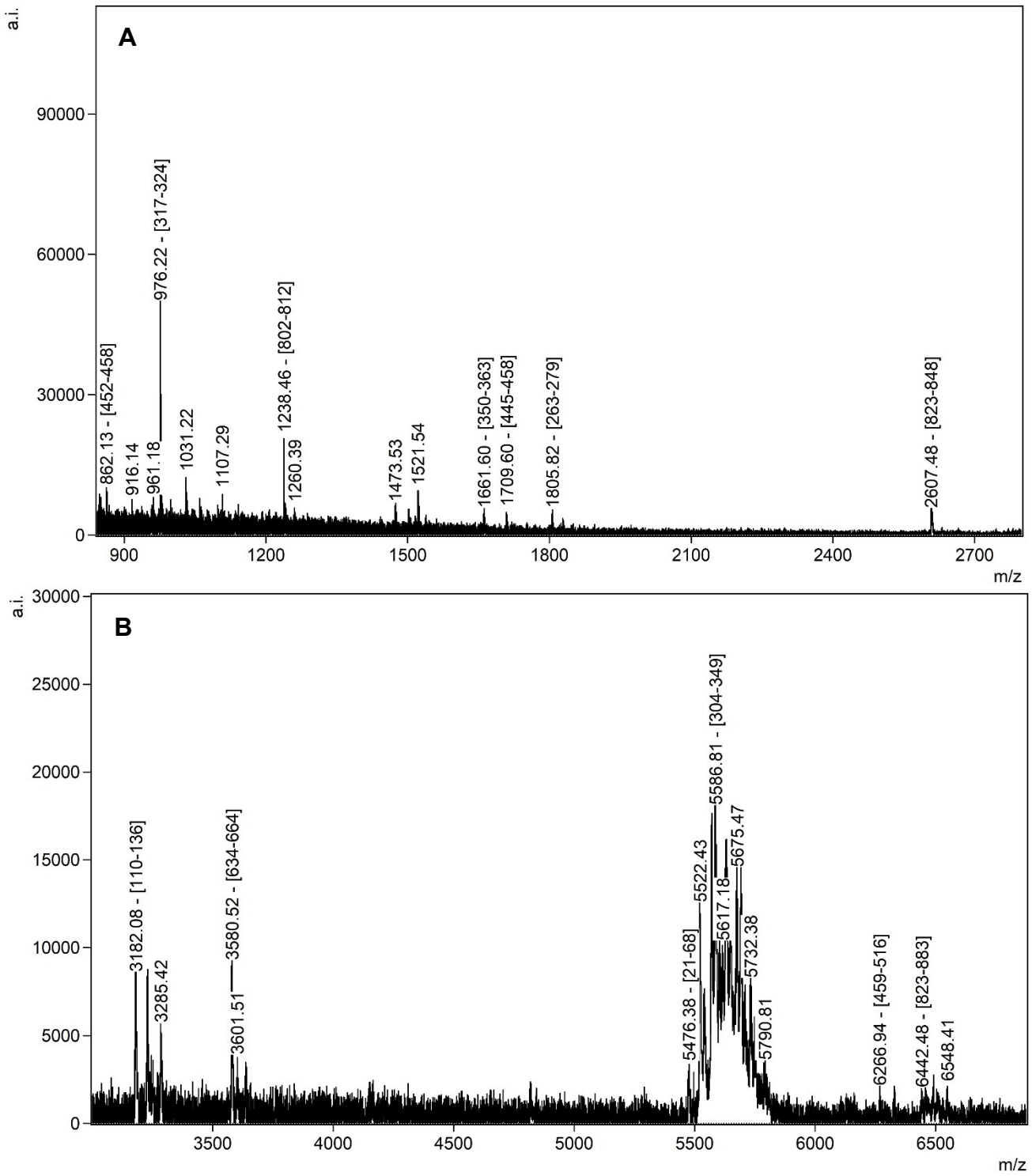

Figure 8.2.31: MALDI-tof mass spectra of the acidic elution (E1) from immobilized mAB-43G7 and tryptic digestion of GAA. (A) shows the lower mass range measured with the DHB matrix (Method: RP), and (B) shows the higher mass range measured with the SDHB matrix (Method: LP).

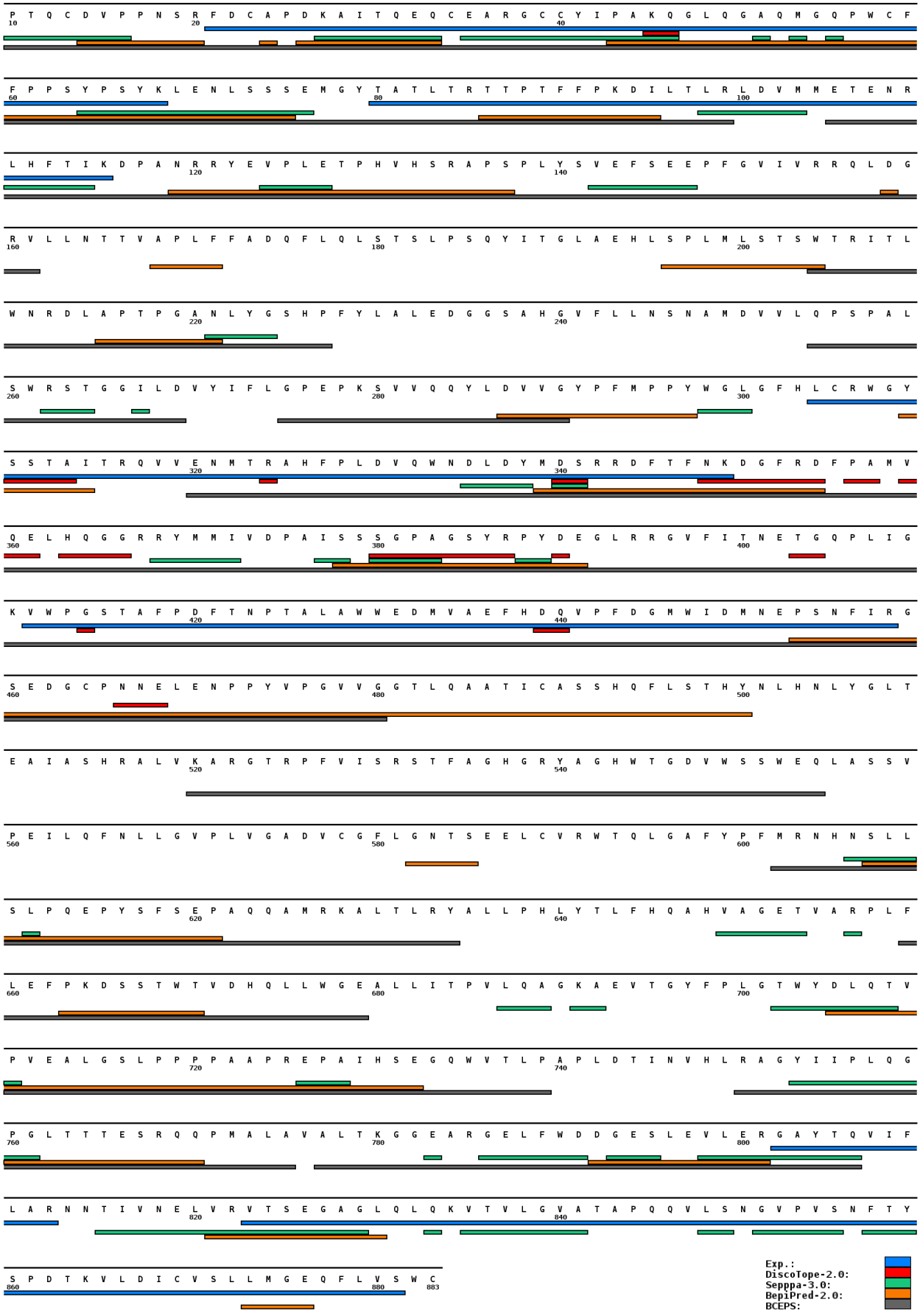

Figure 8.2.32: GAa protein map with experimentally determined epitope results and predictions with DiscoTope-2.0, Seppa-3.0, Bepipred-2.0, and BCEPS.

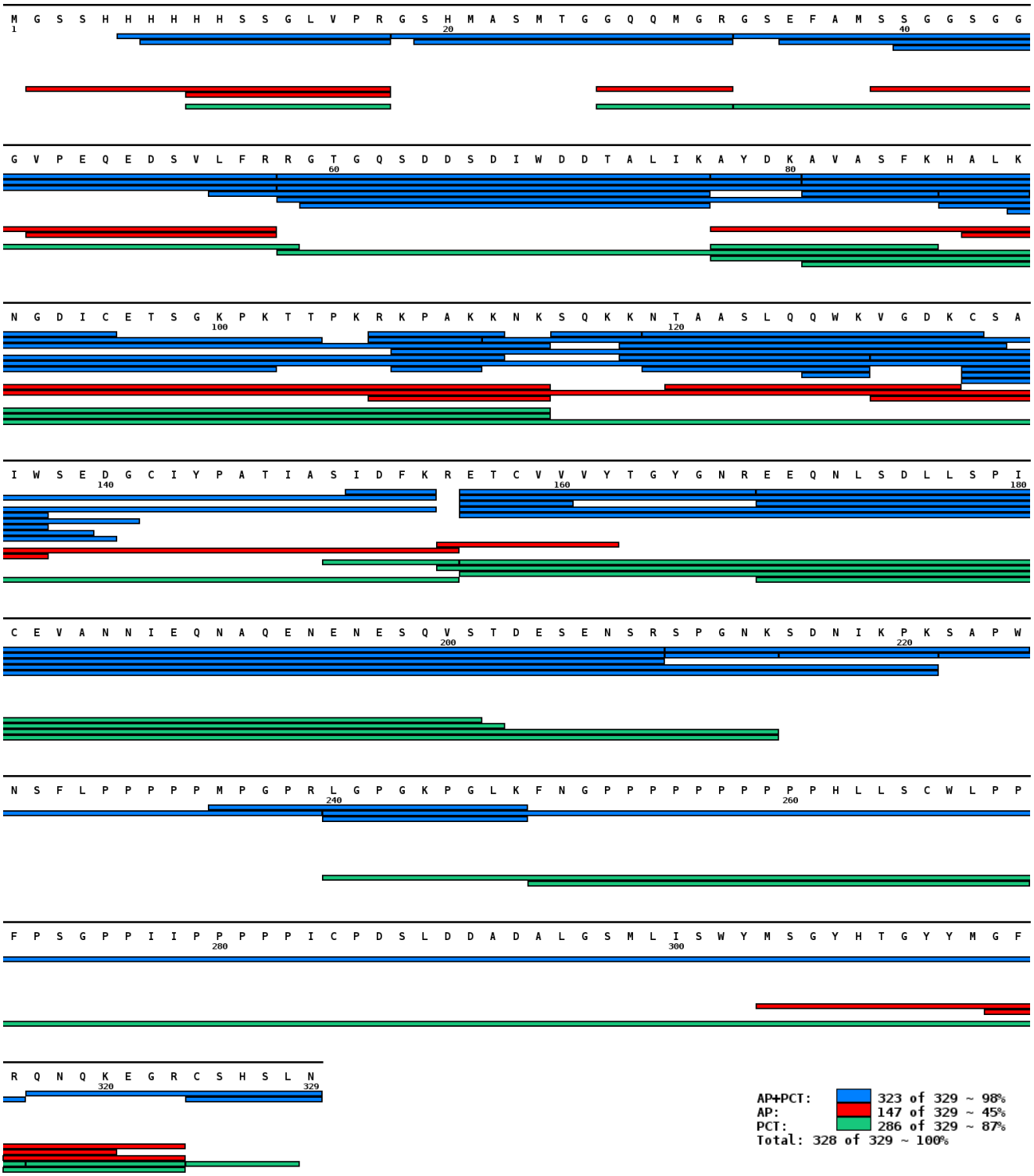

Figure 8.2.33: Protein map of the tryptic digestion of rSMN under AP and PCT conditions. Identical peptide fragments in AP and PCT digestion are shown in blue bars, red bars are peptide fragments only identified in the AP digestion, and green bars are peptide fragments identified in the PCT digestion.

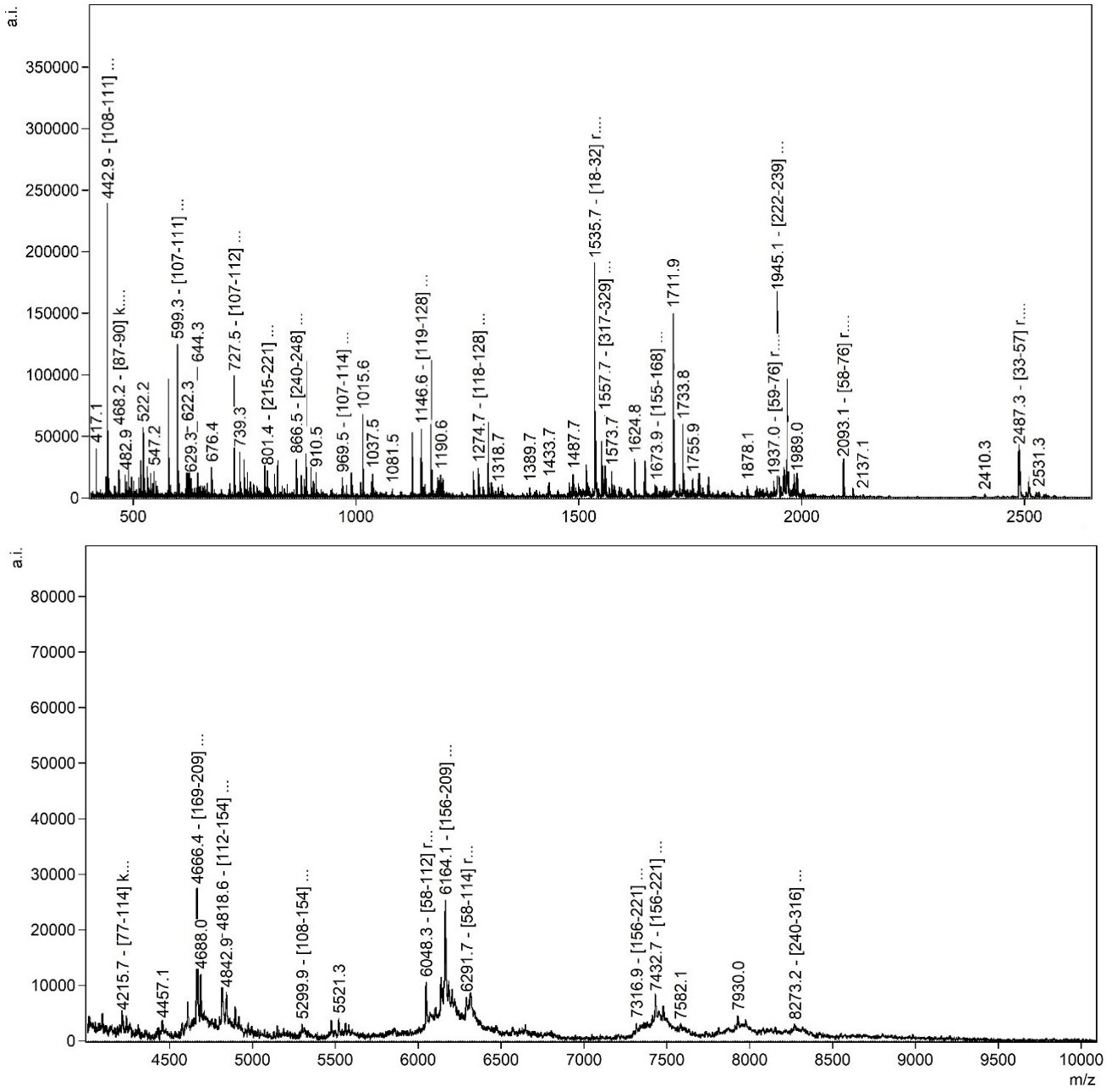

Figure 8.2.34: MALDI-tof mass spectra for smaller and larger tryptic rSMN1 peptide fragments. Highlighted/annotated peaks correlate to fully tryptic peptide fragments. (Upper spectrum: Method: RP; Matrix: DHB) / (Lower spectrum: Method: LP; Matrix: SDHB)

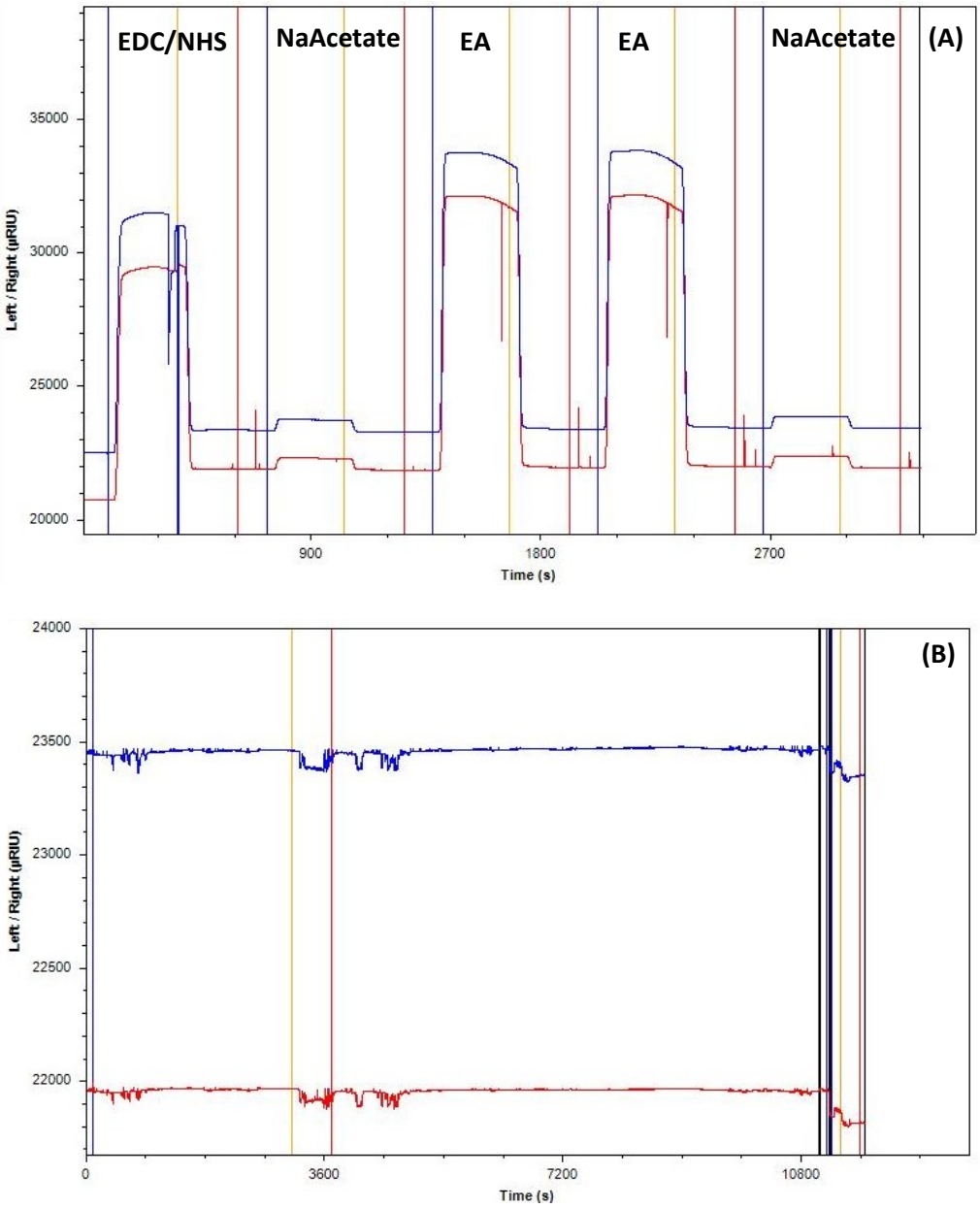

Figure 8.2.35: (A) Preparation of a 16-MHDA functionalized gold chip for the control epitope extraction experiments. An EDC/NHS activation followed by buffer and 1 M ethanolamine (pH 8) injections. (B) Control experiment for the epitope extraction with 5 mM AmBic as running buffer and a flow rate of 5 µL/min or 50 µL/min for the acidified elution. Injection of 10 µg tryptic IL8 in digestion buffer diluted to 300 µL with 5 mM AmBic. Vertical lines: blue marks the start of injection; yellow marks the dissociation start; red indicates the end of the dissociation phase; black shows a stop of recording. Horizontal lines: blue is the signal from the sample channel; red is the signal from the reference channel.

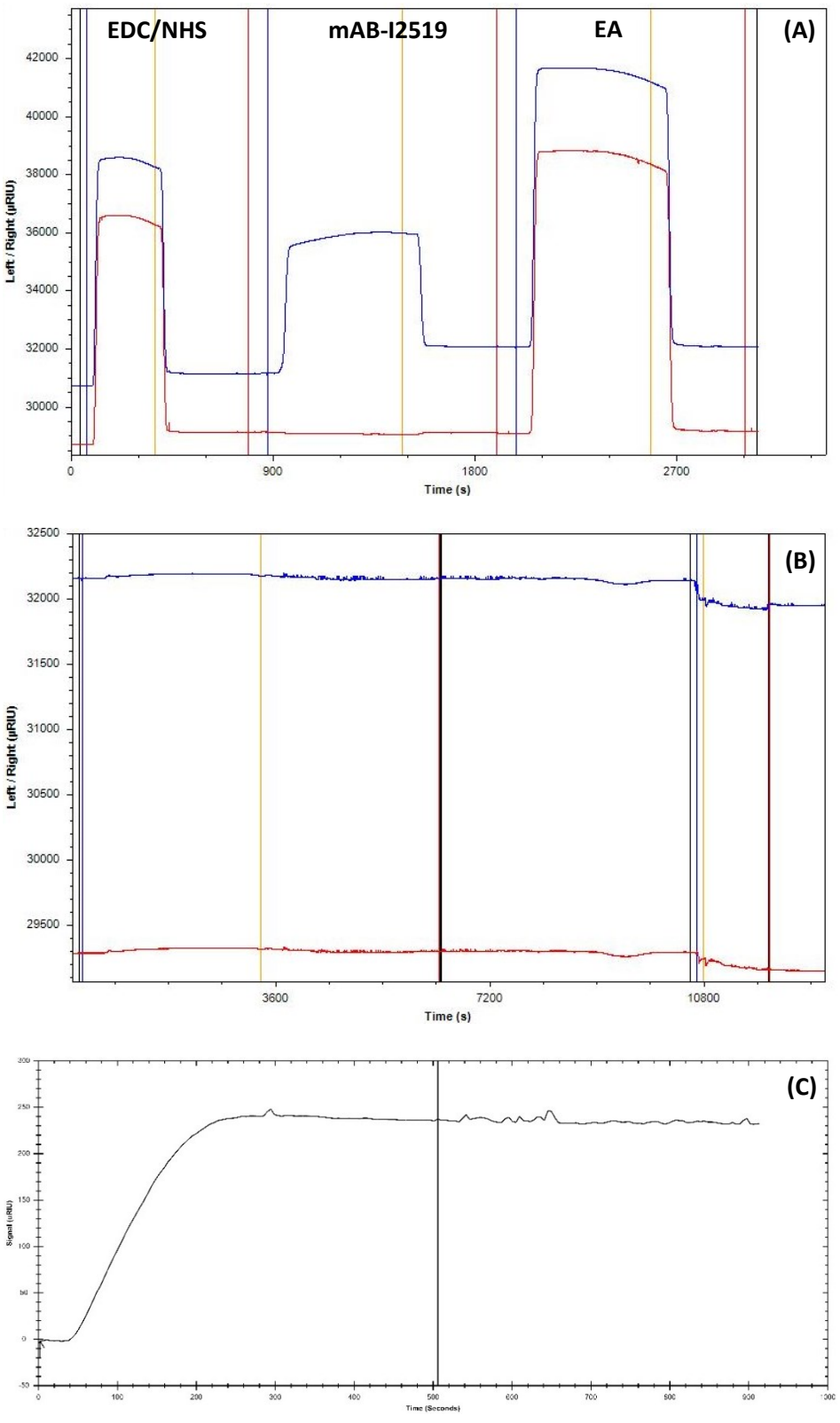

Figure 8.2.36: (A) Immobilization of mAB-I2519 on a 16-MHDA functionalized gold chip. At first, the carboxyl groups on the surface were activated via EDC/NHS, followed by injection of 50 µg mAB-I2519 in 300 µL 30 mM sodium acetate buffer (pH 5) and final capping with 1 M ethanolamine (pH 8). (B) Epitope extraction with 5 mM AmBic as running buffer and a 5 µL/min flow rate or 50 µL/min for the acidified elution. Injection of 10 µg tryptic IL8 in digestion buffer diluted to 300 µl with 5 mM AmBic. (C) Test injection of 500 nM IL8 to prove the successful antibody immobilization (vertical line indicates the start of dissociation phase). Vertical lines: blue marks the start of injection; yellow marks the dissociation start; red indicates the end of the dissociation phase; black shows a stop of recording. Horizontal lines: blue is the signal from the sample channel; red is the signal from the reference channel.

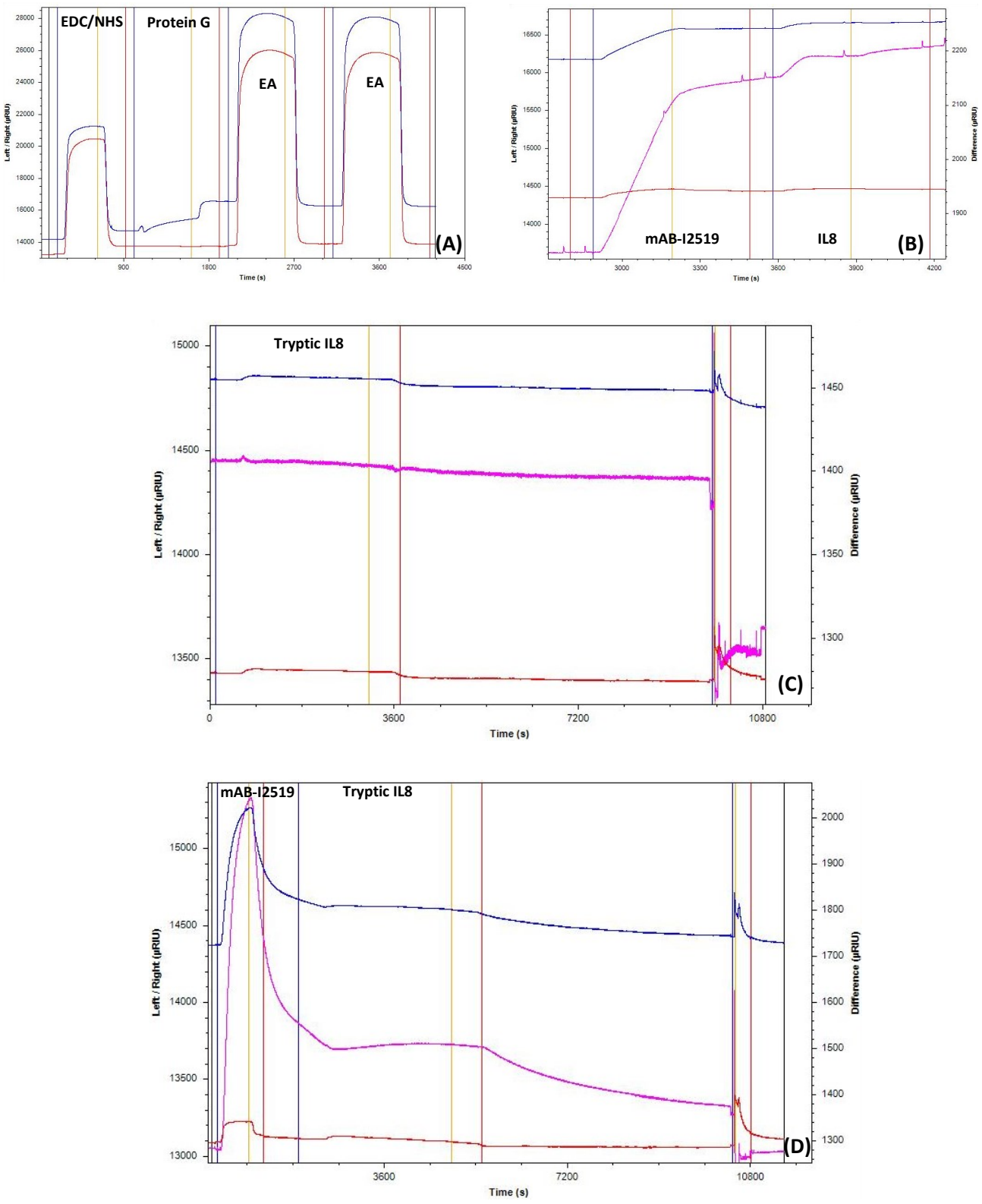

Figure 8.2.37: (A) Immobilization of protein G (50 µg in 300 µL sodium acetate buffer) on a 16-MHDA functionalized gold chip with initial EDC/NHS activation and final ethanolamine capping. (B) Test injection of 12 nM mAB-I2519 in PBS followed by 100 nM IL8 in PBS to test the successful protein G immobilization and principal experimental setup. (C) Control epitope extraction with 5 mM AmBic as running buffer and a 5 µL/min flow rate or 50 µL/min for the acidified elution. Injection of 10 µg tryptic IL8 in digestion buffer diluted to 300 µl with 5 mM AmBic. (D) Epitope extraction with 150 nM mAB-I2519 in PBS (25 µL/min) with 5 mM AmBic as a running buffer at a 5 µL/min flow rate after the antibody injection. 10 µg tryptic IL8 in digestion buffer diluted to 300 µl with 5 mM AmBic was injected with final acidic elution (0.1 % TFA). Vertical lines: blue marks the start of injection; yellow marks the dissociation start; red indicates the end of the dissociation phase; black shows a stop of recording. Horizontal lines: blue is the signal recorded from the sample channel; red is the signal recorded from the reference channel; pink is the difference between the sample and the reference channel.

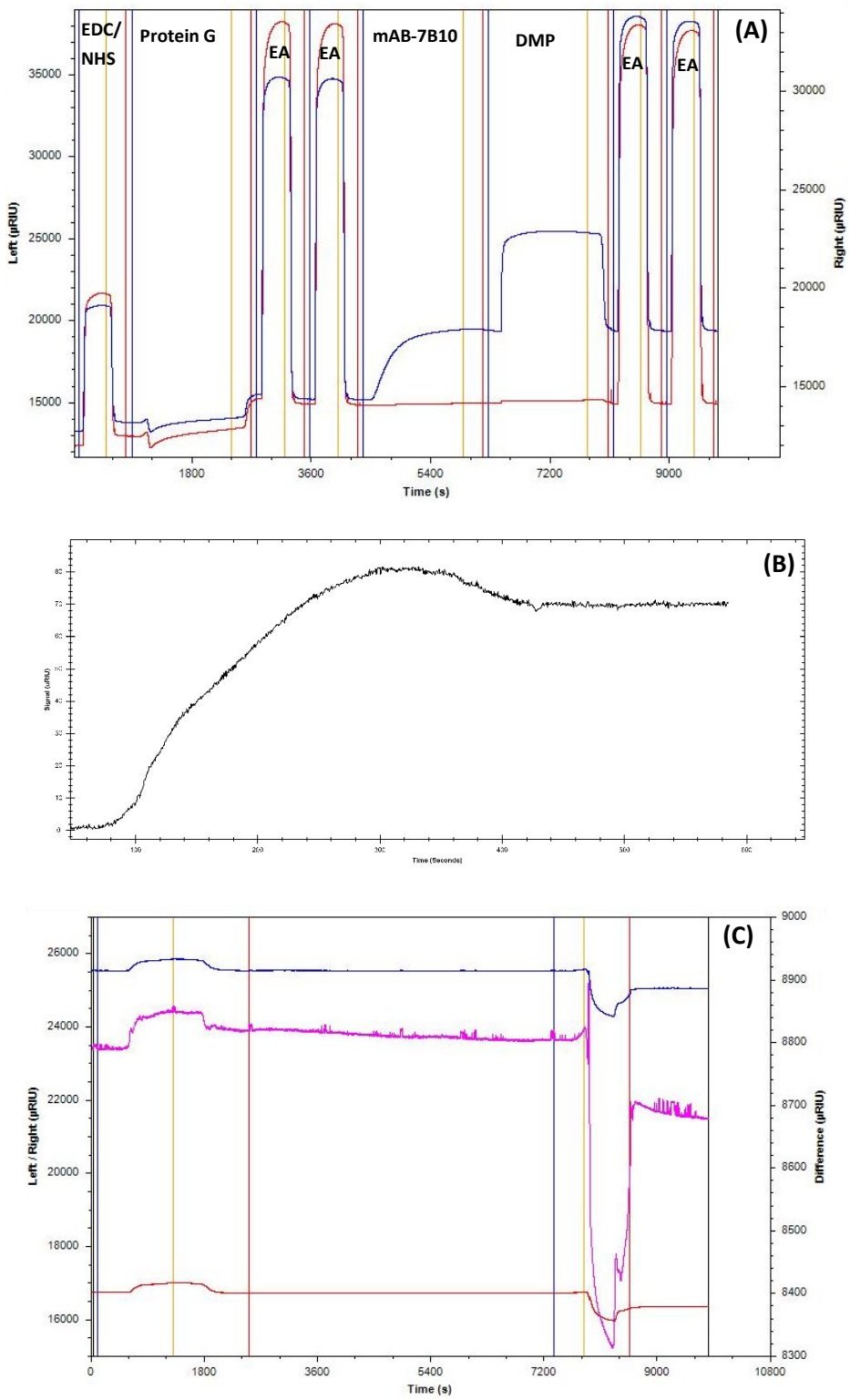

Figure 8.2.38: (A) Immobilization of 60 µg/mL mAB-7B10 (250 µL; NaAcetate buffer pH 5; R = 4238 µRIU) over previously immobilized 200 µg/mL PG (250 µL; sodium acetate buffer) on a 16-MHDA functionalized gold chip with initial EDC/NHS activation, DMP crosslinking of mAB-7B10 to PG and ethanolamine capping (EA). (B) Test injection of 25 nM rSMN in PBS to test the antibody activity. (C) Epitope extraction with 5 µg tryptic rSMN in digestion buffer diluted to 300 µl with PBS. After washing with PBS for 140 minutes, the acidic elution (50 mM glycine with 50 mM HCl) followed. Vertical lines: blue marks start of injection; yellow marks dissociation start; red indicates the end of the dissociation phase; black shows a stop of recording. Horizontal lines: blue - signal recorded from sample channel; red - signal recorded from reference channel; pink - difference of the sample and reference channel.

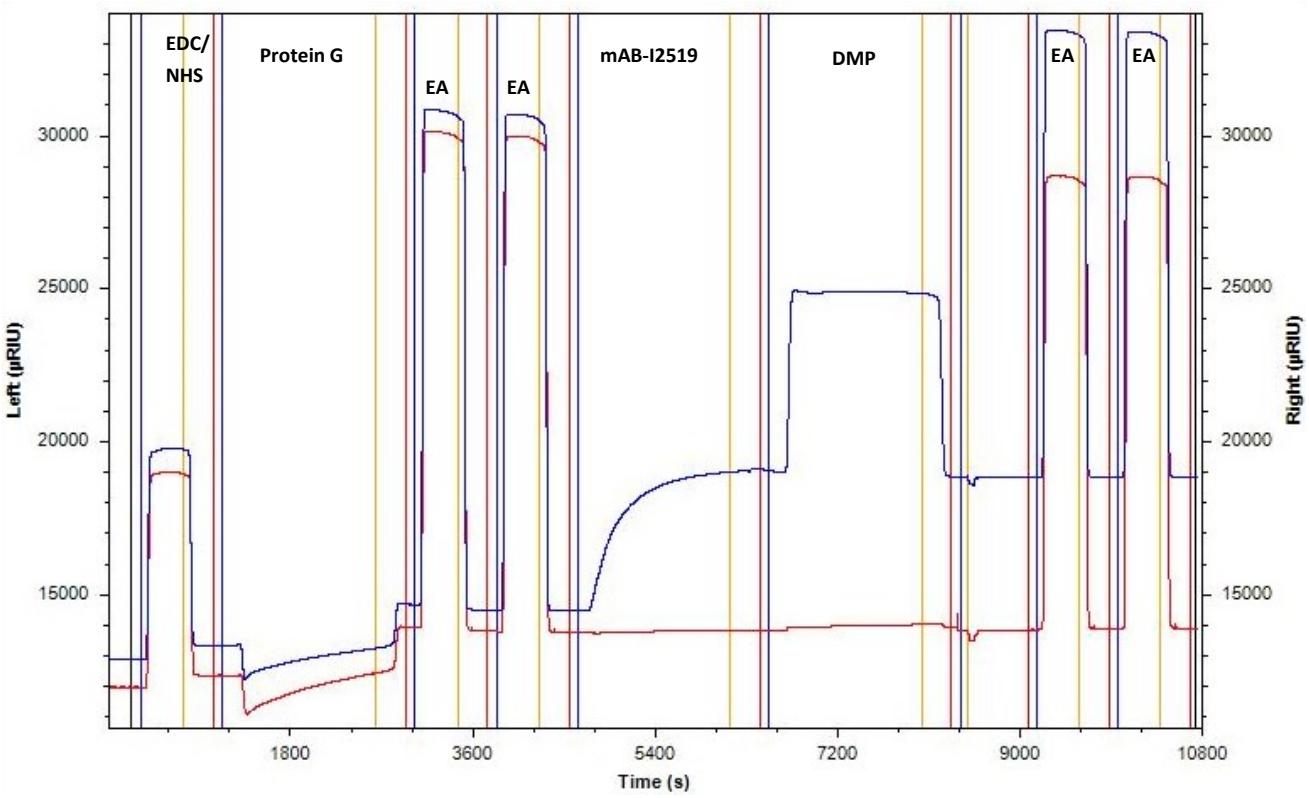

Figure 8.2.39: Immobilization of 40 µg/mL mAB-7B10 (250 µL; NaAcetate buffer pH 5; R = 4442 µRIU) over previously immobilized 200 µg/mL PG (250 µL; sodium acetate buffer) on a 16-MHDA functionalized gold chip with initial EDC/NHS activation, DMP crosslinking of mAB-7B10 to PG and ethanolamine capping (EA). Horizontal lines: blue - signal from the sample channel; red - signal from the reference channel.

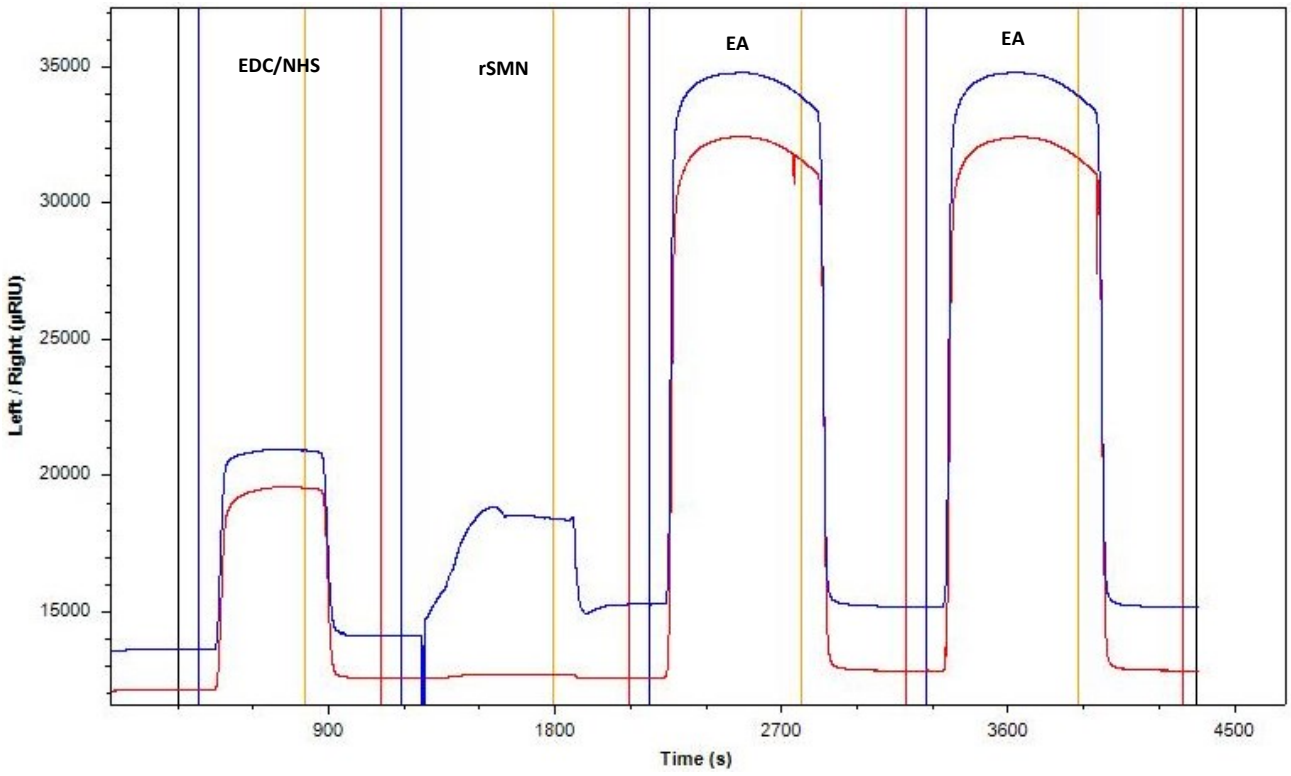

Figure 8.2.40: Immobilization of rSMN (10 µg/mL; 15 µL/min) only on the sample channel (left; blue) with prior EDC/NHS surface activation (25 µL/min; 250 µL; 40 mg/mL EDC; 10 mg/mL NHS, both channels) and two times EA capping (25 µL/min; 1 M; pH 8.5; both channels). 1172 µRIU stable rSMN immobilization was achieved.

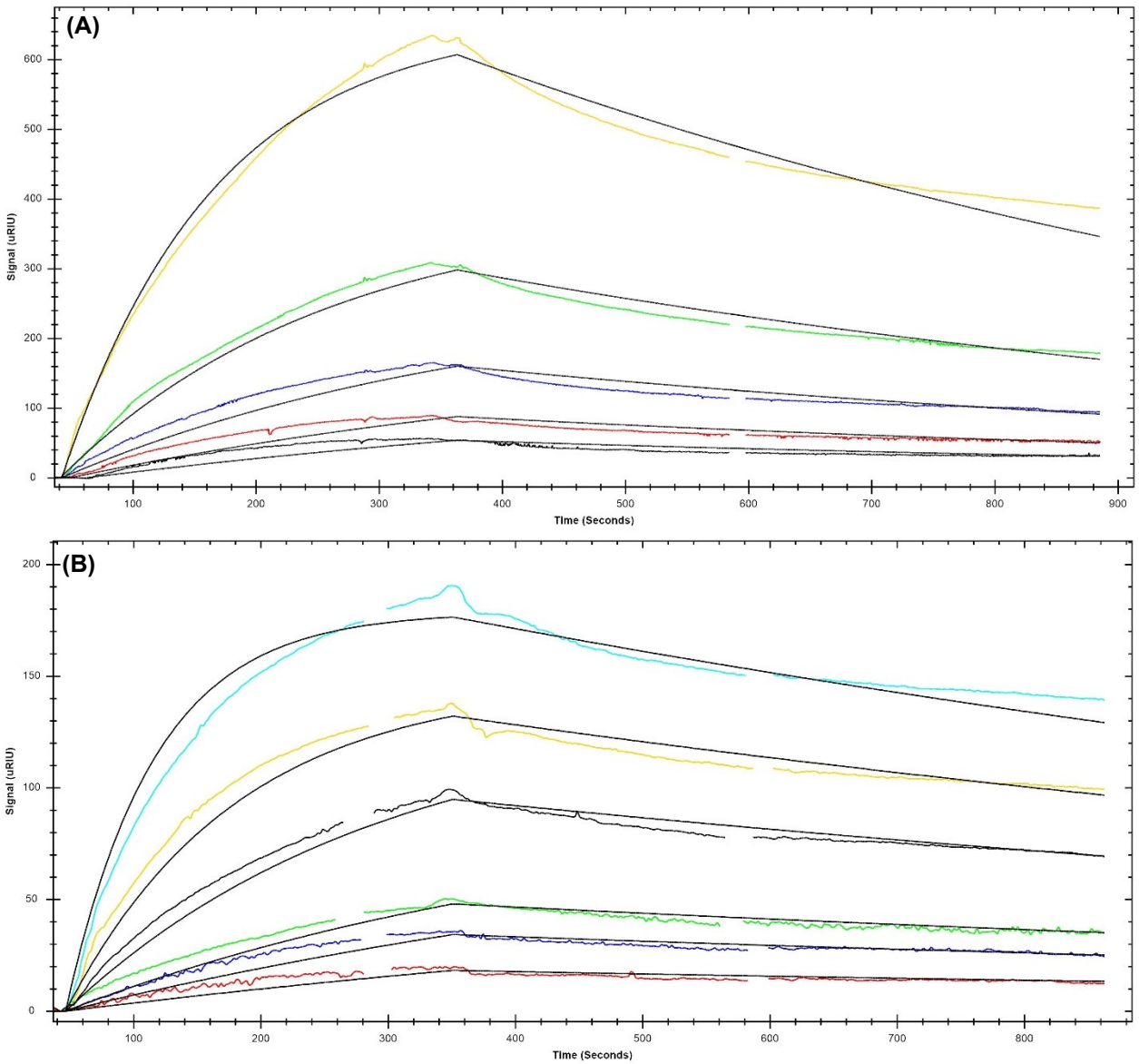

Figure 8.2.41: Senosorgrams for double-referenced curves for the sample and reference channel with buffer and anti-SMN antibody injections over immobilized rSMN. 1:2 dilutions of the antibodies with (A) 10-320 nM IG-1106-2 and (C) 10-320 nM IG-1107-2 were injected. Colored lines represent the measured curves, and black lines represent the 1:1 binding fit.

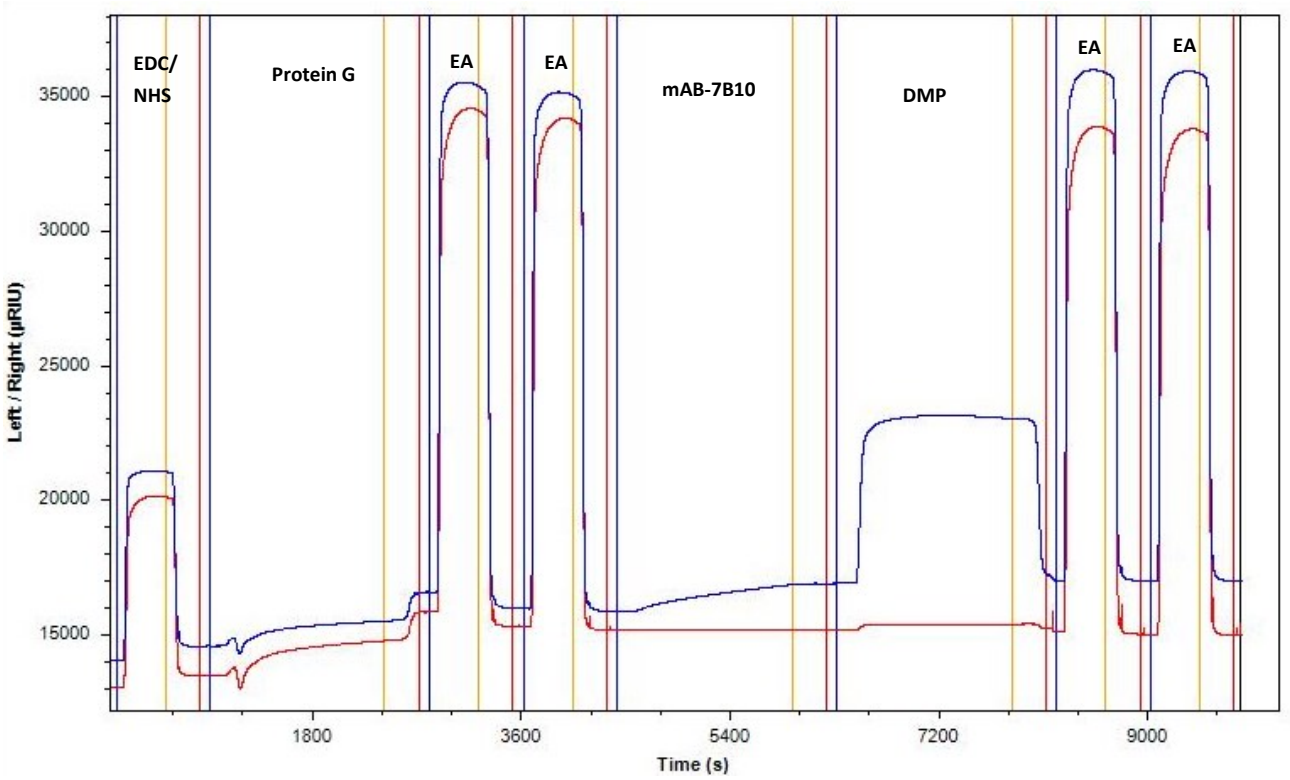

Figure 8.2.42: Immobilization of mAB-7B10 via protein G and DMP crosslinking on an MHDA functionalized gold chip. Initial EDC/NHS activation (25 µL/min; 250 µL; 40 mg/mL EDC; 10 mg/mL NHS) followed by PG injection (10 µL/min; 250 µL; 200 µg/mL) and first EA capping (25 µL/min; 1 M; pH 8.5) over sample (left; blue) and reference channel (right; red). The mAB-7B10 injection (10 µL/min; 8 µg/mL, 250 µL; R = 1055 µRIU) in PBS followed by a DMP injection (10 µL/min; 30 mM; 250 µL) in 0.2 M sodium borate only over the sample channel (left; blue). The last cappings with EA were injected over both channels to avoid completely drying out the reference channel. Horizontal lines: blue - signal recorded from sample channel; red - signal recorded from reference channel; pink - a difference of the sample and reference channel.

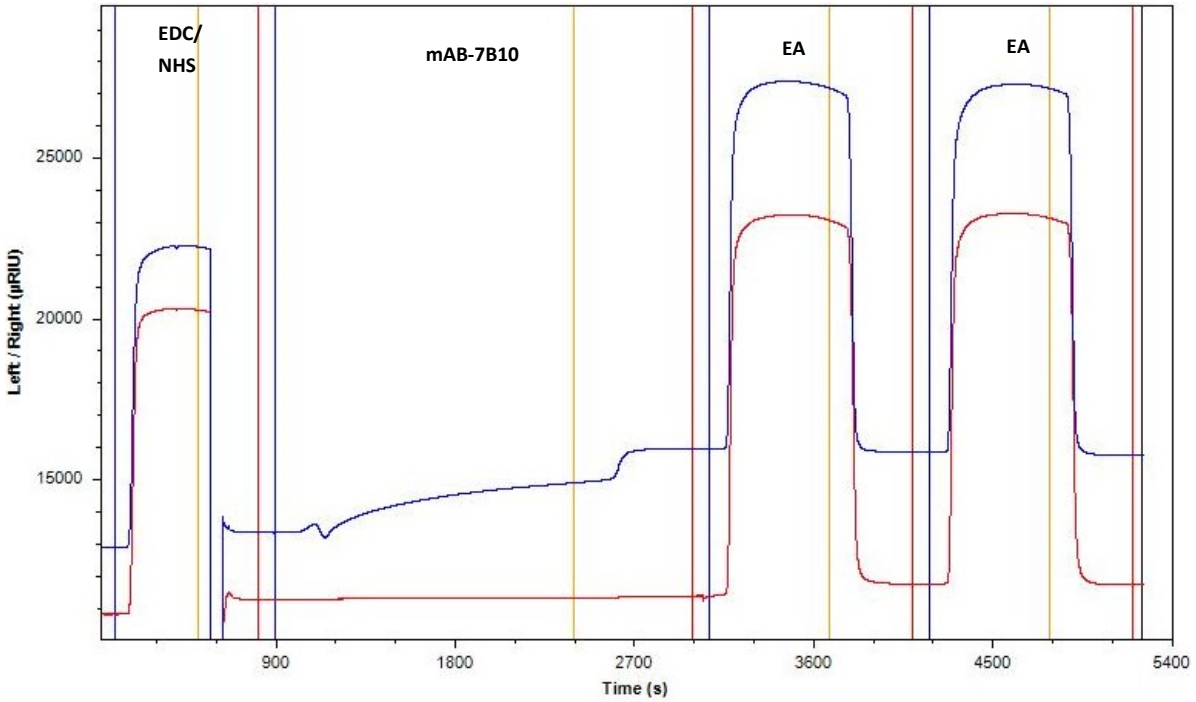

Figure 8.2.43: Immobilization of mAB-7B10 on an MHDA functionalized gold chip. Initial EDC/NHS activation (25 µL/min; 250 µL; 40 mg/mL EDC; 10 mg/mL NHS) followed mAB-7B10 injection (10 µL/min; 250 µL; 200 µg/mL; R = 2600 µRIU) and two EA capping injections (25 µL/min; 1 M; pH 8.5) over sample (left; blue) and reference channel (right; red). Horizontal lines: blue - signal recorded from sample channel; red - signal recorded from reference channel; pink - a difference of the sample and reference channel.

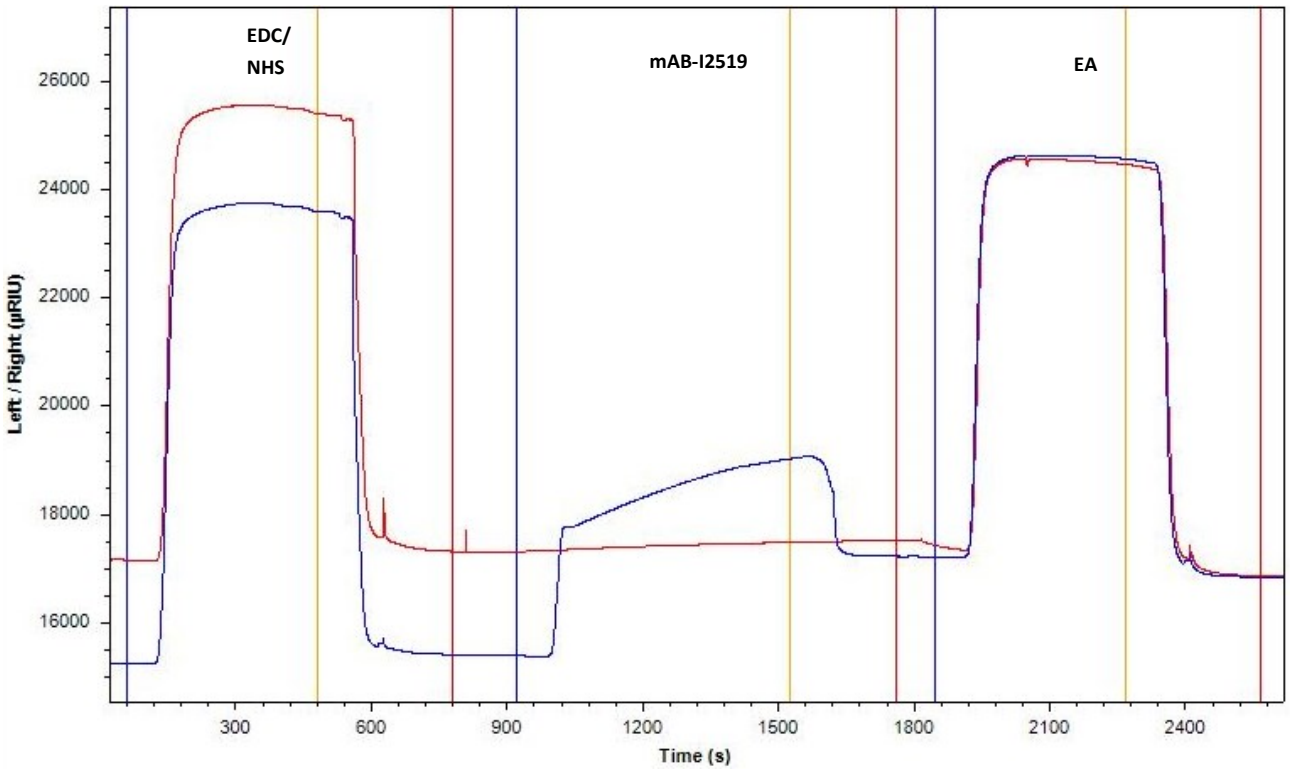

Figure 8.2.44: Immobilization of mAB-I2519 on a dextran functionalized gold chip. Initial EDC/NHS activation (25 µL/min; 250 µL; 40 mg/mL EDC; 10 mg/mL NHS) followed by mAB-I2519 injection (15 µL/min; 250 µL; 60 µg/mL; R = 1833 µRIU) and one EA capping injection (25 µL/min; 1 M; pH 8.5). Activation and capping were done on both sample (left; blue) and reference (right; red) channels and mAB-I2519 was only injected over the sample (left; blue) channel. Horizontal lines: blue is the signal from the sample channel; red is the signal from the reference channel.

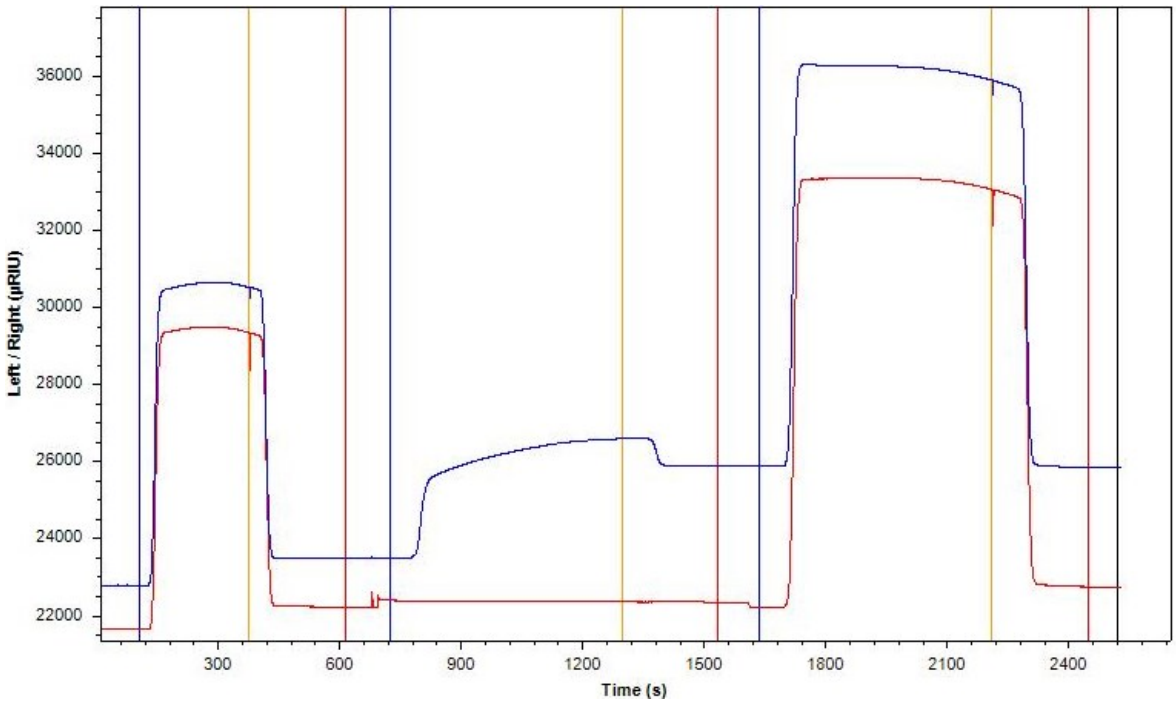

Figure 8.2.45: Immobilization of mAB-I2519 on an MHDA functionalized gold chip. Initial EDC/NHS activation (25 µL/min; 250 µL; 40 mg/mL EDC; 10 mg/mL NHS) followed by mAB-I2519 injection (15 µL/min; 250 µL; 90 µg/mL; R = 2402 µRIU) and one EA capping injection (25 µL/min; 1 M; pH 8.5). Activation and capping were done on both sample (left; blue) and reference (right; red) channels and mAB-I2519 was only injected over the sample (left; blue) channel. Horizontal lines: blue is the signal from the sample channel; red is the signal from the reference channel.

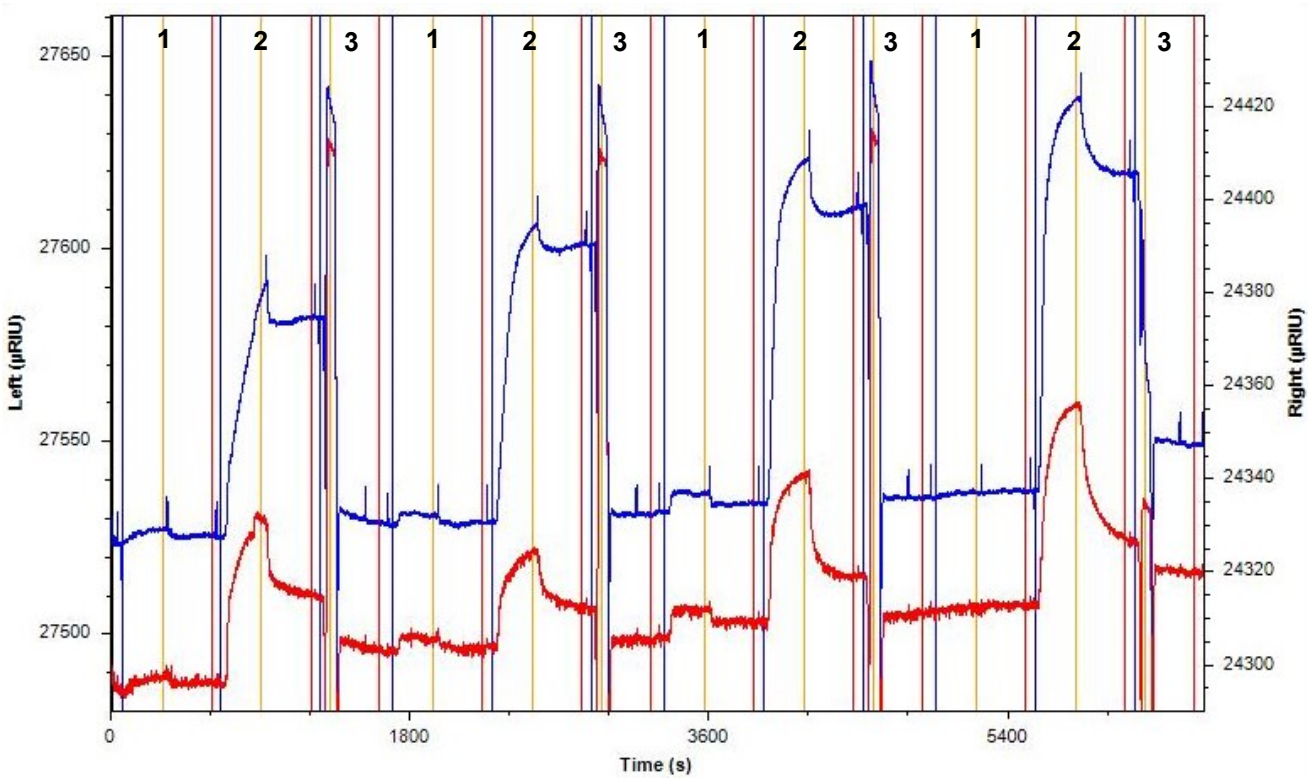

Figure 8.2.46: Raw sensorgram for buffer (**1**), sample (**2**), and regeneration solution (**3**) injections. The sample channel (left; blue) and reference channel (right; red) are shown. The vertical lines indicate the start of injection (blue), the start of dissociation (yellow), and the end of dissociation (red). Two times 250 nM IL8 in PBST were injected, and the regeneration solution consisted of 0.1 M NaCl pH 2.

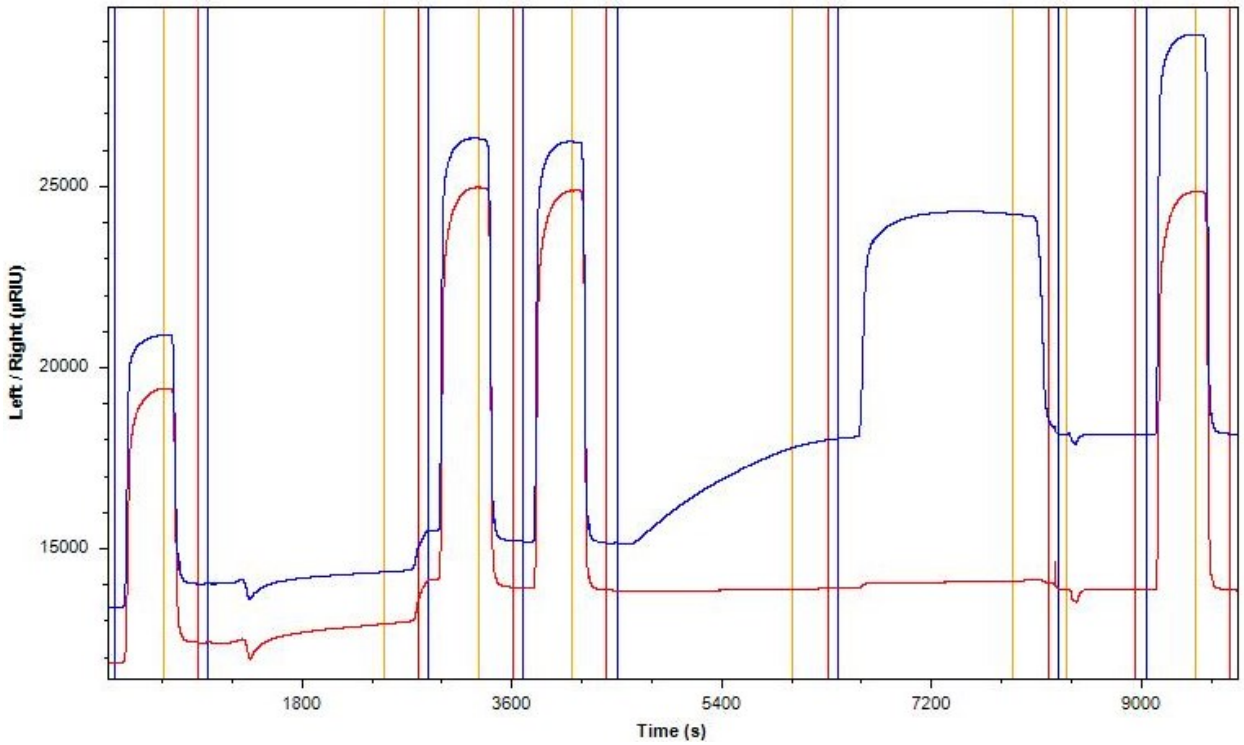

Figure 8.2.47: Immobilization of mAB-I2519 via protein G and DMP crosslinking on an MHDA functionalized gold chip. Initial EDC/NHS activation (25 µL/min; 250 µL; 40 mg/mL EDC; 10 mg/mL NHS) followed PG injection (10 µL/min; 250 µL; 200 µg/mL) and first EA cappings (25 µL/min; 1 M; pH 8.5) over sample (left; blue) and reference channel (right; red). The mAB-I2519 injection (10 µL/min; 20 µg/mL, 250 µL; R = 2924 µRIU) in PBS followed a DMP injection (10 µL/min; 30 mM; 250 µL) in 0.2 M sodium borate, both only over the sample channel (left; blue). The last cappings with EA were injected over both channels to avoid completely drying out the reference channel. Horizontal lines: blue is the signal from the sample channel; red is the signal from the reference channel.

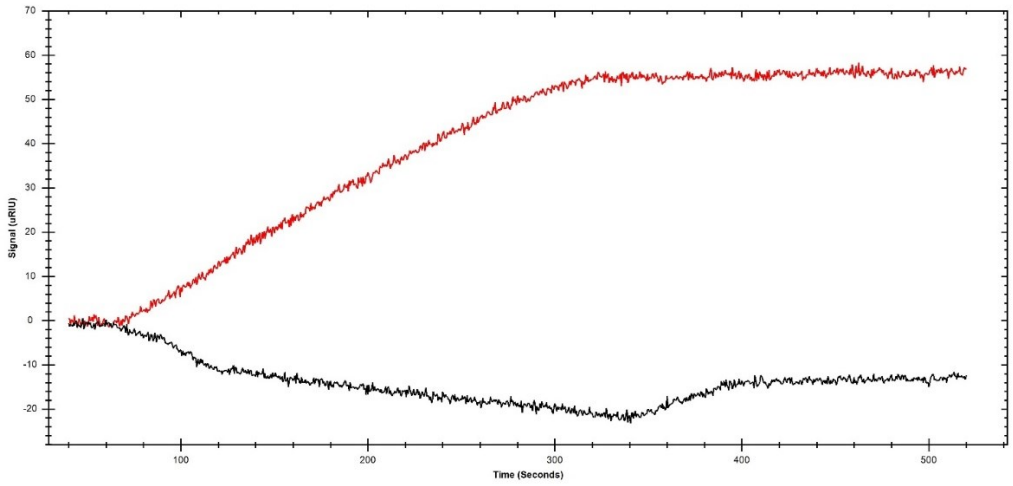

Figure 8.2.48: Sensogram for referenced response curves for a 100 nM IL8 (red) and 200 µM IL8[55-72] (black) injection.

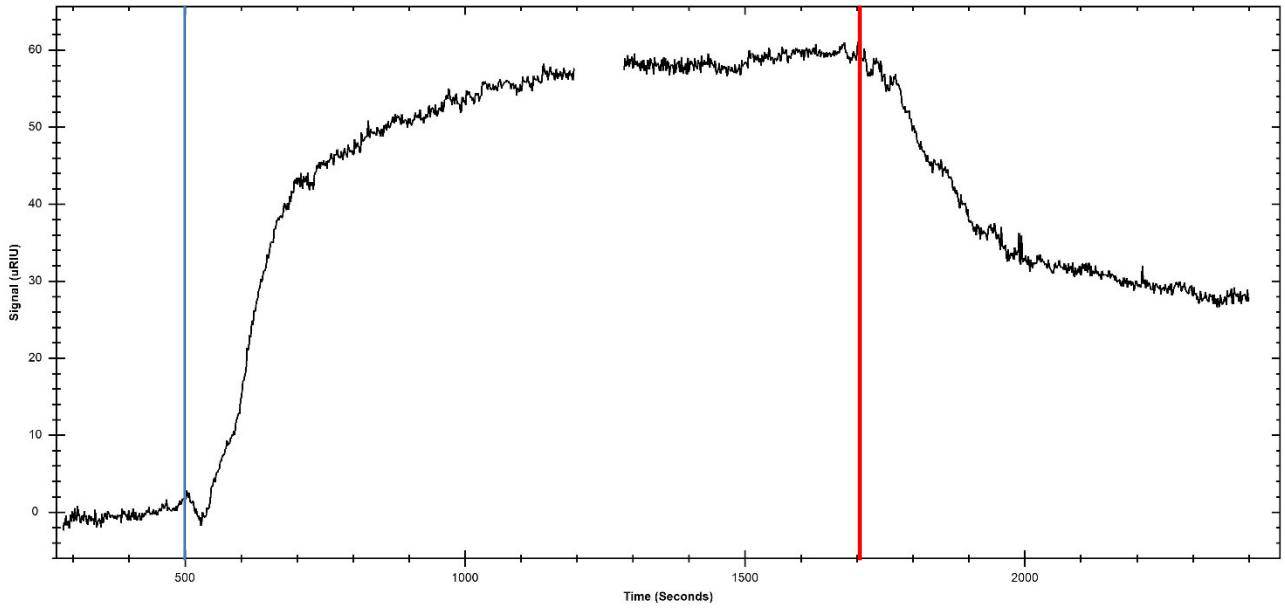

Figure 8.2.49: Epitope extraction with 0.5 µM tryptic rSMN diluted with PBS. The processed sensorgram shows the association (start: blue line) and dissociation (start: red line) without the acidic elution phase (Figure 8.2.38).

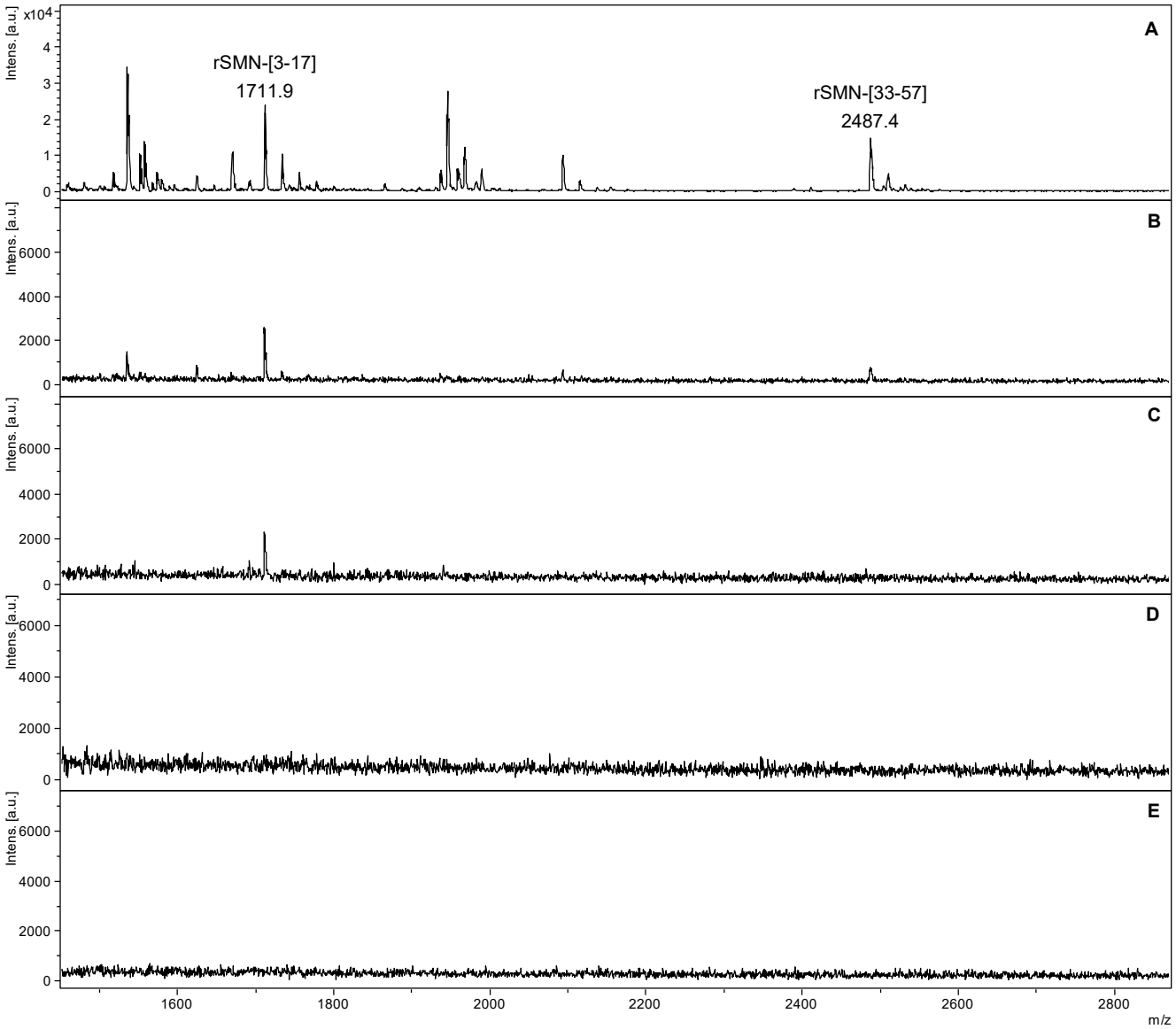

Figure 8.2.50: MALDI-tof MS measurements of selected fractions from the control column and injected tryptic rSMN: (A) Injection fraction; (B) 3rd washing fraction; (C) 5th washing fraction; (D) 20th washing fraction; (E) acidic elution with 0.1 %TFA in MQ. The experiment was executed by Tamsila Khan, and the data were reprocessed. (Method: RP; Matrix: DHB)

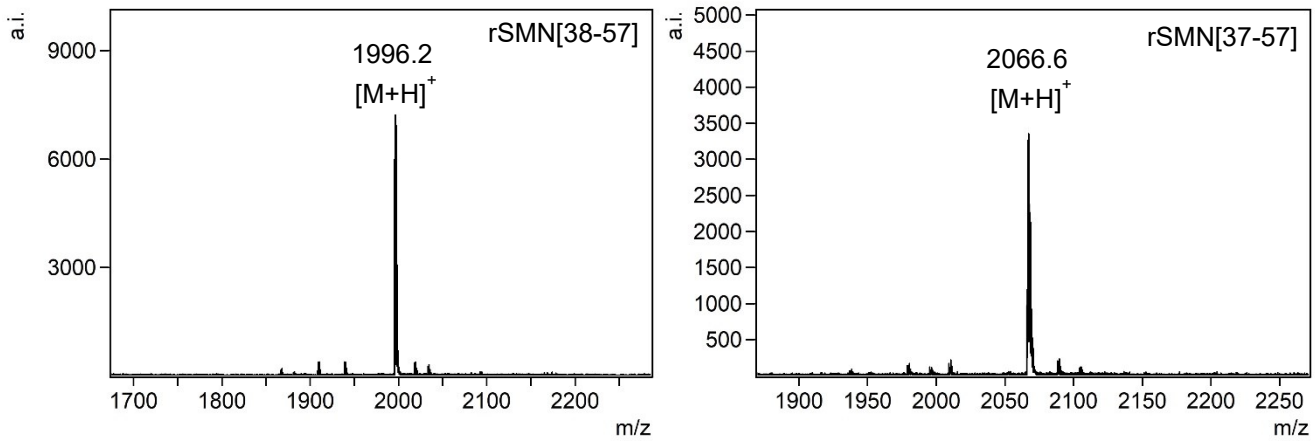

Figure 8.2.51: MALDI-tof MS measurements of the purified peptides and combined fractions for the rSMN peptides: rSMN[38-57] ($[M_{theo.}+H]^+$ = 1995.9) and rSMN[37-57] ($[M_{theo.}+H]^+$ = 2066.9).

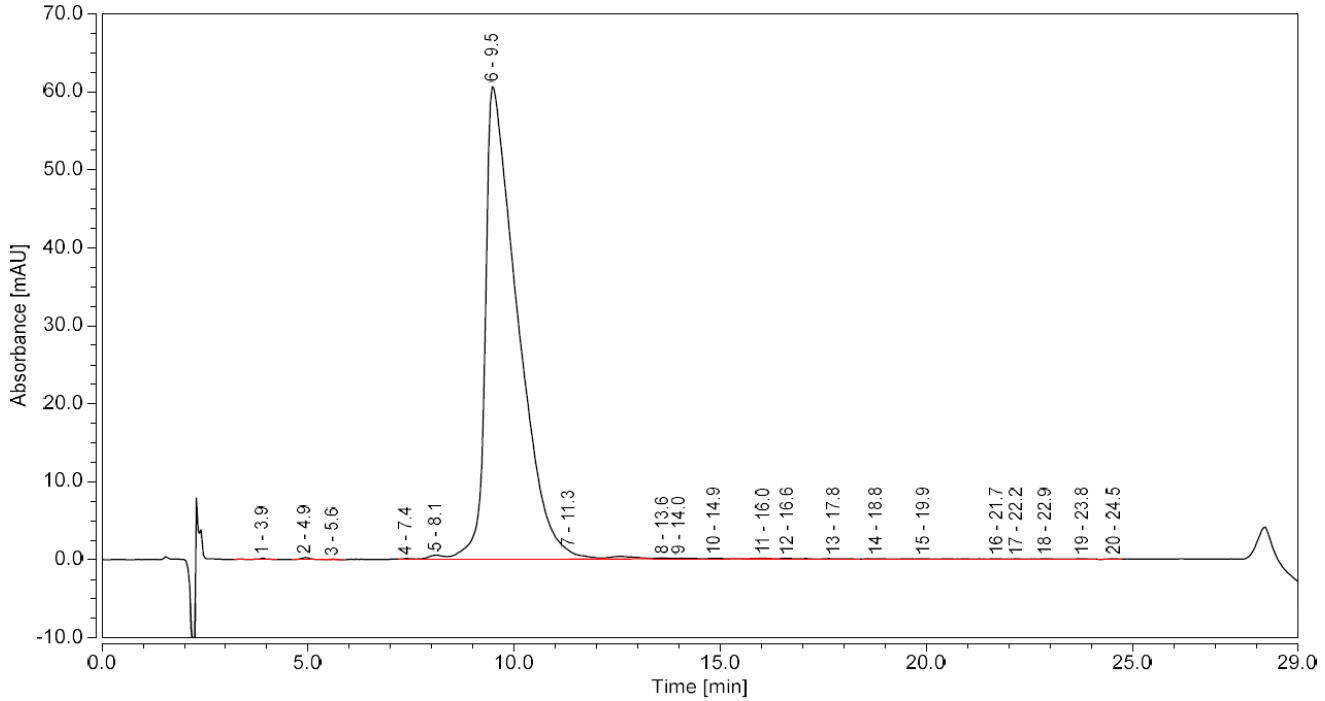

Figure 8.2.52: Chromatogram for the purified peptide rSMN[38-57] with a gradient of 80 % to 74% solvent A from 5 - 25 minutes. Peak-6, with a retention time of 9.5 minutes, corresponds to the peptide rSMN[38-57] with a relative area of 97.6 %. The Vanquish HPLC System (ThermoFisher Scientific, Langerwehe, GER) was used with the RP-C18 column from Macherey-Nagel (Nucelosil 100-5 C18 Nautilus).

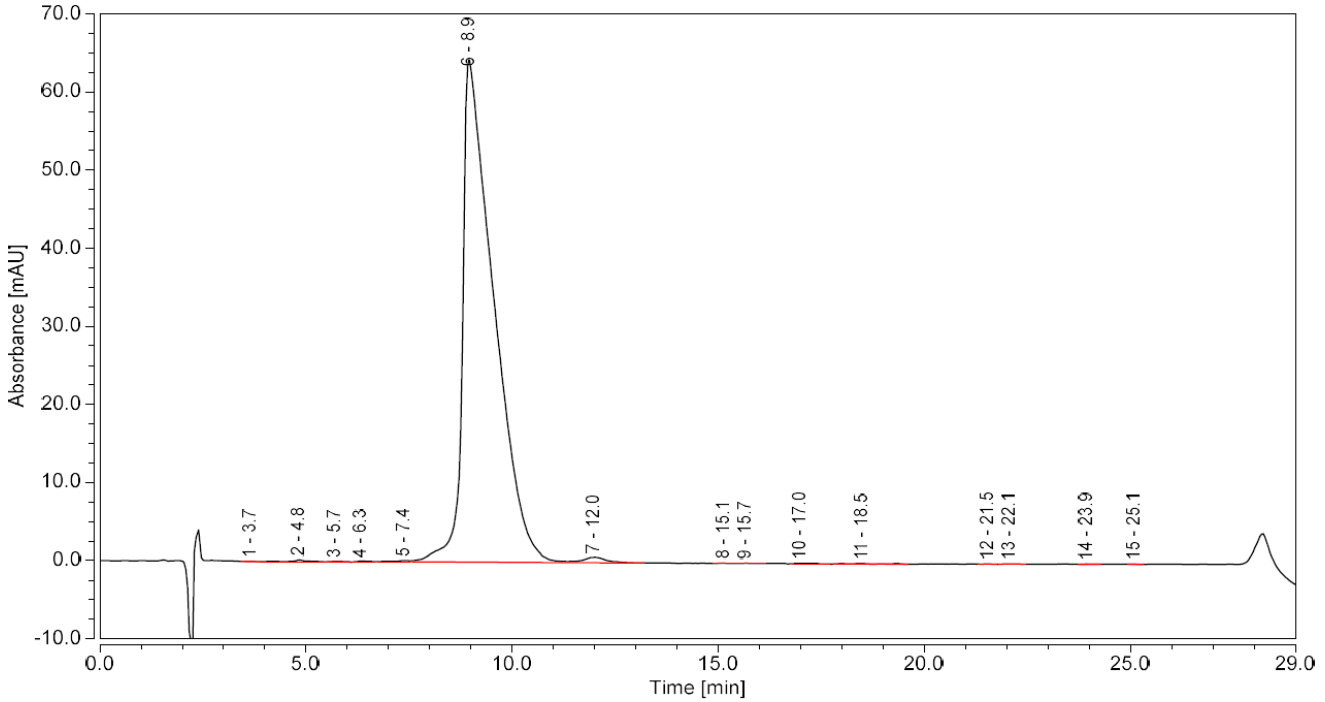

Figure 8.2.53: Chromatogram for the purified peptide rSMN[37-57] with a gradient of 80 % to 70% solvent A from 5 - 25 minutes. Peak-6, with a retention time of 8.9 minutes, corresponds to the peptide rSMN[37-57] with a relative area of 98.6 %. Vanquish HPLC System (ThermoFisher Scientific, Langerwehe, GER) with the RP-C18 column from Macherey-Nagel (Nucelosil 100-5 C18 Nautilus) was used.

List of Figures

List of tables

List of Abbreviations

°C	Degree celsius
µg	Microgram
µL	Microliter
µM	Micromolar
µRIU	Micro-refractive index units
16-MHDA	16-mercaptohexadecanoic acid
3D	Three dimensional
3-HPA	3-hydroxy picolinic acid
AA	Amino acid
Abu	α-aminobutyric acid
AC	Affinity chromatography
ACC	Accuracy
ACN	Acetonitrile
ADA	Anti-drug antibody
AE	Acidic elution
Ala, A	Alanine
AmBic	Ammonium bicarbonate
AMD	Age-related macular degeneration
ANN	Artificial neural networks
APS	Ammonium persulfate
Arg, R	Arginine
Asn, N	Asparagine
Asp, D	Aspartic acid
BCE	B-cell epitope
BLI	Biolayer-interferometry
Boc	Tert-Butyloxycarbonyl
BP	Binding site-forming peptides
BSA	Bovine serum albumin
C	Constant
Cys	Cysteine
c_0	Initial concentration
c_A	Concentration of A
c_{AB}	Concentration of complex AB
c_B	Concentration of B
CC	Chemical crosslinking
CDR	Complementary determining region
C-Met	Mesenchymal-epithelial transition factor
CNBr	Cyanogenbromid
CRIM	Corss-reactive immunological material
cryo-EM	Cryo-electron microscopy
CTSD	Catehpsin D
CV	Column-volume
CXCL8	Interleukin-8
D	Discontinuous
Da	Dalton
DCM	Dichloromethane
DE	Diethyl ether
DHB	2,5-dihydroxy benzoic acid
DIPEA	N, N-Diisopropylethylamine

DMF	Dimethylformamide
DMP	Dimethyl pimelimidate
DNA	Deoxyribonucleic acid
DTT	Dithiothreitol
EA	Ethanolamine
EES	Exonic splicing silencer
EDC	1-Ethyl-3-(3-dimethyl aminopropyl)carbodiimide
ELASA	Enzyme-linked apta-sorbent assay
ELISA	Enzyme-linked immunosorbent assays
EMA	European Medicines Agency
EP	Epoxy
ERT	Enzyme replacement therapy
ESI	Electrospray ionization
EtOH	Ethanol
Fab	Antigen-binding fragment
FC	Crystallizable fragment
FDA	U.S. Food and Drug Administration
fg	Femtogram
Fmoc	Fluorenylmethoxycarbonyl
FP	Fluorescence polarization
g	GRAM
GAA	α-Glucosidse A
GAG	Glycosaminoglycans
GER	Germany
Gln, Q	Glutamine
Glu, E	Glutamic acid
Gly, G	Glycine
GPCR	G-protein coupled receptor
GRT	Gene replacement therapy
h	Hours
H	Heavy
H2O2	Hydrogen peroxide
H2SO4	Sulfuric acid
HBTU	Benzotriazol-1-yloxy(dimethylamino)methylidene]-dimethylazanium;hexafluorophosphate
HCCA	α -hydroxy cinnamic acid
HCl	Hydrochloric acid
HDX	Proton-deuterium exchange
His, H	Histidine
HPLC	High-pressure liquid chromatography
HS(CH2)COOH	16-mercapto hexadecanoic acid
HSA	Human serum albumin
IAA	Iodoacetamide
ICH	International committee for harmonization
Ig	Immunoglobulin
IL1	Interleukin-1
IL8	Interleukin-8
Ile, I	Isoleucine
IOPD	Infantile-onset Pompe disease
ITC	Isothermal titration calorimetry
ITI	Immune tolerance induction
ka	Association rate constant

KA	Equillibrium association constant
KCl	Potassium chloride
kd	Dissociation rate constant
KD	Equillibrium dissociation constant
KH2PO4	Potassium dihydrogen phosphate
KHL	Keyhole limpet hemocyanin
kpsi	Kilopounds per square inch
L	Light, Linear
LC	Liquid chromatography
Leu, L	Leucine
LOD	Limit of detection
LOPD	Late-onset Pompe disease
LOQ	Limit of quantification
LP	Linear mode
LSD	Lysosomal storage disease
Lys, K	Lysine
m/z	mass-to-charge ratio
M6P	Mannose-6-phosphate
mAB	Monoclonal antibody
MALDI	Matrix-assisted laser desorption ionization
MCC	Matthew correlation coefficient
MCS	Missed cleavage site
MCT	Microcentrifugation tubes
MeOH	Methanol
Met, M	Methionine
mg	Milligram
MHC	Major histocompatibility complex
MHDA	16-mercaptohexadecanoic acid
min	Minutes
mL	Milliliter
ML	Machine learning
mm	Millimeter, Millimeter
mM	Millimolar
MQ	MilliQ filtered water
MS	Mass spectrometry
MTBE	Methyl-tert-butylether
MTP	MALDI target plate
MWCO	Molecular weight cutoff
N2	Nitrogen
NaAc	Sodium acetate
NaCl	Sodium chloride
NaH2PO4	Sodium dihydrogen phosphate
NaHCO3	Sodium hydrogen carbonate
NaOH	Sodium hydroxide
NBS	Newborn genetic screening
NCL	Neuronal ceroid lipofuscinoses
ng	Nanogram
NHS	N-hydroxysuccinimide
nm	Nanometer
nM	Nanomolar
NMP	N-methyl-2-pyrrolidone
NMR	Nuclear magnetic resonance spectroscopy

No	Number
pAB	Polyclonal antibody
PAGE	Polyacrylamide gel electrophoresis
Pbf	2,2,4,6,7-pentamethyl dihydrobenzofuran-5-sulfonyl
PBS	Phosphate-buffered saline
PBST	Phosphate buffered saline with Tween-20
PCT	Pressure cycling technology
pCTSD	Pro-cathepsin D
PEG	Polyethylene glycols
PG	Protein G
Phe, F	Phenylalanine
Pmc	2,2,5,7,8-pentamethyl chroman-6-sulfonyl
PNGF	Peptide-N-Glycosidase F
PPI	Protein-protein interactions
Pro, P	Proline
PS	Polystyrene
PVDF	Polyvinylidenfluorid
Q	Quadrupole mass analyzer
QCM	Quartz crystal microbalance
R	Response
R2	Coefficient of determination
RA	Rheumatoid arthritis
Req	Response at equilibrium state
RFR	Random forest regression
Rmax	Response maximum
RNA	Ribonucleic acid
ROC AUC	Receiver operator characteristic area under the curve
RP	Reversed phase, Reflectron mode, Reference peptide
rSMN	Recombinant survival motor neuron protein
RT	Room temperature
S/N	Signal-to-noise ratio
s/s	seconds and seconds
SA	Sinapic acid
SAM	Self-assembled monolayer
SAW	Surface acoustic wave
SDS	Sodium dodecyl sulfate
SEC	Size exclusion chromatography
SELEX	Systematic evolution of ligands by exponential enrichment
Ser, S	Serine
SMA	Spinal muscle atrophy
SMN	Survival motor neuron protein
SMNΔ7	SMN protein C-terminally truncated by 7 amino acids
SPPS	Solid phase peptide synthesis
SPR	Surface Plasmon Resonance
SVM	Support vector machines
TBS	Tris-buffered saline
TBST	Tris-buffered saline with Tween-20
tBu	Tert-Butyl
TEMED	Tetramethylethylenediamine
TFA	Trifluoroacetic acid
Thr, T	Threonine
TNF-α	Tumor necrosis factor-alpha

tof	Time-of-flight
Tris-HCl	Tris(Hydroxymethyl)Methylamine hydrochloride
Trp, W	Tryptophan
Tyr, Y	Tyrosine
u	units
UC	Ultracentrifugation
USA	United States of America
UV	Ultraviolet
V	Variable
v/v	Volume-to-volume
Val, V	Valine
VEGF	Vascular endothelial growth factor
w/w	Weight-to-weight
WBCL	Whole blood cell lysate
WG	Working group
ΔG	Differential free enthalpy
ΔH	Differential enthalpy
ΔS	Differential entropy